2019-12

UPDATED APPROACH TO SHOCK FAILURE ASSESSMENT OF SHIPBOARD EQUIPMENT

Didoszak, Jarema M.

Monterey, CA; Naval Postgraduate School

NAVAL POSTGRADUATE SCHOOL

MONTEREY, CALIFORNIA

DISSERTATION

UPDATED APPROACH TO SHOCK FAILURE ASSESSMENT OF SHIPBOARD EQUIPMENT

by

Jarema M. Didoszak

December 2019

Dissertation Supervisor: Young W. Kwon

THIS PAGE INTENTIONALLY LEFT BLANK

REPORT DOCUMENTATION PAGE			*Form Approved OMB No. 0704-0188*

1. AGENCY USE ONLY *(Leave blank)*	**2. REPORT DATE** December 2019	**3. REPORT TYPE AND DATES COVERED** Dissertation

4. TITLE AND SUBTITLE
UPDATED APPROACH TO SHOCK FAILURE ASSESSMENT OF SHIPBOARD EQUIPMENT

5. FUNDING NUMBERS

6. AUTHOR(S) Jarema M. Didoszak

7. PERFORMING ORGANIZATION NAME(S) AND ADDRESS(ES)
Naval Postgraduate School
Monterey, CA 93943-5000

8. PERFORMING ORGANIZATION REPORT NUMBER

9. SPONSORING / MONITORING AGENCY NAME(S) AND ADDRESS(ES)
N/A

10. SPONSORING / MONITORING AGENCY REPORT NUMBER

11. SUPPLEMENTARY NOTES The views expressed in this thesis are those of the author and do not reflect the official policy or position of the Department of Defense or the U.S. Government.

12a. DISTRIBUTION / AVAILABILITY STATEMENT
Approved for public release. Distribution is unlimited.

12b. DISTRIBUTION CODE
A

13. ABSTRACT (maximum 200 words)

Naval vessels are subjected to underwater explosions that impart a mechanical shock onto the ship structure, its subsystems, equipment and crew. This violent shock loading, although not in direct contact with the ship hull, seeks to cause significant damage and even failure of critical components, potentially rendering vital systems inoperable. To ensure deployment of robust systems, shock hardening of surface ships is established in part through shock qualification of mission-essential shipboard equipment. Current shock qualification methods predominantly rely on demonstration of satisfactory performance under prescribed physical testing schedules using standardized shock test machines. A pass/fail rating is assigned based on post-test operational evaluation and visual inspection of structural elements, not from measured response values. An updated shock failure assessment approach is found through numerical experimentation of standard shock platform models, full ship simulations and reduced order equipment models approximating various shock testing scenarios. Introduction of a simple functional failure representation provides a definite means by which to assess the response severity and time at failure. Threshold values for the peak velocity response and change in displacement are thusly established and proposed as deterministic shock failure criteria in order to reduce uncertainty in the shock qualification of shipboard equipment.

14. SUBJECT TERMS
fluid structure interaction, underwater explosions, ship shock, ship survivability, mechanical shock, equipment fragility, pseudo velocity, failure criteria, peak velocity, change in displacement, shock severity, functional failure, damage boundary

15. NUMBER OF PAGES
246

16. PRICE CODE

17. SECURITY CLASSIFICATION OF REPORT	**18. SECURITY CLASSIFICATION OF THIS PAGE**	**19. SECURITY CLASSIFICATION OF ABSTRACT**	**20. LIMITATION OF ABSTRACT**
Unclassified	Unclassified	Unclassified	UU

NSN 7540-01-280-5500

Standard Form 298 (Rev. 2-89)
Prescribed by ANSI Std. 239-18

THIS PAGE INTENTIONALLY LEFT BLANK

Approved for public release. Distribution is unlimited.

UPDATED APPROACH TO SHOCK FAILURE ASSESSMENT OF SHIPBOARD EQUIPMENT

Jarema M. Didoszak
Civilian, Department of the Navy
BSE, Naval Architecture & Marine Engineering, University of Michigan, 1994
MS, Mechanical Engineering, Naval Postgraduate School, 2004

Submitted in partial fulfillment of the
requirements for the degree of

DOCTOR OF PHILOSOPHY IN MECHANICAL ENGINEERING

from the

NAVAL POSTGRADUATE SCHOOL
December 2019

Approved by:

Young W. Kwon
Department of Mechanical and Aerospace Engineering
Dissertation Supervisor

Joshua H. Gordis
Department of Mechanical and Aerospace Engineering

Fotis A. Papoulias
Department of Systems Engineering

Clyde L. Scandrett
Department of Applied Mathematics

Young S. Shin
Department of Mechanical and Aerospace Engineering

Young W. Kwon
Department of Mechanical and Aerospace Engineering
Dissertation Chair

Approved by:

Garth V. Hobson
Chair, Department of Mechanical and Aerospace Engineering

Orrin D. Moses
Vice Provost of Academic Affairs

THIS PAGE INTENTIONALLY LEFT BLANK

ABSTRACT

Naval vessels are subjected to underwater explosions that impart a mechanical shock onto the ship structure, its subsystems, equipment and crew. This violent shock loading, although not in direct contact with the ship hull, seeks to cause significant damage and even failure of critical components, potentially rendering vital systems inoperable. To ensure deployment of robust systems, shock hardening of surface ships is established in part through shock qualification of mission-essential shipboard equipment. Current shock qualification methods predominantly rely on demonstration of satisfactory performance under prescribed physical testing schedules using standardized shock test machines. A pass/fail rating is assigned based on post-test operational evaluation and visual inspection of structural elements, not from measured response values. An updated shock failure assessment approach is found through numerical experimentation of standard shock platform models, full ship simulations and reduced order equipment models approximating various shock testing scenarios. Introduction of a simple functional failure representation provides a definite means by which to assess the response severity and time at failure. Threshold values for the peak velocity response and change in displacement are thusly established and proposed as deterministic shock failure criteria in order to reduce uncertainty in the shock qualification of shipboard equipment.

THIS PAGE INTENTIONALLY LEFT BLANK

TABLE OF CONTENTS

LIST OF FIGURES

THIS PAGE INTENTIONALLY LEFT BLANK

LIST OF TABLES

THIS PAGE INTENTIONALLY LEFT BLANK

LIST OF ACRONYMS AND ABBREVIATIONS

2D	two-dimensional
3D	three-dimensional
AMS	automatic multi-level sub structuring
AVP	seaplane tender
BUSHIPS	Bureau of Ships
CEM	complex exponential method
COTS	commercial off the shelf
CPU	central processing unit
DDAM	dynamic design analysis method
DDG	guided missile destroyer
DOD	Department of Defense
DOF	degree of freedom
DSF	deck simulating fixture
DSSM	deck simulating shock machine
DYSMAS	Dynamic System Mechanics Advanced Simulation code
EFSP	extended floating shock platform
EMALS	electromagnetic aircraft launch system
EOS	equation of state
ET-M&S	enhanced shock qualification by surrogate testing and modeling & simulation
FEA	finite element analysis
FEM	finite element method
FFT	fast Fourier transform
FMEA	failure mode and effects analysis
FMECA	failure mode and effects criticality analysis
FSI	fluid structure interaction
FSP	floating shock platform
FSST	full ship shock trial
HF	high frequency
HPC	high-performance computing

HWSM	heavyweight shock machine
IEC	International Electrotechnical Commission
IFSP	intermediate floating shock platform
JWL	Jones-Wilkins-Lee
KVM	keyboard, video and mouse
LBP	length between perpendiculars
LCS	littoral combat ship
LFSP	large floating shock platform
LWSM	lightweight shock machine
M&S	modeling and simulation
MDOF	multi degree of freedom
MWSM	medium weight shock machine
NAVSEA	Naval Sea Systems Command
NSWCCD	Naval Surface Warfare Center Carderock Division
NSWC IHEODTD	Naval Surface Warfare Center Indian Head Explosive Ordnance Disposal Technology Division
NPS	Naval Postgraduate School
PCB	printed circuit board
PSI	pounds per square inch
PVSS	pseudo-velocity shock spectrum
RFPM	rational fraction polynomial method
SDOF	single degree of freedom
SHM	simple harmonic motion
SRS	shock response spectrum
UERD	Underwater Explosions Research Division
UNDEX	underwater explosions
VAC	volts of alternating current
V/UHF	very/ultra high frequency
VV&A	verification, validation, and accreditation
WWII	World War II

ACKNOWLEDGMENTS

I would like to first thank my advisor, Distinguished Professor Young Kwon, for providing consistent direction, remarkable foresight and much patience in my pursuit of this research. Without his direct support, this work could not come to fruition.

I am also grateful for the mentorship of Distinguished Professor Emeritus Young Shin. In the many years since first introducing me to "shock and vibrations" as a graduate student, he has graciously provided the guidance and understanding of a visionary leader.

Additionally, I am deeply thankful and blessed for the support of Drs. Clyde Scandrett, Joshua Gordis, and Fotis Papoulias, as members of my dissertation committee. The insight, knowledge, and thoughtfulness they bring forth serves to advance the enlightenment of NPS students each day in the sciences, mathematics, and engineering.

I would like to express my sincerest gratitude to the many outstanding engineers, researchers, technicians and fellow officers here at NPS, and throughout the U.S. Navy engineering enterprise. Collectively, their expertise, feedback, and assistance in my completing this research and further developing an interest in this topic were indispensable.

For the inspiration to become an engineer like my big brother, Slavko, thank you. To my mother and father, Maria and Jarema, they deserve more appreciation than anyone in this world could or will ever know. Мама і тато, дякую вам за все!

I dedicate this work, to my six wonderful sons, Danylo, Stefan, Yuri, Luka, Maksym, and Taras, who stood by, never minding my absence, perhaps not always understanding why. Your sacrifice is not without notice. Remember, it is always about, The Team, The Team, The Team.

Most importantly, I thank my loving wife, Robin, whose unbounded generosity, steadfast devotion, and selfless support of me in this endeavor are what saw me through. God is with us—we can do anything together.

THIS PAGE INTENTIONALLY LEFT BLANK

I. INTRODUCTION

The devastating effects of shock and vibrations have long plagued equipment designers, manufacturers and operators, often resulting in damage to, or failure of, a mechanical system. To engineers, vibration analysis describes the oscillation in a mechanical system, and is conveyed in terms of amplitude and frequency. Thus, it can be thought of simply enough as the motion of a structure, or perhaps as an oscillating force applied to some mechanical system [1]. The response of the system to this input is what ultimately leads to failure of a critical component rendering the device unable to perform as intended.

Often referred to as the "Father of Engineering Mechanics" [2] Stepan Timoshenko, recognized the negative impact of mechanical shock and vibration upon the performance of shipboard and other equipment. While working for the Naval Ministry of St. Petersburg early in his career, he applied his theories related to the buckling of structures, material elasticity, and deflection of beams, and of most importance to this examination, the analyses of elastic foundations and response of objects subjected to these disruptive motions [3]. Displaced by the onslaught of the Bolshevik Army in 1917, he later emigrated to the United States from Kyiv, Ukraine, to work briefly for the Vibration Specialty Company in Pittsburg and later the Westinghouse Electric Company where he explored the subject further [4].

He continued to write on the issues of mechanical vibration, structural loading and behavior of materials [5]. In his 1928 *Vibration Problems in Engineering* [6] Timoshenko detailed the various unique issues that a ship and her equipment experiences during a typical underway period. Examples of this are found in the chapter titles of his work: Forced Torsional Vibration of a Shaft with Several Discs, Vibration of Bars of Variable Cross Section, and Vibration of Hulls of Ships. He discusses the paradox that the ship design has with its very low natural frequency and how it is a mismatch for equipment that is locally loaded and responding within the 10–100 Hz frequency range.

With Timoshenko's influence as a professor of engineering (applied) mechanics at the University of Michigan and later Stanford University, as well as the respect amongst the engineering leaders of the day such as Prandtl, von Karman, Lamb, Taylor and Rayleigh [2], his work spurred others to apply the burgeoning theories in an effort to understand the impact driven events occurring in and around that time such as the shock induced damage of ships during World War II (WWII) [7]–[9].

R.H. Cole, in his seminal book *Underwater Explosions*, would go on to present the underwater shock loading phenomena in great detail [10] based on the work he conducted during the period 1941–1946. Later, Cyril Harris [11], in the second edition of his "Shock and Vibrations Handbook," 1976, went on to describe shock as a component of vibration. Rather than oscillatory in nature, shock excitation is sudden and abrupt, non-periodic such as a pulse, a step, or a transient vibration. Shock is something generally unwanted and needs to be avoided or controlled in order to ensure system performance during violent loading events such as underwater explosions (UNDEX) caused by depth charges, mines and torpedoes. This sudden delivery of energy characterized as an early time transient motion of the shock event is often followed by a more regular oscillatory vibration response of the system in the later time.

Recognizing that these are just the entry points rather than culmination of detailed engineering examinations, the combination of a shock event and the inclusion of highly susceptible equipment that absolutely must perform without issue under the most stringent requirements, such as in a naval combatant vessel, makes the topic of shipboard shock qualification of equipment a relevant and necessary endeavor.

A. SHOCK FAILURE OF SHIPBOARD EQUIPMENT

The U.S. Navy has practiced shock hardening of ships since the unfortunate realization of unexpected losses and unanticipated mission kills resulting from near miss UNDEX of surface combatants and submarines during WWII [12].

Starting from a Bureau of Ships (BUSHIPS) initiated program to increase shock resistance and subsequent early explosives testing at the Norfolk Naval Shipyard at Portsmouth, Virginia, in 1942, UNDEX testing and equipment certification and the

eventual practice of testing for shock hardness at sea has significantly evolved over the last century [13]–[16]. The Underwater Explosions Research Division (UERD) at Naval Surface Warfare Center Carderock Division (NSWCCD), Naval Surface Warfare Center Indian Head Explosive Ordnance Disposal Technology Division (NSWC IHEODTD), Naval Postgraduate School (NPS) and other researchers within the U.S. Navy and shock and vibrations community have devoted much time and effort in understanding this complex topic, its damaging effects on ships, their equipment and crew, and the means by which to mitigate such occurrences within the extremely challenging combat environment.

1. Importance of Shock Qualification

In industry, shock, which is perhaps more appropriately named impact for typical applications, is a key consideration in the manufacture and distribution of products, as it is directly tied to cost. Losses in retail products due to improperly packaged or inadequately designed items result in lost revenue resulting from products damaged during transport or display to consumer or perhaps from missed sales due to a perception of fragile, nonsurvivable items which are to be used on a daily basis. Hand held devices with cracked or chipped screens that flicker can be an annoyance for consumers. Simple bumpers or protective cases can typical mitigate the issue in these cases [17]. However, there are circumstances such as in the case of surface ships where overall life cycle considerations and peak performance at sea under combat conditions is an absolute must. It is of such importance to the U.S. Navy that Naval Sea Systems Command (NAVSEA) code 05P [18] is assigned as the technical warrant holder within the Naval Systems Engineering Directorate (SEA 05) to ensure shock hardness of all U.S. Navy surface combatants.

With regard to naval vessels, reducing total ownership cost is always a concern but more importantly, mission performance, and fight through capability in an austere environment when, ship, equipment and Sailors' lives are at stake cannot be negotiated. Shock qualification of critical equipment and systems is a means to ensure this capability is inherent in the combatants of the U.S. Navy Fleet.

a. Past Experience

The MIL-S-901 series, which is the military specification pertaining to high impact mechanical shock of equipment mounted in ships, is based on WWII experiences of mechanical shock loading at close ranges that resulted in severe shock damage without holing the targeted vessel [19]. Though all can be found in combat situations, of the sources outlined in Table 1, only those circled as non-contact UNDEX are of interest to the current discussion. Contact explosions, that breach the hull plate, damage the vessel by shrapnel or thermal effects, though extremely important in the overall analyses of explosion induced failures, are not of consideration here.

Table 1. Sources of Shock Affecting Combatants. Source: Adapted from [9].

A.	Underwater Explosions		Direct Projectile or Bomb Hits		Firing of Ship's Guns	
B.	Contact	Non-contact	Full Penetration	Partial Penetration	Air Blast	Recoil Shock
C.	Torpedoes	Influence mines	.. Projectiles ..		.. Main battery ..	
	Contact mines	Aerial bombs (near-misses)	.. Aerial bombs ..		.. Secondary batteries ..	
		Depth charges				

Some of the resulting damage documented in these non-contact UNDEX events were found to be hull structure that was displaced (dishing) or stiffeners that buckled (tripped), electrical circuit breakers that tripped, reduction gear that suffered misalignment, hull fittings that were jarred loose, lights where glass globes broke and fans that detached from their base frames. Additionally, valves failed, and gauges and meters became inoperative. Of interest is the fact that contrary to expectations, contact explosions caused little shock damage while holing the vessel. War damage reports [20], such as the one for the USS Chincoteague (AVP 24) indicated that the hull construction, design parameters of the equipment, location of the equipment, foundations and weight are influencing factors

on the potential failure of the items of interest. Figures 1 and 2 illustrate global and local damage caused by non-contact explosions, respectively.

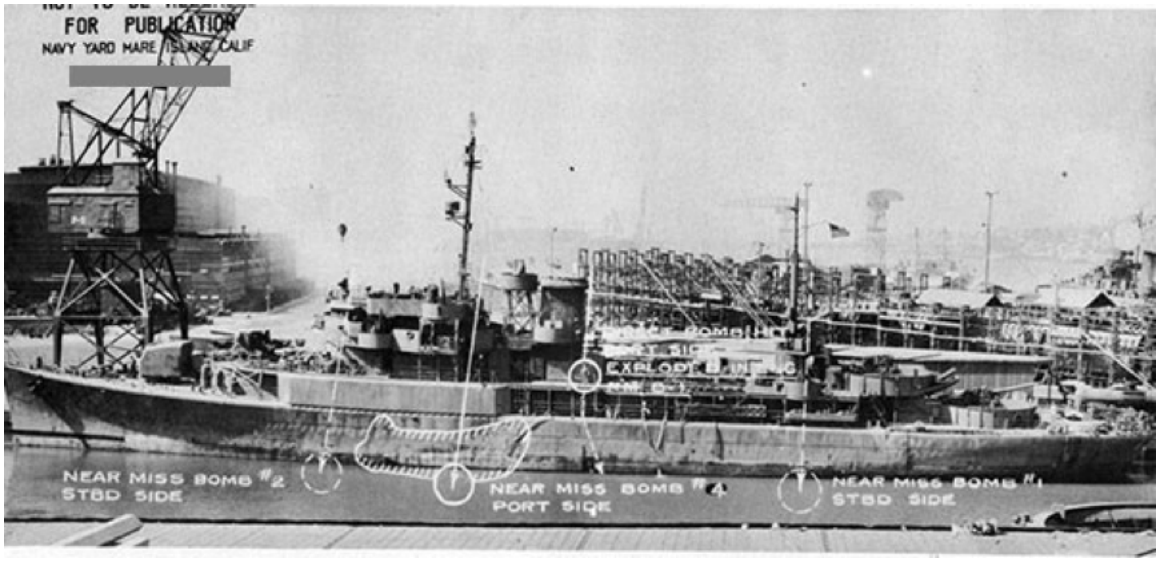

Figure 1. Port Side View of USS Chincoteague (AVP 24) Annotated with Bomb Near Misses. Source: [20].

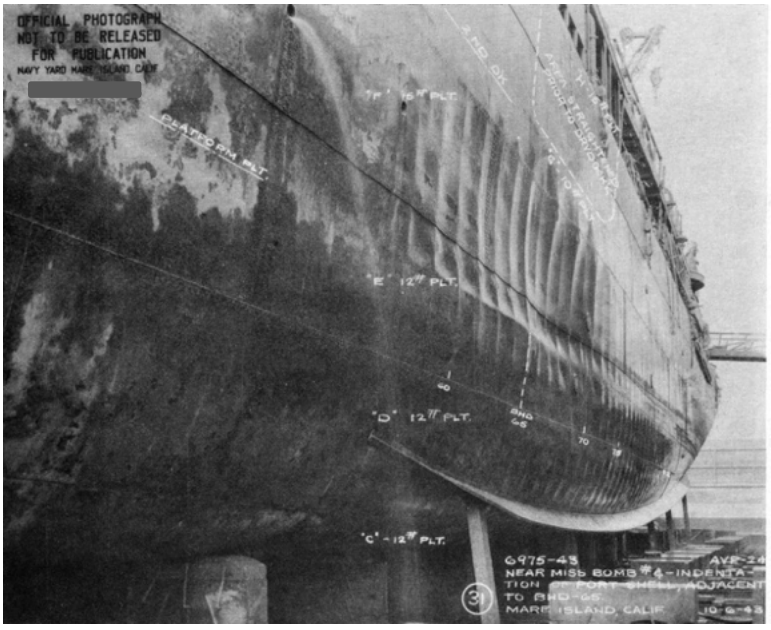

Figure 2. Hull Plate Dishing and Indentation as a Result of Near Miss Bomb No. 4. Source: [20].

b. Present Times

There is no shortage of threats to shipboard systems and equipment in modern times [21]. The charge yield of advisories threats continues to increase and the same problems persist. However, the complexity of systems has evolved and hence so have the types of potential failures points within the ship. Simpler mechanical components of the last century such as pistons, steam pipes and wire tensioning cables are replaced by digital power converters, capacitors and electrical cable connections. For example, an aircraft carrier's primary mission is to transport, launch and recover naval air forces at sea. One mission critical system involved in this operation is the aircraft launch and recovery system. Mechanically driven steam powered catapults have been in use since the early days of naval aviation to help accelerate and vector airframes skyward. Yet today the latest technology, derived from advances in pulsed power, power conditioning, and energy storage, brings the Electromagnetic Aircraft Launch System (EMALS) to ships [22]. Even though the design mission requirement is the same, means to achieve it are new vastly different.

2. Shock Hardening

In order to make a technically sound assessment of how to best validate ship shock hardness against UNDEX, the concept of shock hardening must first be defined. The U.S. Navy instruction "Shock Hardening of Surface Ships," OPNAVINST 9072.2A [23], and other related documents [24-25] describe shock hardening as the ability of a ship to continue to perform its mission in a combat environment without succumbing to shock induced failures resulting from non-contact UNDEX and other extreme loading events.

It is important to understand the scope of shock hardening as it is often confused in the discussion of ship survivability. Ship shock hardening, as described in the context of this current discussion, relates to non-contact underwater explosions and extreme loading events. Contact explosions below or above the waterline which include penetration or holing that produce blast phenomena such as thermal effects and fragmentation are therefore not considered. In U.S. Navy released photos, examples of both contact explosions, such as in the case of USS Cole (DDG 67) attack in the Yemeni port of Aden

in 2000 [26], Figure 3, and non-contact explosions, illustrated by the full ship shock trial (FSST) completed by USS Jackson (LCS 6) in 2016 [28], Figure 4, are provided to show the contrast of these distinct scenarios that produce entirely different shock loading phenomena [30]. These shock trials, which are not shock qualification tests, are mandated in part by U.S. Code Title 10, Part IV, Chapter 139, Section 2366 [31].

Figure 3. Holing Visible on the Port Side of USS Cole (DDG 67) During Heavy Lift. Source: [27].

In further distinguishing the differences in the potential underwater threats, it is known through previous battle damage and testing that the contact explosion generally produces much greater effects in the local area of the charge source. Local deformation of the structure, weapon fragmentation, thermal and blast pressure effects focus damage on the structure, systems and equipment nearer the impact zone. However, in the case of non-contact explosions, there is a predominance of global excitation and which results in unwanted responses to structure and equipment throughout the vessel. Thus, it must be stressed that the proximity and weight of the charge therefore excite the structure, systems and equipment by various means and cause distinct failure modes [32], [33].

Figure 4. USS Jackson (LCS 6) Full Ship Shock Trial. Source: [29].

Non-contact explosions can furthermore be classified into near field and far field shock loading. In the case of a near field explosion the explosive charge is typically closer to the surface, of a smaller yield while nearer to the target. This is in comparison to the far field shock loading case where the charge is very large, at a significant depth and at a great distance from the target. Figure 5 illustrates the three distinct zones that are created by the proximity of the shockwave source. Even though the combination of charge weight, distance and depth may be arranged in such a manner as to dictate a similar shock factor [34], direct scaling cannot be applied, as it is found to be not quite linear in nature as the standoff distance increases with respect to the location of the target [35].

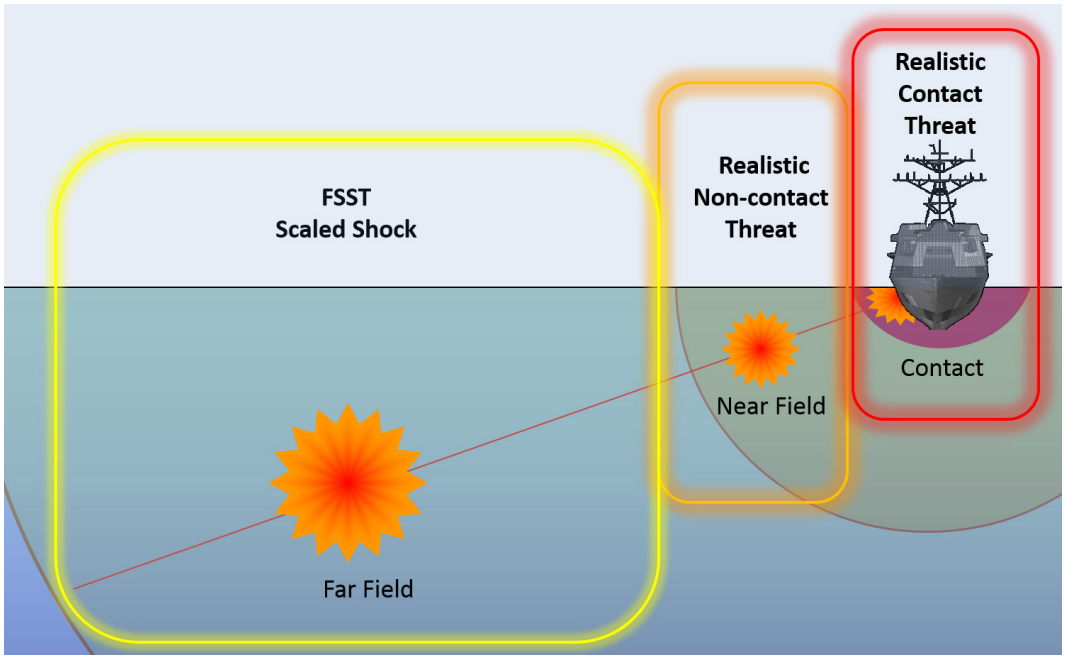

Figure 5. Distinct UNDEX Event Regions

B. LITERATURE REVIEW

In exploring the topic of shock induced failure of shipboard equipment, several primary elements must be examined. A non-exhaustive list includes:

- Shock hardening requirements
- Equipment qualification methods
- Shock qualification standards
- Shock loading mechanisms
- Characterization of failure
- Concept of acceptable losses

While most of these items will be touched upon in some way throughout this research, failure, its overall characterization, the uncertainty inherent in its determination and assessment against available criteria will take center stage.

1. Previous Investigations

As far back as the 1970s, questions arose concerning the proper procedure to test shipboard equipment, systems and their components for the purposes of shock qualification as part of the ship shock hardening program. It was observed that during standard shock trials, circuit breakers that had previously passed qualification tests failed while installed in switchgear assemblies aboard ship which were subjected to shock severities well below the intended survivability level. A study by Clements focused on testing of similar circuit breakers installed in typical electrical switchgear using the lightweight shock machine (LWSM) and mediumweight shock machine (MWSM) [36]. It was concluded that while a greater percentage of circuit breakers passed on the MWSM, due to the increased shock severity in terms of transmitted peak acceleration on the LWSM, nearly all failed using that test method. However, if they passed on the LWSM they also passed on the MWSM. Interestingly, there were found to be significant material condition issues in the structure of the switchgear (equipment case) such as poor welds, and lesser quality of workmanship were also noted. Yet correction of these material issues, though fixing the structural failures, would further increase the severity of the shock delivered to the circuit breakers themselves (i.e., the critical component), as the means of energy dissipation would be removed. Although it was determined that the LWSM provided a more conservative measure of failure in shock qualification testing of these items, the fact that they failed in situ was still an open issue. Additionally, Clement advocated for the need to require operational testing of equipment; the premise being that not only does the equipment need to structurally survive, but it must also continue to perform its intended function.

Introduced post WWII, the routine shock testing of equipment was first accomplished utilizing shock test machines of British design [37]. In addition to the shock qualification of equipment, the U.S. Navy sought to improve overall ship shock survivability through investigation of other design considerations [38]. The result was the MIL-S-901 series [39]. In the early 1990s Bradley et al. [40] reported on an extensive study that revisited the shock qualification of the standard U.S. Navy circuit breaker. The researchers conducted a comparison of shock test methods delineated in the MIL-S-901D [41], testing both the circuit breaker as a primary unit on the LWSM and

additionally as an equipment component on MWSM and floating shock platform (FSP). The FSP had two configurations, one with a tuned deck simulator and the other with the equipment directly mounted to the FSP deck with corresponding fixed ballast in order to match vessel displacement. Their findings were that the loading applied in each case was different, yet the responses varied as a function of their installation type, that is hull mounted or deck mounted. For the hull mounted shipboard components, a circuit breaker and switchboard in this case, there were only marginally differences, whereas the deck mounted equipment displayed much more significant differences. They concluded the following:

1. There were instances where equipment shock qualified on the LWSM failed on the MWSM or the FSP when installed as a component in a larger system. This observation resulted in a recommendation for specific guidelines for installing and mounting of shock qualified equipment on vital shipboard assemblies. Additionally, subsystem tests vice component only tests were recommended as standard practice.

2. There was no information concerning the deck and hull differences for the MWSM, however differences did exist for FSP standard hull and deck simulation testing. One recommendation was for the adoption of a tunable deck simulator for the MWSM. It is conceived that the recent inclusion of the Deck Shock Simulation Machine (DSSM) testing option in MIL-DTL-901E [42] was an eventual result of this.

3. Even though the FSP with tuned deck feature is used preferentially over the standard FSP it is tuned to a generic not specific frequency matching intended installation location on the ship. This test frequency could potentially be anywhere from18-50 Hz not only around a nominal 30 Hz deck frequency. A final recommendation was to test the equipment at additional “tuned” deck frequencies.

The conclusion from this review was that differences exist, especially in deck mounted, equipment testing. It was recommended that the testing be modified in the

LWSM and MWSM to more closely approximate the FSP, which was concluded to be the "most representative" test method. The mounting and structure were also found to have a noticeable influence on smaller components being tested.

Long thought of as the best surrogate for the actual ship environment, the FSP is often considered the "best" shock qualification tool, though certainly not the most cost effective in most cases. This is why physics-based modeling and simulation has taken a prominent place in the resource bin when it comes to shock qualification in recent years.

The 2007 JASON report titled *Navy Ship Underwater Shock Prediction and Testing Capability Study* [43] concluded the following:

> We find that the scientific basis of the component testing procedures is lacking, and that component testing procedures do not necessarily match either the time history of a shock impulse on a ship, or the response a component feels at its location on the ship. Component tests are not done for very large components, and do not address the possibility of failure because of the complex coupling of many components.

Recommendations from their work, which was commissioned by the U.S. Navy to specifically address the potential role of Modeling and Simulation (M&S) in the certification of ship shock hardness included three key points of interest relevant to this study:

> We recommend that the Navy should instrument the lead ship to measure continuously the vibration modes and their associated dampings….
>
> It needs to be determined how well present M&S capability can predict the failure modes of components in Full Ship Shock Trials. This can be done by (i) carrying out comparisons of simulations and observation of failure modes on future shock trials, and (ii) carrying out simulations on recent full ship shock trials….
>
> Uncertainties in component testing procedures for testing to a given threat level must be better documented and understood. For example, the Navy's validated M&S capability for liquid response should be used to determine whether the Keel Shock Factor[1] is the right indicator of "similarity"

[1] Keel Shock Factor — shock severity referenced to the keel and with deference to the angle of incident shock wave with respect to the ship.

between the shock induced by a hostile event and the impulse delivered in the component test program.

From these we can take away the need to a) more effectively address structural damping in ship shock models, b) better understand failure modes of shipboard equipment, and c) reduce uncertainties in component level testing of shipboard systems.

2. What is Currently Being Done

In order to test critical systems and equipment in newly designed and constructed ship classes, the at sea live fire ship shock trial has been seen as the de facto tool to some in the validation of ship shock hardening for decades. However, this in fact is somewhat misleading, and not generally the view accepted by those who are closest to the issue of shock qualification of ships and shipboard equipment. As Fowler [44] points out, the shock trial is not a shock test, nor is it intended to be. It does not provide a means to understand the witnessed failures, or advance the science of shock hardening, it merely demonstrates that the ship hull, systems and equipment, will perform as intended, in the configuration that they were installed. Much goes into the preparation of a shock trial in order to identify potential failures and correct them prior to the event. On the contrary, a shock test is designed to flush out potential design flaws and shock hardening weaknesses through failure assessment.

Thus, as early as the turn of the 21st century, the question was posed "what is the true benefit of these live fire events" and furthermore "is there an alternative method of shock validation that better meets the stringent technical, fiscal and schedule requirements" [45]–[57].

There are currently three options outlined in the U.S. Navy guidance [23]. Those are: 1) Full Ship Shock Trial (FSST), 2) Ship Shock Test Supplemented with M&S (Alternative Shock), and 3) Enhanced Shock Qualification, Surrogate Testing and Modeling and Simulation (referred to herein as ET-M&S). In the 2017 NPS technical report "Assessment of Ship Shock Hardening Validation Options" Kwon et al. [58]. evaluate the three options in the validation of shock hardening for surface ships based upon common business criteria of cost, schedule and performance.

The main strengths and weaknesses for each of the options are summarized in Table 2. From the summary it is clear that in terms of ship structural shock hardness validation, the first option, FSST, directly tests the vessel as built, though not to the full design level. Option 2 fails to produce the correct UNDEX loading while Option 3 can provide data up to and beyond the full design level, though requires additional validation of the model by alternative means. With respect to ship systems and equipment, Options 1 and 2 are able to test the entire vessel at once but to only a reduced loading condition, leaving the result as undesirable due to the implicit uncertainty. It is impractical for all systems and equipment to be directly assessed via Option 3, though through selective design of the analysis, based on prior equipment level shock validation, more focused and meaningful testing and investigations can lead to crucial discoveries at the prescribed design level. Once again in the case of crewmember shock assessment, there is some benefit from the reduced level of shock sustained by the crew present aboard during the live fire test series, though the number of Sailors subjected to and "trained" is insignificant. Option 2 is however plagued by an inability to fully match the UNDEX loading. Though not directly "tested' via Option 3, ET-M&S does provide the ability to collect data regarding crewmember response.

The following key findings are made based on previous investigation of the shock hardening validation options [59].

- FSST has been very beneficial to date in understanding potential failures affecting the ship mission.
- FSST has provided sound data and experience in order to validate evolving M&S techniques.
- Future use of FSST would provide only limited benefit considering the cost, schedule, and environmental impact, and hence results in a diminishing return on investment at this point.
- ET-M&S uses M&S and targeted testing to mitigate shock risk.

As technology improves, ET-M&S will continue to advance and provide enhanced capabilities in mitigation of ship shock risk while no major changes are expected in future FSST.

Table 2. Summary of Options Strengths and Weaknesses. Source: [58].

		1. FSST	2. Alternative Shock	3. ET-M&S
Ship Structure Shock Hardness	Pros	Obtains physical data under UNDEX	Obtains physical data via testing	Considers design level conditions
	Cons	Performed at reduced shock level	Not representative of UNDEX loading	Requires validation by other means
Equipment & Systems Shock Hardness	Pros	Validates all systems & equipment	Checks all systems & equipment	Checks equipment at desired design level
	Cons	Validation at a reduced threat level	Reduced UNDEX loading	Checks only pre-selected equipment. Requires validation
Crew Shock Hardness	Pros	Provides limited information	Provides limited information	Could be modeled via supplemental testing
	Cons	Performed at reduced shock level	Not representative of UNDEX loading	Not directly addressed in M&S

3. Existing Methods of Shock Validation

There are several ways to characterize damage due to shock and vibration. Some address the system globally, while other are specific to shipboard equipment at the component level. Coupled systems of components and subsystems are not adequately addressed in the testing procedures [42] and are typically addressed in an ad hoc manner.

As evidenced by the previously cited reports [43], [59], there is certainly a need to carry out additional studies in vibrations and mechanical shocks related to shipboard equipment design. Lalanne [60] discusses the need for first projecting the dynamic strain and stress that these events bring onto the system. Deformation or fracture of structural materials being pushed beyond their material limit, is typically mentioned when discussing failure. However, the failure could be such that functional failure results where the material has not exceeded a physical limit causing the damage. Rather it could be an electrical short, open circuit, separation at a connection point, optical misalignment, or other occurrence that prevents the component, equipment or system from performing its function as designed [33], [61], [62]. These functional failures could cause intermittent or permanent failures resulting in operational degradation or inability to prevent the entire ship system from accomplishing the required mission.

A cursory review and comparison of failure characterization with the Damage Boundary method [63], Dynamic Design Analysis Method (DDAM) [64] and other equipment response criteria such as the Shock Response Spectra (SRS) equipment level thresholds, which are used in ANSI/ASA S2.62-2009 [65], is conducted.

a. Damage Boundary Method

In order to overcome shock damage associated with the transportation and handing of commercial products, Newton [63] proposed a fragility assessment theory and test procedure. In this he strove to find the most severe shock likely to be encountered and the maximum shock that the item would tolerate. From this the appropriate cushioning and packaging could be designed to protect the product.

Newton assumes that the most severe shock typically results from package handling operations. Thus, the critical drop height above a non-resilient horizontal surface was found from systematic testing and accommodations for the transport and product storage could be optimized, ensuring a safe limit to the acceleration and change in velocity [66]. It was also concluded from his and subsequent work [67]–[69] that item fragility is linked directly to the type of item being tested.

In the Boundary Damage method developed by Newton, a damage region is defined based on the critical velocity change, v , and the critical acceleration, A_c ,of the component, at the onset of failure in the repeated testing of the physical article. Newton concluded that the peak acceleration transmitted to the item, A_p , over an effective duration of time, τ_e , of the acceleration pulse, define the velocity change as found in Equation 1.1.

$$v = A_p \tau_e \tag{1.1}$$

It was also recognized [63] that for a given shock there was a strong dependence between the component frequency, f_c , and the peak acceleration where,

$$\begin{aligned} f_c \tau_e &< \frac{1}{6}, \quad A_c \text{ is dependent on } v \\ f_c \tau_e &> \frac{1}{6}, \quad A_c \geq A_p \end{aligned} \tag{1.2}$$

Figure 6 illustrates the process of testing at increasing velocities until initial failure, and then subsequent acceleration step increases to initiate failure due to a critical acceleration value of the drop test.

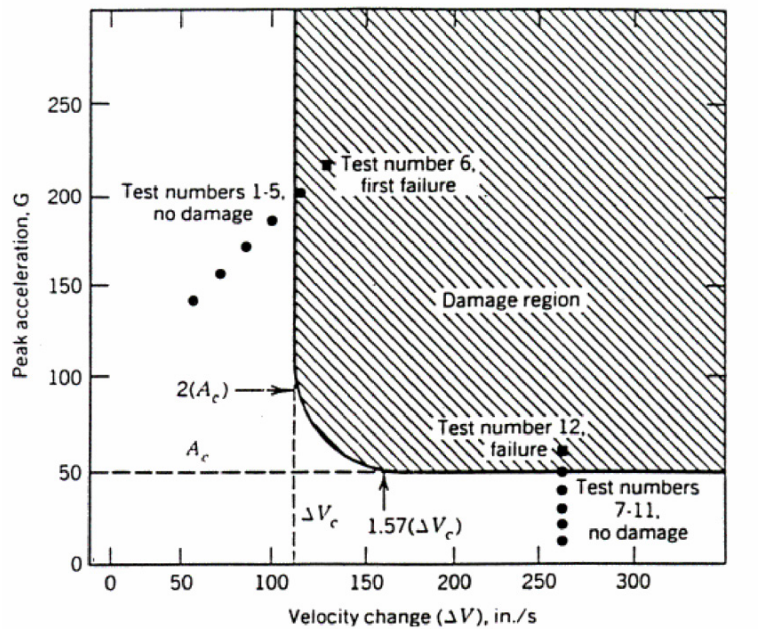

Figure 6. Boundary Damage Method. Source: [63].

This approach is highly repeatable but has an obvious determent in the fact that numerous "identical" test articles must be tested to failure in this approach. One may see where in a full-scale production run, wasting a few samples from a lot of thousands or millions may be well worth the cost of the breakage. However, for a low rate of production or one-off situation, this is not an acceptable failure determination method.

b. DDAM

When specified, DDAM provides a numerical approach to finding yield forces, strains, and displacements on a structure or equipment, to the engineer. A modal analysis is performed on the structure, reducing the system to a mass-elastic system [64]. The results from the modal analysis are used to generate an effective modal weight. Using coefficients determined from empirical data gathered from experimental testing and reported in NRL 1396 [64], the accelerations and velocities of the system are calculated and applied to the structure, resulting in the shock input response to the system.

Shock Design Criteria for Surface Ships, T907-AJ-DPC-120/3010, [25], is the governing document for using the DDAM approach for shock qualification. This document was revised in September 2017 and its superseded version was NAVSEA 0908-LP-000-3010 Rev 1[24]. The T907-AJ-DPC-120/3010 is based off the research of O'Hara and Belsheim in the early 1960s [64]. While the DDAM process allows for equipment certification, it is primarily used for structure or foundation analysis. The first reason for this is a result of the foundations that mount the equipment to the ship deck. These additional pieces of light structure are usually designed late in the ship's design and construction phase, as the ship builder and equipment engineers will go through multiple design revisions. As such, foundations are usually added after the ship and equipment designs have been finalized and accepted. The second is that, as previously mentioned, the DDAM analysis reduces the system to a mass-elastic system. The U.S. Navy's preference is that all physically testable equipment be tested in accordance with the MIL-DTL-901E. As a result, NAVSEA approval is required to certify operational equipment with DDAM. This preference for physical testing over modeling is shown in Figure 7, where, if the

equipment can be tested on one of the physical machines previously mentioned, only NAVSEA concurrence will allow shock qualification for Grade A equipment with DDAM.

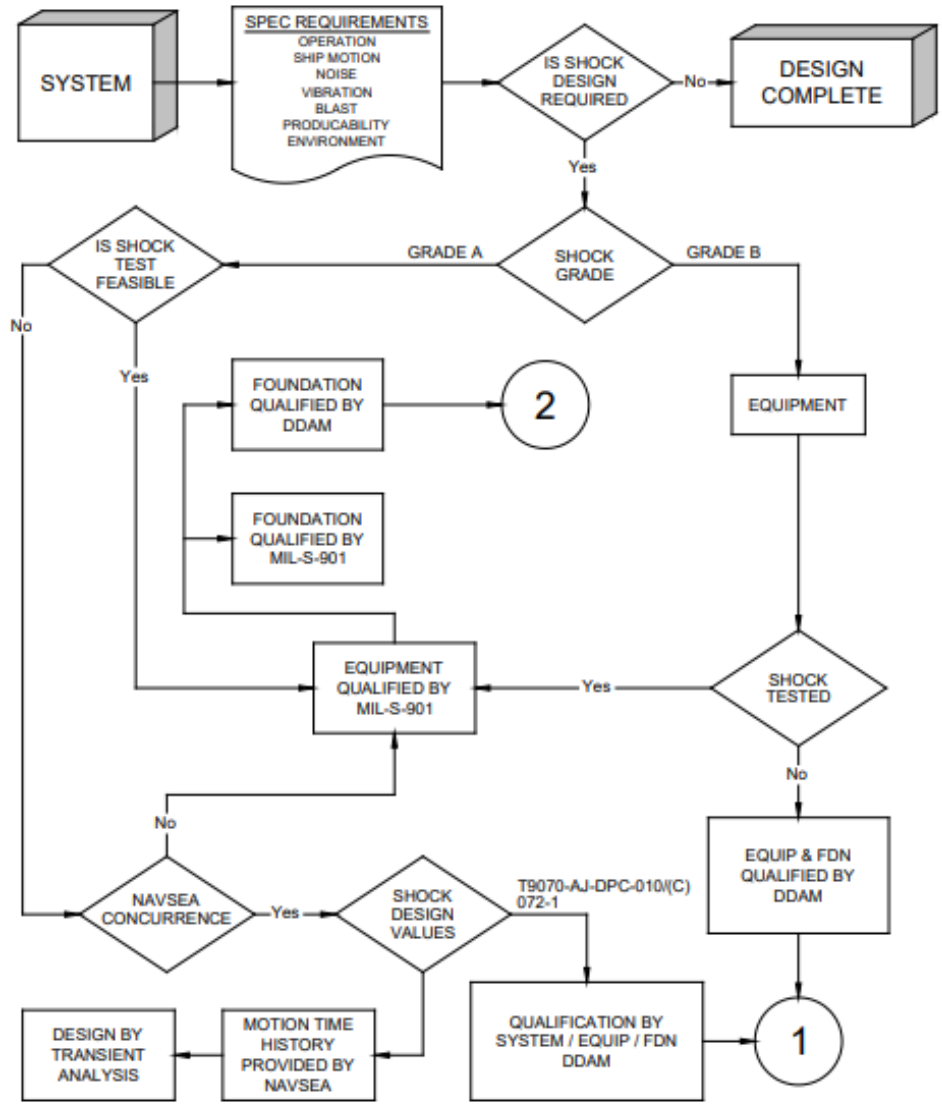

Figure 7. Selection Flow Chart for DDAM. Source: [25].

Explanation of the basic DDAM process is found in reference [64]. The DDAM results provide a means for comparison of total stress at a point to the maximum allowable stress. Results from the DDAM analysis may also be plotted in terms of SRS, as illustrated in Figure 8, and described in MIL-STD-810G [70].

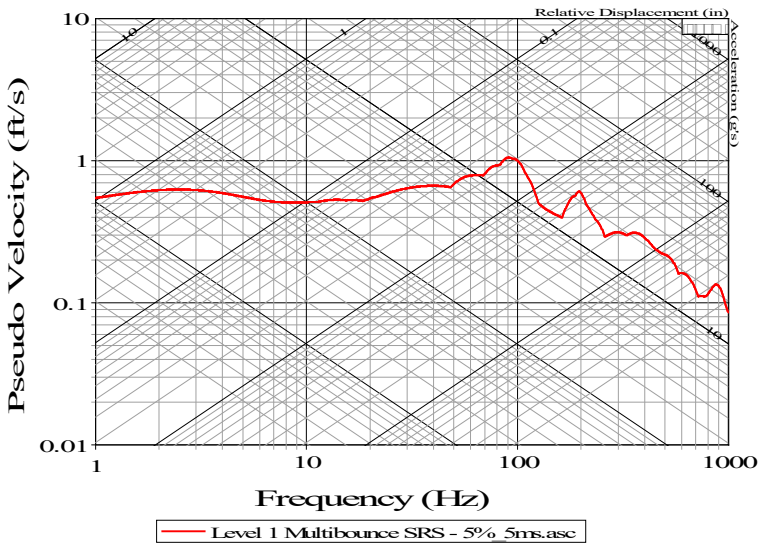

Figure 8. Shock response spectra. Source: [70].

C. RESEARCH OBJECTIVE

The overall goal of this research is to develop a more robust approach for shock qualification of shipboard equipment through implementation of a failure criterion in order to reduce the uncertainty in component and subsystem level testing.

The ultimate objective is to then use this method in conjunction with existing shock qualification standards such as MIL-DTL-901E for the prediction of potential failure in Shock Class A and B designated vital electronic equipment aboard ships subjected to potential shock induced damage resulting from a violent impulse loading such as an UNDEX.

In order to achieve this several key items need be determined in sufficient detail for the particular case of interest. A printed circuit board (PCB), common to many shipboard systems, is used as an example. In the case of a PCB, and its onboard components, there is a linkage that exists between the structural response of the ship, the equipment cabinet, card itself and all the related connections and transmission paths that deliver the shock from the detonation source through the water and on to the target. However, modeling this in enough detail, is in and of itself an extremely difficult task, as one might imagine, since every ship, even within a ship class, is constructed differently at the detailed level, and

inevitably its very characteristics change throughout the life of the ship due to normal use, modernization and repair.

To simplify the approach, we assume a common functional failure scheme for the critical element, wherein the board itself deflects and an exposed component makes contact with another in close proximity, causing an electrical short. This results in a failure to the system, which could be either permanent or temporary, or even lead to cascading failure effects system wide. Here in this scenario it is determined absent of influence from the physical location, specific structural properties and/or other variables beyond the local properties of the given PCB. Even still this is a complex problem with many unique characteristics and parameters. To generalize this further, we can take a simplified functional failure model as our surrogate, to use as a "test," (i.e., something that will clearly give a pass/fail condition). For instance, the contact of two offset cantilevered beams constrained by a spring at the tip and attached to the equipment case, which are free to respond to base acceleration input from an UNDEX represents this failure mode in this study.

1. Significance of Research

To date prescribed failure criteria do not exist, nor are mandated by shock qualification of shipboard equipment per the MIL-DTL-901-E. In accordance with the current procedures, qualification is tied to the confirmation of structural adequacy. This is accomplished via inspection and in some cases visual or instrumented verification of proper system function. An informative, comprehensive, easily deployable and cost-effective means of failure analysis and shock hardness validation remains a priority as the breadth of systems, equipment and components that fall within the authority of the guidelines is vast, and the inability to clearly determine shock hardness performance is undesirable.

2. Improving Shock Hardness in Shipboard Equipment

The existing requirement to physically test a fair number of systems and equipment in the shock qualification process affords the opportunity to gather and retain equipment specific data. The model is improved by measuring parameters such as base excitation with

an installed accelerometer during shock testing in order to reduce total ownership cost starting with the ship design phase. This is accomplished by reducing the uncertainty in the key parameter performance as related to shock hardness.

This may then be used to enhance the creation of engineering models for further shock assessment and evaluation of perspective designs, modifications to existing designs, or insight into the alternate placement of the equipment within the ship. One possibility is to refine the finite element method (FEM) model to more accurately represent the article being tested. Another is to ensure the test is accurately predicting the most critical response (acceleration, velocity, or displacement), or perhaps the combination of these. and others. These will then be used to determine the pass/fail criterion of the equipment being examined.

D. HYPOTHESIS

If you remove the uncertainty in failure assessment by leveraging M&S and targeted testing, you will be able to determine how well the equipment performed with respect to the given threshold and can compare it against the stated objectives, rather than merely grading it as a *pass* or *fail*.

1. Velocity and Change of Displacement Failure

By using current shock test loading and measuring critical component response during MIL-901E shock qualification of equipment we can more accurately predict equipment functional failure due to shock based on the combined criteria of maximum velocity response and change of displacement. Only in the case that both shock response parameters are exceeded is the equipment determined to have failed. Nominal values are assigned for both factors using reduced order modeling of equipment functional failure and realistic shock loading values.

2. Reduced Order Model Use for Failure Assessment

Depending on the complexity of the critical element in the shipboard equipment or system, simplified FEM models of the component can be used along with ship shock models in order to simulate various loading conditions and equipment configurations. If

detailed FEM models of the equipment are available, they may be reduced to a simplified state in which the basic functional failure can be observed. Equipment submitted for physical testing in the absence of a FEM model will require a simple model to be built. Rigid body models with springs, and simple multi degree of freedom MDOF models (mass-spring systems) are also candidates for reduced modelling as detailed FEM models of equipment tend to increase simulation run times due to discretely modeled elements of disproportionate size as compared to the larger structural elements found in ship shock models.

E. RESEARCH OVERVIEW

Unlike most engineering failure evaluations where the damage loading and failure mode is known and well characterized, there is an inherent uncertainty in the true loading that the equipment is subjected to during the broad scope of combat environment operations. Thus, using a "limit" or envelope that uniquely defines failure in all instances during the shock qualification of shipboard equipment is ambiguous at best. "Is it the maximum acceleration, velocity, displacement, their rate of change, the accumulated energies resulting from each or a combination of these results that inflicts the unacceptable level of damage in the form of material or functional failure to the shipboard system, equipment, or more precisely some critical component therein?" Good question, and that is why this must be examined further.

1. General Process

First, we review the existing ship shock hardening standards found in MIL-DTL-901E and other instructions that govern the shock qualification of shipboard equipment. From these we take the various types of testing approaches and methods available to "qualify" typical shipboard subsystems, equipment and components and select the most representative.

Next, we use a simple equipment case with overlapping asymmetric dual cantilevered beams, interconnected by a soft spring at the tip, as the surrogate test article for use in our M&S of the shock response investigation. The FEM model is run through

simulations of the typical loading that would be applied in the LSWM test, FSP test and sample shipboard installations using a full ship model.

From these simulations, acceleration, velocity and displacement response, in the primary (vertical) response direction, are obtained and analyzed. Functional failure of the cantilevered beam subsystem is characterized by contact of the beam tips, or near contact (within 1 cm). Similarly, equivalent single degree of freedom (SDOF) spring-mass systems are substituted for the detailed box model in each case and compared with the results.

Having verified the similar response between the top of the equipment case and its simplified SDOF spring mass system, the spring-mass systems are placed throughout the detailed FEM model of the ship and subjected to a wide array of shock inducing events with selected parameters to exercise various features of the UNDEX phenomena (near field, far field, small weight, large weight, whipping, global, local loads, etc.)

We do not know where the equipment will eventually be located. But if we have a FEM model of the ship and would like to place the equipment in a certain location, then we can check that equipment location to see if it will *pass* or *fail*. What this does is bridge the gap of uncertainty in shock qualification by bringing realistic threat weapon loading to equipment placed at an actual shipboard location to verify equipment shock hardness of existing equipment, influence placement of proposed equipment or provide design input for new equipment. Use of these criteria then would alleviate the need for physical testing matching combat threat levels.

2. Potential Results

It is anticipated that this work will result in the ability to use a reduced order model as a representative means of showing the functional failure region where critical components of shipboard equipment will not pass current shock qualification standards based on standard shock test methods. Based on this information potential redesign, isolation, or relocation of the item being investigated can be recommended in order to further verify shock hardening of the ship in which the equipment will be utilized.

THIS PAGE INTENTIONALLY LEFT BLANK

II. BACKGROUND

In order to fully grasp the complexity of the underwater explosion problem space we must first understand the environment of the shock event that loads the equipment from the water through the ship hull and its structure, ultimately initiating the system response at the attachment point. Next, we must investigate the concept of failure, how and when it occurs once responding to the base acceleration input. And finally, we must review the current practice for shock hardening and shipboard equipment validation so as to provide a reference for the new approach to failure determination that is researched within the study.

A. UNDEX PHENOMENA

The UNDEX environment is a very complex space. This section aims to provide a cursory overview of the type of loading mechanisms associated with non-contact, chemical explosions common to naval undersea warfare.

1. Problem Space

The underwater domain is complicated. Figure 9 illustrates the complexity well. When a high explosive is detonated in this region, many phenomena occur during this brief yet devastating energetic event. There are dominate features such as the direct shock wave (incident pressure wave) between the source (charge) and the target, and surface reflection or rarefaction waves which occur at the air water interface. Some are strictly dependent on the UNDEX scenario, such as the bottom reflected waves that either direct reflections back toward the surface or headwaves that travel through the ocean bottom medium and then retransmit to the water at a distance from the impact point. Additionally, a large bulk cavitation zone, local cavitation, vertical plume, jetting, spray dome, gas globe or bubble oscillation and reloading, bulk cavitation closure (zipper) pulse are all present to varying degrees as a function of charge type, weight and detonation depth.

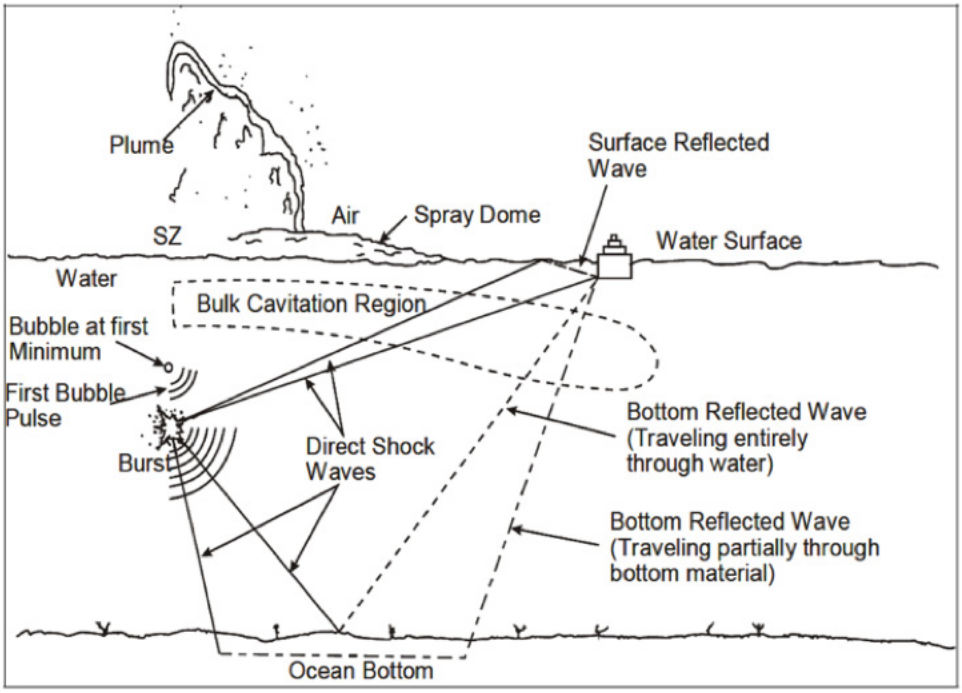

Figure 9. Underwater Shock Phenomena. Source: [30].

In determining the severity of an UNDEX it is necessary to account for the various underwater explosion phenomena that are occurring beneath the surface. First, there is the incident shock wave front in the form of a compressive pressure wave that acts directly against the hull of the ship. There is also a surface reflection or rarefaction wave, which is tensile in nature which causes the formation of a bulk cavitation zone. Within this region the tug and pull of upward momentum of the shock front, hydrostatic pressure and gravity, results in the water layer's separation or spallation of the fluid particles, due to the fluid's inability to maintain more than a couple of pounds per square inch (psi) of tensile pressure.

Beyond the initial shock front, there is the gas bubble that is formed by the lingering explosion products that have nowhere to go once the chemical reaction has occurred. These gases expand radially outward from the point source and grow until the hydrostatic pressure overcomes the outbound force and drives them to collapse, causing a secondary explosion due to the compression of non-expended explosive materials remaining in the bubble.

There can also be a bottom, side or other reflected compressive waves that form due to the geometry of the problem environment. Shallow sea bottoms, restricted

navigation channels and other boundaries result in additional pressure loading on a structure in close proximity. Figure 10 illustrates the pressure propagation direction.

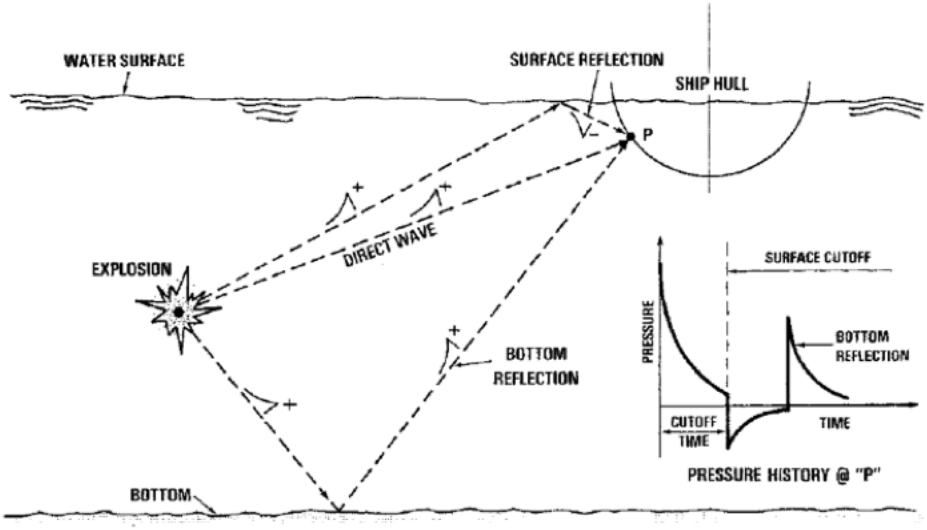

Figure 10. Shockwave Propagation and Reflections. Source: [30].

The governing equations [71] that describe the interactions of the shockwave front, the seabed and surface which follow are collectively known as the Similitude Equations for Underwater Shockwave Performance. The maximum pressure at the shock front, P_{max}, given in Equation 2.1, is dependent on the charge weight, W, radial standoff distance, R, and charge type specific coefficients and exponents developed from empirical data [72].

$$P_{\max} = k_p \left(\frac{W^{1/3}}{R} \right)^{\alpha_p} \tag{2.1}$$

Using the charge weight, and standoff distance again, with previously determined coefficient and exponentials [71], the time (decay) constant, θ, is calculated via Equation 2.2.

$$\theta = k_\theta W^{1/3} \left(\frac{W^{1/3}}{R} \right)^{\alpha_\theta} \tag{2.2}$$

The impulse is then determined via Equation 2.3.

$$I = k_I W^{1/3} \left(\frac{W^{1/3}}{R} \right)^{\alpha_I} \tag{2.3}$$

And the Energy, E, is found by Equation 2.4, again using charge type specific values.

$$E = k_E W^{1/3} \left(\frac{W^{1/3}}{R} \right)^{\alpha_E} \tag{2.4}$$

where

W = Charge Weight (lb)
R = Slant Range (ft)
k_i = Similitude Coefficient
α_i = Similitude Exponent

Additionally, empirical equations describe the characteristics of the formation and oscillation of the UNDEX produced bubble. The first bubble period is calculated using Equation 2.5.

$$T_1 = K \left(\frac{W^{1/3}}{Z^{5/6}} \right) \cdot \left(1 - 0.1 \frac{A_{\max}}{D} \right) \tag{2.5}$$

The last term in the bubble period equation is the free-surface correction for shallow water detonations. The maximum bubble radius, A_{max}, is given as Equation 2.6.

$$A_{\max} = J \left(\frac{W}{Z} \right)^{1/3} \tag{2.6}$$

where

D = Charge Depth (ft)
W = Charge Weight (lb)
Z = Hyrdrostatic Head (ft)
J = Bubble Radius Coefficient
K = Bubble Period Coefficient

2. Types of Shock Loading

There are many types of shock loading that can be experienced onboard ship. Some of these excitations are naturally occurring such as the slamming of a ship's bow through the crest of a wave while others are imposed through forced mechanical motions resulting from chemical generated explosions as in the case of a mine strike. To help understand the types of loading occurring on the ship hull and consequently to the internal structure, equipment and finally transmitted to the critical components, one can refer to Table 3, taken from Naval Shock Analysis and Design [73] which provides several common examples of shock loading.

It is important to note that there are multiple components to the force that is experienced by a body moved from its equilibrium position, whether static or dynamic in nature, such as in the case of a rolling ship impacted by sea waves. For example, using an event that may be familiar, Table 3 illustrates that an ordinary aircraft takeoff may result in 0.5 g force and have a duration of 10–40 seconds, while a catapult assisted take off from an aircraft carrier may come closer to 6 g in only a 10^{th} of that time. An underwater explosion from a non-contact mine or near miss, can deliver 40–2000 g on the order of 0.1 seconds, or merely a 10^{th} the time of the catapult launch [73].

Table 3. Approximate Duration and Magnitude of Some Short-Duration Acceleration Loads. Source: [73].

Type of operation	Acceleration, g	Duration, sec
Elevators:		
Average in "fast service"	0.1–0.2	1–5
Comfort limit	0.3	
Emergency deceleration	2.5	
Public transit:		
Normal acceleration and deceleration	0.1–0.2	5
Emergency stop braking from 70 mph	0.4	2.5
Automobiles:		
Comfortable stop	0.25	5–8
Very undesirable	0.45	3–5
Maximum obtainable	0.7	3
Crash (potentially survivable)	20–100	<0.1
Aircraft:		
Ordinary take-off	0.5	>10
Catapult take-off	2.5–6	1.5
Crash landing (potentially survivable)	20–100	
Seat ejection	10–15	0.25
Man:		
Parachute opening, 40,000 ft	33	0.2–0.5
6,000 ft	8.5	0.5
Parachute landing	3–4	0.1–0.2
Fall into fireman's net	20	0.1
Approximate survival limit with well-distributed forces (fall into deep snow bank)	200	0.015–0.03
Head:		
Adult head falling from 6 ft onto hard surface	250	0.007
Voluntarily tolerated impact with protective headgear	18–23	0.02

The input signal or loading may also be characterized by its shape or form. Several signals may have the same peak acceleration, or impulse yet excite the object of interest in a completely different manner resulting in varied responses to the shock loading. Figure 11 contains various examples of acceleration time histories and their corresponding Fourier amplitude and phase spectra. Of these, the last one, labeled as (e) and named "complex" is most representative of typical ship shock loading.

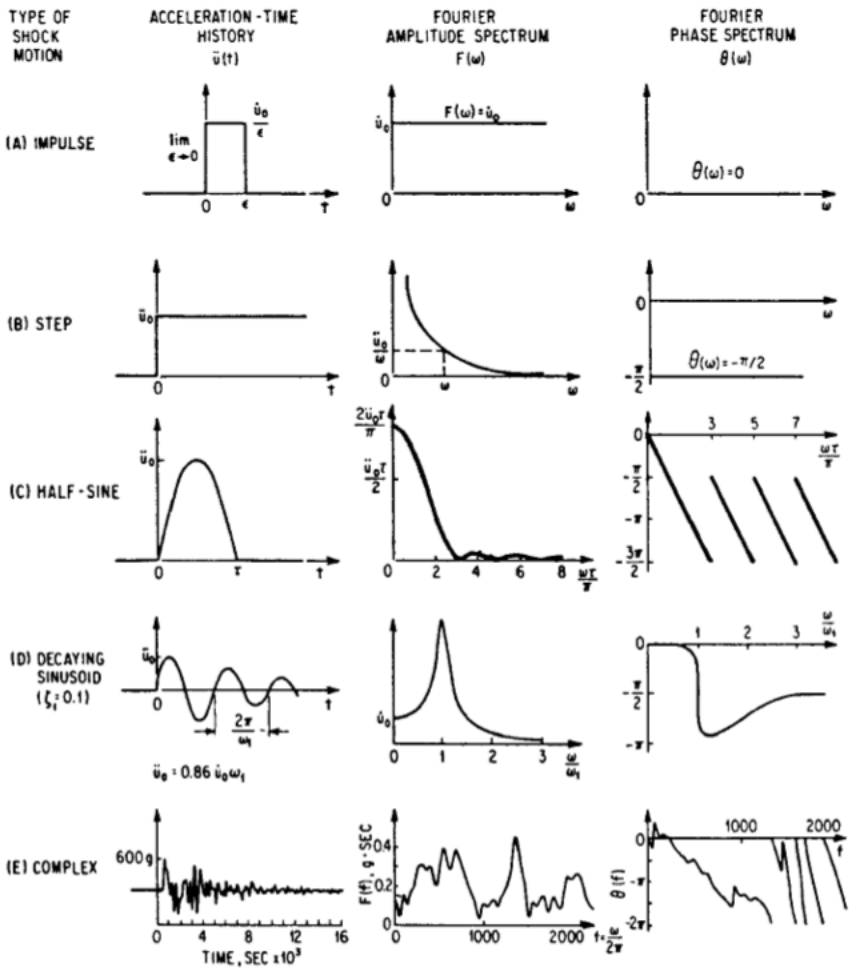

Figure 11. Examples of Shock Acceleration Time-History, Fourier Amplitude and Phase Spectra. Source: [11].

a. Incident Loading

In UNDEX there is a uniqueness in the response motion, somewhat independent of the location of the source. Base acceleration is typically the governing forcing input to the system, and its corresponding response motion is vertical velocity, predominately upward, perpendicular to the air-water interface, and greater in magnitude than other directions. This is best explained via an example. In Figure 12 the peak vertical velocity response (green) is approximately 5.7 m/s, while the athwartship response (blue) is 1.7 m/s and the fore and aft response (red) is approximately 0.25 m/s. The secondary (lateral) response is on the order of 1/3 the vertical response and the tertiary (axial) response is usually

negligible. Thus, the investigation will center primarily on the vertical velocity response motion.

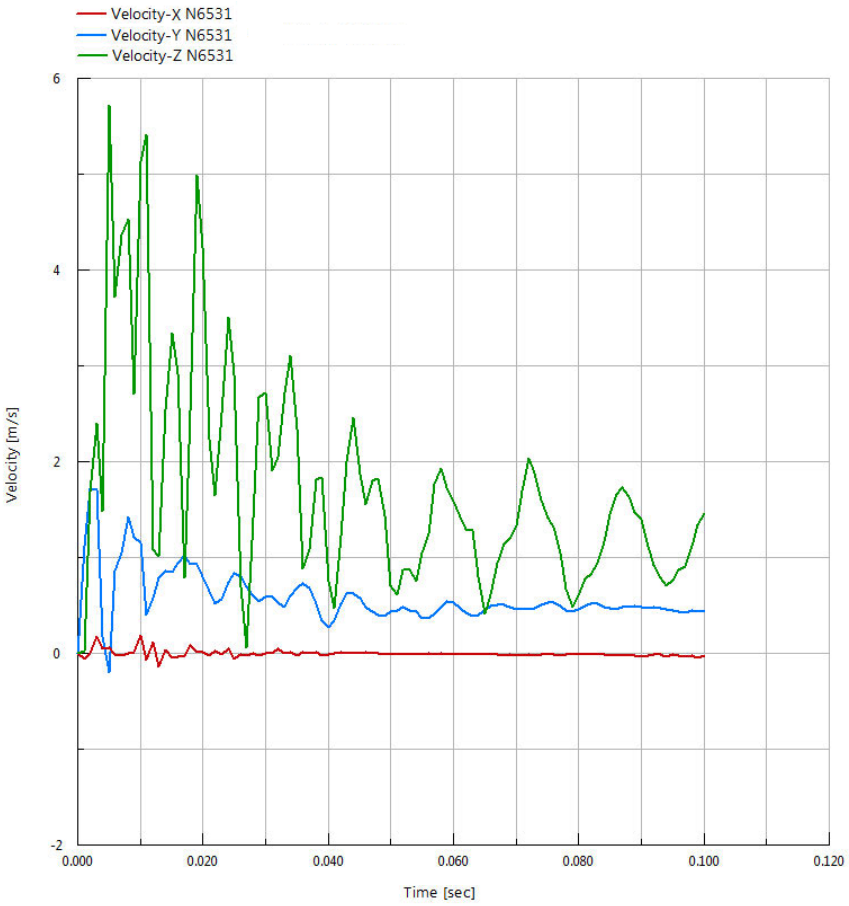

Figure 12. Relative Magnitudes of Typical UNDEX Velocity Response per Direction Axis

b. Bulk Cavitation Zone

It is appropriate to note that these phenomena occurring in the underwater explosion event scenario are not fixed in time and influence the overall response differently throughout the transient and into the steady state response phases. These are dynamic events and thus the ultimate shock severity which is of most interest to engineers and ship designers, is dependent on various characteristics that fall into one of the three following

categories: a) the explosive charge, b) the fluid domain boundaries, and c) target location, in addition to time.

The primary characteristics of the explosive charge, such as the charge weight, depth and explosive type, are used to determine maximum pressure, decay constant, bubble radius, and bubble oscillation frequency, as a function of time through the aforementioned similitude equations, which were based on empirical test data. All have a direct impact on the resulting size of the bulk cavitation zone, which opens and closes quickly after the shock front passes.

The following series of figures, Figures 13–15, were generated using Equations 2.41 through 2.44. These plots illustrate the dramatic change that seemingly minor changes in depth, charge size and even charge type have on the maximum radius of the bulk cavitation zone.

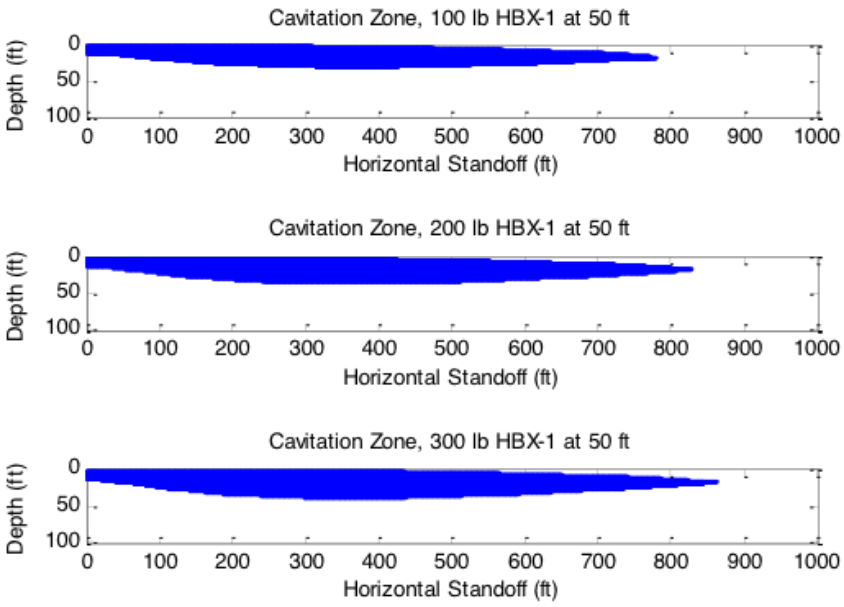

Figure 13. Bulk Cavitation Zone at Constant Depth with Varying Charge Weights

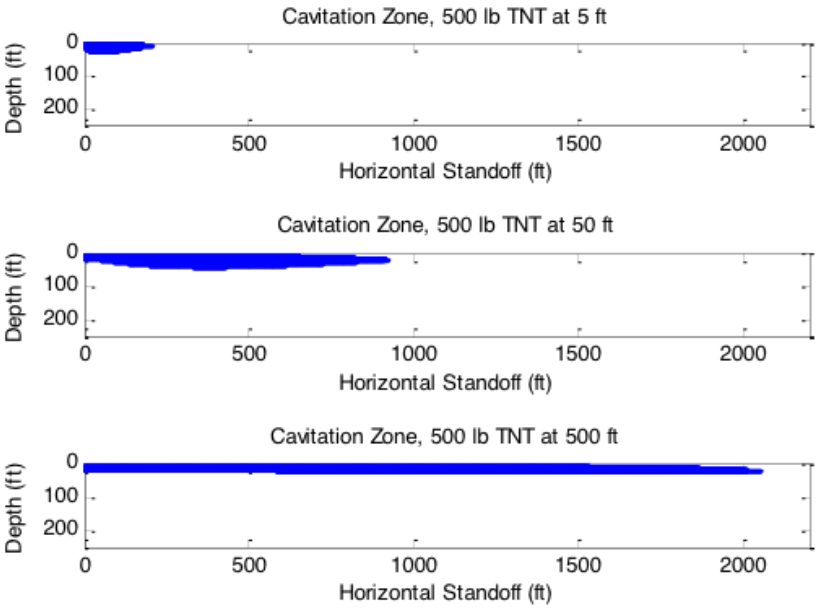

Figure 14. Bulk Cavitation Zone with Constant Charge Weight at Varying Charge Depths

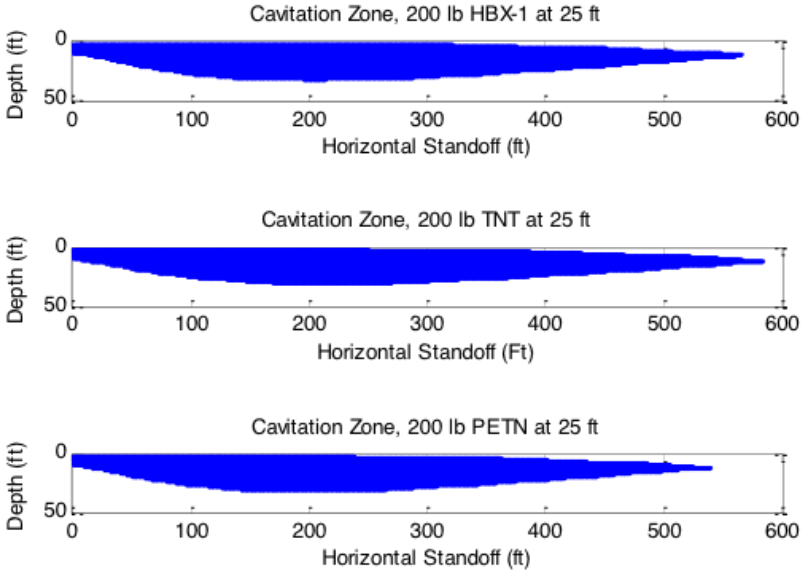

Figure 15. Bulk Cavitation Zone at Constant Charge Weight and Depth with Varying Explosive Type

It should be noted that in the preceding figures, the maximum extent of the bulk cavitation zone was plotted. In reality, the region expands and contracts during the shock event. The cross-sectional area of this region can be described by calculating the upper and lower boundaries of the bulk cavitation zone [30], *F(x,y)* and *G(x,y)*, as depicted in Figure 16.

The equations are described here in a 2D space by the functions

$$F(x,y) = K_1\left(\frac{W^{1/3}}{r_1}\right)^{\alpha_1} e^{-\frac{(r_2-r_1)}{C\theta}} + P_{atm} + \gamma y - K_1\left(\frac{W^{1/3}}{r_2}\right)^{\alpha_1} = 0 \tag{2.7}$$

where

$$r_1 = \sqrt{(D-y)^2 + x^2} \tag{2.8}$$

and

$$r_2 = \sqrt{(D+y)^2 + x^2} \tag{2.9}$$

while

$$G(x,y) = -\frac{P_i}{C\theta}\left\{1 + \left[\frac{r_2 - 2D\left(\frac{D+y}{r_2}\right)}{r_1}\right]\left[\frac{A_2 r_2}{r_1} - A_2 - 1\right]\right\} - \frac{A_1 P_i}{r_1^2}\left[r_2 - 2D\left(\frac{D+y}{r_2}\right)\right] + \gamma\left(\frac{D+y}{r_2}\right) + \frac{A_1}{r_2}\left(P_i + P_{atm} + \gamma y\right) = 0 \tag{2.10}$$

The parameter inputs for Equations 2.7–Equation 2.10 are:

(x, y) = horizontal range and vertical depth of a point

r_1 = standoff distance from the charge to the point

r_2 = standoff distance from the image charge to the point

C = acoustic velocity in water

W = charge weight

D = charge depth

θ = decay constant

P_{atm} = atmospheric pressure

P_i = incident pressure

γ = weight density of water

K_1, A_1, K_2, A_2 = shockwave parameters, specific to explosive type

F(x,y) and *G(x,y)*, are found via the method of images [74], however these slices of the cavitated fluid cross section are found to be uniform about the centerline of the charge and form the full 3D toroid shape of the bulk cavitation zone when spun about the vertical axis. The duration, rate of opening and closure pressure are all determined based on the instantaneous velocities of the upper and lower boundaries and the geometries of the bulk cavitation zone as previously detailed [75].

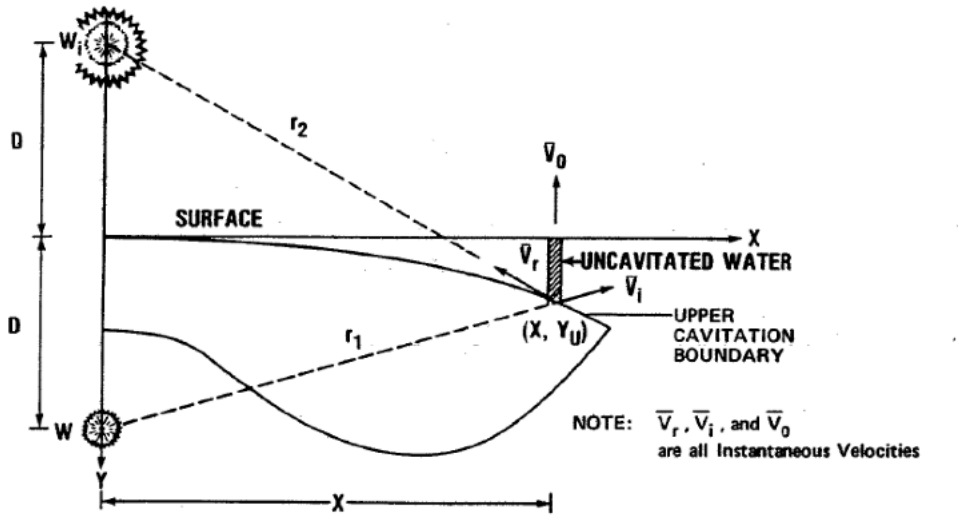

Figure 16. Cavitation Zone Boundaries. Source: [30].

c. Bottom Reflection

Figure 17 brings in another of the factors in play during the undersea explosion. The proximity of the charge to the surface and the target, affect the pressure propagation, which is fully described by hydrodynamics [77] and the empirically developed underwater shock formulae [71] presented earlier in this section.

However, it is sometimes the case that the sea bottom is present as the lower boundary, while the sides are modeled as infinite or free boundaries, where no reflection is expected. Inspecting Figure 17, we find that the target is the FSP floating at the surface jut right of center in this cross section of the fluid-structure domain, while the bulk cavitation zone is represented as the white area. The curved black dotted line represents the advancing shockwave reflection. The sea bottom is modeled here as semi permeable solid elements.

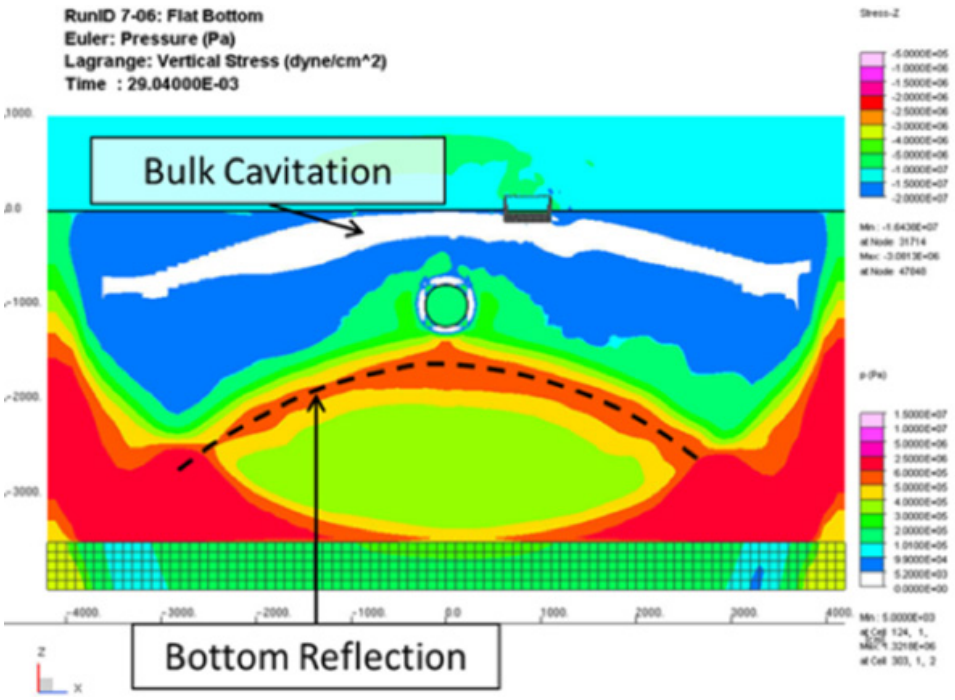

Figure 17. Sea Bottom Reflection of Shockwave. Source: [76].

Due to the shallow nature of the sea bottom, the reflected pulse results in additional pressure loading in quick succession after the initial pressure front loading on the target. The magnitude of the reflected compression wave is also relatively high as compared to

the initial pulse. This is due to the reflective nature of the semi rigid sea bottom. If the bottom were solid, dense and rigid, the pressure at the interface boundary would become twice the pressure with respect to time; approximating a fully reflective structure. A softer bottom such as sand, or a deeper bottom would both reduce the reflected wave magnitude and drive it further away from the initial pulse in time as both are governed by the equation

$$P(t) = P_{\max} e^{-\frac{t-t_1}{\theta}} \tag{2.11}$$

where $P_{\max}$ and θ are previously defined as Equations 2.1 and Equation 2.2.

The effects of different bottom surfaces are observed in Figure 18. Contoured bottom, shallow water effects can focus or scatter bottom reflections and impact bubble pulse period and timing. The distinct type of ocean bottom (shape and material) influences the pressure loading on the target while also delaying the bubble pulse.

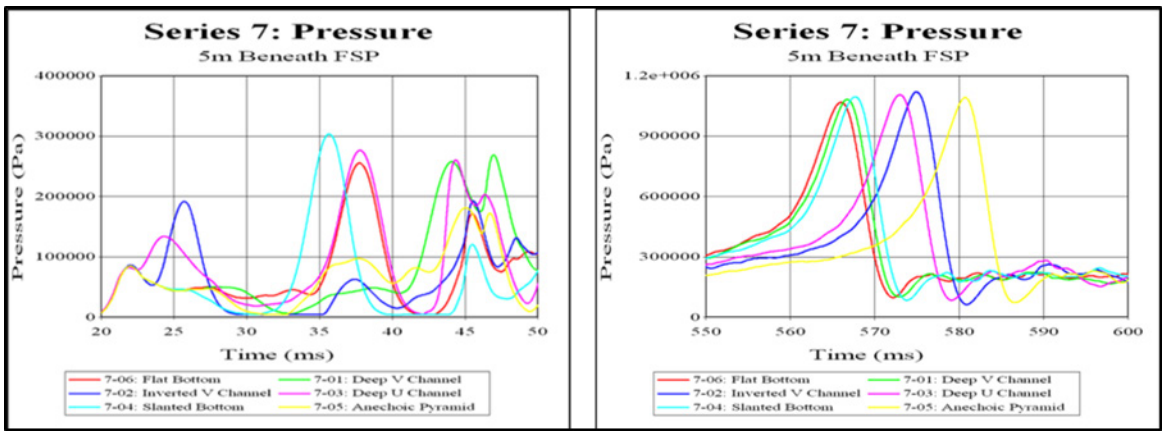

a) Variance in Pressure Loading, b) Delay in Bubble Pulse.

Figure 18. Comparison of Pressure Data for Various Ocean Bottom Models. Source: [78].

After the shock pressure front has expanded radially outward from the detonation point, a highly compressed, superheated gaseous bubble forms [79]. This globe expands outward until the internal pressure is less than the hydrostatic pressure of the surrounding water. Growing to a maximum radius that is greater than the actual equilibrium point, due

to momentum, the bubble rapidly implodes upon itself and provides a “reloading” pulse, and again begins to re-expand. This cycle continues until all the oxygen and remaining combustible materials have been expended within the bubble or when it breaches the surface and freely vents. Figure 19 illustrates this gas bubble oscillation and the migration path towards the surface which accompanies this process.

All of the various types of loading associated with UNDEX are presented by Ilamni [80] as a summary of pressure time histories and associated fringe pressure plots in Figure 20. It is indeed a complex loading process with multiple inputs both in the early time transient phase and late time steady state response periods.

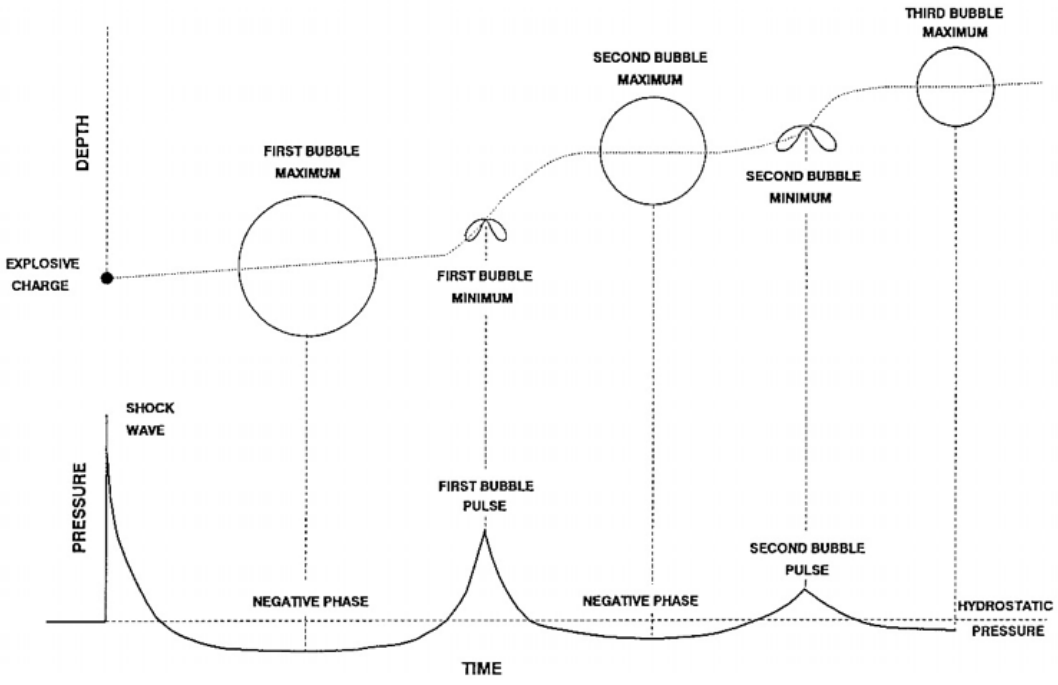

Figure 19. Bubble Migration and Pulse Cycle. Source: [79].

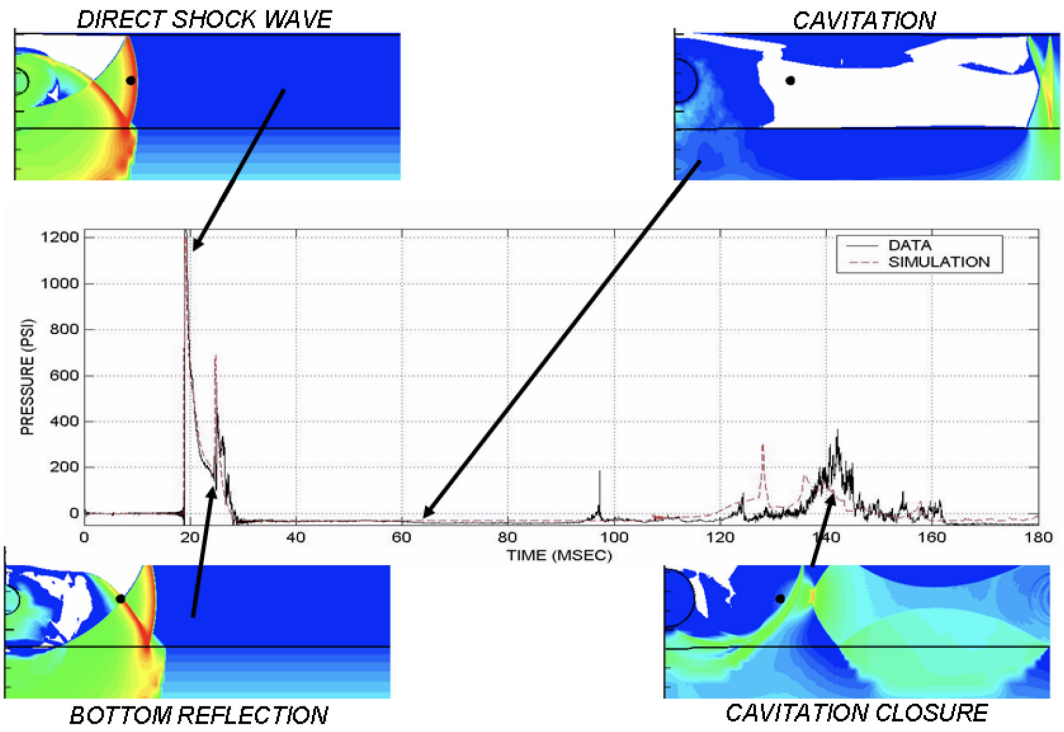

Figure 20. Various Elements of UNDEX Loading. Source: [80].

B. EQUIPMENT FAILURE

Having described the UNDEX phenomena and loading mechanism that the shipboard equipment will be excited by, we turn our attention to explaining equipment failure.

System, equipment or component failure can broadly be described as the item's inability to perform the task, function or service it was intended by the original design. Herein the assumptions are such that this failure is initiated by an UNDEX shock event and that the critical item is related to shipboard equipment meant for service on a naval surface combatant. Figure 21 illustrates the author's concept of what failure may mean in general within the context of shock loading. The ordinate describes the energy input into the equipment system that cannot be relieved by the system and its shock response, while the abscissa dictates the duration or quantity of this excitation condition with respect to some physical failure mechanism based on material properties such as yield limit of the critical component.

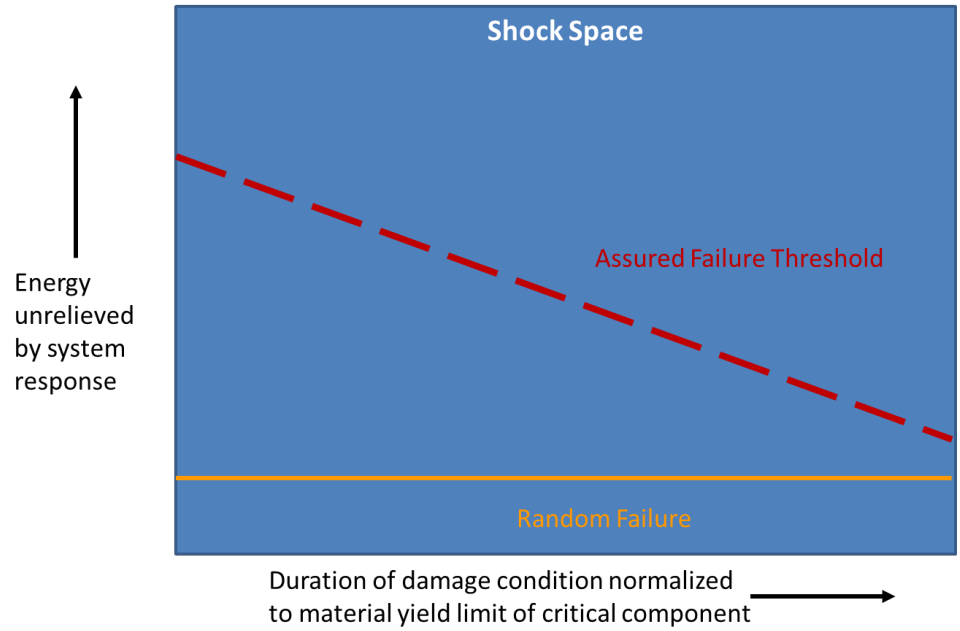

Figure 21. A Concept of Failure in the Shock Domain

Failure mode effect and analysis (FMEA) [81] and the related failure mode effect and criticality analysis (FMECA) [82], an extension of FMEA, were developed because of the military's need to better understand failure in mission critical items and seek improved design practices to ensure robust, reliable, resilient hardware for combat use. The FMEA approach separates failure modes, defined as the general manner in which the function of an items fails and failure mechanism or the actual cause for the failure. An example of this may be that a transmitted signal is weak or intermittent instead of steady due to built-up corrosion on the terminal contacts of the sending unit which are exposed to the salt air. The ultimate failure effect, and hence the immediate consequence, is that the system does not send the correct signal; failing to operate correctly thus degrades the mission performance. When examining these failures, the probability, severity, and detection must also be considered. One limitation of this approach is that only one failure mode is considered at a time, and all other inputs are held constant and in their nominal conditions [83].

1. When Does the Expected Failure Occur?

In normal products or systems there is a typical equipment failure model as displayed in Figure 22. In terms of ship construction and life cycle, the initial time frame

relates to failures occurring in the "post launch" phase where errors or issues are uncovered primarily through "live" testing and subsequent operation of equipment. The end time frame is characterized by failures later in time and increase due to fatigue, material property deterioration, yield due to applied stress, etc. Goodman and other established criteria address this, though only in terms of material failure (stress), as depicted in Figure 23.

However, the true area of interest lays in the middle region where unknown failures and predicted failures due to normal use are relatively low and chance encounters with shock events, in this case, need to be planned for and their performance verified well before that "debugging phase" commences.

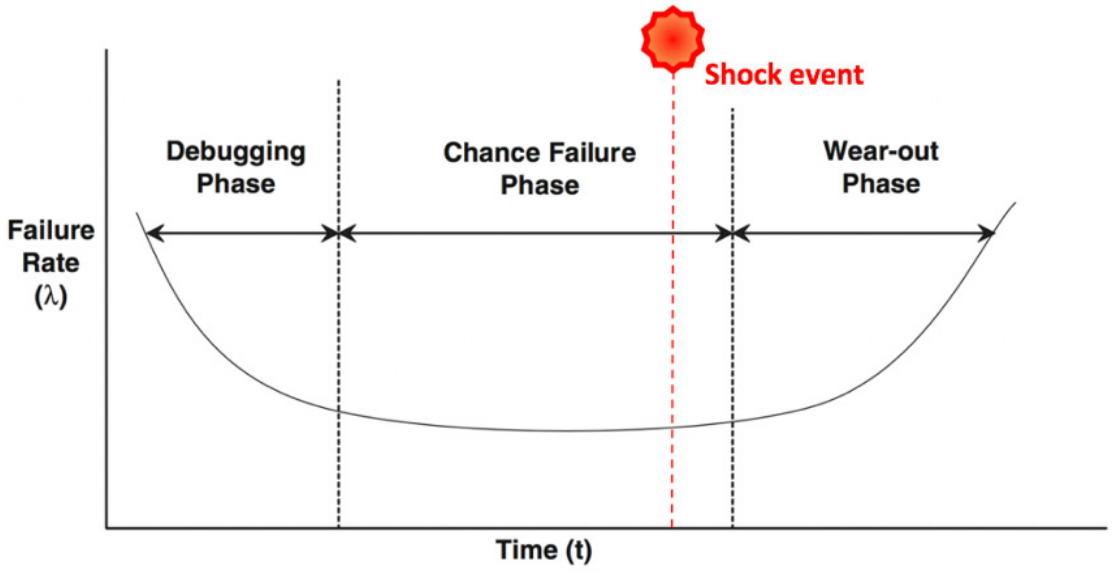

Figure 22. Generic Bathtub Failure Curve. Source: Adapted from [84].

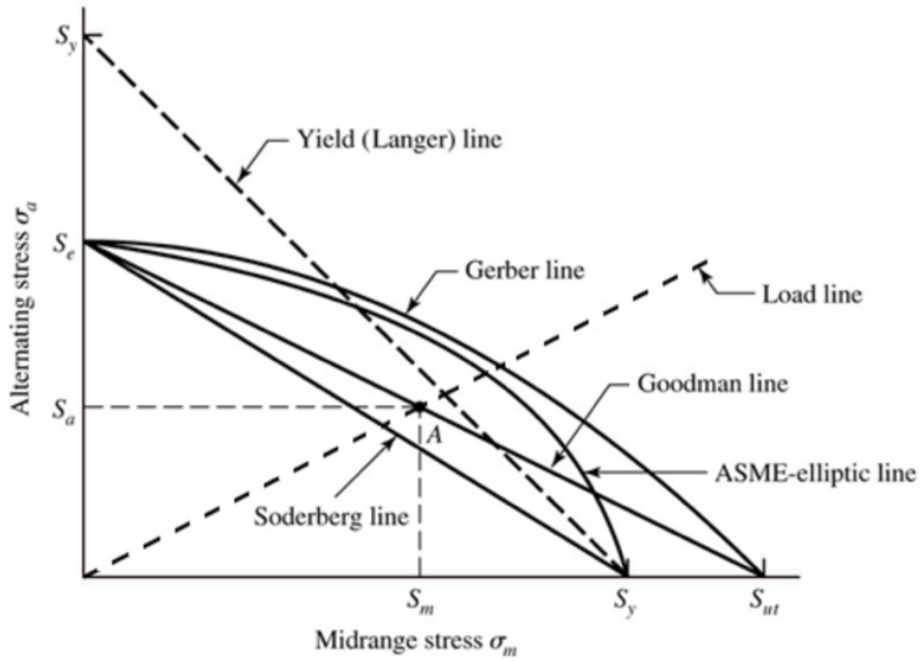

Figure 23. Summary of Fatigue Failure Resulting from Varying Loads. Source: [85].

The problem here is that peak loads on the equipment are not static, that is to say that load amplitudes are varying with time. As displayed in Figure 20, load fluctuates with time during a shock event. Even prior to the shock event, vibrations experienced during normal operations at sea are constantly loading and unloading equipment [86], which requires a primary examination such as that expressed in Figure 23.

The type of excitation is also important to consider. Global motions that are moving the main hull girder and main deck structure are typically at a much lower frequency, and act as mainly sinusoidal carrier waves, while the local random loading result in excitation to equipment and systems at all frequencies and over a wide range of amplitudes. Rigid body modes of response are also present [73]. Hence, finding a convenient means to measure the point at which the component "breaks" is daunting with so many design considerations and operational factors. Furthermore, as shown in Figure 22, whereas most components enjoy a long mid-life with relatively lower concern for failure, less the chance encounter, this is the very condition that shock hardening of equipment looks to mitigate; an extreme event.

2. What Does It Mean to Fail?

If we take our example of a PCB and some critical component on the board which is necessary for the proper functionality of a much larger system, we can determine the failure of that system through a traditional failure analysis approach. Steinberg gives a very detailed account in his book of electronic failures [87]. The different means are summarized here as failures are due to (1) high stress, (2) high acceleration, (3) high displacement, (4) electrical malfunction. His survey of damage models & associated criterion is reproduced here [61]:

a. Displacement

$$Y = Y_o \sin \Omega t \tag{2.12}$$

b. Velocity

$$V = \frac{dY}{dt} = -\Omega Y_o \cos \Omega t \tag{2.13}$$

c. Acceleration

$$A = \frac{d^2Y}{dt^2} = -\Omega^2 Y_o \sin \Omega t \tag{2.14}$$

d. Maximum Acceleration

$$A_{\max} = \Omega^2 Y_o \tag{2.15}$$

e. Maximum Acceleration (gravity unit)

$$G = \frac{A_{\max}}{g} = \frac{\Omega^2 Y_o}{g} = \frac{\left(2\pi f\right)^2 Y_o}{g}$$
$$G = \frac{\left(2\pi f\right)^2 Y_o}{9.8}, \text{where } Y_o \text{ is given in meters.} \tag{2.16}$$

f. Transmissibility

$$Q = \frac{F_{out}}{F_{in}} \tag{2.17}$$

g. Velocity Shock

$$\frac{1}{2}KY^2 = \frac{1}{2}MV^2 \rightarrow Y = \sqrt{\frac{M}{K}}V \tag{2.18}$$

From Equation 2.15, the maximum acceleration can then be found as

$$A_{\max} = Y\Omega^2 = Y\frac{K}{M} \tag{2.19}$$

and this result makes the gravity unit maximum acceleration

$$G_{\max} = \frac{A_{\max}}{g} = \frac{Y}{g}\frac{K}{M} = \frac{V}{g}\sqrt{\frac{K}{M}} = \frac{V\Omega}{g} \tag{2.20}$$

Of these, the final type, velocity shock, which is not a new concept in shipboard equipment shock validation, is best suited for the broader scope outside of just electronics. As early as the 1960s Gaberson and Chalmers [88] pointed to the concept of pseudo velocity and an absolute limit of 508 cm/s (200 in/s) as the failure threshold. However, these authors also conjectured the need for shape of the impulse or loading signal as a disqualifier for such a definite value.

3. When Has It Failed?

Perhaps the correct question to ask is, what does the word failure actually imply? Material, functional? Momentary, temporary, permanent? Several broad categories that characterize engineering failure are material failure, fatigue or corrosion, manufacturing error and unexpected circumstances. Discarding the errors in manufacturing and process, we look toward material failures and functional failures as the focus.

a. Material Failure

Material failure deals with traditional insufficiency of strength, change in form, etc. Common mechanical failure mechanisms are: fracture, ductile failure, elastic deformation, creep, fatigue, impact, spalling, wear, brinelling, thermal shock, radiation damage and corrosion [89–91].

Classical approaches to establishing a failure criterion are typically linked to material failure. By setting a boundary limit, let's say a maximum stress equal to a prescribed value, and designing in a safety factor to ensure that largest expected stress will not exceed that limit in the specified operational environment, one can definitively evaluate performance of the equipment against a standard. Detection may be by visual cue, or precise measurement, but either way it is deterministic, within some small error band.

b. Functional Failure

More recently, U.S. Navy vessels subjected to shock environments, whether during testing, trials or combat, have experienced failures less so related to the material failures in strength, yield, stress or, deformation and have tended to succumb to greater numbers of functional failures. Ships becoming less prone to unknown material failures is an encouraging sign that significant portions of the shock qualification approach are indeed improving overall shock hardening of ship systems. Yet there are no shortage of functional failures occurring in these same events.

Typical FMEA failure conditions outlined by the MIL-DTL-1629 [82] are stated as:

- Premature operation
- Failure to operate at a prescribed time
- Intermittent operation
- Failure to cease operation at a prescribe time
- Loss of output or failure during operation
- Degraded output or operational capability
- Other unique failure conditions, as applicable based upon given characteristic and operational requirements or constraints.

With regard to functional failure, first the function that will fail must be identified; second, the correct representation of the predetermined critical failure must be achieved; third, there must be a quantitative means by which to measure the failure; and lastly, the

functional failure must be consistent and repeatable given similar operating conditions, material property characteristics and loading environments.

c. Other Failures Types

Process failures fall into this category. Outlined in FMEA, process failures result from the wrong operation or use, which was not intended by the original design, or when another operational factor or processes have altered the environment in which the item of interest is used. In terms of this study, these failures are not of immediate interest.

4. What Does Acceptance Imply?

Failure criteria is one way of looking at the item while acceptance criterion is another. This could be as simple as a visual inspection, observing that nothing appears to have broken. A step further would be to add the condition that the intended function is still able to be performed. It is presumed that a quantitative measure is the best approach to providing an accurate assessment of performance under specified conditions. And that this would then provide a well-informed acceptance recommendation upon completion of the evaluation.

For example, in the testing of electrical equipment, IEC 60068-2 “Electrical Equipment and Product Standards,” which was developed by the International Electrotechnical Commission (IEC) [92] is commonly used to assess the products ability to perform and survive under conditions such as transportation, storage, and various operational environments. In particular IEC 60068-2-27 [93] relates to shock while IEC 60068-2-6 relates to vibrations [94]. Figure 24 shows several commercial and military standards for shock.

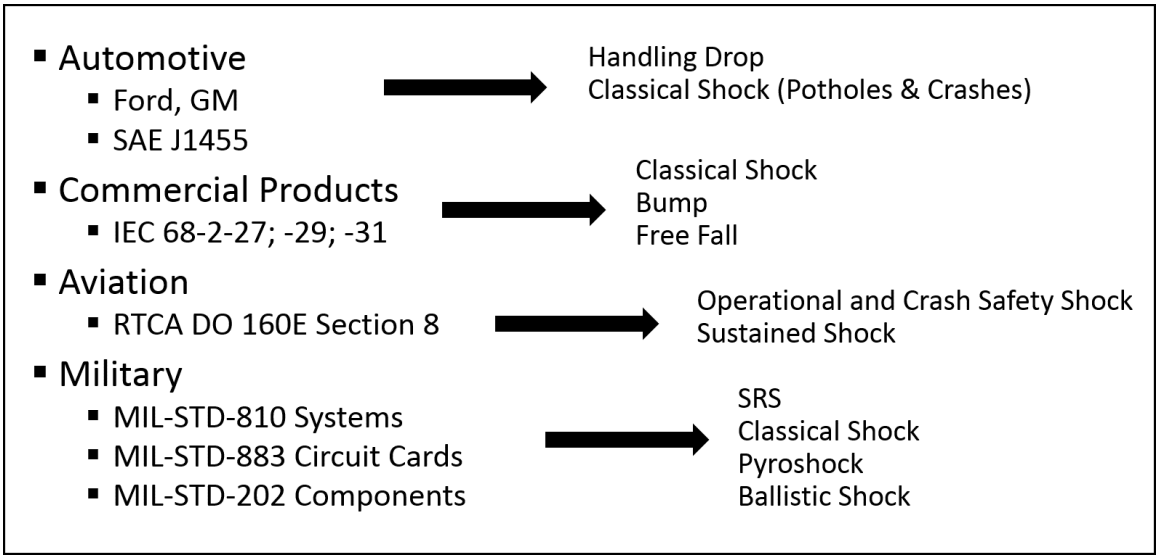

Figure 24. List of Various Shock Standards

a. Acceptance Criteria

So, when is the equipment considered shock qualified and accepted for use in the field? A specification for environmental conditions and test ETSI EN 300 019–2-4 V2.5.1 (2018-07) [95], can be used as an example for telecommunications equipment testing. There are many tests called out as required for this equipment. Temperature cycling, corrosion resistance, vibration, earthquake resistance and other tests may be required dependent on the application and installation of the equipment. The IEC standards and others are the basis for performing these tests. This document then specifies the desirable outcome using a performance criterion set such as the one quoted here for earthquake testing per IEC 60068-2-57 [96] and shown in Table 4.

Performance criterion C:

> The equipment shall function according to the manufacturer specifications before and after the tests. No degradation of performance or loss of function is allowed below the performance level specified by the manufacturer when the apparatus is used as intended. If the minimum performance level is not specified by the manufacturer, then this may be deduced from the product description and documentation and what the user may reasonably expect from the apparatus if used as intended.

During the application of the test, temporary loss of function is allowed but after the test the equipment shall restore to the normal functionality without replacement of components, manual rebooting or human intervention. The equipment shall sustain the test without permanent structural or mechanical damage.

Table 4. Testing Specifications for Earthquake Test. Source: [96].

Environmental parameter			Environmental Class 4.X	Environmental test specification T 4.X: Earthquake test					
Type	**Parameter**	**Detail parameter**	**Characteristic severity**	**Test severity**	**Duration**	**Reference**	**Method**	**Performance criterion**	**Notes**
Earthquake	Time-history	RRS	Fig.1, tab.7	Fig.1, tab.7		IEC 60068-2-57 [13]	Ff: time-history method	C	(see note)
		Frequency range (Hz)	0,3 - 50	1 - 35					
		ZPA (m/s^2)	5	5					
		Axes		3	30 s				
		Damping ratio (%)		2					
NOTE: (Earthquake). Time history signal Verteq II specified in ATIS T1.0600329 [5] shall be used. RRS (Required Response Spectrum). ZPA (Zero Period Acceleration). The equipment under test mounted in the "in use" position. The testing configuration shall be worst case in terms of weight and stiffness. The influence of connections, piping, cables, etc. shall be taken into account when mounting the specimen. The normal "in service" mounting structure of the specimen shall be included in the test. Single-axis excitation shall be used; simultaneous multi-axis excitation is also acceptable, but it is not recommended since, in general, multi-axis testing gives less reproducible test results. The three testing axes can be reduced to two horizontal axes if the equipment, after the vibration response investigation in the vertical axis, does not exhibit any resonance below 20 Hz. The strong part of the time-history should be at least 15 s. The duration of each time-history signal shall be 30 s. One time-history shall be applied along each axis.									

What the reader is asked to notice is the vagueness in the actual specification. The prescribed loading is given in the details of Table 4, yet the criterion for system performance is left without a measurable specification, value or way to determine failure.

b. Design Spectra

An additional approach to ensuring that the equipment will pass shock qualification standards is through use of a shock design spectra. Commonly referred to as “envelopes,” these tools prescribe a limiting displacement in the low frequency range, a constant maximum velocity in the mid frequency range and a limiting acceleration region in the upper frequency range. In the example provided in Figure 25 for the FSP, the velocity shock region, which is relatively flat in the 10–80 Hz, gives a spectrum similar to MWSM motion [73]. The vertical, athwartship and fore and aft response directions all have their own spectra which follow a similar pattern to the typical input in Figure 12. Since these guides were based on the deck loading of the FSP under standard MIL-S-901D tests, the equipment designer may choose to use these as a design tool for their shipboard equipment which is subject to shock qualification.

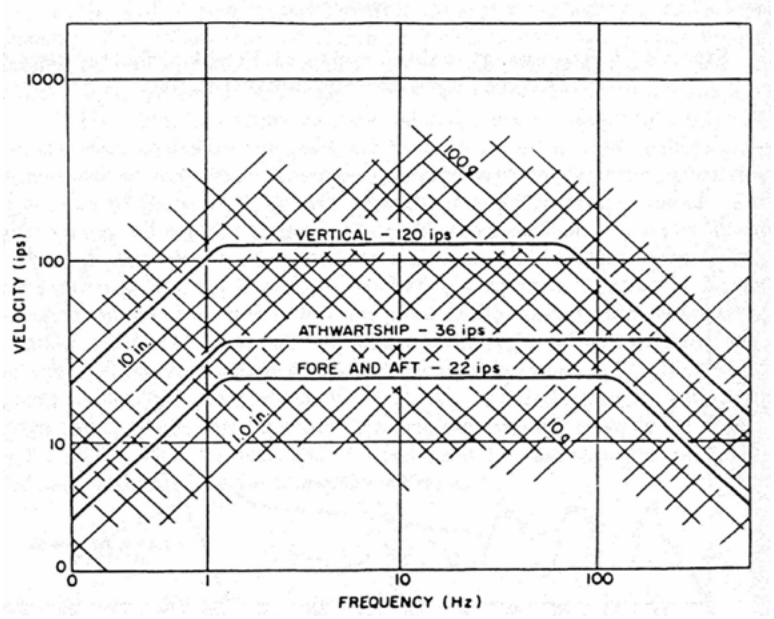

Figure 25. Design Spectra for a Floating Shock Platform. Source: [73].

c. Standards

As commercial off the shelf (COTS) equipment has become more and more prevalent over the years and is now commonly found throughout current military systems, the continued implementation, update and adherence to standards is vitally important in ensuring proper engineering processes, procedure, practices and methods [97]. This holds true for both industry and military standards. To this point, recently work was conducted in the area of equipment fragility by Lang [98] and Gaberson to support ANSI (2009) [65] and ASTM (2010) [99].

C. SHOCK HARDENING APPROACH

The U.S. Navy uses a standard shock hardening approach to shipboard equipment validation, as outlined in the MIL-DTL-901-E [42] and other guiding U.S. Navy documents [23], [25].

1. Approach

With the goal of reducing lost capability in an UNDEX environment, ship systems and equipment are subjected to a shock hardening program that is to ensure their

performance mirrors the level of ship structure and crewmember shock hardness. More robust design, shock isolation of equipment and modification of COTS, are all pursued in conjunction with the shock qualification of equipment and systems for shipboard use.

In accordance with [23], NAVSEA is tasked with:

1. Identifying the shock qualification requirement.
2. Issuing shock qualification approval, ensuring functional requirements are met.
3. Ensuring cost-effectiveness is incorporated into this program.
4. Implementing a process to assess and certify shipboard equipment after new construction, modernization or conversion of ships occurs.
5. Developing and implementing a shock hardness assurance, maintenance and surveillance program during the ship service life.
6. Providing approval on non-conformance with Navy requirements.

Furthermore, the shipboard equipment and systems are categorized into Grade A and Grade B items, the former being "[items] required to maintain performance of direct and vital support of mission essential areas aboard shock hardened ships under and after exposure to a shock event," and the latter, "items [that] shall not present a hazard to the host ship, other nearby Grade A equipment, and ship's force under exposure to shipboard shock [23]. "

As noted, previously, the three current options for validating integrated ship system shock hardness are: 1) Full Ship Shock Trial (FSST), 2) Ship Shock Test Supplemented with M&S (Alternative Shock), and 3) Enhanced Shock Qualification, Surrogate Testing and Modeling and Simulation (referred to herein as ET-M&S). Of these, the third option, which is further described as: "this test-based process centers on three elements: a thorough shock qualification program, targeted surrogate testing, and VV&A modeling and simulation focused on the prediction of the ship's mission performance capabilities after shock events," is of most interest in this study.

2. Methods

The method used to demonstrate shock hardness in surface ships is detailed in T9072-AF-PRO-010 [100], and the MIL-S-901D, superseded in June 2017 by MIL-DTL-901E. These documents convey the standard process for verifying the ability of critical shipboard equipment and systems to withstand the shock environment.

Recently updated to include a further categorization of items to be tested as principal unit, subsidiary component, or subassembly and the equipment class (Type A, B, C), MIL-DTL-901E includes specifications for shock testing via lightweight and mediumweight shock test machines, the heavyweight (floating shock platform) explosive based tests and the more recently approved medium weight deck simulating machine for deck mounted equipment, the Deck Simulating Shock Machine (DSSM). Additionally, the instruction covers the primary, Grade A and secondary Grade B equipment which are essential to the survivability and mission performance of the ship system.

An updated shock test flow chart taken from [42] guides vendors and reviewers through the acceptable shock hardness qualification process for equipment as shown in Figure 26.

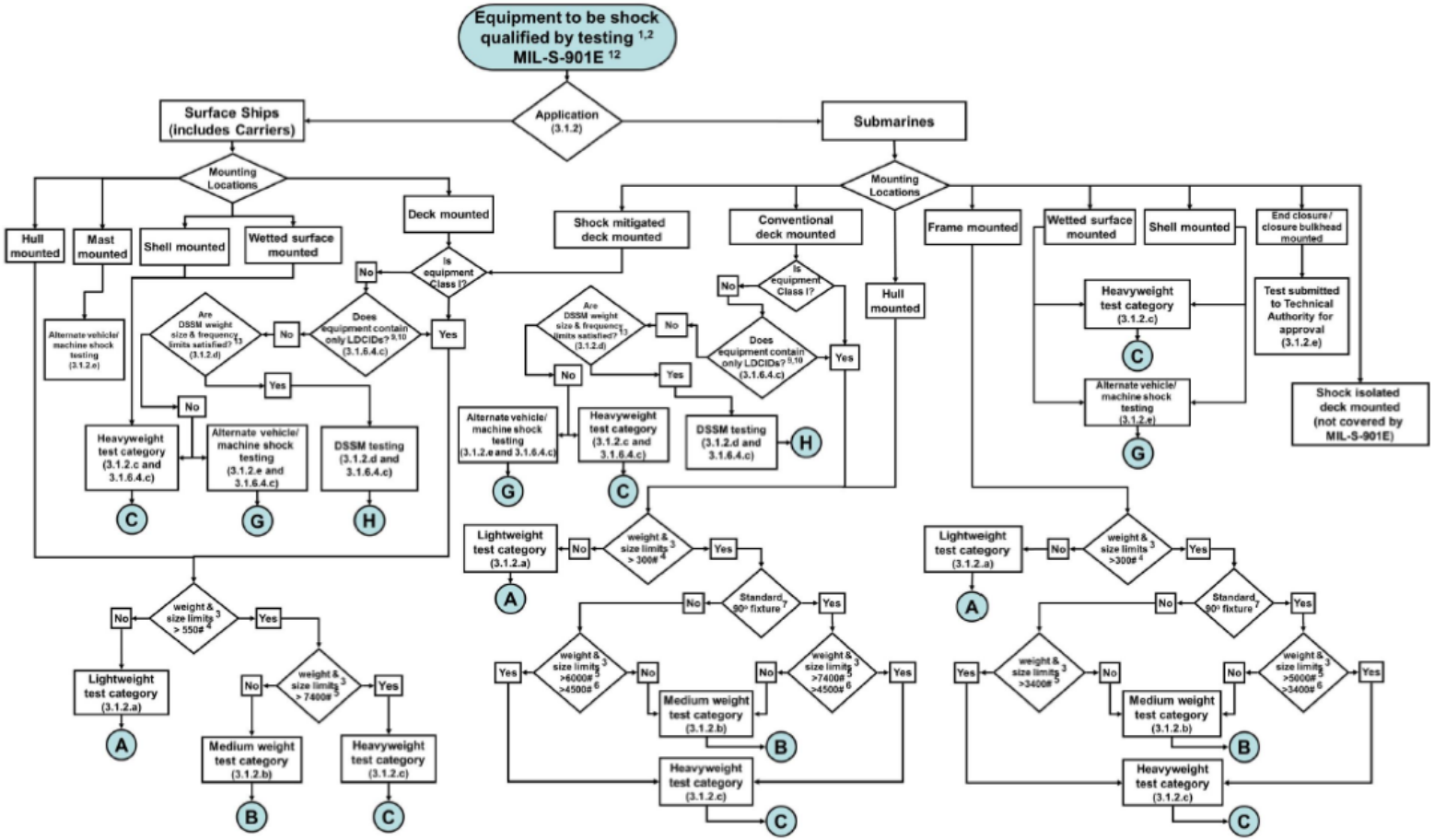

FIGURE 22. Flowcharts of testing requirements for qualification of equipment by shock testing. (Sheet 1 of 10)

Figure 26. Equipment Shock Qualification Process. Source: [42].

As this investigation is limited to surface ships, only those applicable portions of the chart are discussed. The flow chart is laid out, corresponding to a mounting location-driven test plan where the choices are: hull mounted, mast mounted, shell mounted, wetted surface mounted and deck mounted. The equipment class (I/II/III), weight and size, and test vehicle frequency limitations further determine the appropriate path for testing of the candidate equipment. The primary choices for testing the subsystem, equipment or component are: Heavyweight (FSP), MWSM, LWSM, DSSM and alternate vehicle testing. To provide some point of reference as to where these shock qualification tests fall in comparison to other UNDEX events, Table 5 compares the charge weight and standoff range with expected response type.

Table 5. Table of Sample Charge Weights

Name	**Charge Type**	**Charge Weight** (lb)	**Standoff Range**	**Response Type**
FSST	HBX-1	10,000-40,000	Far Field	Global
Torpedo	PBXN-103	500-1000	Near Field	Hull Whipping
Depth Charge	TNT	220	Near Field	Local
Mine	TNT	220	Contact	Local
FSP (901-E)	HBX-1	60	Near Field	Global/Local

3. Shock Tests

In order to ensure that the tests are carried out in a standard fashion, several test platforms or shock machines are used. The primary ones used in shock qualifications testing are described here. Initial velocities for the shock test machines are estimated based on reference [101] and range from 190.5-304.8 cm/s (75-120 in/s), depending on the total test weight. Additional background and procedures for conducting the shock tests cited here are available in [102].

a. Light Weight Shock Machine

The lightweight shock test is performed on the lightweight shock machine (LWSM). It is used to test articles up to 226.8 kg (550 lb) and of a practical size. As observed in Figure 27 the equipment is mounted on the anvil plate and struck from the top, back and side via a gravity dropped pendulum striker.

Figure 27. Light Weight Shock Machine. Source: [103].

b. Medium Weight Shock Machine

The medium weight shock test is performed on the mediumweight shock machine (MWSM). It is used to test deck mounted equipment of up to 3,356.6 kg (7,400 lb). The MWSM has the ability to be tilted or have the standard 90-degree fixture installed. Figure 28 displays a shipboard combat systems operator counsel mounted atop the MWSM with the deck simulating shock test fixture installed.

Figure 28. Medium Weight Shock Machine. Source: [104].

c. Floating Shock Platform

The heavyweight shock test is performed on one of the various sizes of floating shock platform (FSP) which is alternately known by the name heavyweight shock machine (HWSM). A standard FSP, as shown in Figure 29, is 8.53 m (28 ft) in length and has a 27,215.5 kg (60,000 lb) limit, while the large floating shock platform (LFSP) has a limit of 181,436.9 kg (400,000 lb). These, as well as the extended FSP (EFSP) and intermediate FSP (IFSP) are described in detail in [42]. This is considered to most closely approximate the actual combat shock environment as the barge is afloat in water and loaded by a

conventional explosive charge produced shock wave vice a mechanically achieved impact pulse.

A deck simulating fixture (DSF) is often fitted within the FSP to provide the correct base frequency, that is, one that approximates the ship deck structure. Figure 30 is an engineering sketch of the most basic of several DSF options used in the FSP.

Figure 29. Standard Floating Shock Platform. Source: [105].

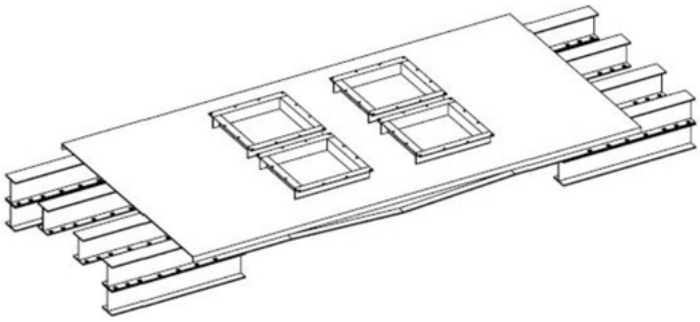

Figure 30. FSP Deck Simulating Fixture. Source: [106].

d. Deck Simulating Shock Machine

The deck simulating shock machine (DSSM) is used to perform the medium weight deck simulating shock test. This is the most recent addition to the shock testing line up. One such test unit is shown in Figure 31. It is capable of taking equipment up to 453.59 kg (1,000 lb) for isolated payloads.

Figure 31. Deck Shock Simulator Module. Source: [107].

e. Alternate Shock Test Vehicles/Machines

In some instances, other alternate shock test machines or specialty vehicles may be employed to shock test systems and equipment as outlined in [42]. These items generally do not meet the weight and/or form factor requirements to facilitate use of the standard test platforms.

III. INVESTIGATION OF CURRENT APPROACH

The current approach, which is described in the NAVSEA Technical Publication T9072-AF-PRO-010 [100] and detailed in NAVSEA T9070-AJ-DPC-120/3010 [25], is designed around the requirement for shock hardening of surface ships as stated in OPNAVISNT 9072.2A [23]. The OPNAV instruction states that the "shock hardening of Navy ships' systems and subsystems is required to a level balanced with primary hull structure and personnel survivability." This is attested to in previous combat operations and realistic testing findings showing that the hull and personnel were more resilient to shock. An enclosure to reference [23] further states a need to "validate the integrated ship system shock hardness as well as select the lead or an early ship of each shock hardened class that shall be subjected to the shock validation process as part of post-delivery test and trials when required." This is verbiage that questionably prompts the use of scaled design level shock as a pseudo certification of *pass/fail* for the shock qualification of ships and equipment.

A review of terms is prudent before proceeding. With regard to system testing, "verify" is defined as a test of a system to ensure all specified requirements are met at a particular stage of development. The term "validate" is defined as the activity that ensures the stakeholder's true needs and expectations are met. And finally, "qualification," as referred to in qualification testing, is denoted as tests typically performed with a production ready product up to design level. This is in contrast to the intended goal of introducing failure as is the case in a developmental test [108].

Currently the FSST is used as the gold standard for comparisons, yet it does not actually represent the objective of shock qualification, which is to "verify the ability of shipboard installations to withstand shock loadings due to the effects of nuclear or conventional weapons or environmental mechanical shock during operation [42]."

Figure 32 represents the entire design-test space for items of interest in UNDEX related shock. While the FSST does theoretically exercise the entire vessel, its systems and installed equipment in situ, as opposed to mounted on a test stand, the shock severity is significantly less than the equipment would potentially see in a combat event, and thus the collected data must be extrapolated to the full design or combat threat level. Surrogate tests

using scaled models, systems, sub-system, equipment and component level testing reach design limits in shock severity but may not accurately capture all of the interactions of the ship, deck, surrounding equipment, and transmission path potentially influencing the shock response of the test article. However, these component level tests can be used with physics-based M&S, which is valid throughout the design space presented in Figure 32, to inform shock hardness qualification.

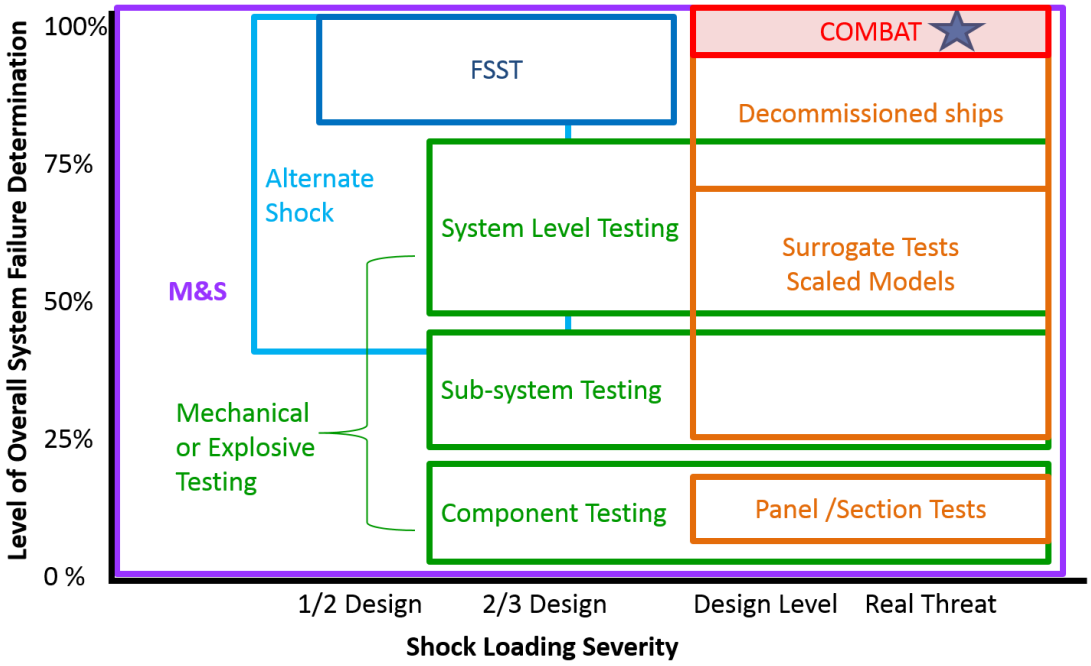

Figure 32. Shock Hardness Evaluation Space. Source: [58].

A. EXAMPLE CASE OF EQUIPMENT VALIDATION

An example case of an electronics equipment cabinet is used to explore the current procedure for a vendor working to achieve shock qualification acceptance for their equipment for further use in U.S. Navy surface ships.

A typical heavy weight shock test was conducted, and the results presented in a shock test report [109]. The system being tested consisted of several electronics equipment cabinets and electronic subsystem and equipment. The average weight of each equipment

cabinet including associated electronics was approximately 362.9 kg (800 lb). The AN/SSQ-137 (V) 1 Rack weighed nearly 136.1 kg (300 lb) and the electronics equipment load another 226.8 kg (500 lb) on average. The size of the cabinet was approximately 182.9 cm x 55.9 cm x 86.4 cm (72 in x 22 in x 34 in), with an approximate center of gravity in the vertical direction of 86.36 cm (34 in) from the cabinet base. Approved isolators were installed for the testing, and the equipment was receiving 110VAC power during the test series. The major electronics consisted of a HF receiver system, V/UHF receiver, server gear, switches and other hardware typical to this type of installation. Figure 33 provides a visual reference of the FSP (test barge) and test equipment while Figure 34 provides detail regarding the typical placement of accelerometers on the equipment cabinet.

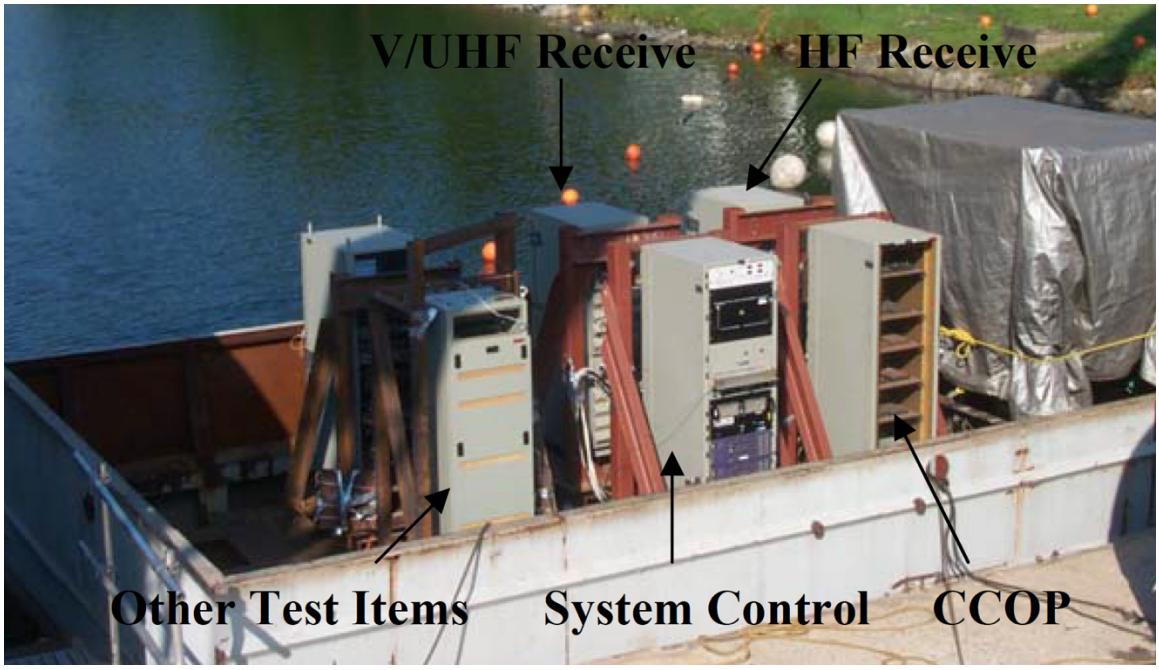

Figure 33. FSP Loaded with Electronic Equipment Cabinets for Shock Test. Source: [109].

From the test report [109] we are provided with the basic setup and test configuration information. The test series for this electronics equipment, equipment case and accessories was conducted in accordance with MIL-S-901D [41] and 901D Document No. D00231-QTP-001, using the FSP, constructed in accordance with BUSHIPS Drawing

No. 645–1973904. Again, it should be noted here that MIL-S-901D has been superseded by MIL-DTL-901E since that time, but this example case remains relevant. The standard 27.22 kg (60 lb) HBX-1 charges suspended at a depth of 7.32 m (24 ft) below the surface of the water were utilized in the testing with horizontal standoff distances measured from the center of the charge to the FSP side hull plating. After Shot 3, the test items were rotated 90 degrees in order to meet requirements for unlimited orientation [42]. The equipment being tested was designated as Shock Grade A, Class II. Table 6 provides the explosive shock test "shot" sequence, and horizontal standoff distances, while Figure 35 depicts the shot progression.

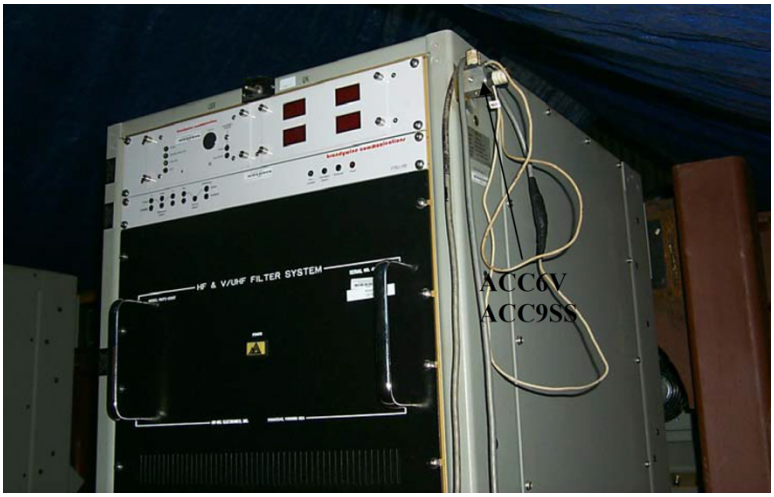

Figure 34. Shipboard Equipment Cabinet and Electronics with Response Accelerometer Placement Shown. Source: [109].

In accordance with the shock qualification test procedure outlined in [41], the "Shock Test Acceptance Criteria" cited in the report is stated as:

> In addition to the acceptance criteria presented in Section 3.1.10 of MIL-S-901D (Navy), the following was also considered as acceptance criteria for meeting the shock test requirements:
>
> The test item continues to perform its intended functions following the test series.
>
> A momentary malfunction shall be considered acceptable if it is automatically self-correcting.

No part of the test item that may be considered a hazard to personnel or Grade A equipment shall break or come adrift.

The test item shall not demonstrate a potential for fire hazard. Any evidence of electrical shorts, release of flame, smoke, or sparks shall be cause for rejection unless otherwise approved by the acceptance authority.

Minor physical damage to the test item, such as small cracks, minor yielding of structure, out-of-tolerance clearances, and similar damage shall not be cause for shock test disapproval unless such damage causes unacceptable impairment of equipment performance, results in a hazard, or results in a substantially shortened equipment useful life.

Table 6. Test Series for FSP Shock Qualification Test. Source: [109].

Shot/MIL-S-901DTest Number	Standoff Distance	Deck Frequency	Charge Location
1/2	30 feet	14 ± 2 Hz.	Along the athwartship centerline of the FSP
2/3	25 feet	14 ± 2 Hz.	Along the athwartship centerline of the FSP
3/4	20 feet	14 ± 2 Hz.	Along the athwartship centerline of the FSP
4/4 Rotated	20 feet	14 ± 2 Hz.	Along the athwartship centerline of the FSP

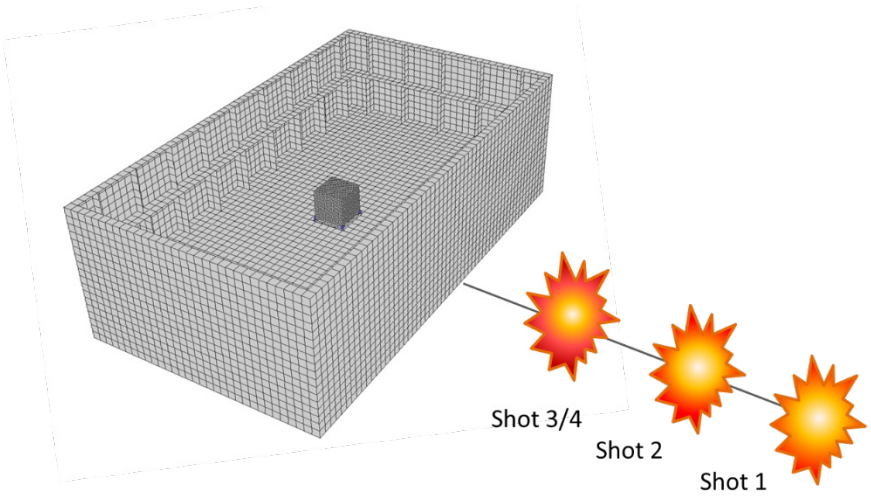

Figure 35. Shot Progression for FSP Testing

The deck frequency of thee installed DSF in the FSP was tuned to 13.1 Hz. Test instrumentation consisted of one velocity meter mounted in the inner bottom, closest side to the UNDEX and 10 accelerometers placed on the DSF, or top or bottom of the equipment racks. These would provide measured data for shock loading, base acceleration and equipment response, respectively. As typical in UNDEX analysis, the data was low pass filtered at 250Hz.

Prior to the test, a survey was conducted to find that all equipment was properly installed with no visual deficiencies noted. Operational tests of the equipment were also satisfactorily completed.

The testing progressed and resulted in the following observations. In Shot 1, the 9.14 m (30 ft) standoff distance, while there was no visual indication of any issues, the KVM switch did not function. The HF Receiver, V/UHF Receiver, and Systems Control Rack were not operational even with a reset. The resolution is that the power required to be cycled. After Shot 2, 7.62 m (25 ft) the same result occurred as with Shot 1, the KVM switch, HF Receiver, V/UHF Receiver and Systems Control Rack were not operation and required cycling the system power to restore the systems to operation. This took nearly 10 minutes in each case. Shot 3, which is the actual shock qualification loading, resulted in failure of a circuit breaker in the V/UHF receiver rack. However, in this case unlike with the less intense loading, a simple reset rendered the device fully operational. The final test, Shot 4, which is set at the same shock factor as Shot 3, finds the equipment rotated 90 degrees with regard to the charge axis. This time the HF receiver rack was not operating properly post shock. In this case the equipment rack was rebooted and proceeded to operate properly.

1. What Works

In assessing the overall performance of the equipment in the given example of these electronics systems cabinets, there were no structural issues noted. This is most likely due to the fact that the cabinet itself is of a mature design. However, the equipment load, and arrangement may affect the shock response and performance over that of the equipment cabinet itself. Whether or not the equipment itself gained shock qualification is not of

immediate interest here, rather it is the test process itself. We find that the review of the qualification is two-fold in that first, "Did the process result in adherence to the stated criteria?" and second, "Was that the correct measure of performance?"

The shock test report indicates that the equipment did not function after the test without manipulation of the systems or power source. The implication is that at least some of the listed criteria were not met. So as a simple *pass/fail* test, the goal has been achieved. Rework of the system in some fashion was thus required and presumably another series of tests would be performed prior to certification of the equipment systems as shock qualified for service aboard U.S. Navy vessels.

The overall shock qualification process (slightly revised by reference [25] since the time of this test), is provided in Figure 36. As implied by flowchart, shock testing is the preferred path to shock qualification of shipboard equipment, but not the only one.

2. What Doesn't Work

When investigating the given shock qualification test example, one has to ponder the fact that there were failures in the operational performance, a function failure, of the equipment at less than qualification level shock factors. In Shot 1 and 2 complete power cycling of the system was required in order to restore the functionality of the electronic system, while at closer standoff ranges in Shot 3 and 4 a reset of a circuit breaker and reboot of the system were all that was required to recover.

A review of the associated acceleration and velocity time history records from the base of the DSF and the inner bottom indicate, as expected, a nearly linear increase with decreasing standoff ranges. Table 7 provides these values with their associated shock factors, and corresponding peak recorded accelerations. What is of interest is that in the case of Shot 3, the V/UHF Receiver system with the circuit breaker that tripped was associated with a peak acceleration of only 176.52 m/s^2 (18.01 g's), which is approximately 20% less than the overall peak response acceleration recorded in Shot 3. Additionally, in Shots 1 and 2 where the peak acceleration across the systems was as low as half that of Shot 3, full power cycling was required to recover functionality.

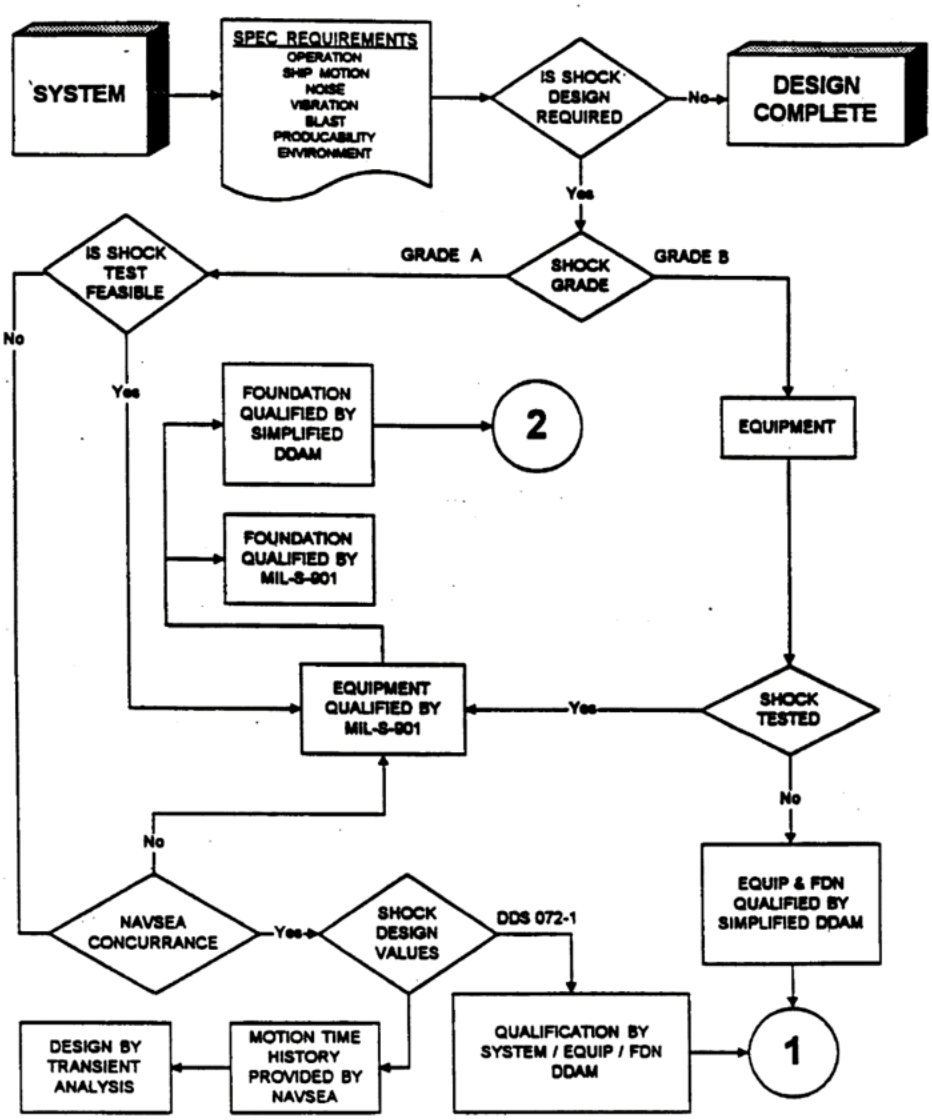

Figure 36. Shock Qualification Approach. Source: [23].

Investigation of this example case and others [110] then points us to the fact that the procedure does not require analysis of "how" or "why" the failures occurred, or deference by what means. In fact, the shock test report is just that, a means to state whether the equipment passed or failed the shipboard equipment shock qualification process.

Table 7. Recorded Data from Test Series. Source: [109].

Shot No.	1	2	3
Standoff (ft)	30	25	20
Shock Factor	0.16	0.19	0.22
V_{M1} (ft/s)	11.67	12.84	14.78
A_{DSF} (g)	35	37	45
A_{peak} (g)	10.5	20.3	22.0

B. NEED FOR IMPROVEMENT

The aforementioned example of the equipment cabinet shock qualification test is perhaps cause for concern with regard to the uncertainty in practices currently employed by equipment manufacturers, ship designers and the shock testing community. This point is not accusatory, nor self-promoting but rather to merely state that we can and should do better collectively as a shock community at tackling this incredibly difficult problem.

1. Uncertainty in Failure

As was previously described in the familiar specifications and others from abroad such as the SSC [86], IEC [93]–[94], and ETSI [95], shock qualification criteria are not definitive in nature. There is generally no easily addressed nor predetermined value that if exceeded, or failed to achieve, would result in a test failure. Visual and functional performance are typical criteria. While this may facilitate test reporting, comparison and cost savings, there remains a question as to how well the specimen actually performed. Without being able to quantify that performance in some more definitive manner, it leaves operational commanders with no true sense of the capability in their mission critical systems, equipment nor the individual components that are likely to fail and leave them vulnerable at the worst possible moment following a shock event at sea.

A quick search may reveal a host of uncertainties in the examination of testing and data. Parameter uncertainty, aleatoric (statistical) uncertainty, epistemic (systemic) and interpolation uncertainty are just some examples of this. Respectively, the aforementioned can be thought of as uncertainties in values such as material properties, the existence of

“unknown” factors where all others are consistent between data sets, exclusion of a critical “known” factors or principles such as gravity effects, and in the last case, a lack of available data leading to predictions based on interpolated results. All of these uncertainties exist in relation to the shock qualification problem, at least to some degree. However, the goal is to first quantify the uncertainty, and then to reduce it by offering a deterministic measure to the test specimen performance.

One way to do this is to first ensure that the methods applied will minimize the appearance of uncertainty in the data. For example, when physical test data is compared to analytical solutions or computer simulations there is the potential for a difference in results once comparison of both are made. Figure 37 illustrates how this uncertainty may creep in. The test shows the actual performance is based on the accuracy of the measurement, yet the analytical result is rooted in proven calculations coming from established physical principals. However as is the case in this plot, there is some disparity between the two apparent solutions which the user must first reconcile to even establish a basis for assessment of failure. Minimization of these differences is key to establishing a basis for our criterion investigation. Specific ways to mitigate these differences, such as through improvement in structural damping within the model are discussed in Chapter IV.

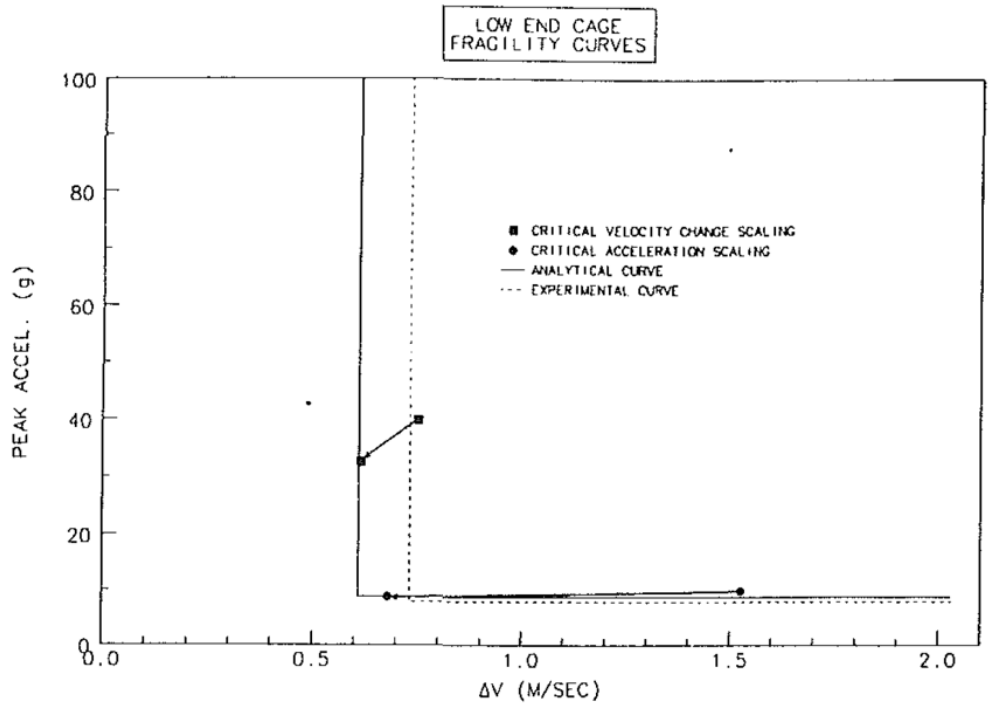

Figure 37. Sample Experimental/Analytical Fragility Curve for Sheet Metal Case. Source: [111].

Naturally, in modeling and simulation there is always the desire to minimize the difference between the actual measured and numerically derived results. Figure 38 presents how the comparison of the measured results and analytical solutions or simulation uncertainty can be related. The solid curve represents the mean predicated values over the entire data range based on the experimental and simulated results. Thus, in the data presented in Figure 37 we see that the dotted curve, which represents a confidence index to the prediction, bounds the area, greater than an approximate change in velocity of 0.75 m/s and a peak acceleration of 147.1 m/s^2 (15g's), where the values would be expected to fall.

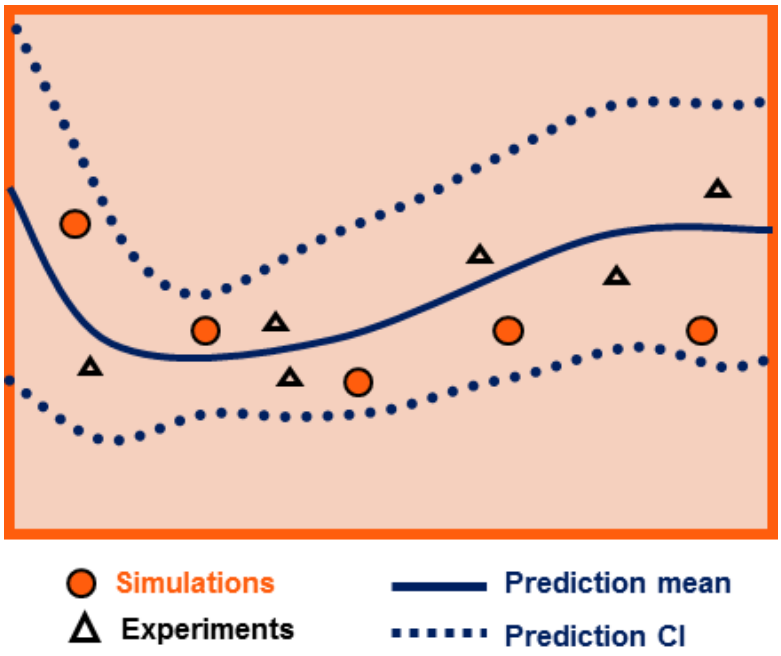

Figure 38. Uncertainty Quantification. Source: [112].

However, beyond this still lies the true uncertainty in the actual failure criterion. Using the current approach to shock qualification it is difficult to quantify the proximity to failure for either a test specimen that *passed*, or even if it *failed.* More simply put, how close to failure is the test specimen under the given input and environmental conditions? Is there a margin of "safety," or did it fail by a long shot?

In order to determine this in a strict engineering sense, one would need to perform numerous tests at increasing shock levels until the precise point of failure was achieved. For assurance, the test series would need to be repeated in order to have a consistent set of replicates. In order to make this a useful measure, a range of loading conditions and configurations would be best suited to forming a predicted mean curve of actual failure for this one test article. Modeling and simulation could then be used to extend the curve by extrapolating the test data once congruence was achieved between the model and the actual recorded data, as in Figure 38. From numerical data, a diagram showing the response as a function of input, could then be plotted against the previously determined regions of passage and failure such as illustrated in Figure 39.

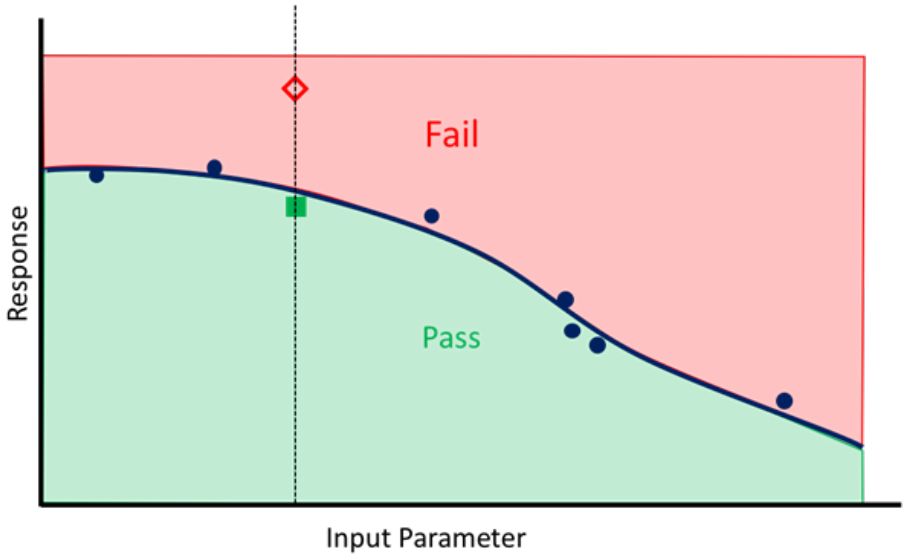

Figure 39. Proximity to Failure Threshold

When necessary, a future test or simulation could be conducted and assessed against the known failure zone. At the same intensity, or shock factor, the response may then be categorized as a *pass*, as illustrated by the closed green square in Figure 39, or a *fail*, which corresponds the open red diamond marker. Currently, this it is not clear. Without a deterministic measure of the response, as to the true proximity to the failure threshold, which is defined here by the black curve for all input values, it just states that the test falls somewhere along the vertical line corresponding to the selected input parameter.

Mere mention of the input shock loading also evokes cause to contemplate further divergences when evaluating the uncertainty of failure in the assessment process. Test platforms are not consistent in the way that the shock loading is delivered, as shown in Figure 40. Furthermore, absent of a formal requirement to record sensor data associated with each instance of the shock qualification test, future analyses pertaining to the tested equipment and test setup used are invalidated and would require to be repeated.

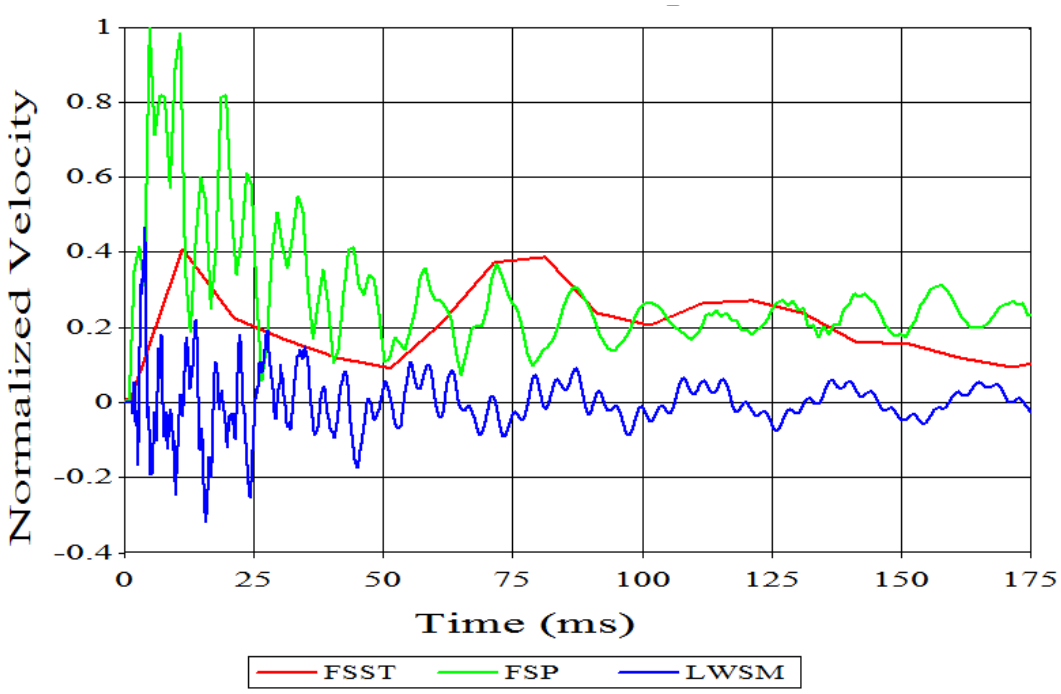

Figure 40. Inconsistency of Input in Shock Loading

2. Informed Failure Testing

Beyond the obvious material failure compliance related to engineering design (strength, deflection, etc.) and situational failure issues attested to improper installation, unauthorized modification or poor workmanship during fabrication or assembly, there must be a more definitive and quantifiable measure of failure in shock qualification of shipboard equipment.

Through careful examination of the system or equipment, down to the component level, a critical component, that, which is likely to fail, must become the focus of the failure analysis in determining shock qualification rating of the test specimen. With the tools available to engineers of the day, this is quite possible where perhaps in the past simple test observation was not merely adequate but all that was practical given the constraint of that time period.

By defining tailored failure criteria based on the ship system delivered shock loading and critical component response under simulated shock conditions, the uncertainty

in failure can be reduced as compared to conventional shock qualification testing alone. The methodology, procedure and applicability of this updated approach are described in the following chapters.

THIS PAGE INTENTIONALLY LEFT BLANK

IV. ADDRESSING SHIP SHOCK MODELING

The modeling and simulation process, procedures and unique issues that come with UNDEX and more specifically system response to fluid structure interaction (FSI) will be addressed in this chapter and accompanying appendices.

A. UNDEX EVENT MODELING AND SIMULATION

The UNDEX event is modeled using the Dynamic System Mechanics Advanced Simulation (DYSMAS) hydrocode suite [113]. Use of DYSMAS allows for the coupling of the fluid-structure problem through a power coupler interface that accurately translates the shock pressure loading from the Eulerian solver *Gemini* [114] to the structural solver *Dyna3D*/*Paradyn* [115], [116]. Mature in their software development cycle, these finite element codes have been through the DOD M&S verification, validation and accreditation (VV&A) process independently for use in the UNDEX class of problems, as well as in a fully coupled state [117], [118].

1. Shock Geometry

The FSP is used here to describe the general setup and explanation of the FSI coupling between the ship structure, the surrounding fluid, the source location and shock front propagation produced by detonation of the explosive charge within the simulation. The basic arrangement and process used in the full ship modeling and simulation is similar.

As previously explained, in a typical heavyweight (FSP) shock test series, four shots, of increasing shock factor are detonated abeam of the vessel, at correspondingly closer ranges. In the most severe of the four test shots, Shot 3/4, the FSP is subjected to an underwater explosion resulting from a 27.22 kg (60 lb) HBX-1 charge, with a change in equipment aspect, by 90 degrees in the final shot. The charge location is centered amidships, with radial standoff components in the vertical direction of 7.315 m (24ft) below the water's surface, and 6.096 m (20 ft) lateral offset from barge edge. These are orthogonal distances labeled as R_V and R_H, in Figure 41, respectively, while the radial standoff, R, is approximately 9.52 m (31.24 ft) to the point where the barge floor meets the

side. The barge has a draft, *T*, of approximately 1.22 m (4 ft) in the lightship condition. The overall shock event geometry is illustrated in Figure 41 from a 2D perspective of a cross-section viewed from the "bow" of the FSP.

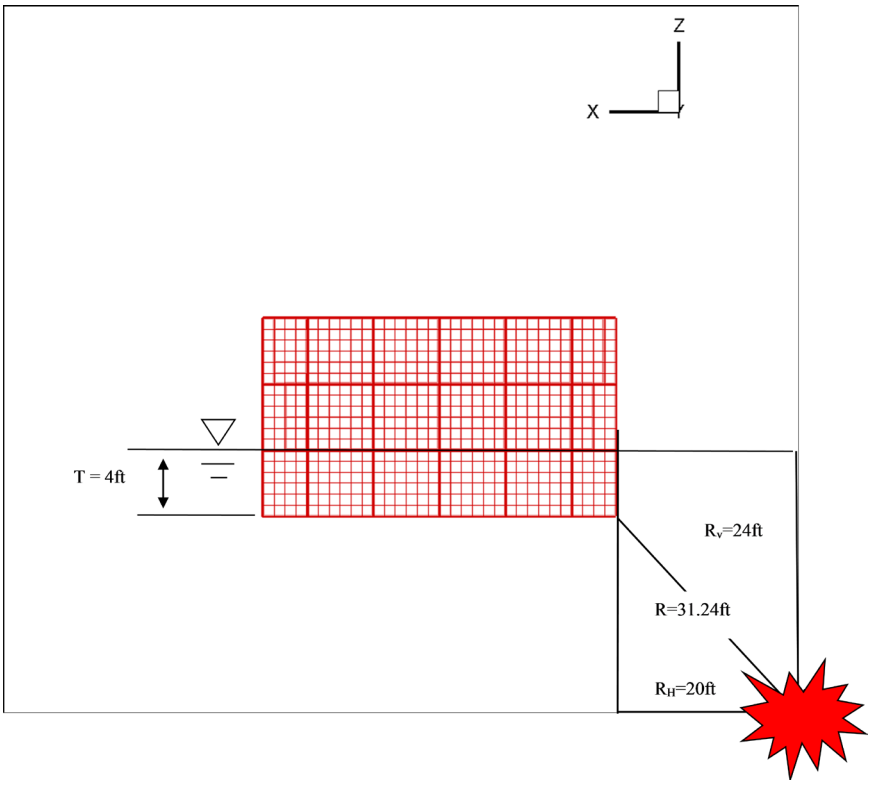

Figure 41. XZ Plane View of FSP Showing Charge Location Offset at Amidships

Figure 42 provides a view of a slice of the fluid and the structure as modeled in the finite element analysis (FEA) program, while Figure 43 provides a full 3D perspective of the bounding box of fluid that surrounded the structural model for this simulation.

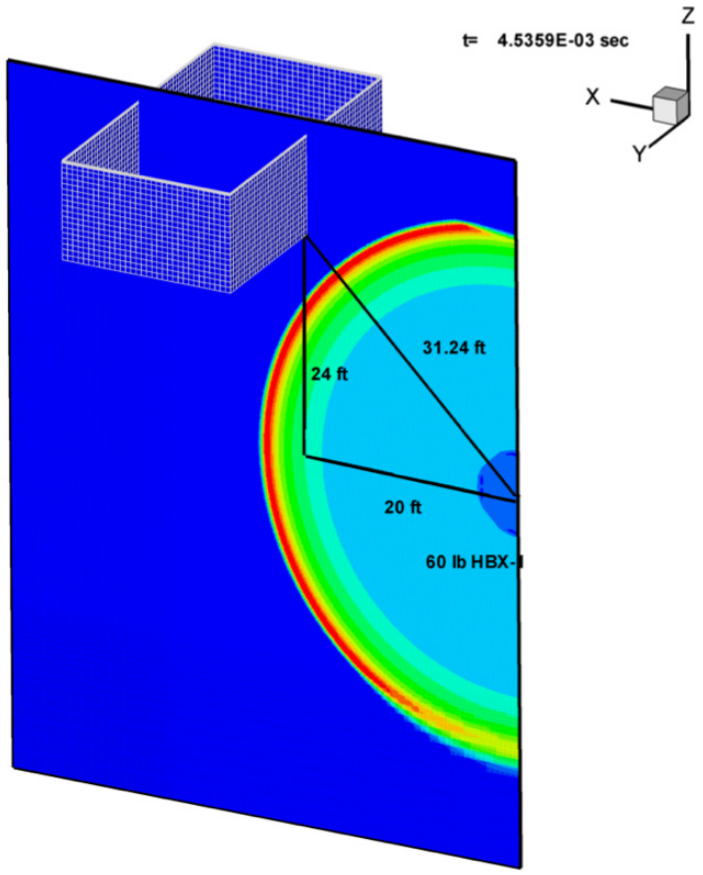

Figure 42. XZ Plane View of FSP Structure Coupled to Fluid Model

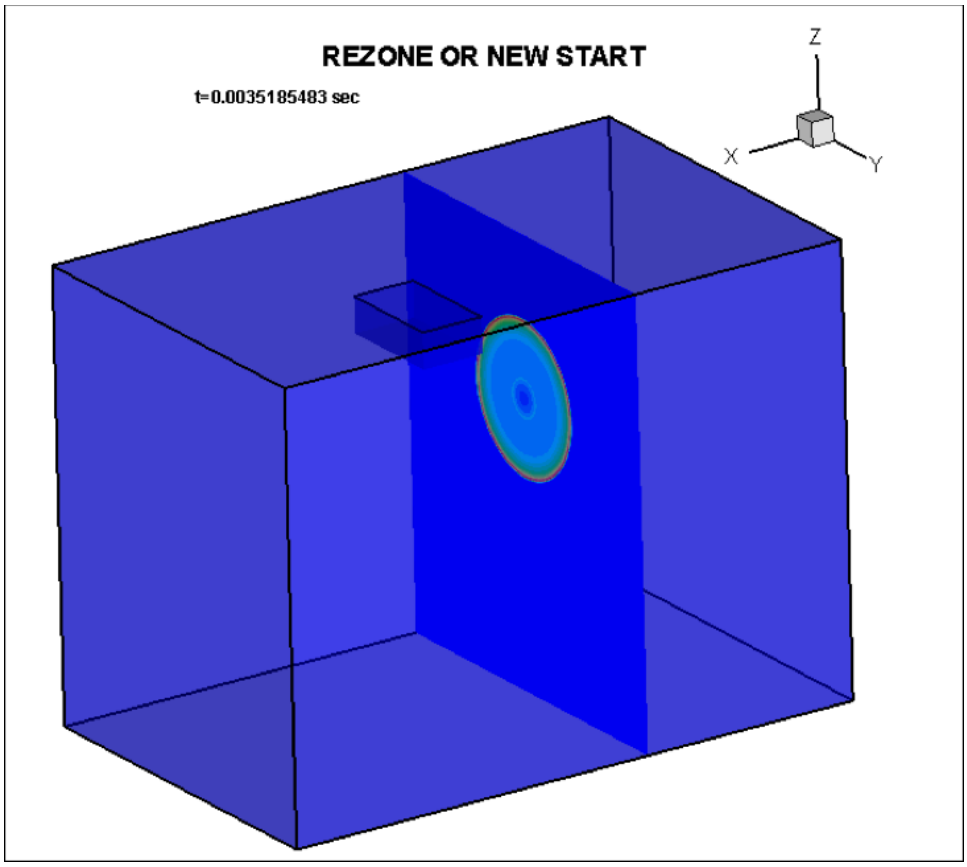

Figure 43. 3D Visualization of the Fully Coupled FSI Model

2. Fluid Model

For fully coupled problems, careful attention must be taken in the creation of the mesh, selection of the fluid properties and boundaries. As observed in Figure 43, the structural model is dwarfed by the volume of water that is necessary to be carried in the fluid model. Details of the fluid model generation and explosive charge setup are provided in Appendix A.

a. Fluid Domain

Proper selection of the correct fluid domain is critical to achieving the most accurate and efficient result. It was shown in Walters et al. [78], that the ocean bottom proximity, shape and material composition significantly affect the delivered shockwave loading phase and amplitude. Similarly, the mesh density and boundary treatment of the fluid domain can

affect the shock loading of the vessel. The density and quality of the mesh in and around the fluid structure interaction boundary was found to be of great importance by Hart [119], however perhaps not as important as the wall boundary condition of the fluid [120]. The amount of fluid that must be modeled and what type of radiation boundary is required is still more of an art than a science and is often problem dependent [121].

b. Ocean Bottom

It was observed in some cases of the standard barge testing that the measured response and simulations did not compare well beyond the first portion of the time history and can be affected by the sea bottom, or sides of the test pond. An example of the difference in reflected pressures at a specified point vertically distant to the reflected boundary is presented here. Figure 44 provides a visual comparison of three fluid models; one with a hard bottom or fully reflecting wall condition set at 45.72 m (150 ft), (left), another with a 9.14 m (30ft) sand bottom added below the same depth of water (center), and a 150 m (492 ft) deep water column (right). Table 8 gives the change in pressure at a point at an equal distance beneath the source point and demonstrated the increase in witnessed pressure due to the bottom reflection. The recommendation given is to use a deep ocean scenario for modeling and simulation during shock qualification testing, if possible or to minimize bottom reflections via other available methods.

Table 8. Influence of Ocean Bottom Boundary on Pressure Wave Reflection

Zmin	ΔP (psi)
Wall at 150 ft	89.25
Wall at 150 ft + 30 ft Sand	19.05
Wall at 492 ft (deep water)	0.15

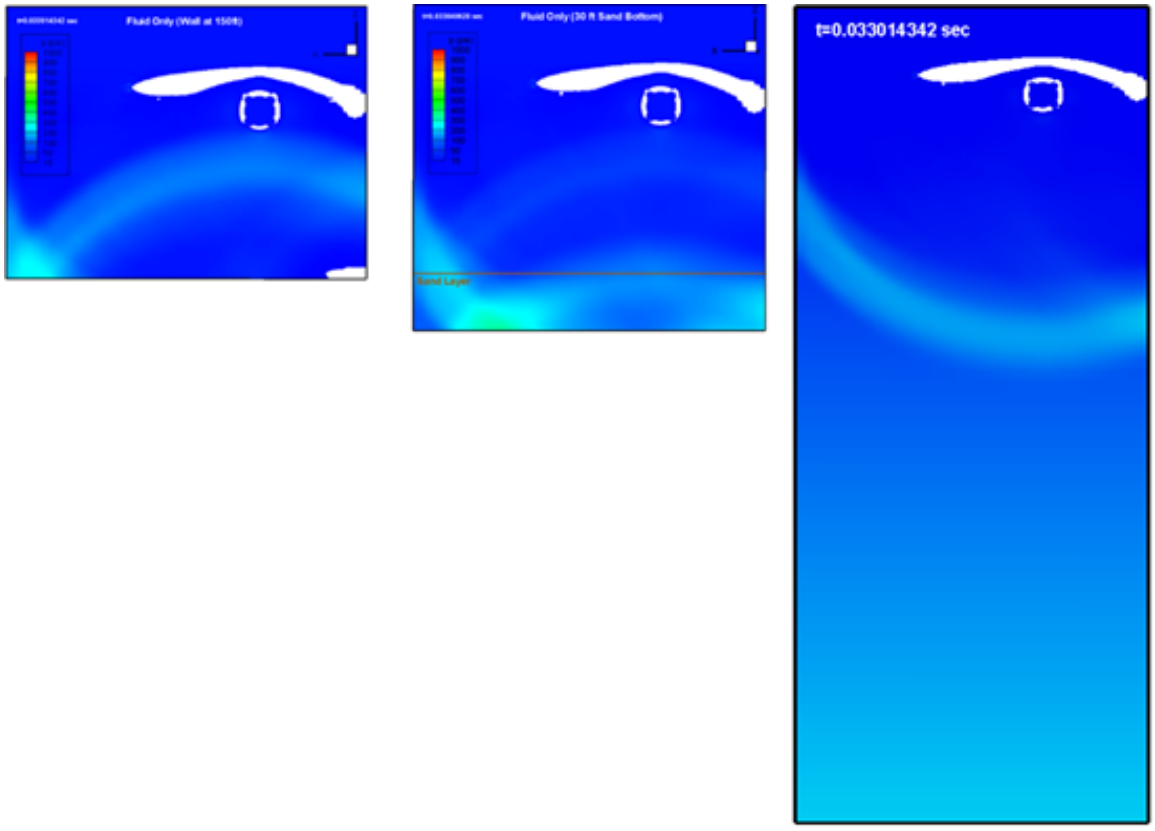

a) Hard Bottom, b) Sand Bottom, c) Deep Ocean Bottom.

Figure 44. Comparison of Bottom Treatment Effects

B. IMPROVED SHIP SHOCK MODEL

There continues to be an increase in computer capability. Today's FEM solvers and hydrocodes handle multi-million nodes and degrees of freedom without issue. Naturally there is a desire to discretely model every aspect of the equipment and its environment. Yet more nodes and central processing units (CPU) are not necessarily always the answer when it comes to resolving modeling issues that plague research. Rather the model, which is a surrogate for the physical function (shock loading), and the input parameters must first be properly prepared to accurately produce the output (response) of the event being simulated. Some of the various ways that this can be accomplished is through better problem definition, through more accurate representation of the boundaries, and review of model properties. Refinement of the mesh does aid precision, in some circumstances, yet perhaps

not as much as does the revision in a treatment of a core modeling process utilized within the simulation.

System damping, well known to be an incessant impediment in the correlation of the physical response and numerical method simulations, is one such example. A selection of the improved damping method study, which shows promise for further investigation and implementation, is documented here for potential adaptation in the recommended shock qualification updated approach based on functional failure.

1. Ship Structural Damping

Damping has long been an issue with ship shock modeling and simulation. Numerous studies have been conducted [122]–[125]. The results from a recent survey of damping approaches [126] found that there still exists a need to improve the damping model used in the shock simulation of ships. As part of this larger effort, damping models were studied and a revised approach to ship structural damping is presented.

2. Improved Ship Damping Models

An updated multi-stage damping model [125] based on traditional Rayleigh damping [127] was proposed for ship systems under UNDEX loading. The proposed structural damping model consists of two stages. During the early time response, only mass proportional damping is applied and then later, only stiffness proportional damping is applied to the structural model. In this manner, overdamping of high frequency responses at early times is avoided while the low frequency response is preserved throughout the late time response. Inasmuch, this damping model fully represents the dynamic behaviors of the complex ship structures subjected to UNDEX loading. This is accomplished by the proper selection of proportional constants related to mass and stiffness proportional damping, determination of the optimal transition timing from mass proportional damping to stiffness proportional damping and grouping of structural sections for determination and use of different damping values.

a. Background

Dynamic characteristics of structural behavior in many complex structures can be difficult to model. Damping is certainly one of these. This is in part due to the myriad of ways that damping transcends the model such as material damping, frictional damping, fluid damping, etc. [128], [129]. The ability to measure and quantify each of these unique damping types is challenging even in the simplest of cases. In the case of a system as varied, complex and densely packed as a naval combatant, the issue of damping is nearly incomprehensible. In order to simplify the complex systems of equations of motion for the ship model, a viscous damping model is used in describing the structural characteristics. From a review of fundamental vibrations, we recall that the damping force is proportional to the structural velocity. The proportional constant is called the damping coefficient.

In the time domain, the most general viscous damping model consists of a uniquely assigned damping coefficient for every DOF in a structural FEM model. These may also vary as a function of time. A graphical depiction of this is shown in Figure 45. This is easy to understand and track, yet with ship structural models ranging in the millions of DOF, this is clearly not practical. This necessitates a simplified approach such as the one summarized here.

First, the total number of DOF is grouped such that those DOF in each group have the same damping value. Secondly, the damping value in each group is assumed to be piecewise constant from interval to interval over a range of time. An example of this is shown in Figure 46 with two groups. As the damping model is further simplified, we find that the most simplified damping model is when all DOF have the same damping value and remain constant throughout the entire time interval. Convenient as it may be, this type of reduced model does not usually do well in representing the damping behaviors of a complex structure. Therefore, it is necessary to find a damping model which is simple yet still accurately represents a complex damping behavior.

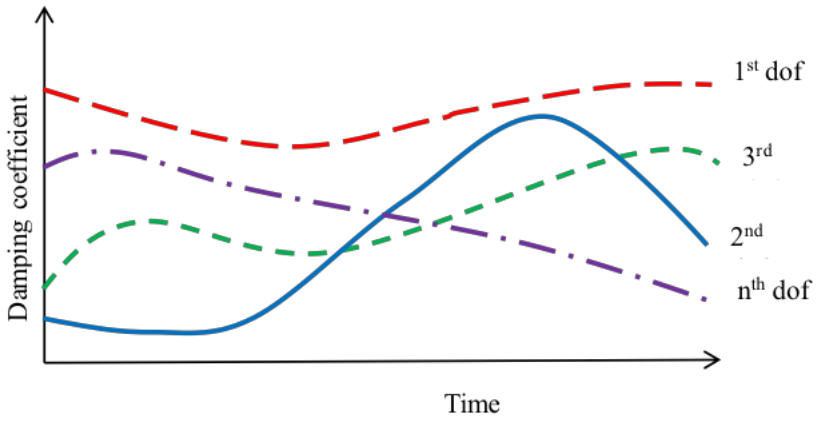

Figure 45. General Damping Model. Source: [125].

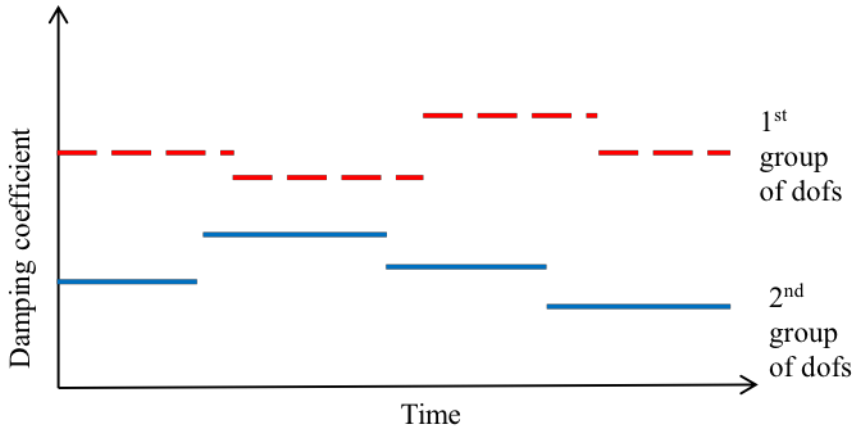

Figure 46. Simplified Damping Model. Source: [125].

b. Damping Models

First, traditional Rayleigh damping methods are discussed and then the proposed damping model is presented.

(1) Rayleigh Damping

Proportional (Rayleigh) damping is one of the most common approaches to damping, and thusly it is used as a damping model in most FEA programs. Hence, starting with this approach, Rayleigh damping is expressed as

$$[C] = \alpha[M] + \beta[K] \tag{4.1}$$

where $[C]$ is the damping matrix, $[M]$ is the mass matrix, $[K]$ is the stiffness matrix, and α and β, are proportional coefficients. We see then that Rayleigh damping is constructed from the mass and stiffness matrices of the structural system. From modal analysis, the damping factor ς can be expressed as

$$\varsigma = \alpha \frac{1}{2\omega} + \beta \frac{\omega}{2} \tag{4.2}$$

in which ω is the natural frequency of the system. The coefficient α, associated with the mass matrix, results in a large damping factor for low frequencies while β, which is associated with the stiffness matrix, yields large damping factors at high frequencies.

Considering a single DOF system with a mass, spring, and damper, the equation of motion is then

$$m\ddot{u} + c\dot{u} + ku = F \tag{4.3}$$

where *m*, *c*, and *k* are the mass, damping and spring constants; *u* is the displacement value; *F* is the force applied to the mass. The superimposed dot denotes the temporal derivative in the equation of motion. When the excitation force is the impulse function, the equation of motion can be rewritten as

$$\ddot{u} + 2\zeta\omega_n\dot{u} + \omega_n^2 u = \delta(t) \tag{4.4}$$

in which ζ is the damping factor which is defined as

$$\zeta = \frac{c}{2\sqrt{km}} \tag{4.5}$$

ω_n is the natural frequency which is equal to

$$\omega_n = \sqrt{\frac{k}{m}} \tag{4.6}$$

and $\delta(t)$ is then the delta function.

The solution to Equation 4.4 with the initial conditions of $u(0) = \dot{u}(0) = 0$ is given as

$$u(t) = \frac{\widehat{F}}{m\omega_n\sqrt{1-\zeta^2}} e^{-\zeta\omega_n t} \sin\left(\sqrt{1-\zeta^2}\,\omega_n t\right) \tag{4.7}$$

$$\dot{u}(t) = \frac{\widehat{F}}{m\omega_n\sqrt{1-\zeta^2}} e^{-\zeta\omega_n t} \left[-\zeta\omega_n \sin\left(\sqrt{1-\zeta^2}\,\omega_n t\right) + \omega_n\sqrt{1-\zeta^2}\cos\left(\sqrt{1-\zeta^2}\,\omega_n t\right)\right] \tag{4.8}$$

For high frequency motion, (i.e., a large ω_n value), the exponential term $e^{-\zeta\omega_n t}$ diminishes quickly in the early time response. The stiffness driven proportional damping with a non-zero β value increases the damping coefficient ζ for a large natural frequency. Then the product value $\zeta\omega_n$ accelerates the decay. Therefore, stiffness portioned damping tends to overdamp the structural response at early time. On the other hand, for low frequency motion, (i.e., a small ω_n value), $e^{-\zeta\omega_n t}$ decreases faster in time when the mass proportional damping has a non-zero α value.

A typical velocity response from an UNDEX test is shown in Figure 47. As shown in the figure, the early response consists of mostly high frequency components. The response in the early time is very important because peak values often occur during this period. Next it is observed that the late time response consists of a dominant lower frequency curve superimposed with high frequency components. Here the high frequency oscillations have a small magnitude. This suggests that the high frequency components should be preserved in the early time response while the low frequency components must not be suppressed in the late time response.

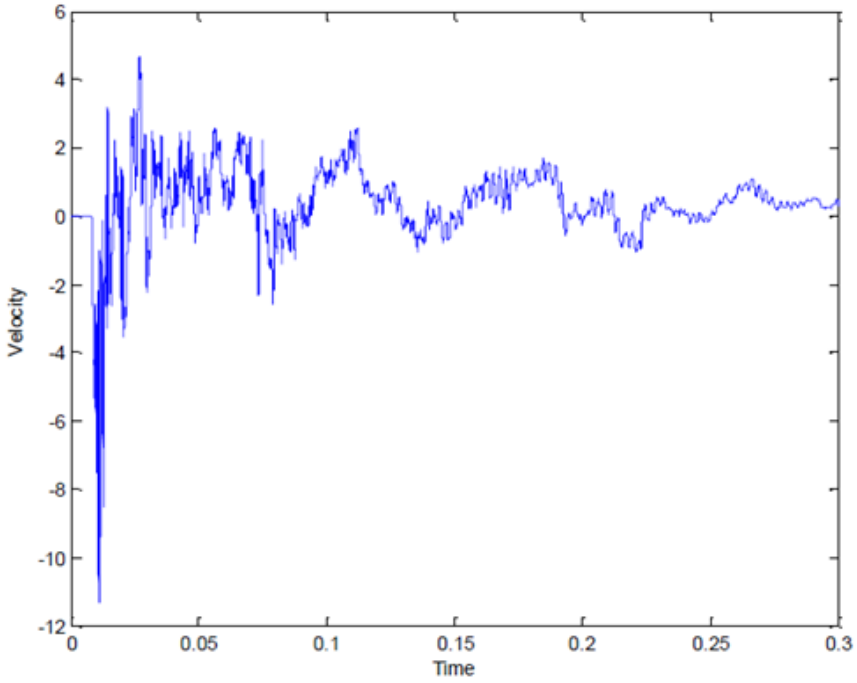

Figure 47. Typical Shock Velocity Profile. Source: [125].

(2) Proposed Damping

As previously discussed, the high frequency response should not be suppressed early in the response record in order to fully preserve the peak values. As a result, stiffness proportional damping is then not suitable for early time response. However, high frequency components may be neglected in later times. Consequently, a two-stage damping scheme is proposed as:

$$[C] = \begin{cases} \alpha[M] & t \le T_o \\ \beta[K] & t > T_o \end{cases} \tag{4.9}$$

Therefore, the proposed damping fully represents the early time high frequency response and the late time low frequency response. Three parameters are to be determined, α, β, and T_o. For a large structure which may have different damping characteristics from section to section, the proposed damping may be applied in a piece-wise sense by section. In that case, the three damping parameters may vary from section to section.

(3) Determination of Damping Parameters and Grouping

The three necessary damping parameters are determined from experimental data. The proportional constants are extracted from experimental data such as velocity time histories using techniques such as the complex exponential method (CEM), the rational fraction polynomial method (RFPM), etc [129]. These techniques provide the natural frequencies and damping factors. The natural frequencies are separated into two groups; low and high frequency groups. The range of frequencies that belong to the low or high frequency group depends on the structural system. In general, reviewing the structural response as shown in Figure 46 suggests that any frequency active at early times belongs to the high frequency group while the others belong to the low frequency group. The mass proportional damping coefficient α values are then computed from the high frequency natural frequencies and damping factors. In a like manner, the stiffness proportional damping coefficient β values are determined from the low frequency group. The computed α and β values are then averaged for the single measured data.

This process is repeated for all measured responses at all locations within the structure. Then, the computed proportional damping values are compared between locations to determine if there are sizable differences in the α and β values. The locations which have comparable values are grouped together by α and β values. This grouping may result in multiple sections of which each section has a different level of the damping. Then, the α and β values within each section are averaged and used for that section of the FEA model. The expectation here is that those sections are expected to match different zones and/or different materials within the structural model that is to be analyzed. However, because damping may vary significantly within the same zone and material, the zones may be subdivided further into multiple zones such that different damping values are assigned to each of those zones, as necessary.

(4) Transition Time

As the damping model given in Equation 4.9 is applied, a transition time, T_o, is also required. This is the time that separates the response into the high frequency dominant and

low frequency dominant time ranges. For example, reviewing Figure 47 suggests that the high frequency group dominants until a time of 0.08 s. Thus, we set T_o = 0.08.

In general, T_o is expected to vary depending on the applied loading. The typical pressure profile in time for an UNDEX shock loading is shown in Figure 48. Shock pressure decays exponentially, and is expressed as

$$P = P_o e^{-\theta t} \tag{4.10}$$

where P_o is the peak pressure and θ is the decay constant. Equation 4.10 states that the velocity response for an impulse loading decays exponentially as a function of the natural frequency, which is proportional to the θ value. The transition time, T_o, is taken as a function of the natural frequency and the decay constant as shown in Equation 4.11

$$T_o = f(\omega_{\max}, \theta) \tag{4.11}$$

where the dominate maximum frequency typically occurs in the initial response. It is practical to choose T_o after the initial peak.

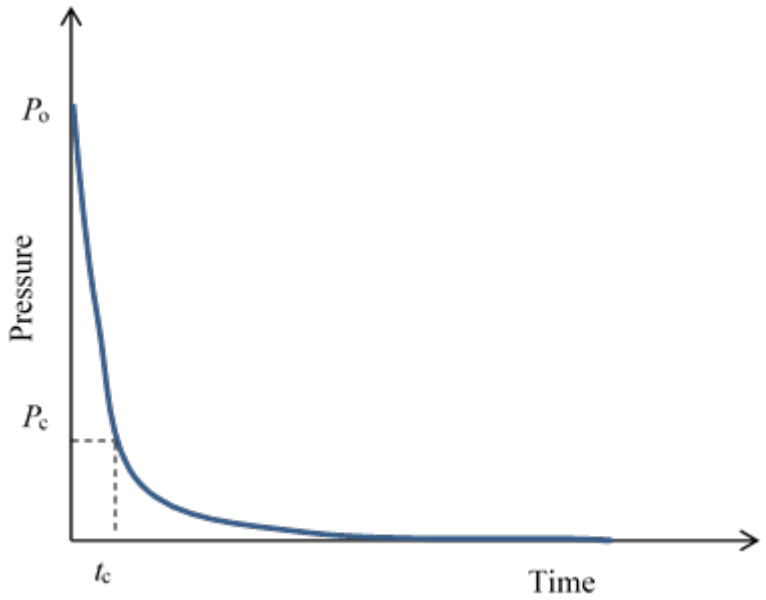

Figure 48. Typical UNDEX Shock Loading Pressure

c. Numerical Example

Several numerical examples were conducted during the development of the damping model. The discrete spring-mass-damper system is presented here. A clamped beam model was also investigated and is available for review separately in [125].

(1) Discrete Spring-Mass-Damper System

The first numerical example, which consists of the discrete masses, springs, and dampers, is sketched in Figure 49. The equation of motion for mass m_1 is

$$\begin{aligned} m_1\ddot{u}_1 &= -k_1u_1 + k_2(u_2 - u_1) - c_1\dot{u}_1 + c_2(\dot{u}_2 - \dot{u}_1) \\ m_1\ddot{u}_1 &+ (c_1 + c_2)\dot{u}_1 - c_2\dot{u}_2 + (k_1 + k_2)u_1 - k_2u_2 = 0 \end{aligned} \tag{4.12}$$

The equation of motion for mass m_2 through m_4 is

$$\begin{aligned} m_i\ddot{u}_i &= -k_i(u_i - u_{i-1}) + k_{i+1}(u_{i+1} - u_i) - c_i(\dot{u}_i - \dot{u}_{i-1}) + c_{i+1}(\dot{u}_{i+1} - \dot{u}_i) \\ m_i\ddot{u}_i &- c_i\dot{u}_{i-1} + (c_i + c_{i+1})\dot{u}_i - c_{i+1}\dot{u}_{i+1} - k_iu_{i-1} + (k_i + k_{i+1})u_i - k_{i+1}u_{i+1} = 0 \end{aligned} \tag{4.13}$$

The equation of motion for mass m_5 is

$$\begin{aligned} m_5\ddot{u}_5 &= -k_5(u_5 - u_4) - c_5(\dot{u}_5 - \dot{u}_4) \\ m_5\ddot{u}_5 &- c_5\dot{u}_4 + c_5\dot{u}_5 - k_5u_4 + k_5u_5 = 0 \end{aligned} \tag{4.14}$$

The final matrix equation becomes

$$[M]\{\ddot{U}\} + [C]\{\dot{U}\} + [K]\{U\} = \{F\} \tag{4.15}$$

where

$$[M] = \begin{bmatrix} m_1 & & & & \\ & m_2 & & & \\ & & m_3 & & \\ & & & m_4 & \\ & & & & m_5 \end{bmatrix} \tag{4.16}$$

$$[C]=\begin{bmatrix} c_1+c_2 & -c_2 & & & \\ -c_2 & c_2+c_3 & -c_3 & & \\ & -c_3 & c_3+c_4 & -c_4 & \\ & & -c_4 & c_4+c_5 & -c_5 \\ & & & -c_5 & c_5 \end{bmatrix} \tag{4.17}$$

$$[K]=\begin{bmatrix} k_1+k_2 & -k_2 & & & \\ -k_2 & k_2+k_3 & -k_3 & & \\ & -k_3 & k_3+k_4 & -k_4 & \\ & & -k_4 & k_4+k_5 & -k_5 \\ & & & -k_5 & k_5 \end{bmatrix} \tag{4.18}$$

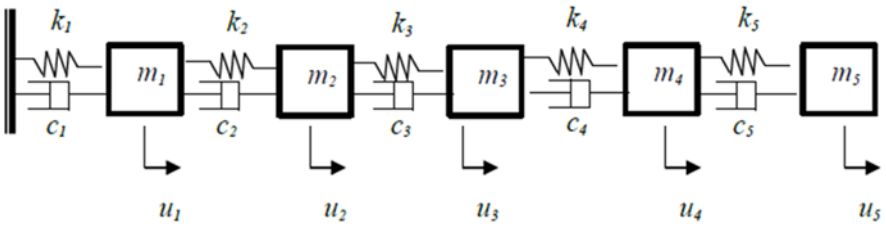

Figure 49. System Consisting of Lumped Masses, Linear Springs, and Dampers.

Even though it is easy enough to analytically solve the damping matrix, we will assume that it is unknown. Instead we use the dynamic response of the system, in order to construct the damping matrix, as would be the case in a more complex system. Using the predicted damping matrix, the system is again analyzed. The predicted dynamic responses are compared to the exact dynamic responses, which are obtained using the exact damping matrix. As we try to construct the damping matrix, we will use the damping model described above.

As the first case, the following data is used:

$$m_1 = 10,\ m_2 = 20,\ m_3 = 30,\ m_4 = 10,\ m_5 = 20$$
$$c_1 = 300,\ c_2 = 100,\ c_3 = 200,\ c_4 = 100,\ c_5 = 200$$
$$k_1 = 1x10^5,\ k_2 = 2x10^5,\ k_3 = 1x10^4,\ k_4 = 4x10^5,\ k_5 = 1x10^5$$
$$F_1 = F_2 = F_3 = F_4 = 0,\ F_5 = \begin{cases} -100 & t \le 5x10^{-4} \\ 0 & t > 5x10^{-4} \end{cases}$$

All units were assumed to be consistent. The matrix equation, Equation 4.15, was solved using the central difference scheme, which is explicit and conditionally stable.

The proposed two-stage damping model for this case is then given in terms of the calculated proportional damping values:

$$\begin{cases} \alpha = 8 & t \le 0.2 \\ \beta = 0.005 & t > 0.2 \end{cases} \tag{4.19}$$

The predicted velocity of the fifth mass is compared to the theoretical velocity in Figure 50. There is slight overshoot by the predicted response, but good agreement between the two, overall. When either only α or β values are used, the prediction does not agree with the theoretical result. Figure 51 and Figure 52 show the comparisons for these cases. Similarly, using both α or β values fails to produce an acceptable result as shown in Figure 53.

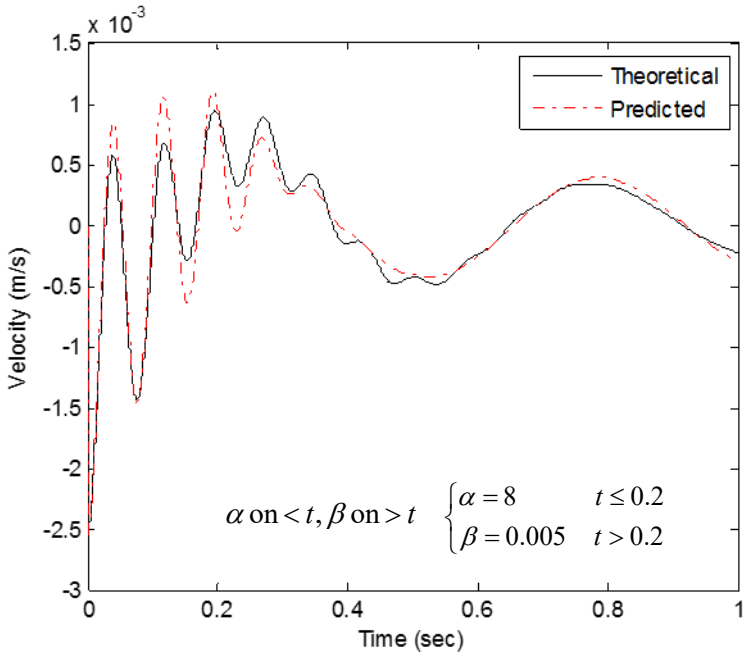

Figure 50. Comparison of the Velocity of the Fifth Mass with Proposed Two-stage Damping Model

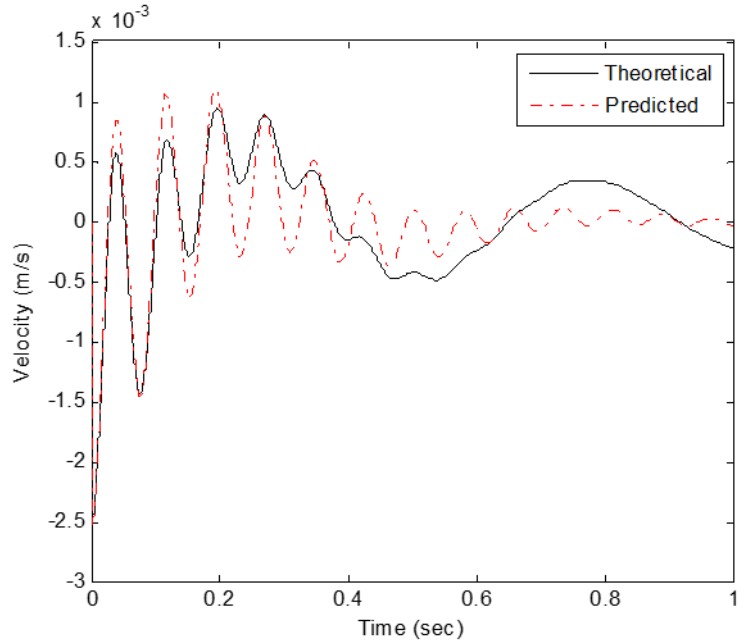

Figure 51. Comparison of the Velocity of the Fifth Mass with Mass Proportional Damping Only

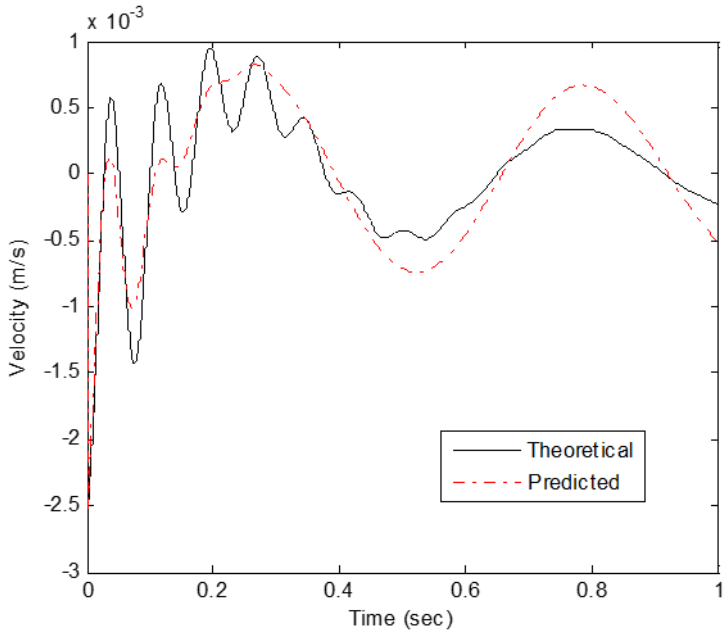

Figure 52. Comparison of the Velocity of the Fifth Mass with Stiffness Proportional Damping Only

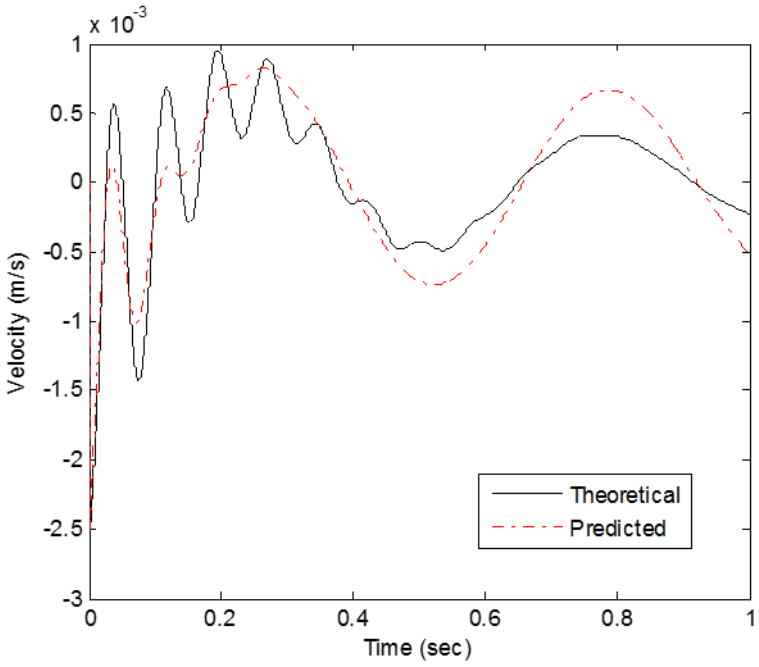

Figure 53. Comparison of the Velocity of the Fifth Mass with both Mass and Stiffness Proportional Damping Activated Over All Time

In order to demonstrate the multiple grouping of damping, the viscous damping constants were changed for the previous example while other variables were held constant with the same values as before. The new damping constants are then found to be $c_1 = 300,\ c_2 = 100,\ c_3 = 200,\ c_4 = 1000,\ c_5 = 2000.$

As shown earlier, the fourth and fifth dampers have damping constants with one order of magnitude higher than the rest. In this case, two groups are created; one group for the first three DOFs and the other group for the last two DOFs. The following damping values were used in this analysis.

$$\begin{cases} \alpha = 2.5 & t \le 0.2 \\ \beta = 0.015 & t > 0.2 \end{cases} \quad \text{for group 1} \tag{4.20}$$

$$\begin{cases} \alpha = 5.0 & t \le 0.2 \\ \beta = 0.02 & t > 0.2 \end{cases} \quad \text{for group 2} \tag{4.21}$$

For comparison of their responses to the theoretical results, node 3 is selected for group 1 and node 5 is chosen for group 2, respectively. As is evident in the examination of Figure 54 and Figure 55, the predicted results agree well with the theoretical data for the DOFs in both groups. Other examples corroborating the applicability of this updated damping model are found in [125], as is a discussion regarding negligible impact on critical time step size when incorporating this damping scheme while using explicit time integration solvers.

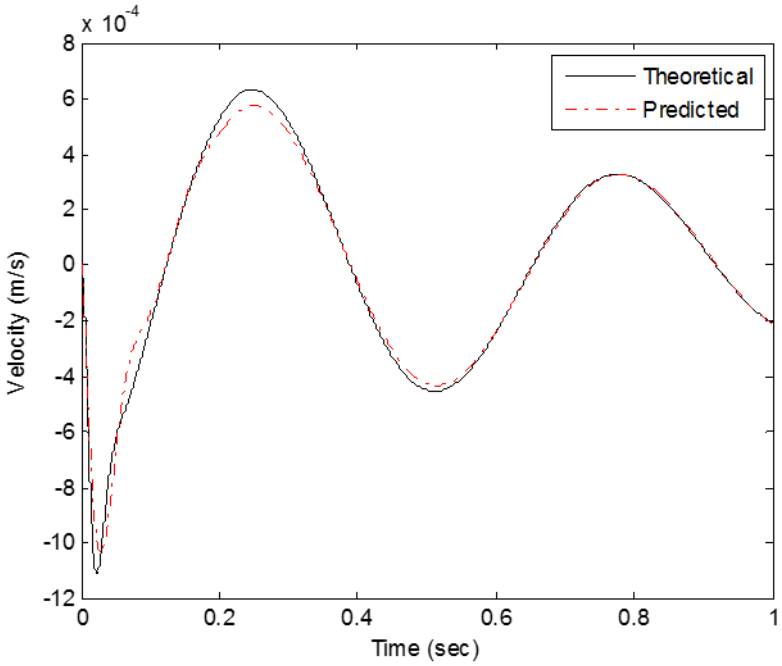

Figure 54. Comparison of the Velocity of the Third Mass in Group 1 with Two-stage Damping Model

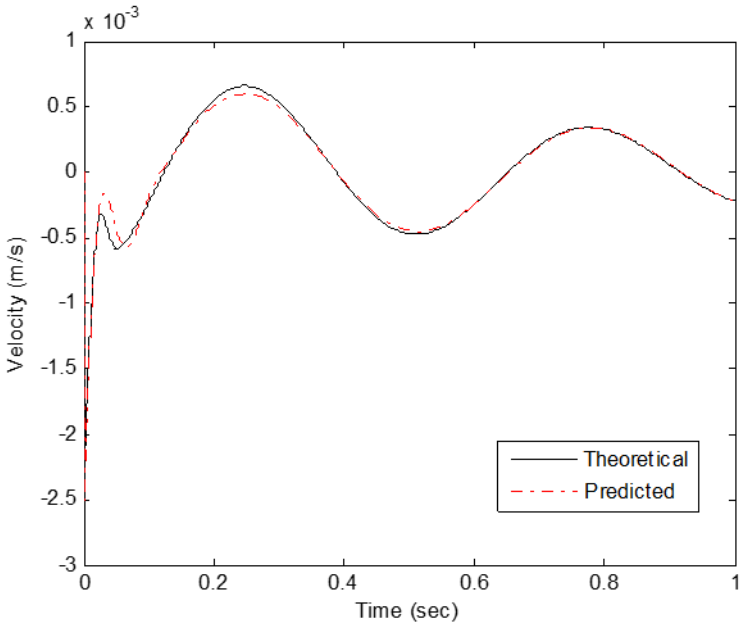

Figure 55. Comparison of the Velocity of the Fifth Mass in Group 2 with Two-stage Damping Model

d. Floating Shock Platform Study

Next the proportional damping method was applied to the UNDEX scenario using the FSP with DSF installed. Response data was obtained from a series of shock qualification tests that were conducted by NSWCCD at the Aberdeen Test Center, Briar Point Test Pond in Aberdeen, MD, in April 2012. This test series was carried out in accordance with MIL-S-901-D and is fully describe in [130]. The event was well instrumented, and the setup of the physical barge and corresponding model are shown in Figure 56 and Figure 57.

Figure 56. Floating Shock Platform with DSF Installed. Source: [130].

The FSP test case was chosen as a representative case in order to further investigate the updated damping procedure due to its simplicity and wide range of use in UNDEX testing. However, when the model was exercised with the proposed damping strategy it was found to be a somewhat impractical choice. Several damping mass proportional and stiffness proportional values sets (α, β) were investigated as well as the transition timing. The steady state response region, as shown in Figure 58 of the FSP velocity time history plot, was used to calculate a 0.163 damping ratio which corresponds to the first mode response of approximately 7–8 Hz, based on the log decrement measurement. A damping ratio of 0.15–0.18 was obtained from the result of the CEM solver.

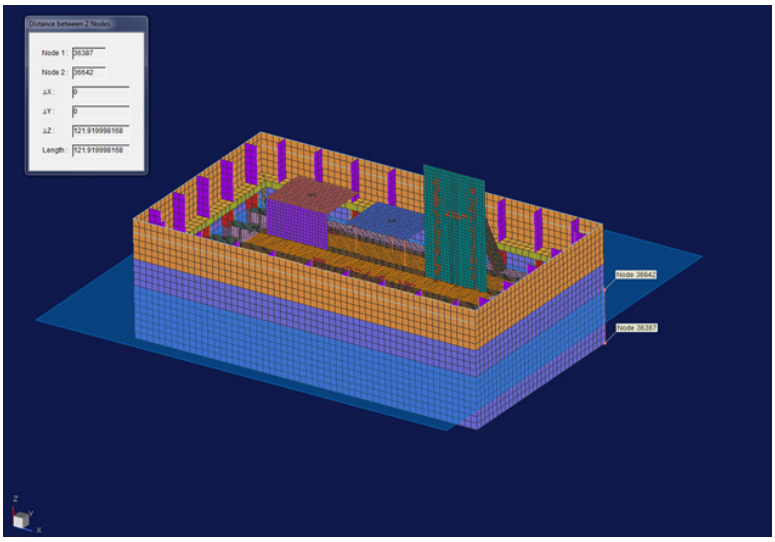

Figure 57. Finite Element Model of FSP Showing Waterline

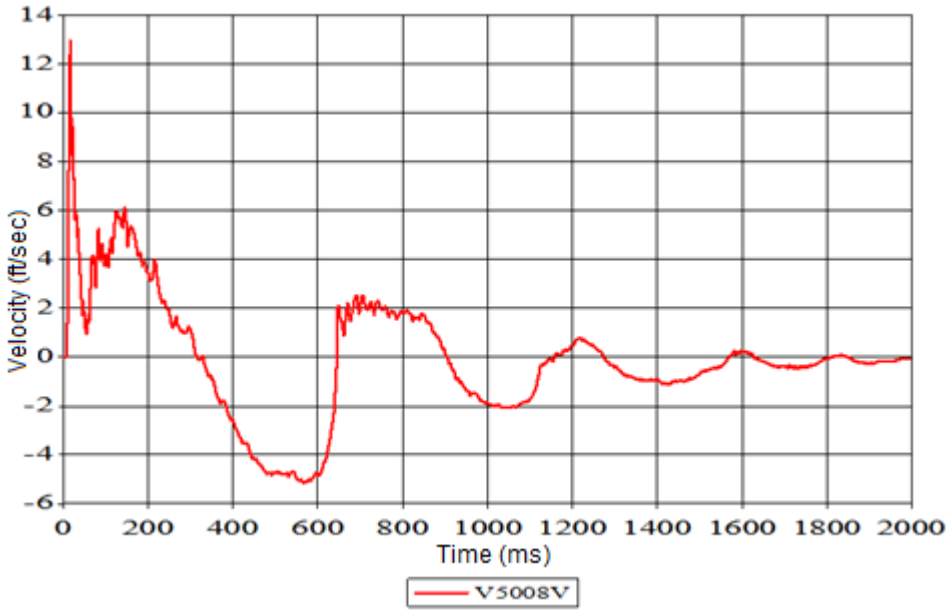

Figure 58. FSP Vertical Velocity Response Time History

Several locations were chosen throughout the FSP for analysis using the described method. However, comparison of the numerical and experimental data showed that the structure has only negligible damping. It was found that the undamped numerical model of the FSP agreed well with the experimental data. This suggested that the proposed damping model is not appropriate for application to the FSP structural model. Figure 59 provides a

sample comparison of the undamped numerical model and experimental result for a vertical velocity meter (V5004V) from the tests. The initial peak vertical response correlates well, but the numerical damping model fails to track once the damping has time to take affect at approximately 30 ms.

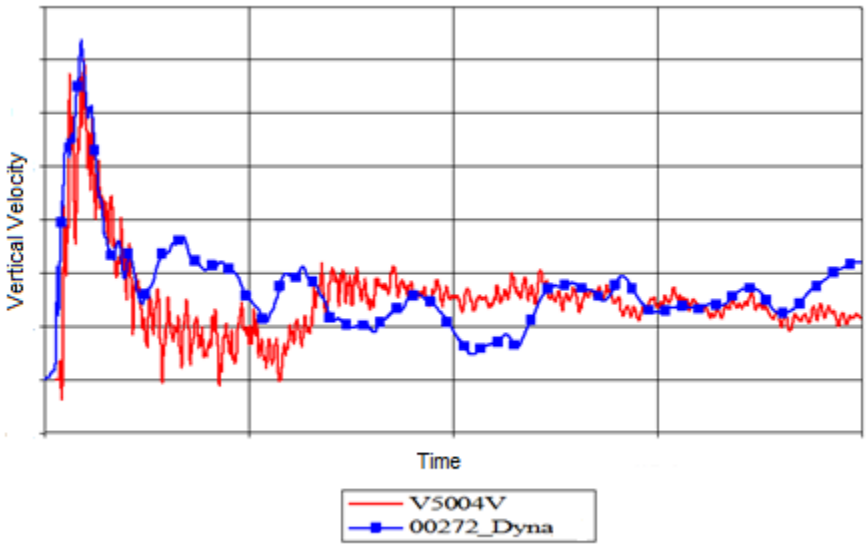

Figure 59. Comparison of Undamped Numerical Data and Experimental Result for FSP

e. Full Ship Study

Following the FSP study, a more extensive study utilizing a full ship model was completed in order to determine if the proposed damping method would be applicable in other ship models. The full ship shock model used for this purpose possesses a greater variety of damping mechanisms than the fairly uniform and rigid FSP. Details of this study are available in the supplemental data analyses.

3. Damping Model Summary

A modified Rayleigh damping method was proposed and evaluated using both analytical and experimental cases. The proposed damping technique applies to either mass

or stiffness proportional damping, α and, or β values, discretely applied during the respective time period of the response by way of T_o, the transition time parameter. This two-stage approach may be applied successively through the duration of the dynamic response based upon the loading input. This is of special interest for UNDEX where the excitation has many components such the initial shockwave, cavitation closure and bubble pulsation which occur at different times. The selection of damping coefficient values may vary from section to section of the structure if damping is not uniform within the structure. Similarly, the transition time may be adjusted for different sections within the structure, as it is tied to the time of shock front arrival.

Determination of the proper proportional damping values is based on previously known values or derived from the use of numerical techniques such as the complex exponential method applied to experimental data. The optimal transition time is suggested such that the mass proportional damping is deactivated in the model shortly after the initial dominate peak response is reached. By doing so, this preserves the late time response.

C. REDUCED ORDER STRUCTURE MODELS

This section describes the various structural models that were used in the preliminary studies supporting equipment cabinet failure criteria development. While detailed equipment models may exist in some instances, the use of reduced order models is desirable as a means of minimizing modeling costs as well as simulation run time.

1. Representative Equipment Model

There were four main types of equipment model representations used in this work. The detailed shell model, two-part rigid body model, simple rigid body model and spring mass model, as illustrated in Figure 60, provided a framework for the equipment model simulations and numerical experimentation. Several versions of each were created to facilitate certain aspects of the research, such as mass effects, stiffness effects, center of gravity (mass distribution) variations and others.

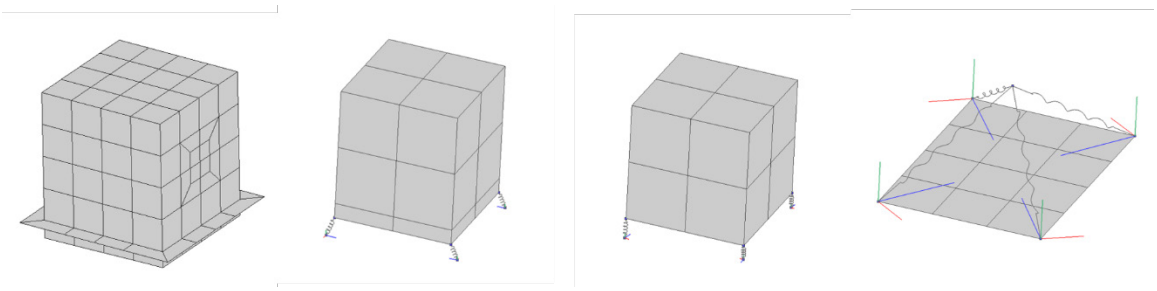

a) Detailed Shell, b) Two Part Rigid Body, c) Simple Rigid Body, d) Spring Mass.

Figure 60. Equipment Cabinet Models of Varying DOF

2. Equipment Cabinet Model

A series of equipment models were generated for the FEA based on a standard shipboard electronics equipment cabinet. These models included coarse and refined shell elements, models with and without deck mounting (foundations), spring isolation equipped models and models directly mounted to the deck. Figure 61 provides an exterior view of the final version of the equipment cabinet model with functional failure model (not visible) and explicitly modeled deck foundation. This model was the primary model used in the FSP and full ship study analyses.

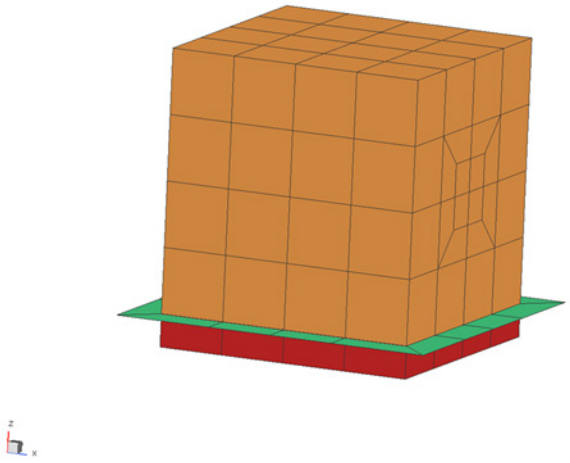

Figure 61. Coarse Mesh Equipment Case Shell Model

3. Rigid Body Model

The rigid body model with spring isolators attached at the bottom corners of the equipment case, as shown in Figure 62, was also investigated. The mass was made consistent with that of the detailed shell model by varying the density of the material. Additionally, the center of gravity was adjusted to match that of the detailed shell model, Figure 61, by using a second rigid body mass of a different density and affixed to the base through a fixed interface in order to compensate for the offset in height and mass of the foundation. The spring isolator values provided consistent stiffness with the other models.

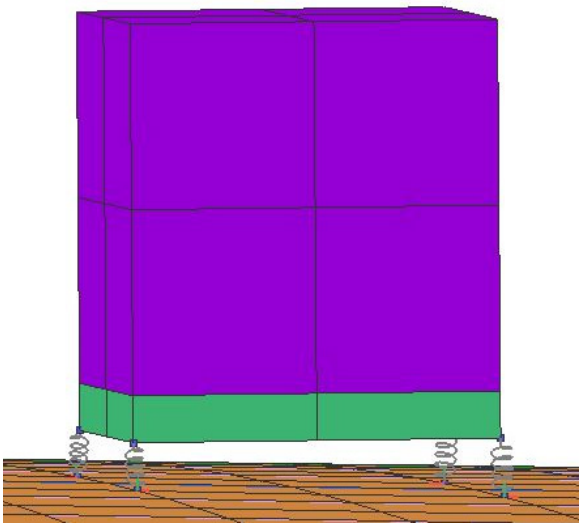

Figure 62. Rigid Body Model with Spring Isolators

4. Spring Mass System Model

A simple spring mass model was also created for analysis and is illustrated in Figure 63. Again, the model stiffness and center of gravity were persevered in relation to the other models through the use of specified spring constants and prescribed nodal mass at the appropriate height above the deck.

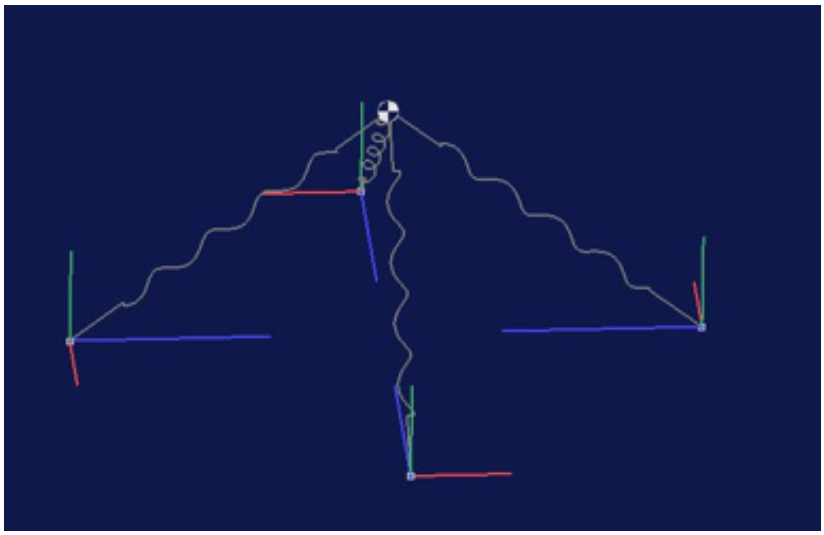

Figure 63. Simple Spring Mass Model

5. Shock Test Platform Models

The FSP, LWSM and a retired naval surface combatant model were used as the shock test platforms in these modeling and simulation analyses.

a. LWSM

A FEM model was created to represent the LWSM based on the fixture drawing from reference [42]. The major components of the model are the backing plate, channels, attachment plate and impactor. Dimensions and materials of the model are consistent with construction and testing standards for the LWSM. The complete model, with simple spring mass system affixed as a represented test article is shown in Figure 64. The impactor has a mass of $1.71e^5$ g (nearly 400 lb) with an initial vertical velocity of 215 cm/s (approximately 86 in/s) and is striking the backing plate from the Z direction, as depicted in Figure 65, in accordance with [42].

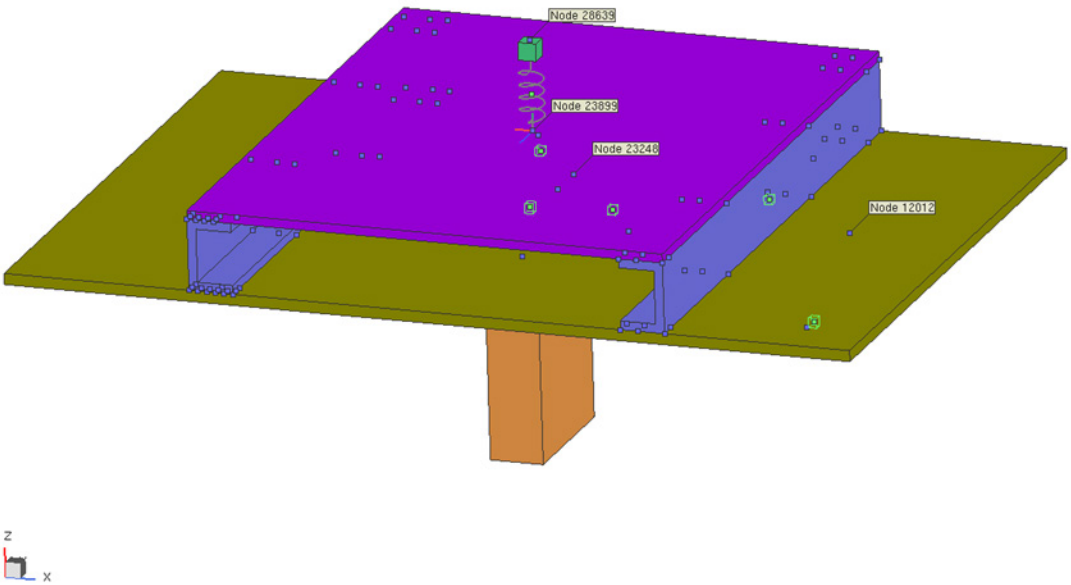

Figure 64. LWSM Model with SDOF Equipment Model

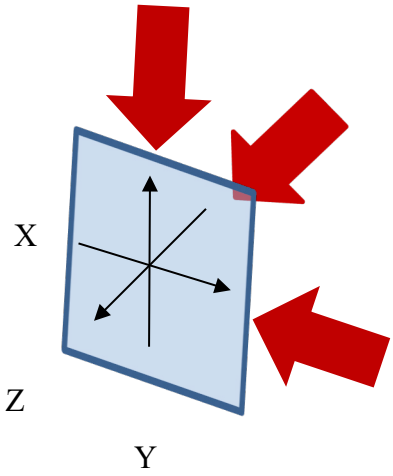

Figure 65. Application Direction of Impacts to LWSM

The nominal response of the LWSM model was verified using the SDOF system and observation of the displacement, velocity and acceleration, as shown in Figures 66–68.

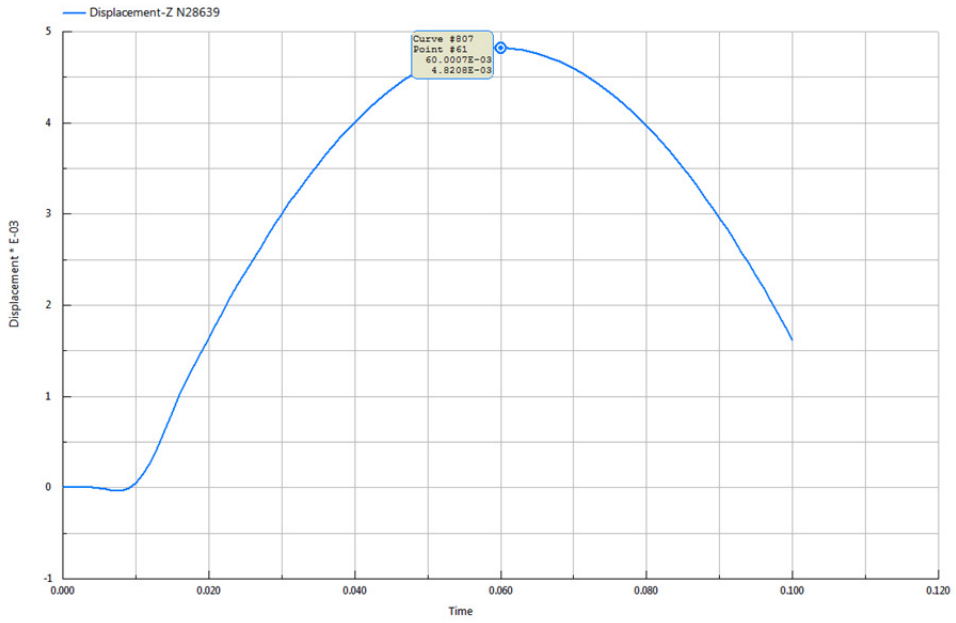

Figure 66. Vertical Displacement Response of Spring Mass System during LWSM Simulation

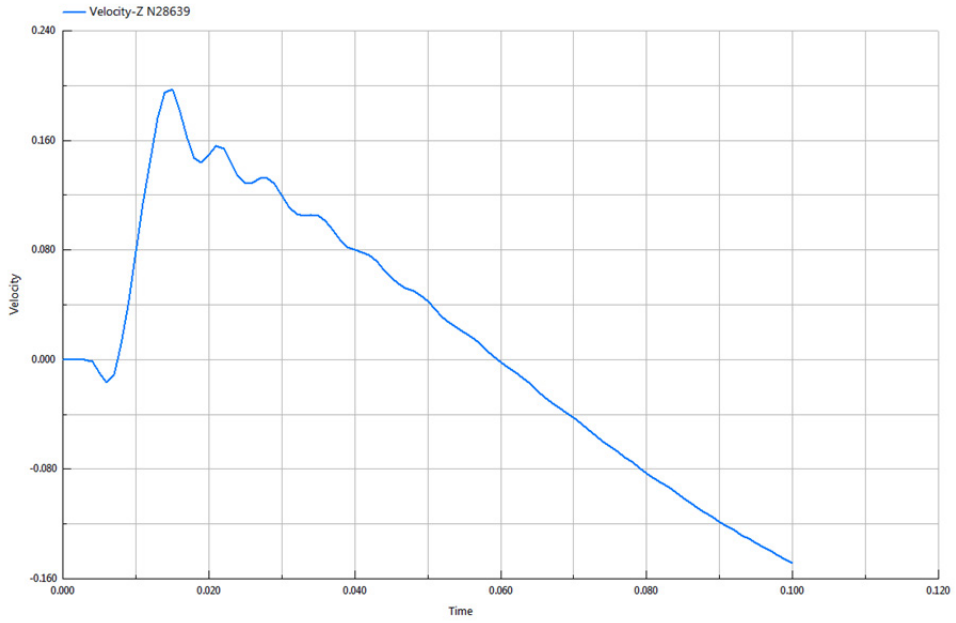

Figure 67. Vertical Velocity Response of Spring Mass System during LWSM Simulation

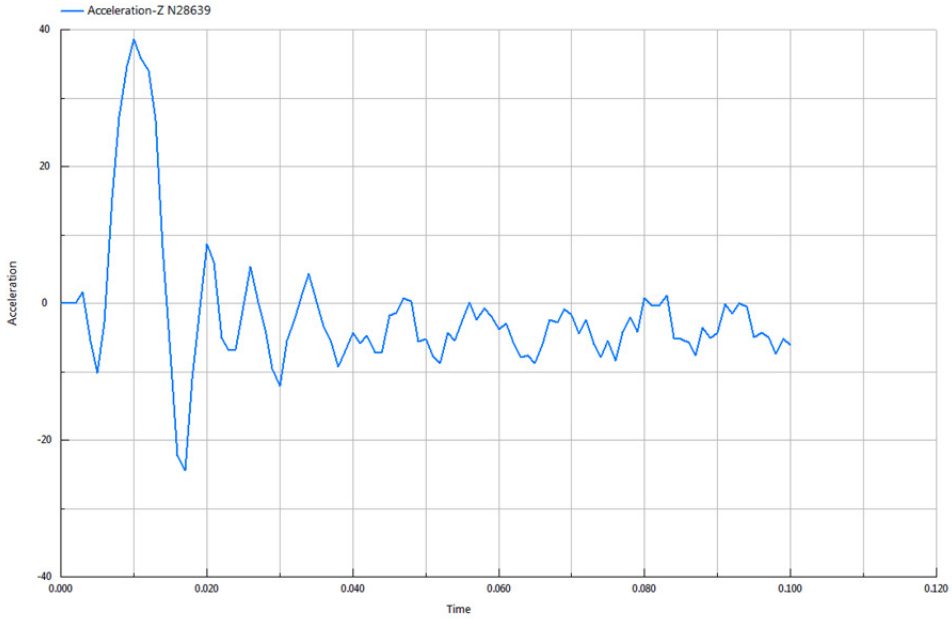

Figure 68. Vertical Acceleration Response of Spring Mass System during LWSM Simulation

Figures 69–72 represent select vertical displacement response plots during the simulation. Plots for 5, 25, 50 and 75 ms are included. The color fringe indicates displacement values, the blue to yellow colors are in the negative direction, while the orange to pink colors are in the positive direction. The impactor is observed to move away from the back of the strike plate as the time after impact increases. The edge of the LWSM model is constrained.

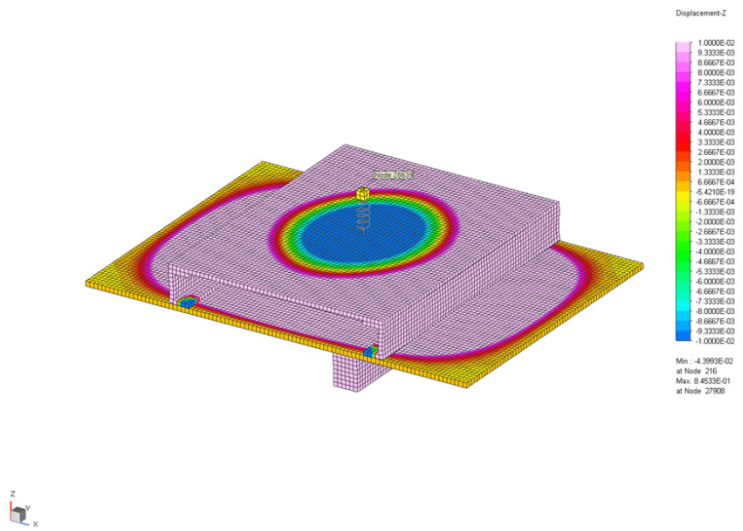

Figure 69. Vertical Displacement Response at Time = 5 ms

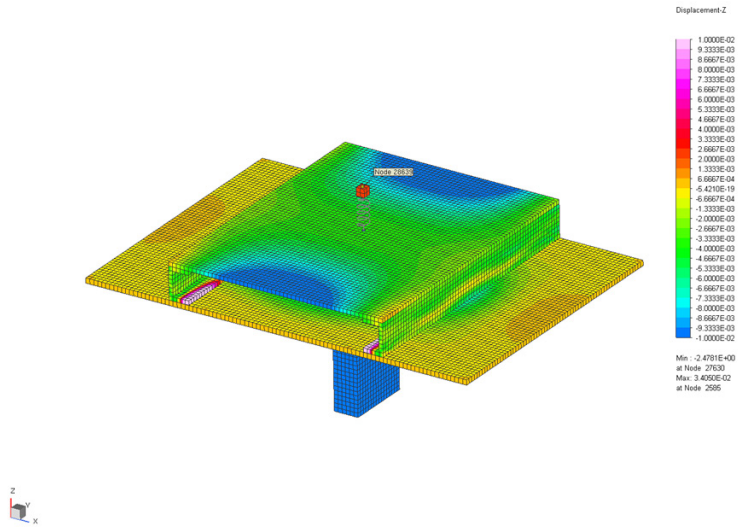

Figure 70. Displacement Response at Time = 25 ms

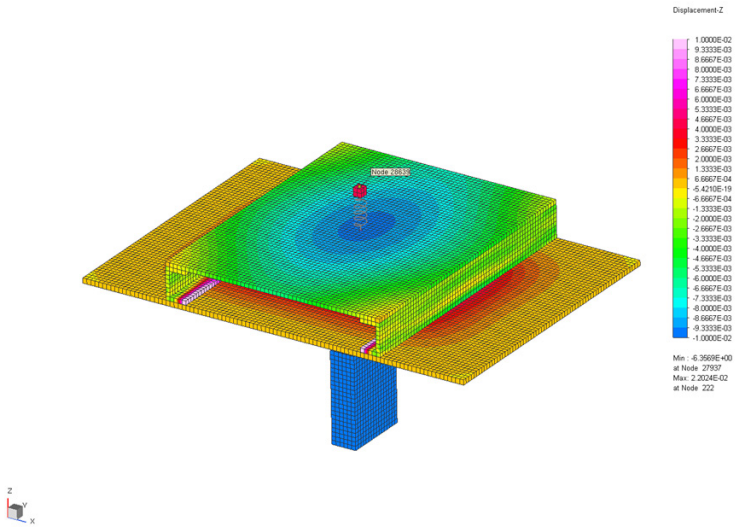

Figure 71. Displacement Response at Time = 50 ms

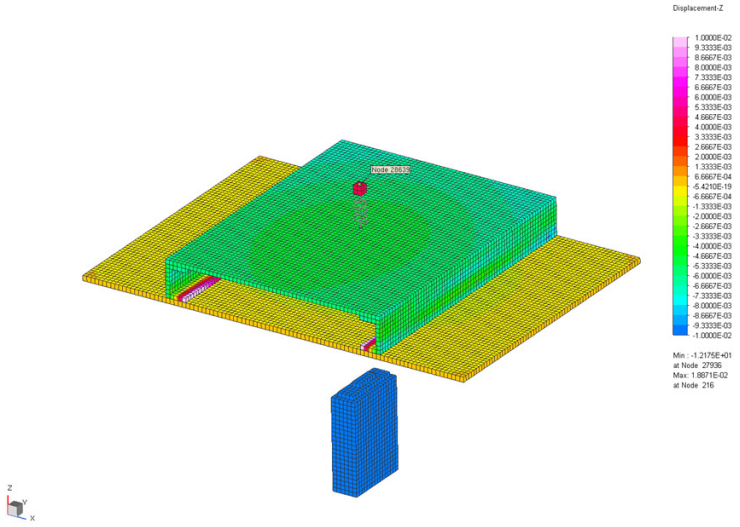

Figure 72. Displacement Response at Time = 75 ms

The equipment case detailed shell model was also analyzed using the LWSM model. Figure 73 displays the setup of the LWSM model with the equipment cabinet model.

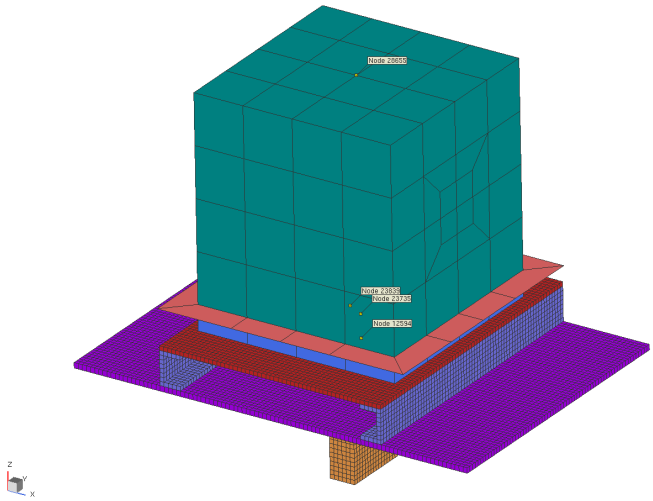

Figure 73. LWSM Model with Detailed Shell Equipment Case Model

The following plot, shown in Figure 74, is of the base plate structural velocity response at the point opposite of the impactor. The two models, the point mass (blue) and the detailed shell model (red) are compared. While the initial peak and early time response matches well, the oscillatory nature of the point mass dominates the response and dampens out smoothly as a result of the spring constant (stiffness) that was applied from separate modal analysis of the equipment model. It was determined that the detailed model, which partially extended over the car channels supports has additional input to the system via local interaction in contrast to the cleaner response of the spring mass system located at the center of the place. As the transient response dies out the low frequency test plate global motion dominates. Subsequent simulations using the LWSM model concentrated on the reduced order spring mass model vice the more detailed shell model for this reason.

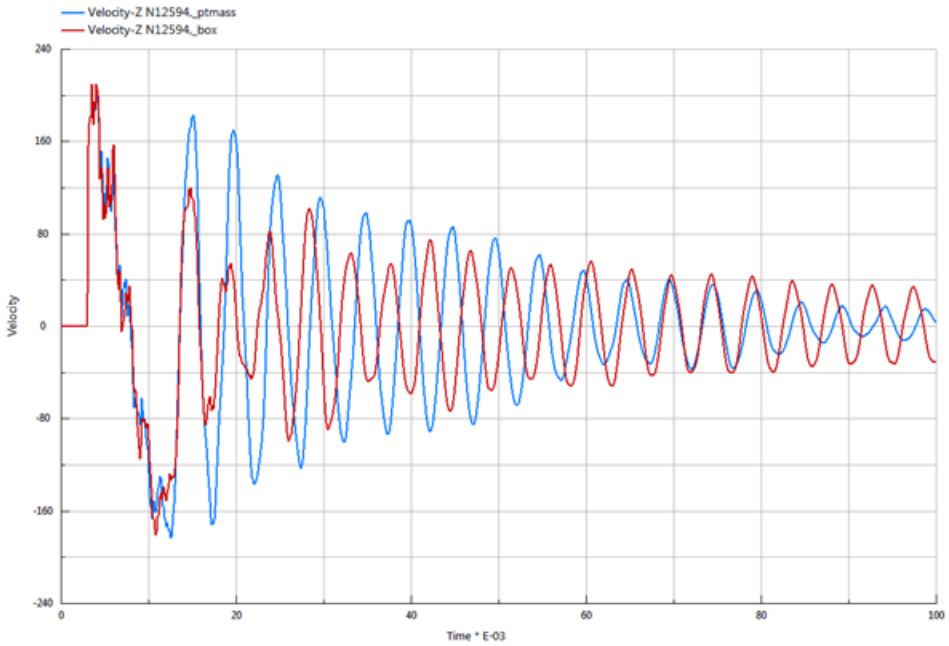

Figure 74. Comparison of Input Loading Response on LWSM Backing Plate

b. Ship Shock Models

Details regarding the FSP and full ship shock FEM models are found in the supplement data analyses.

THIS PAGE INTENTIONALLY LEFT BLANK

V. FAILURE ASSESSMENT PROCESS

The U.S. Navy has practiced shock hardening of ships ever since the unfortunate realization of unexpected losses and unanticipated mission kills resulting from near misses. A means by which to address these failures is necessary. Thus, in this chapter, first the method of failure determination is established. Next the equipment response is analyzed for trends from the collected data. Then new failure criteria are proposed. And finally, additional influences on the failure criteria are investigated.

A. INVESTIGATION OF FAILURE VIA MODELING AND SIMULATION

The LWSM, standard and tuned deck FSP, and a full ship shock models were used to represent platforms for different shock loading translated to the shipboard equipment models. The LWSM was a locally generated model based on MIL-S-901-D specifications provided to all equipment vendors. The FSP models were existing shock models provided courtesy of NSWCCD. The full ship model used is a verified and validated ship model employed in several extensive series of UNDEX modeling and simulations projects.

1. Equipment Models

The equipment case model was investigated in many variants. Some of these were detailed shell models with the cantilever beam system representative of functional failure, while others were rigid body mass models, and even single degree of freedom simple spring mass systems were used in these analyses. Additionally, the mounting of these models to the ship deck or test platform was varied as well. Shock isolation mounts modeled as simple springs, detailed deck foundations, spot weld constraints and direct attachment to the deck were all options considered by the various models depicted in Figure 75, which gives a visual summary of all model combinations explored.

The upper row in Figure 75, variants a-d represents the detailed shell model of the equipment case including the cantilevered beams representing the functional test. Several versions of the basic model with refinements in mesh density were initially investigated with a nominal 7.62 cm (3 in) or 15.24 cm (6 in) uniform mesh was ultimately found to be

satisfactory for the purposes of this investigation. The middle row of Figure 75, variants e-h, represents the different combinations of rigid body elements that were used throughout various studies related to this work. The yellow to blue color change denotes two rigid body masses of different densities tied together at a common interface to represent the equipment case and foundation in variants g and h. The bottom row of Figure 75, variants i-k, represents the simple spring mass models that were used in this to approximate the higher fidelity detailed equipment case models as a reduced order model.

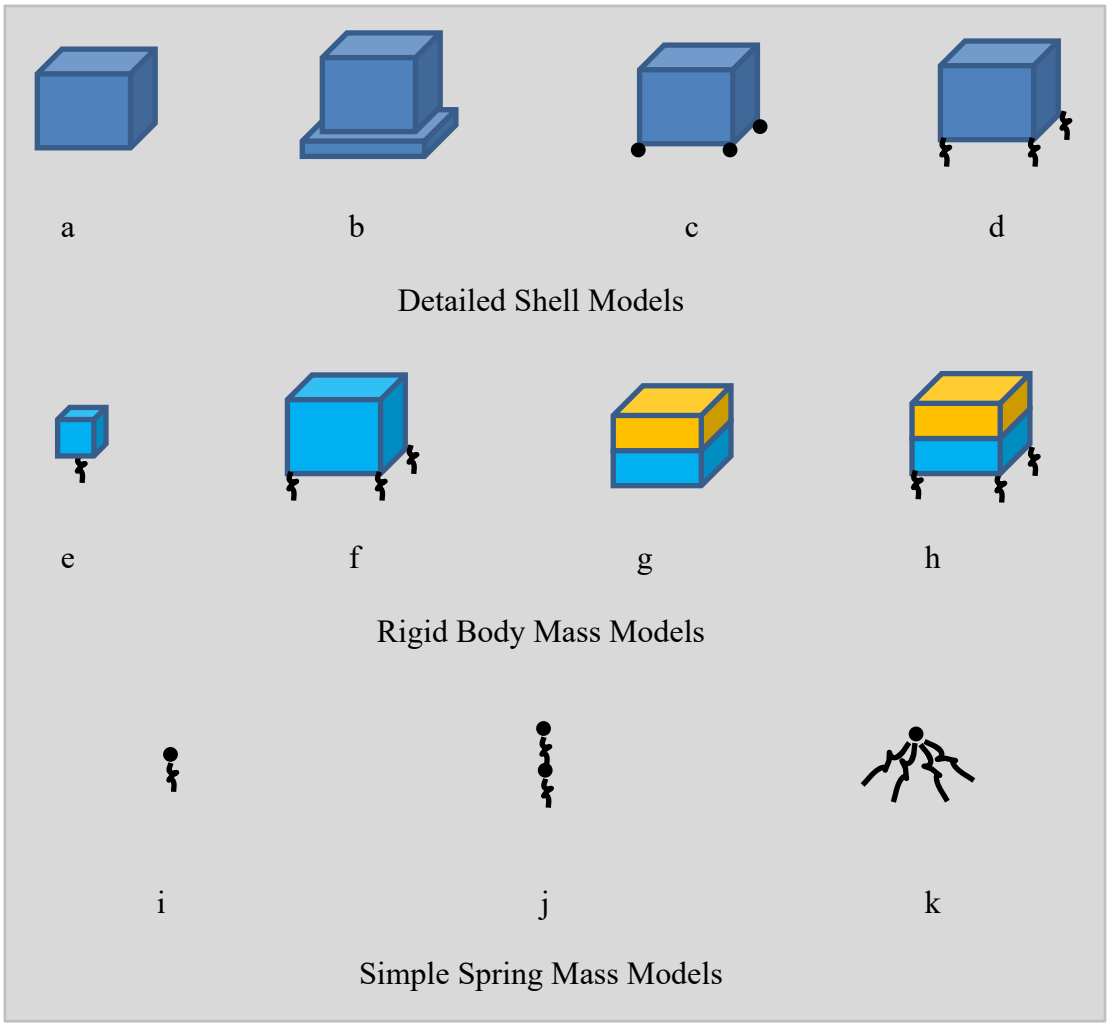

Figure 75. Equipment Case Model Variants

The finite element shell model of the full equipment case is shown in Figure 76. The version of the model illustrated here was created with a uniform 15.24 cm (6 in) mesh and included an explicitly modeled deck mounting (foundation). The dual cantilevered beam "test system" to be used for determination of functional failure is also modeled using shell elements but with a finer 7.62 cm (3 in) mesh, and a spring attachment near the free end of each of the beams which were separated by 7.62 cm (3 in). The beams possessed different stiffness properties in which the lower, shorter beam was much more rigid that the upper beam. Both were attached at opposite ends of the equipment case, near the center of side panel. No beam elements were used in the construction of this model.

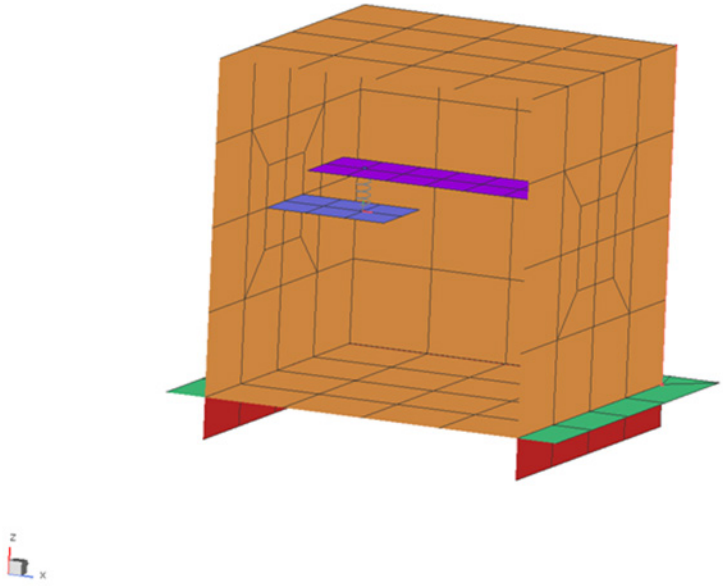

Figure 76. Equipment Cabinet with Functional Failure Model and Foundation

In each case the reduced order model was matched to the detailed shell model. Modal analysis was performed in ABAQUS [131] in order to determine the natural frequency of the equipment case, cantilevered beam setup, deck foundation or other components and configurations. From these analyses and fast Fourier transform (FFT) of the simple spring mass system acceleration time histories at different weights, a fundamental frequency was found to be approximately 120 Hz for the simple box case and

approximately 140 Hz for the box and accompanying foundation. The cantilevered beam setup was included in both determinations. Additional details regarding the modal analysis for these models are available in Appendix C.

As an example, variant h (from Figure 75) of the equipment case model, which models the equipment case and foundation using a two-part rigid body mass and spring system is used to demonstrate the process. With a system mass of 1.33875e^5 g, using Equation 5.1, a spring constant, $k_{spring} \approx 26.6e^{10} \frac{g}{\sec^2}$ was calculated for each of the four springs

$$f = \frac{1}{2\pi}\left(\sqrt{\frac{k}{m}}\right) \tag{5.1}$$

when the frequency, *f*, was taken as 142 Hz.

2. FSP Studies

The equipment case was tested on the FSP. A series of simulation runs were made at different standoff distances approximating the typical FSP test schedule. Test geometry was set as previously described. Figure 77 is provided for reference to the location of the test article, deck, and explosive source in the standard FSP barge configuration. Figure 78 is an example of the vertical displacement and pressure loading of the coupled model.

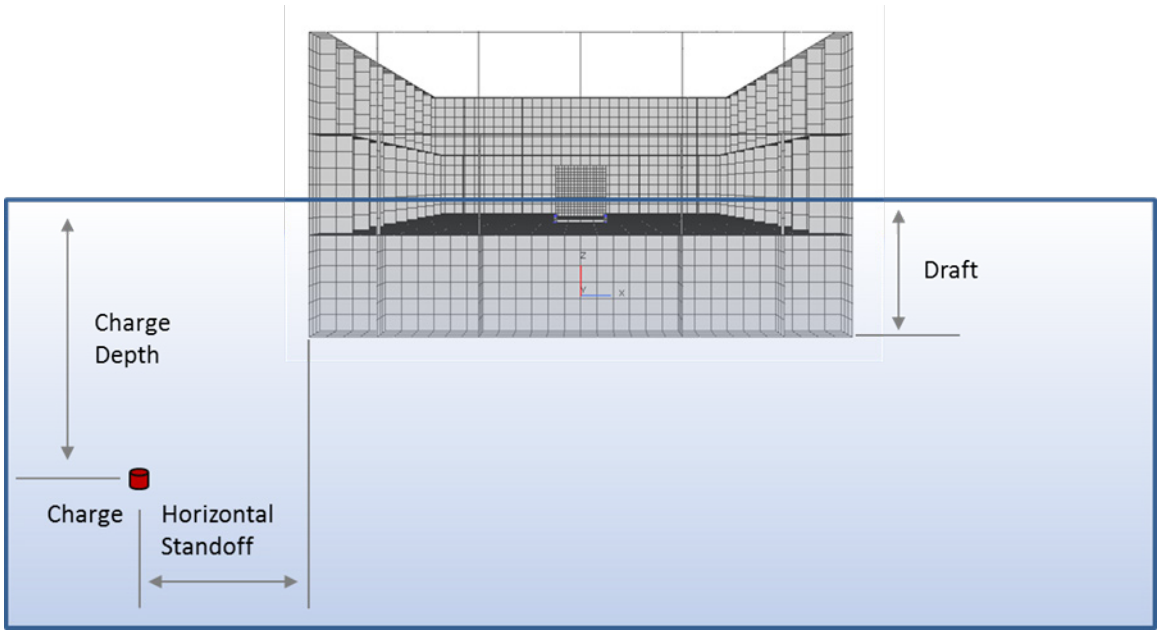

Figure 77. Floating Shock Platform Test Geometry

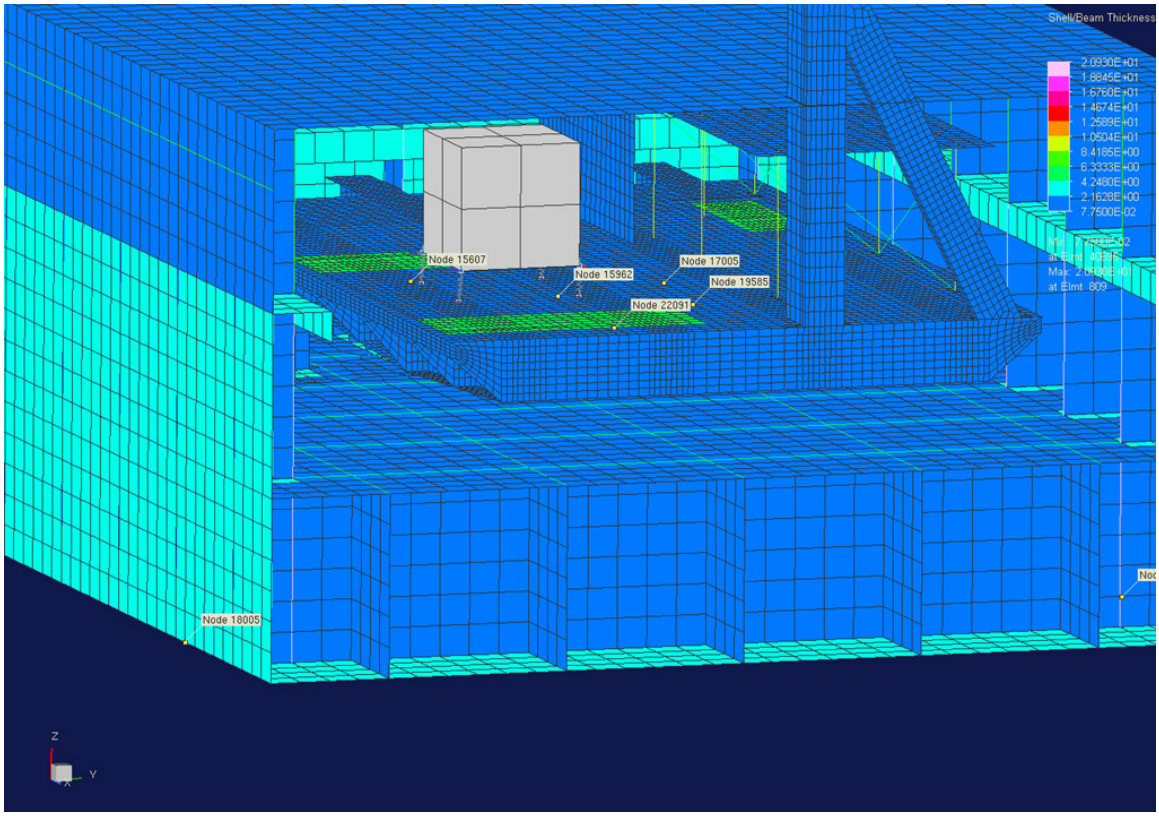

Figure 78. Simulation of Equipment Model on FSP

Further details and analyses regarding the FSP studies are provided in Appendix C.

3. Ship Studies

Details for the ship studies are provided in the supplemental data analyses.

4. Equipment Model Variants

Throughout the investigations, various model variants from Figure 79 were considered. Figure 80 illustrates how a similar case from [42] is depicted with the cabinet structure, foundation, hard mounted and isolated components and subassemblies.

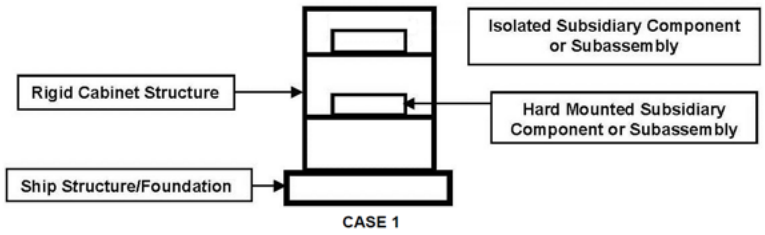

Figure 79. Equipment Cabinet Example Case. Source: [42].

A brief description follows of each model and setup, while full details are found in Appendix B.

a. Deck Spring Isolator Mounted

Direct mounted variants of the model were compared with spring isolator mounted equipment. The spring isolator values were selected based on modal analysis results.

b. Foundation Mounted

Comparisons were conducted with the mass directly mounted to the deck, spot welded and mounted using a typical equipment foundation design.

c. Rigid Body Mass

A study was conducted to examine the potential of using simple rigid body models in place of the fully modeled equipment case and critical component. All 15 detailed box

models in the full ship structural model were replaced by a simplified spring mass model. The model was constructed from two rigid masses to ensure that the mass of the foundation, and case, were properly distributed. Four springs with a stiffness representing the foundation elasticity were placed between the rigid box model and deck at a distance of approximately 7.62 cm (3 in) in the vertical direction.

The analysis presented here is for the amidships location, however all three longitudinal locations were compared with similar results. Figure 80 shows that the loading and response for a hull reference node are nearly identical for both the detailed shell model (blue) and the rigid body model (red) vertical acceleration time histories from the full ship shock simulation.

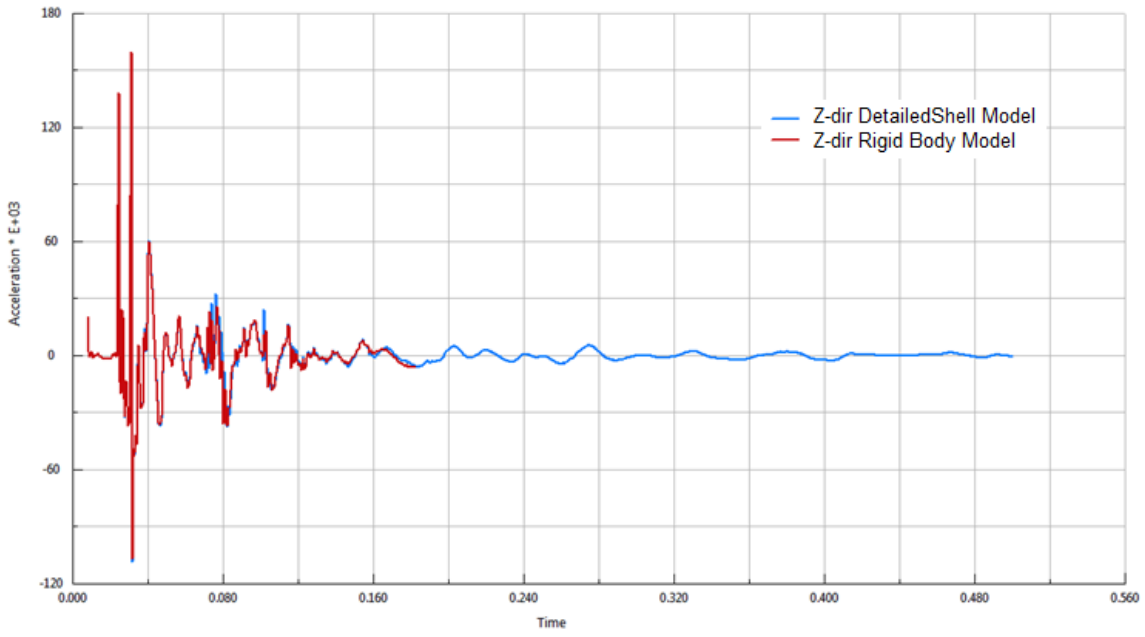

Figure 80. Verification of Loading on Ship Using Hull Reference Node

It was found that the response of the top center node on the equipment case was in line with that of the same node location on the rigid body spring mass model. Figure 81 and Figure 82 illustrate the minor differences in vertical velocity response for sample locations within the ship. First the detailed shell equipment model (blue) is compared with

the two-part rigid body mass model (red) in Figure 81. The rigid body model precisely matches the first peak and does well in matching the subsequent peaks, though not exactly.

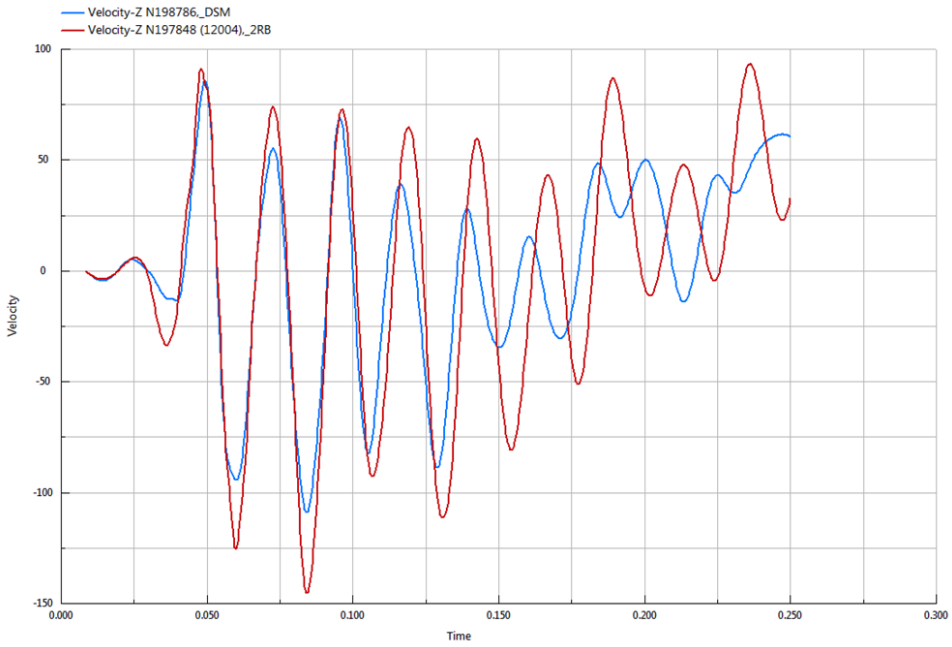

Figure 81. Velocity Response Comparison of Detailed Shell Model and Rigid Body Mass Model

In Figure 82 we find that the simple reduced order spring mass model (red) nearly matched the vertical velocity response of the detailed shell model (blue) over the entire 200 ms time history. Together these two results and others from the data set from throughout the ship indicate that the use of a properly specified reduced order model is permissible.

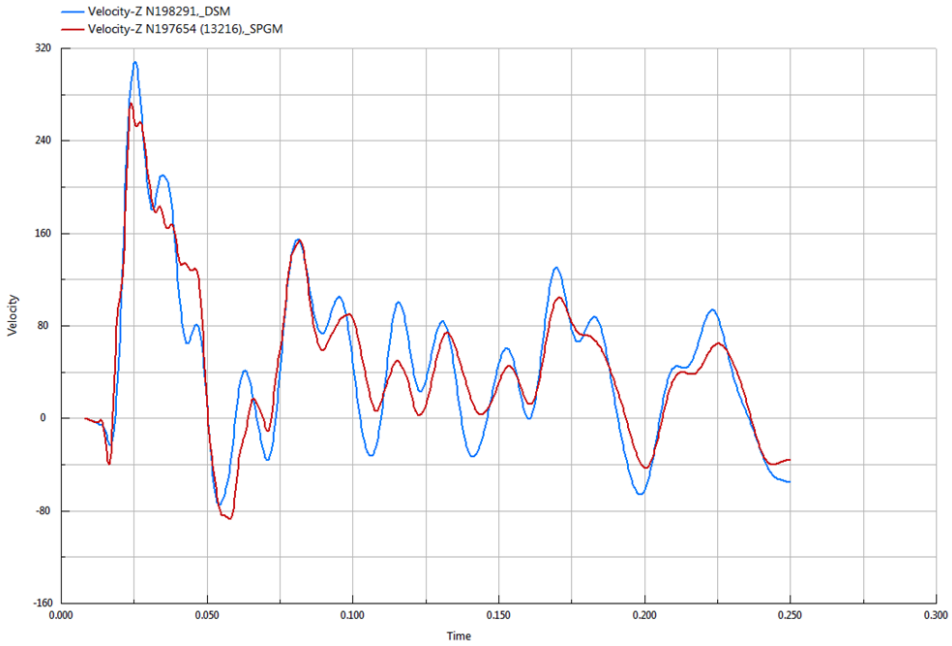

Figure 82. Velocity Response Comparison of Detailed Shell Model and Spring Mass Model

B. ANALYSES OF FAILURE PARAMETERS

Since different shock qualification tests result in various excitations, which may not be representative of the *actual* loading on the shipboard equipment subjected to UNDEX in a combat environment, there needs to be a way to connect these together in a common manner. Once a validated numerical model representing the equipment is available, functional failure against a recognized standard is required; something akin to the material failure assessment which is necessitated by any discussion of shock qualification.

Extensive amounts of data were collected in the FSP, full ship and reduced-order model studies. So, what is to be used as a method of comparison between tests, response parameters and ultimately as a criterion?

1. Functional Failure Determination

Functional failure was used as the initial pass or fail criterion. The assumption was also made that the equipment case, foundation and other components would not fail due to

engineering material properties such as stress, strain, etc. These values were not of particular interest in the current study, but all collected data has been retained for future efforts complimentary to the present one in order to reinforce the results.

Observation of the motion of the upper and lower beam tips from Figure 76, was utilized in order to determine whether the component failed. If the relative position of the cantilevered beam tips overlapped, they were determined to have made contact, and thus failure occurred. In Figure 83 careful inspection shows that the much more flexible upper beam oscillating at a frequency of approximately 12 Hz nearly strikes the much more rigid lower beam which is deflecting very slowly at an approximately 1 second period. While the minimum relative position of the two beams comes close throughout the time history as they respond to the shock input loading at the base of the FSP, the dashed circle highlights the time around 0.1 s where failure nearly occurred. Comparing this time history plot where no failure occurred with the identical model setup at a slightly closer 5.49 m (18 ft) horizontal standoff distance vice the 6.1 m (20 ft) horizontal in Figure 83, we find that contact is evident in Figure 84. Inspecting the overlap of the two curves representing the upper beam (red) and the lower beam (blue) within the dashed circle, we find that failure is determined to occur at time 0.09 s.

It should be noted that the data past this point in time is unreliable and was not used in the analyses since the fully elastic nature of the shell elements is not representative of the physics occurring within the physical material at and beyond the point of first contact. Evaluation of the potential damage occurring within the model, and thus by association, the actual component that is being represented here, is not the focus, nor at all necessary as the instance of failure is used to definitively mark the failure threshold. It must be stated that the use of the dual offset cantilevered beams is not unique in quantifying the functional failure that occurs. That is to say, it is not the only type of test that can be used. Many other types of functional failure tests could be implemented to exact a comparable result. In fact, one of the elements necessary to the successful application of this approach is to tailor the functional failure test to the critical component within the shipboard equipment or system.

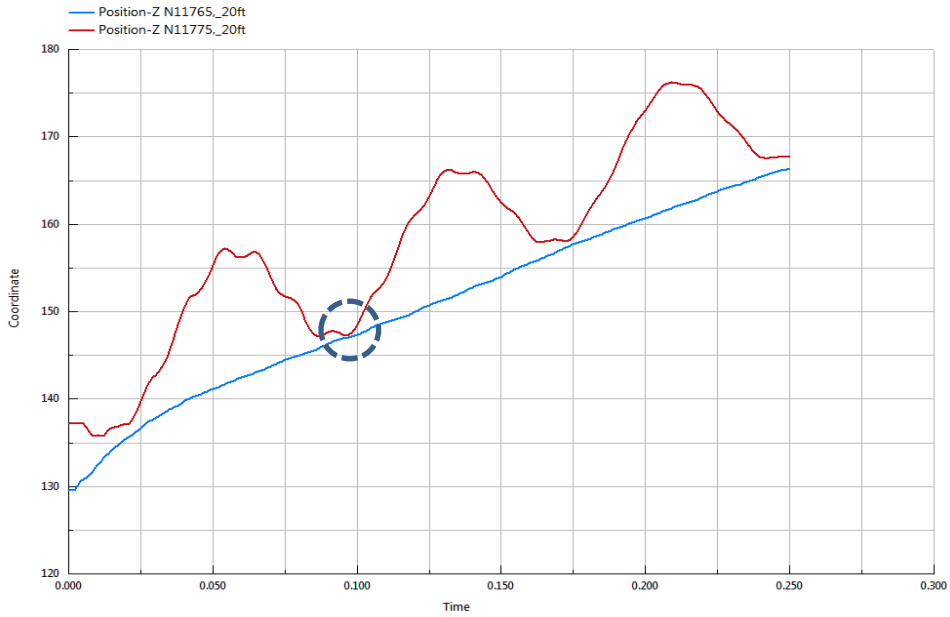

Figure 83. FSP Non-failed Equipment Model

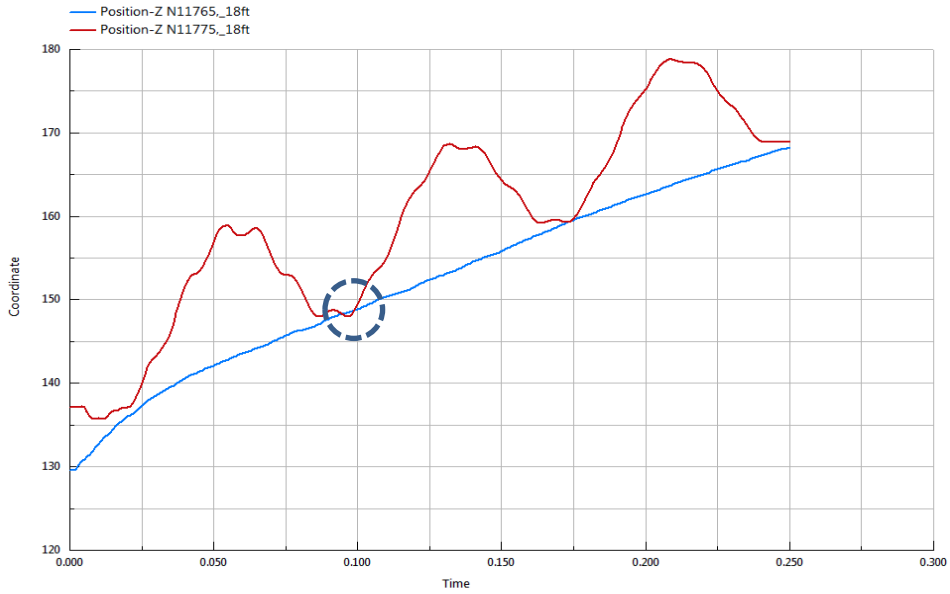

Figure 84. FSP Failed Equipment Model

The use of a contact point failure stems from the original idea to look at failure of electronic components mounted on a PCB within a mission essential piece of equipment. Figure 85 depicts a hypothetical but thought-provoking scenario, where a capacitor with some significant mass mounted to a PCB may layover due to repeated oscillation while responding to a shock load, making contact with another component on the board and create a short, causing an unplanned electrical discharge and ultimately functional failure of that component, equipment or system. Similar concepts for functional failure models such as a simple piston model for fluid dynamic failure modes can be conceived and modeled via finite element methods for real world issues related to extreme shock loading such as surge in mass flow rate through piping systems. Hence mechanics, fluid dynamics, and other failure mode types can be approximated given some consideration to their physics and the issue experienced in past equipment failures under shock loading.

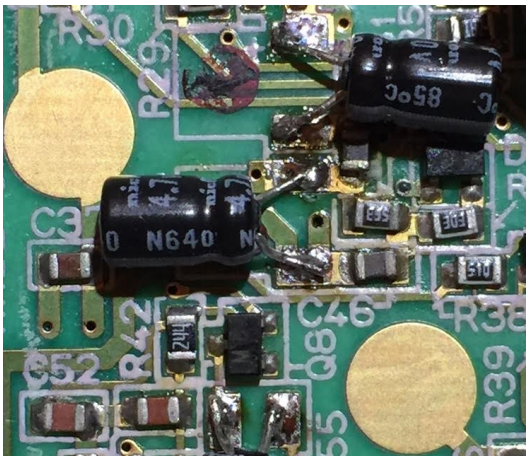

Figure 85. Bent Capacitor on PCB with Damaged Connection Point. Source: [132].

2. Equipment Response Correlation

Once the failure mode, failure mechanism and instance in time are identified and modeled correctly, the next task is determining what response, or combination of response factors can definitively describe the equipment characteristics at the point of this functional failure. Acceleration, velocity, and displacement are the naturally candidates in this pursuit.

Motion can be described in terms of acceleration, velocity or displacement of an entire mass or just the location of interest within a body. The familiar equation of motion,

$$m\ddot{x}(t) + c\dot{x}(t) + kx(t) = f(t) \tag{5.2}$$

relates the motion of the mass, with damping and stiffness through the acceleration, velocity and displacement as a result of a forcing function, *f(t)*. In the case of shock loading, such as discussed herein, Figure 86, is applicable as it also includes the shock loading as impact with a rigid base, *z(t),* and the response motion of the mass, *x(t).*

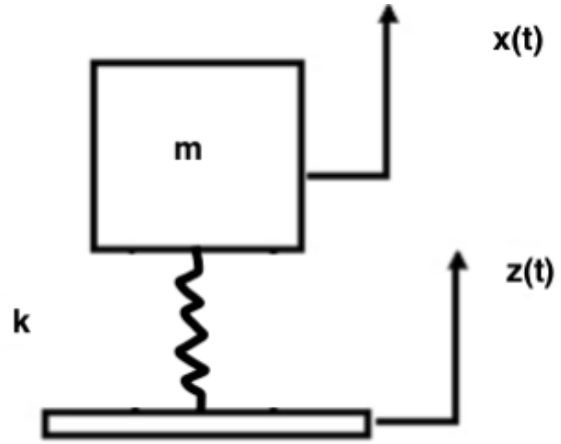

Figure 86. Single Degree of Freedom System

Looking at the response motion of the mass subjected to the base input motion, and neglecting system damping, for now, the equation of motion becomes

$$\begin{aligned} &m\ddot{x}(t) + c\dot{x}(t) + kx(t) = kz(t) \\ &let\ x(t) = y(t) + z(t) \\ &m\left[\ddot{y}(t) + \ddot{z}(t)\right] + k\left[y(t) + z(t)\right] = kz(t) \\ &m\ddot{y}(t) + ky(t) = -m\ddot{z}(t) \end{aligned} \tag{5.3}$$

where y*(t)* is the relative motion between the base input and the response of the mass.

From this we see the time and position are key in describing the motion response. Based on Newtonian Mechanics during our testing or numerical experimentation we may

choose to track and record the displacement of our point of interest, or the derivative of that position with respect to time finding velocity, or acceleration, the derivative of velocity with respect to time. Conversely, we may integrate from the acceleration to gain the velocity or once again to find the displacement. The results of these efforts are recorded in shock response time histories, such as those found in Figure 87, which comes from a generic FSP shock test.

Valuable information related to the response of the body or mass is included within these time histories. The curve may be used to determine peak response values, local maxima and minima, or accumulated response to a particular point. Additionally, each time history of the motion provides information in the temporal sense as well. Acceleration corresponding to early time, displacement to late time, and velocity throughout the mechanical range of response frequencies (approximately 10–100 Hz). The FFT can thusly be determined from the acceleration history. Additionally, the SRS may be produced for further analysis.

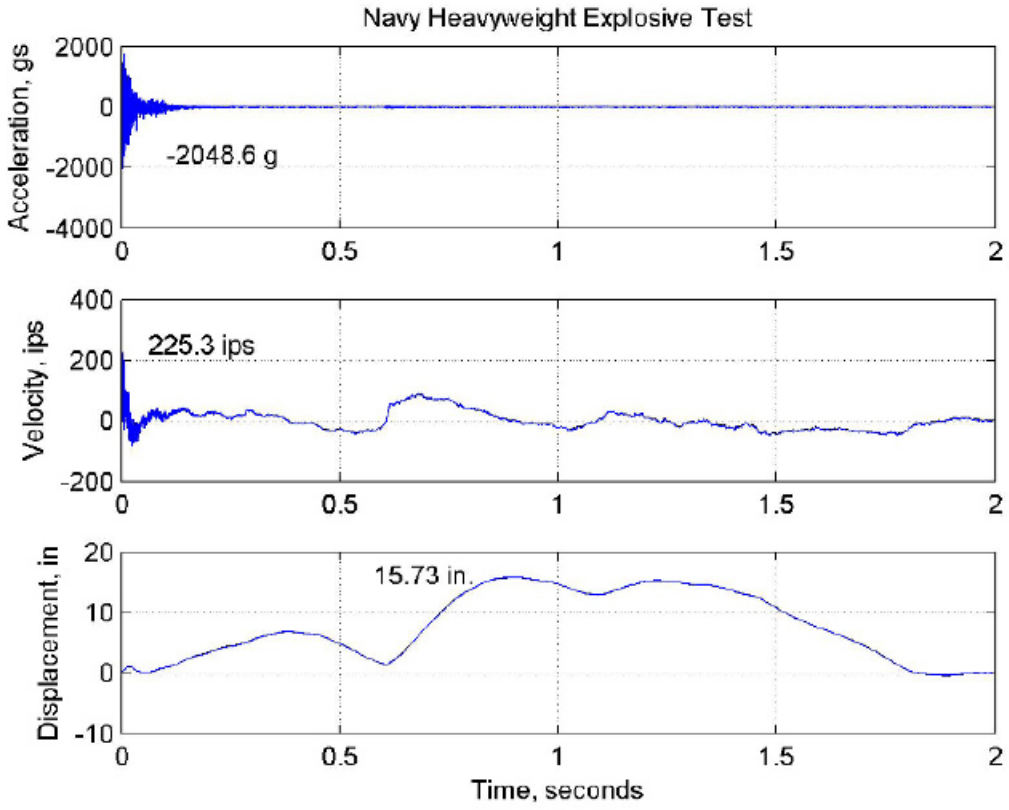

Figure 87. Typical Record of Shock Loading for Standard FSP Test. Source: [133].

In the current study, the top dead center nodal position of the equipment case was selected as the primary location in assessing the shock response. This particular node is at the center of the shell plate structure. Additional data was also collected from the top and bottom corners, side panel, and bottom plate of the equipment case model, the deck beneath the model and foundation, depending on which configuration of the model was utilized in the simulation.

Here the simulated response of the equipment case top, determined via time differencing methods (Gemini and DYNA), is compared for the FSP with a series of horizontal standoff distances at 6.096, 7.62 and 9.144 m (20, 25 and 30 ft) in a series of three plots, one each for acceleration, velocity and displacement in Figures 88–90. The accelerations are compared in Figure 88. It is observed that there is very little occurring in

the time times beyond 100 ms, and that all are similar in response with the amplitude increasing as a function of closure in standoff distance.

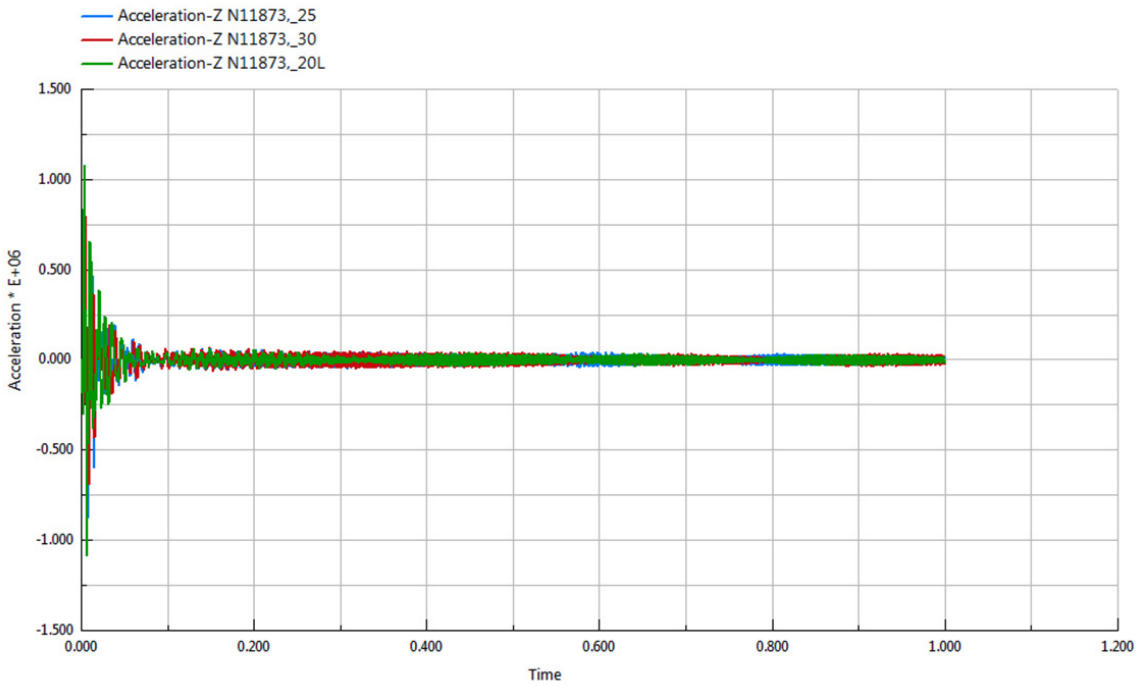

Figure 88. Acceleration Response of Equipment Case Top

Next the velocity was compared. Again, the results are very similar. As expected, the magnitude of the velocity response is dominated by the data that is obtained from the closest test at 6.096 m (20 ft) standoff range as shown in Figure 89.

Finally, the displacement of the top shell plate node is observed in Figure 90. The displacements are consistent and in the early time only vary by 1 cm or less, leaving greater deviation in displacement after the bubble pulse reloading occurs in the vicinity of 700 ms.

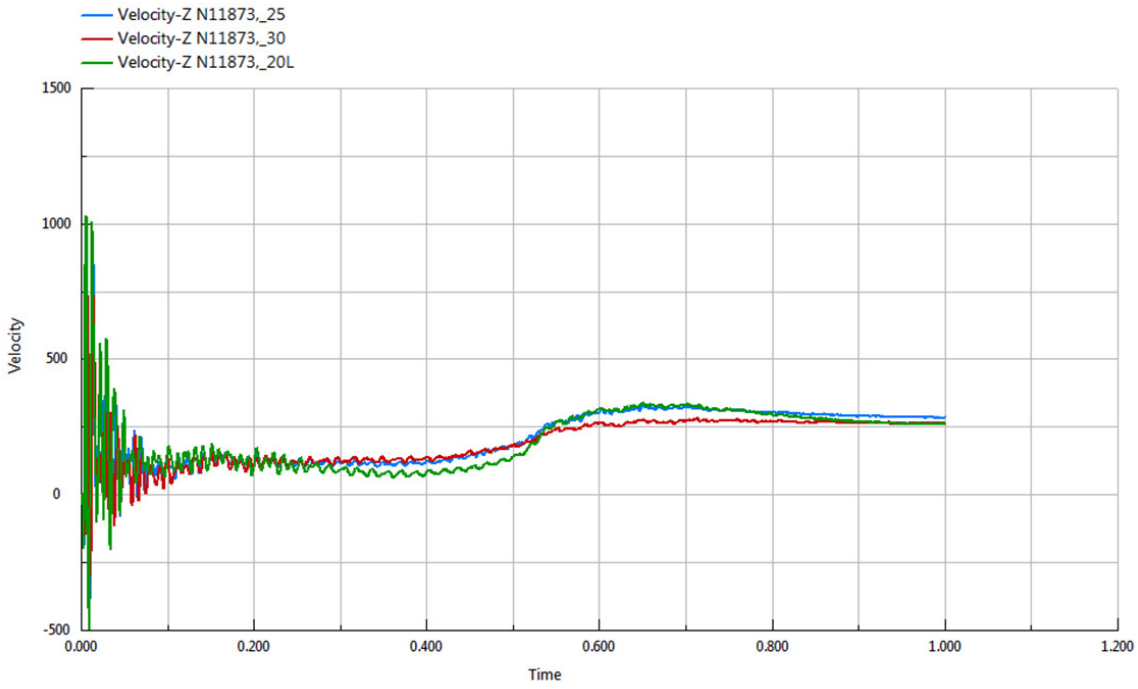

Figure 89. Velocity Response of Equipment Case Top

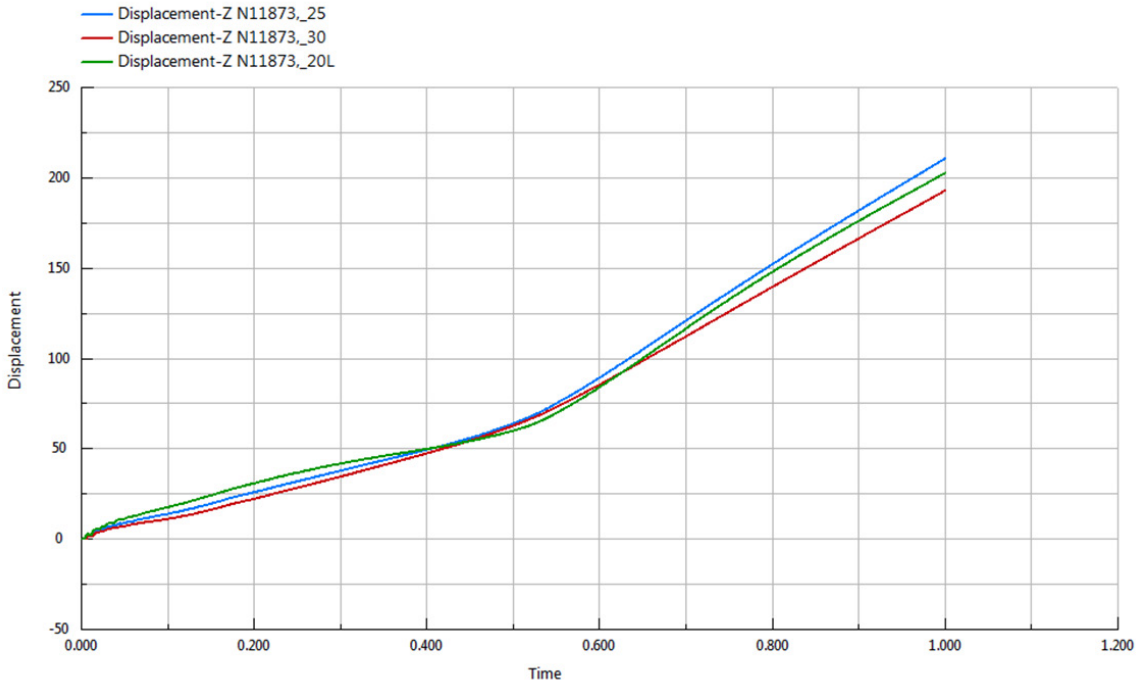

Figure 90. Displacement Response of Equipment Case Top

3. Evaluation of Failure

Nearly 50 years ago, Gaberson and Eubanks [134] first set about evaluating failure. Shock hardness was described by them as "the highest amplitude shock spectrum of any shock loading that the equipment was have known to survive." They later found when testing squirrel cage blower and motor assemblies, as shown in Figure 91, that the blowers failed structurally in all but one out of six shock qualification tests. Figure 92 is an example of the damage sustained during the various types of standard shock tests were performed as listed in Table 9. In the case of the FSP, MSWM and LWSM which should provide the same result, there was disagreement. Knowing that the FSP testing is designed to be conservative in nature, the fact remains that failure occurred in every test less the LWSM, which is by far the most extensively used test platform for shipboard equipment shock qualification by vendors seeking approval for U.S. Navy acquisition and installation in combatant vessels.

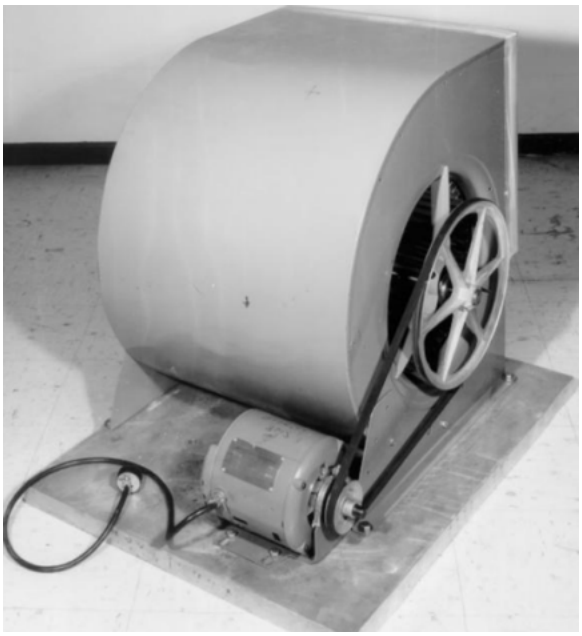

Figure 91. Squirrel Cage Blower and Motor Assembly. Source: [134].

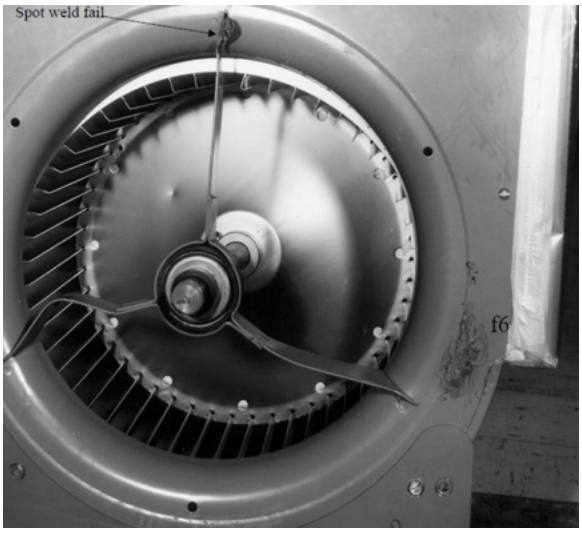

Figure 92. Damage to Squirrel Cage Blower. Source: [133].

Table 9. Squirrel Cage Blower Test Series. Source: Adapted from [134].

Test Name	Shock Test Platform
HS54	54-inch drop; half sine
TP60	60-inch drop; terminal peak
PB24	24-inch drop; onto a hard phenolic block
LW72	72-inch hammer drop; LWSM
MW36	36-inch drop; half sine
HW4	Shot 4; FSP

Table 10 provides detail on the maximum pseudo velocity, given in in/s, and peak acceleration in g's, for each test. Pseudo-Velocity shock spectrum (PVSS), as expressed in equation 5.4, is the maximum absolute value of relative displacement for a SDOF system multiplied by its corresponding frequency.

$$PV_i = \omega_i q_{i_{\max}} \tag{5.4}$$

The greatest velocity response is found in the MWSM test while the least is in the LWSM test. However, in contrast, the peak acceleration is recorded in the LWSM while the terminal peak and half-sine tests provide the least. Examination of Figure 93 shows the varying amplitudes of acceleration response for the tests. The plot labeled LW72 is the only blower to survive without damage, yet it exhibited the greatest absolute acceleration response and has much higher frequency content than all but the heavyweight shock test, denoted as HW4, which had a similar peak acceleration and time history plot. However, the velocity response of HW4 was nearly double that of LW72, at approximately 762 cm/s (300 in/s) per the results listed in Table 10.

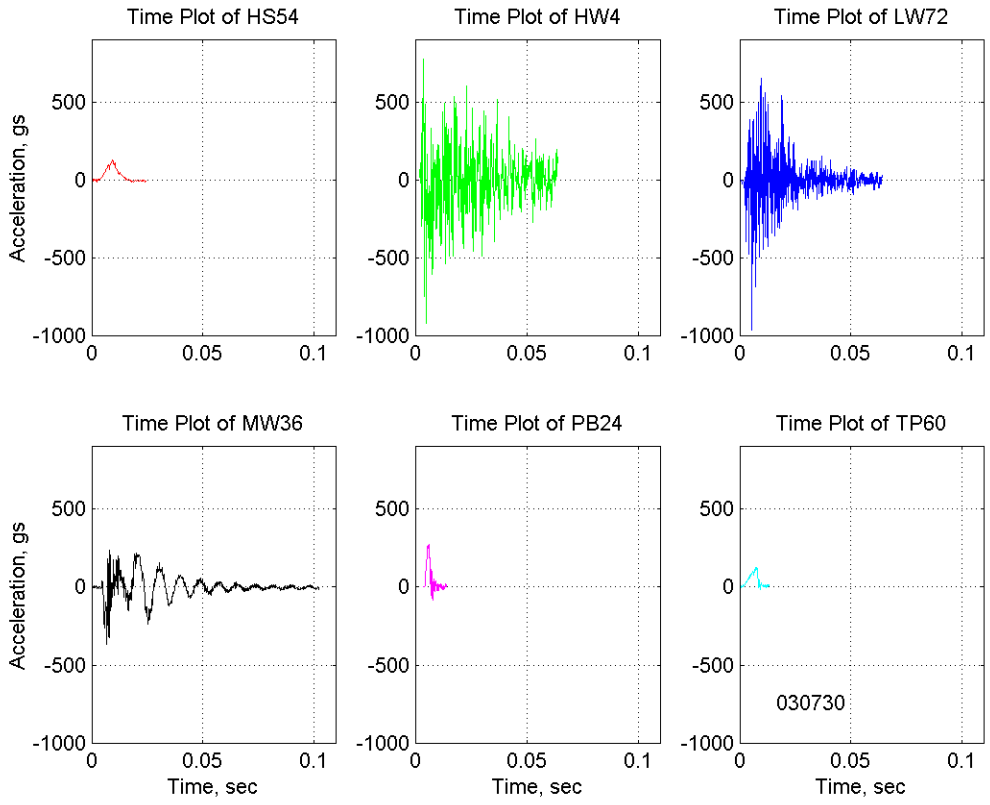

Figure 93. Shock Response Spectra for Six Different Shock Tests of Squirrel Cage Blower Motors. Source: [134].

Table 10. Squirrel Cage Blower Test Results. Source: Adapted from [134].

Test	HS54	HW4	LW72	MW36	PB24	TP60
Result	Fail	Fail	Pass	Fail	Fail	Fail
Type	Drop	Shock	Impact	Impact	Drop	Peak V
PSVel	~250	>300	~150	>400	~180	~180
A_{max}	<200	>900	~950	>350	~250	<200

Careful examination of Figure 94, the SRS for the acceleration time histories of the six tests performed on the set of squirrel cage motors, shows that there is a distinct value as a maximum in the vicinity of 381 cm/s (150 in/s) that many not be exceeded or failure will result. But additionally, from Table 10, there also needs to be a large acceleration value as well that is met in the frequency range of 10–100 Hz for that failure to occur.

Here again, as with Newton's Damage Boundary method, we appreciate that more than one response parameter may need to be set as a condition for failure to occur. In the approach to setting a damage threshold using PVSS, Gaberson equated a constant velocity level to shock severity. This was done in part as stress is proportional to velocity. While this makes for consistent evaluation across various shock loading types when using SRS, it also implies that it is best suited for the aforementioned frequency range of "mechanical" shock.

Recalling that Newton [63] purported that the use of multiple parameters, peak acceleration and change in velocity, for the characterization of failure in a critical component, was sufficient to bound the damage region based on threshold values determined through the very repeatable drop testing of low-cost items produced in mass quantity. This information was used to make changes to the item itself or design packaging to mitigate the shock response. Unfortunately, the shipboard shock environment is not as predictable as the transport, display and handling of consumer electronics and the like.

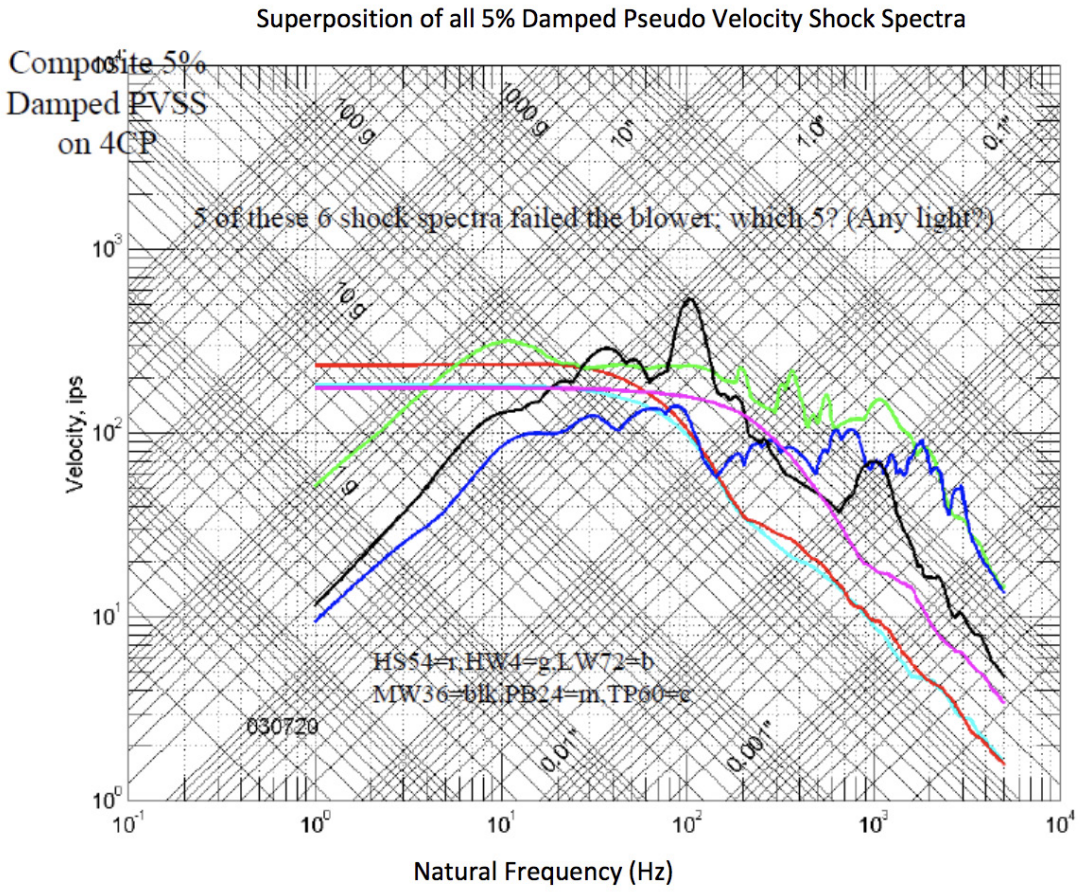

Figure 94. Damped PVSS for All Six Blowers. Source: [134].

C. DEVELOPMENT OF NEW FAILURE PREDICTION APPROACH

The new approach is developed here using several different test cases. These are based in part on the complimentary studies or structural damping, mesh refinement, and other modeling. The underlying investigations of equipment failure include the full ship model, standard FSP, FSP with DSF and various detailed shell, rigid body, and simple spring mass models. A LWSM model is also created and used to further aid in the determination of the response characteristics and applicability of reduced order models within full ship shock models.

In general terms the following approach was implemented in order to determine suitable failure criteria.

1. Functional Failure Model Development

Since numerical analysis does not provide an inherent method of assessing functional (operational) status during the simulation of a physical event such as the post-shock operation of a computer monitor, a functional failure model was implemented. Here the functional failure is represented by the contact of two vertically offset cantilevered beams connected at the tip by a soft spring within the detailed shell model of the equipment cabinet. The purpose of this test apparatus, as best illustrated in Figure 76, is to mimic the failure mode of the critical component of the system, in a FEM model of some representative shipboard equipment.

2. Improved Structural Damping of the Ship Model

As previously described, an improved damping scheme for the FEM of a ship model was developed in [125] to provide more accurate response prediction in the full ship analysis cases. Important to this study is the placement of the equipment and actual physical situation capturing the ship system damping that is not appreciated in the sterile test stand environment of LWSM, MWSM, and FSP testing.

3. Shipboard Equipment Study using Numerical Experimentation

Motion response time histories from select nodal points in the detailed shell equipment cabinet are extracted from the LWSM, FSP, and full ship shock model results. The functional failure model provides temporal information regarding the failure point while the structure offers data to analyze corresponding response maxima for the representative equipment cabinet.

4. Employ Reduced Order Models for Shock Assessment

Once parameter limits for failure are determined based on the functional failure model, and shock test loading, simple spring mass systems are employed at locations of interest throughout the full ship shock FEM model for realistic shock threat simulation. The response of the reduced order model is then used as input to assess against, or corroborate with, results from detailed FEM models or physical equipment tests or analyses.

In this section, we focus on the threshold values that distinguish failed equipment based on the functional failure model and motion response values sampled from the data.

1. Failure Determination in Shipboard Equipment

The approach begins with the identification of the equipment and critical component. The equipment model is placed on the test platform or ship model and the desired shock loading is applied. From the simulation data, a point of interest is selected for the key response to be computed up to the time of functional failure. The process is repeated for various loadings and locations throughout the ship model, if available. From these data a failure zone diagram is created based on the peak velocity and change of displacement corresponding to functional failure in the equipment model.

2. Data Trends

Data was obtained from the simulation runs that were conducted as part of the analysis. Comparisons were completed for the rigid body model and the detailed shell model. Table 11 provides results of the forward, midships and aft shot geometries for the ship model and results of the functional failure assessment at each of the 15 equipment locations. Table 12 provides a sample of the data, in this case of maximum displacement, evaluated against functional failure. This is an example of just one equipment configuration, the detailed shell model with spring isolation. Similar data were obtained in all cases examined.

Displacement of the equipment cabinet (case) was investigated to gain insight into the low frequency motion response. Table 12 shows the results of the functional failure study as compared to the absolute displacement of the center top node in the detailed shell model. The values are given in cm. Functional failure occurred in equipment cases with as little as 2.1 cm displacement and as great 15.1 cm measured at the top center reference node. Yet it is also observed that in other cases the corresponding node of interest had a maximum vertical displacement of 19.2 cm without failure. And in still another case a displacement of only 3.6 cm resulted in a “nearly failed” outcome, as indicated by the yellow color in equipment case No.10 for the aft shot location.

Table 11. Shipboard Locations of Functional Failure

Case No.	Location	Aft	Mid	Fwd
1	Top of Mast	Fail	Fail	Fail
2	Fantail	Pass	Pass	Pass
3	Aft DC Deck	Pass	Pass	Pass
4	Shaft Alley	Pass	Pass	Pass
5	Top Dead Center	Fail	Fail	Fail
6	Middle Dead Center	Pass	Fail	Pass
7	Bottom Dead Center	Pass	Pass	Pass
8	Comm Center	Pass	Fail	Fail
9	Pilot House	Fail	Fail	Fail
10	Center Triplet	Pass	Pass	Pass
11	Stbd Triplet	Pass	Pass	Pass
12	Port Triplet	Pass	Pass	Pass
13	Fwd Qtr Bottom	Pass	Pass	Pass
14	Foc'sle Weax Deck	Pass	Pass	Pass
15	Foc'sle DC Deck	Pass	Pass	Pass

In order to correlate the data to a useful parameter we first started by looking at data trends in motion response. Figures 95–98 show some of the initial attempts to conduct trend analysis by using a linear reference from the origin of the ship model, at the bow.

The change in displacement was plotted in Figure 95 as the area found under the curve. Here somewhat of a trend was observed. Even though there was not an absolute cutoff value, all of the functional failures highlighted in Table 12 occurred at or above a corresponding area of approximately of 4000 cm^2. In this figure, the marker shapes correspond to the simulation series where the "aft," "mid," and "fwd" labels reflect the longitudinal position of the charge. The red dotted horizontal line represents this threshold value. All red colored markers, which represent failed results, fall above this line. However, there were also values (marked in green) that did not exhibit functional failure at points well above this threshold; at double and triple the value in some cases.

Table 12. Overall Displacement Results for Ship Cases

Case No.	Location	Aft (cm)	Mid (cm)	Fwd (cm)
1	Top of Mast	2.467	18.374	7.739
2	Fantail	17.386	13.457	9.837
3	Aft DC Deck	16.08	12.112	8.479
4	Shaft Alley	14.909	10.0162	6.639
5	Top Dead Center	4.29	12.748	4.071
6	Middle Dead Center	8.298	12.178	9.433
7	Bottom Dead Center	8.129	11.725	9.193
8	Comm Center	6.502	12.19	10.021
9	Pilot House	2.175	15.11	5.994
10	Center Triplet	3.618	14.894	13.944
11	Stbd Triplet	4.992	16.614	14.489
12	Port Triplet	2.131	13.264	13.369
13	Fwd Qtr Bottom	3.403	17.801	15.423
14	Foc'sle Weax Deck	9.473	26.23	19.249
15	Foc'sle DC Deck	8.927	24.845	18.648

Clearly from this result, neither the maximum vertical velocity response nor the corresponding change in displacement alone could be used as a viable failure criterion. Plotting overall (absolute) maximum acceleration against the velocity, and other untested combinations, displayed in Figures 96–98, was attempted without any apparent promising results. For clarity, the maximum velocity, V_{max}, is defined as the maximum velocity occurring prior to the onset of functional failure in the model, while the overall maximum velocity, V_M, is defined as the overall greatest absolute value of velocity found throughout the entire time history.

For instance, in Figure 98, the maximum displacement response is plotted against the ship length (longitudinal position). In this plot the data tends to show the greatest relative displacement toward the bow and stern while the predominance of functional failures occurred amidships. This trend holds true with all charge loading conditions investigated.

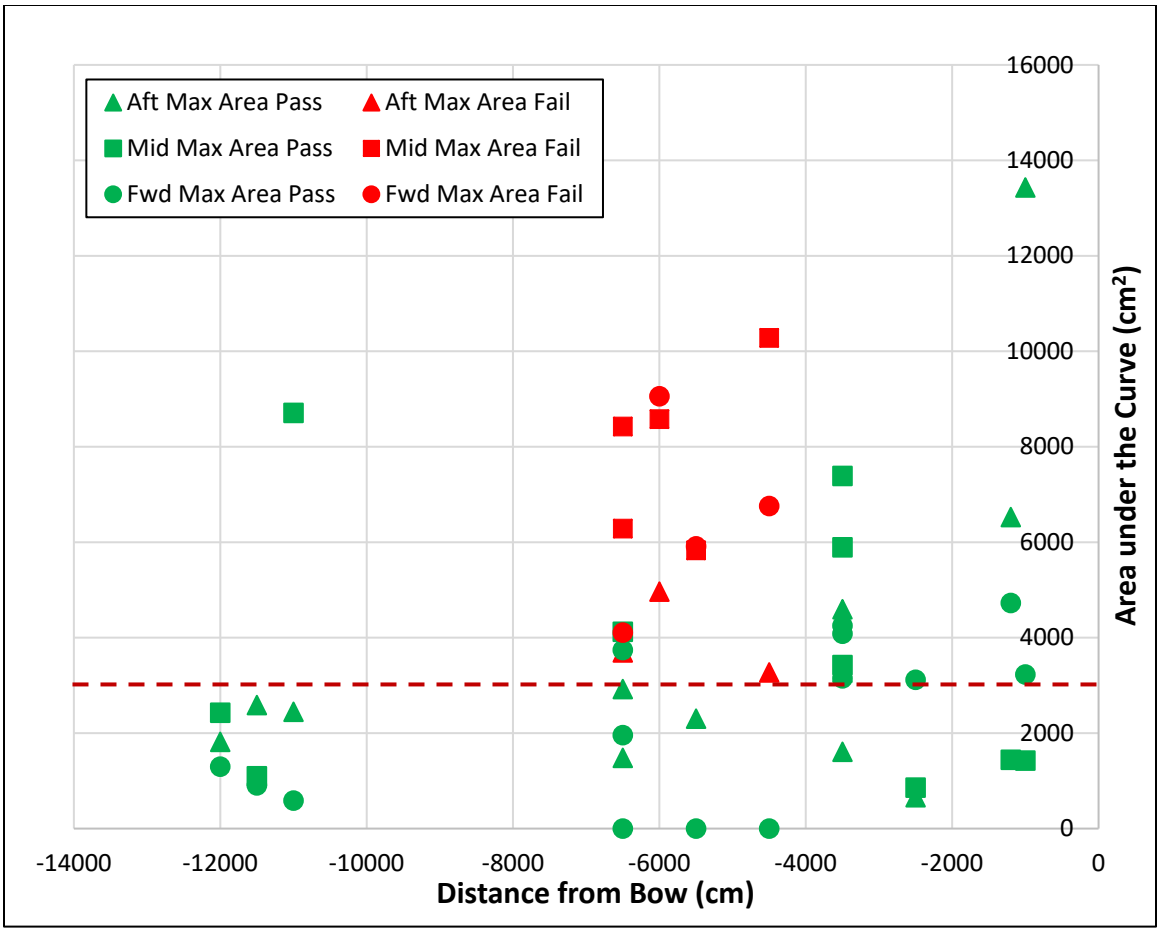

Figure 95. Maximum Area Under the Velocity Curve with Respect to Longitudinal Shipboard Position

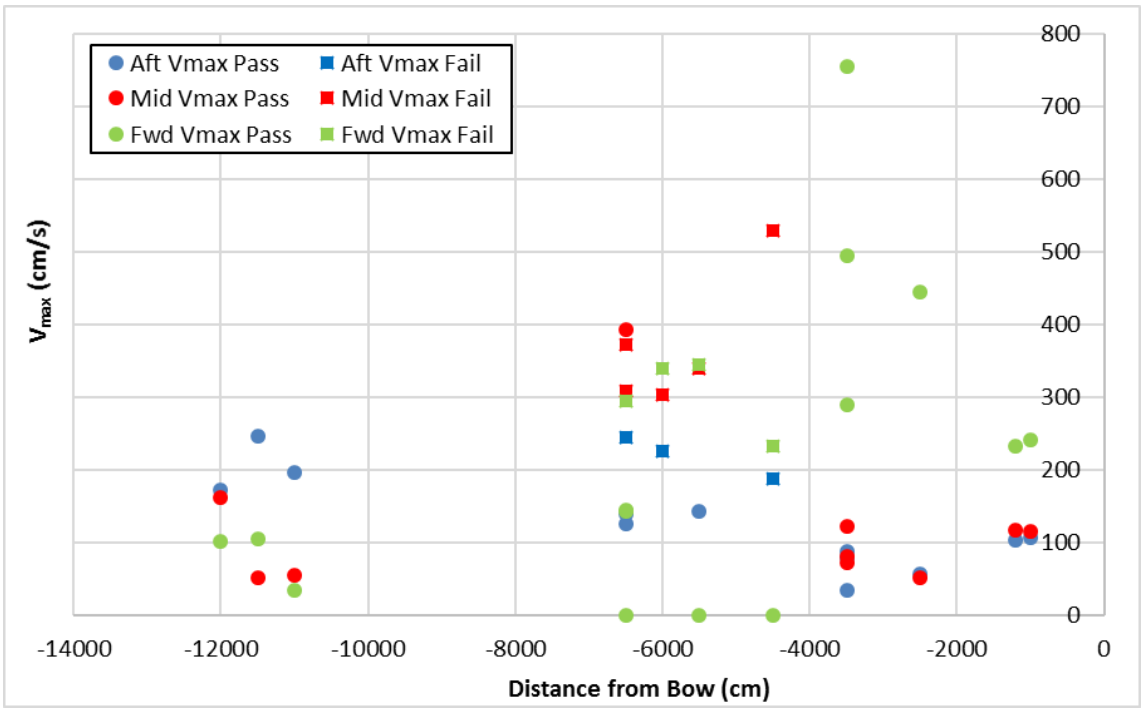

Figure 96. Maximum Velocity with Respect to Longitudinal Shipboard Position

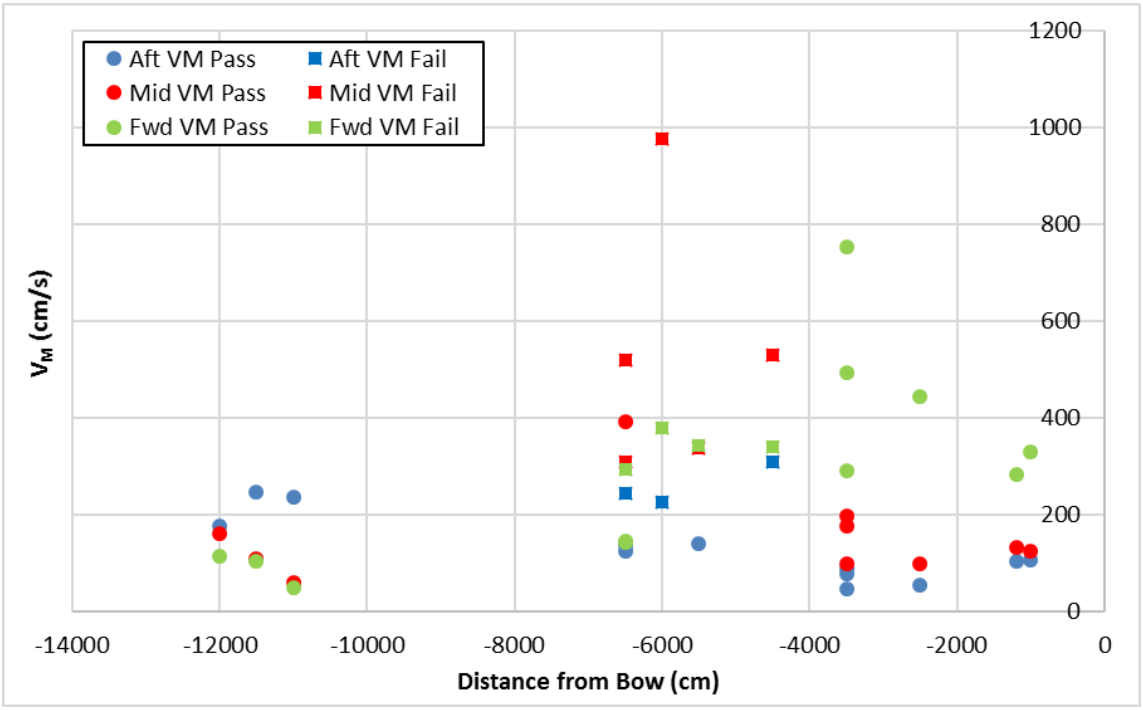

Figure 97. Overall Maximum Velocity with Respect to the Longitudinal Shipboard Position

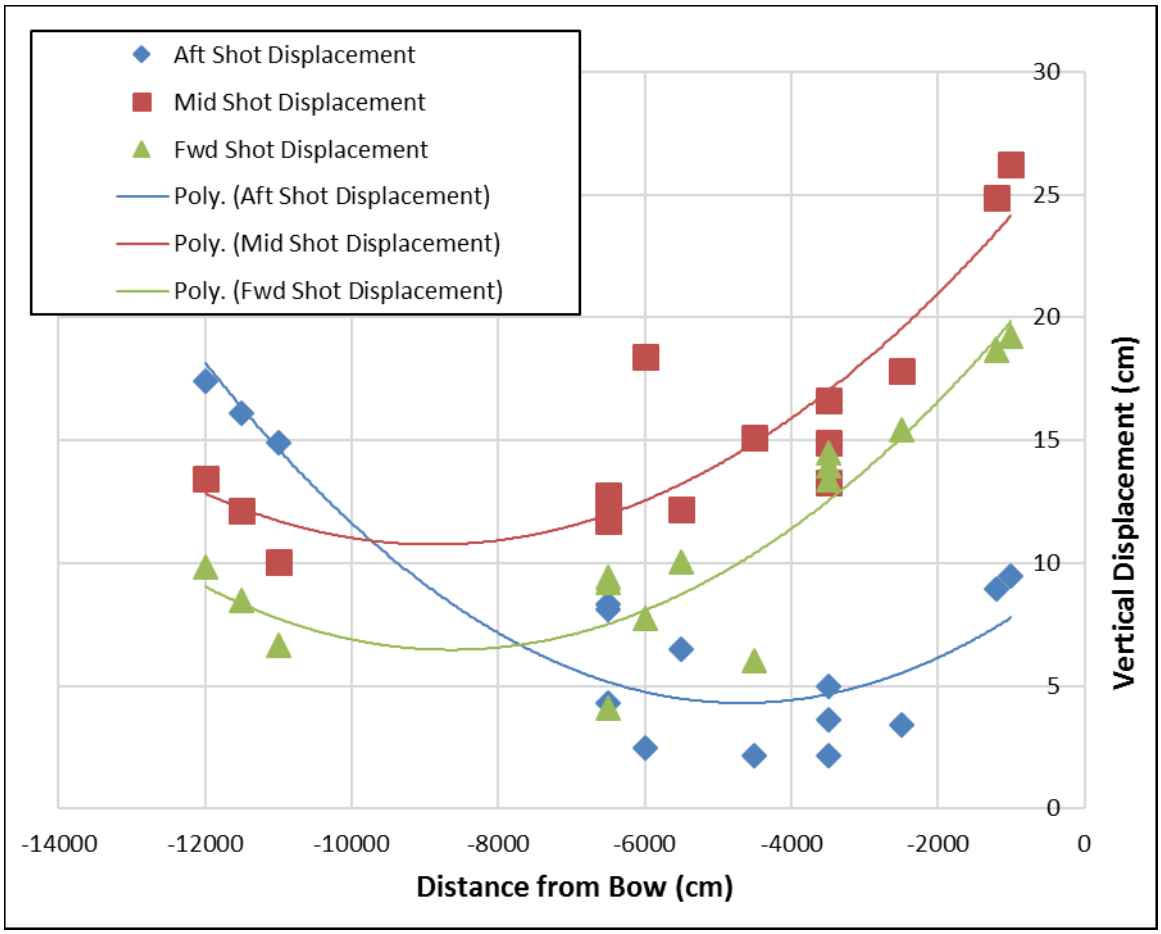

Figure 98. Maximum Displacement with Respect to Longitudinal Shipboard Position

In the following series of plots, Figure 99–Figure 105, red markers indicate failure, while the green markers represent the equipment models that "survived" the simulated UNDEX loading based on the functional failure model response. The marker shapes represent the various loading cases or test series for which the data was gathered.

Data was plotted for overall maximum acceleration, A_M, against overall maximum velocity, as is illustrated in Figure 99. Even though there is some clustering of like data points, there are also failures that fall well beyond the average values for both acceleration and velocity.

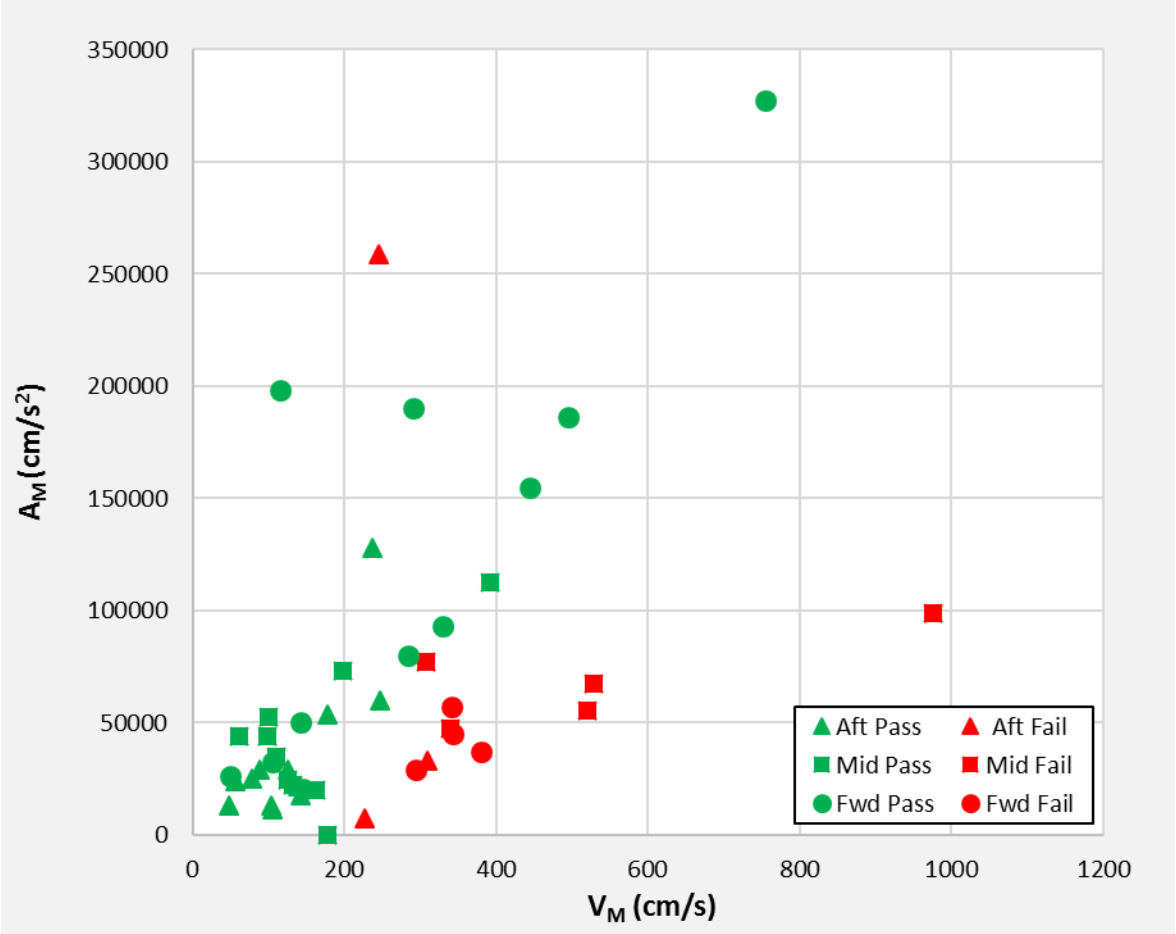

Figure 99. Overall Maximum Acceleration vs. Overall Maximum Velocity

Next the simulated data is compared to a standard Newton Boundary Damage method approach with the peak acceleration and change in velocity values plotted against one another. Figure 100 illustrates the acceleration plotted against the change in velocity obtained from the current study data. As is apparent from this figure, there is the beginning of a separation in the groupings of data nearer to the origin, yet at higher accelerations and greater values of change in velocity this is also not a good match for the data from this study.

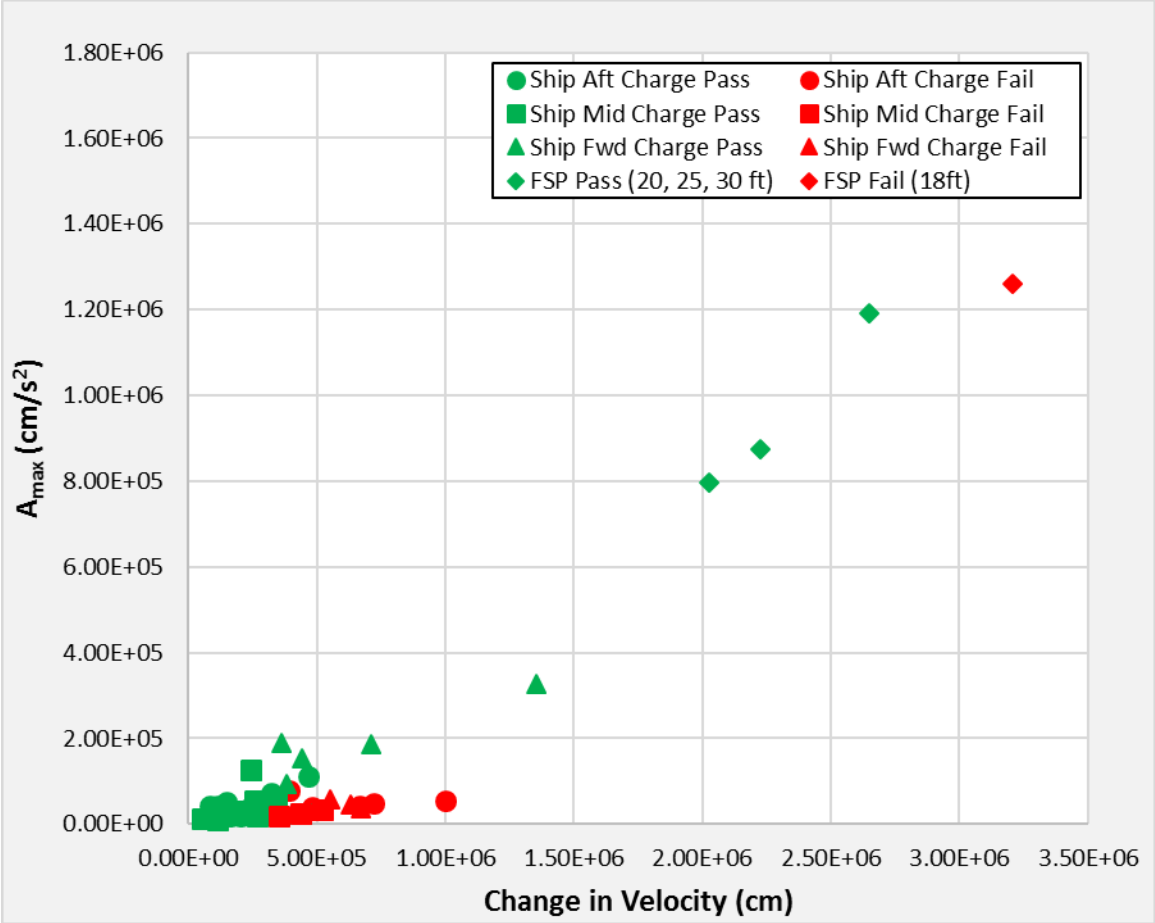

Figure 100. Maximum Acceleration vs. Change in Velocity

Furthermore, the data from the ship and FSP models is distinctly separate, with the full ship data clustered below 2.0e5 cm/s^2 and 1.0e6 cm for peak acceleration and change in velocity, respectively. The FSP data, indicated by the sparely positioned diamond shaped markers in the upper right corner of the plot are somewhat better behaved, but are based only on a few data points. Neither grouping gives a clear delineation as does the sample plot of the damage boundary method in Figure 101, which uses peak acceleration and change in velocity as parameters.

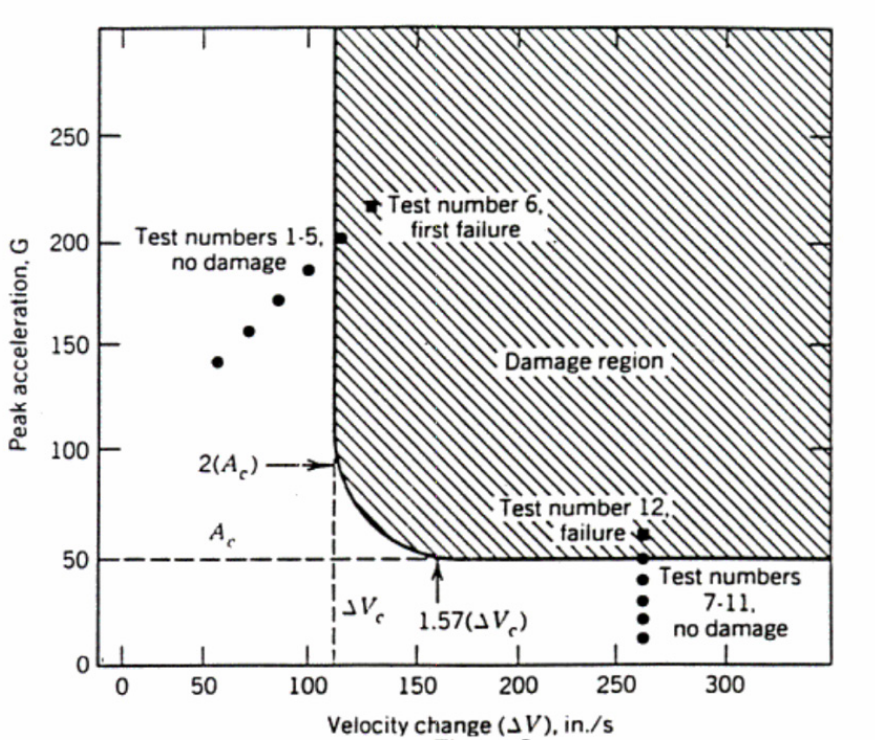

Figure 101. Acceleration vs. Change in Velocity plot. Source: [63].

Following up on the previously described potential findings with the velocity and displacement, maximum acceleration was plotted against change in displacement in Figure 102. Unfortunately, this combination of motion response factors only provides a plot that mainly commingles the data near the abscissa in the case of the full ship simulation with the FSP data again distinctly separate. The FSP is found with a minimum acceleration at 8.0e5, while the maximum ship acceleration values are only half of that.

In Figure 103 the maximum velocity is plotted against the change in velocity. This attempt too was unsuccessful in realizing a solid trend.

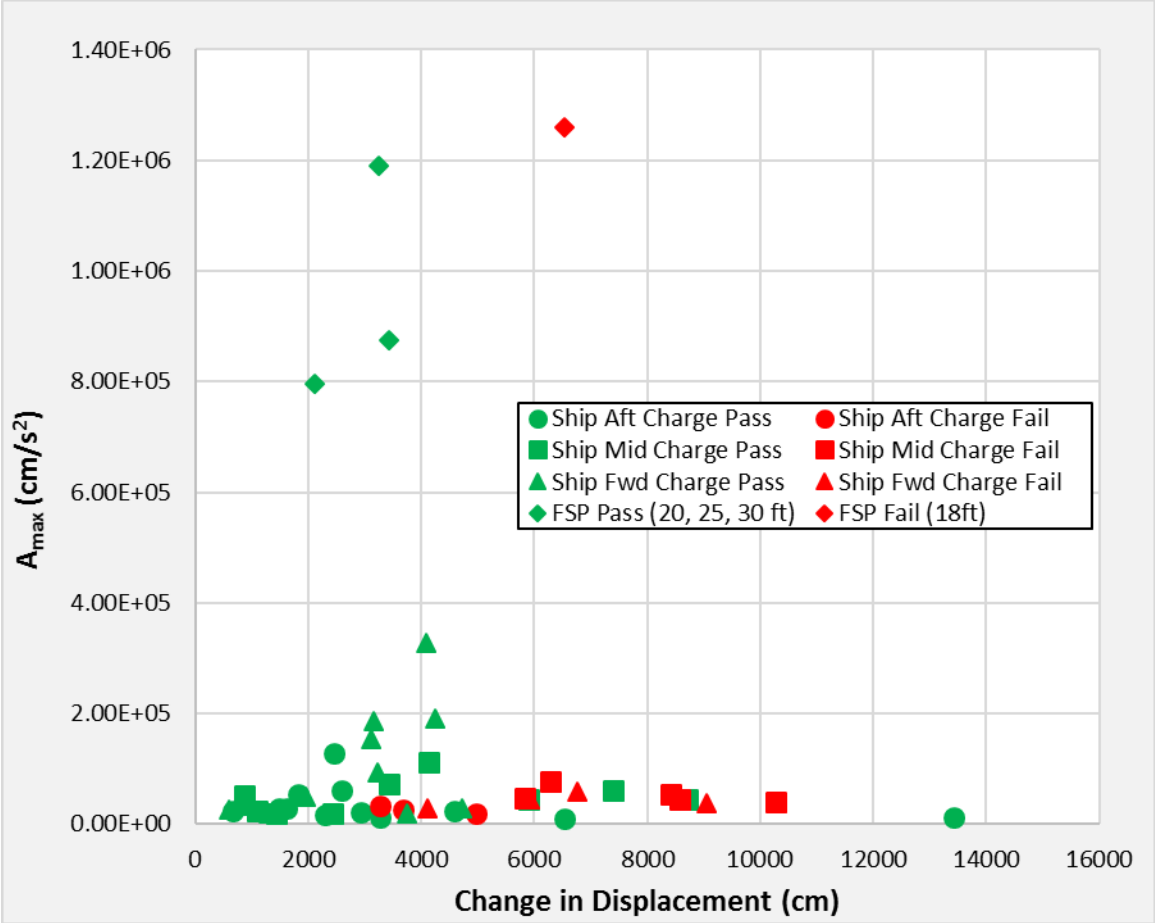

Figure 102. Maximum Acceleration vs. Change in Displacement

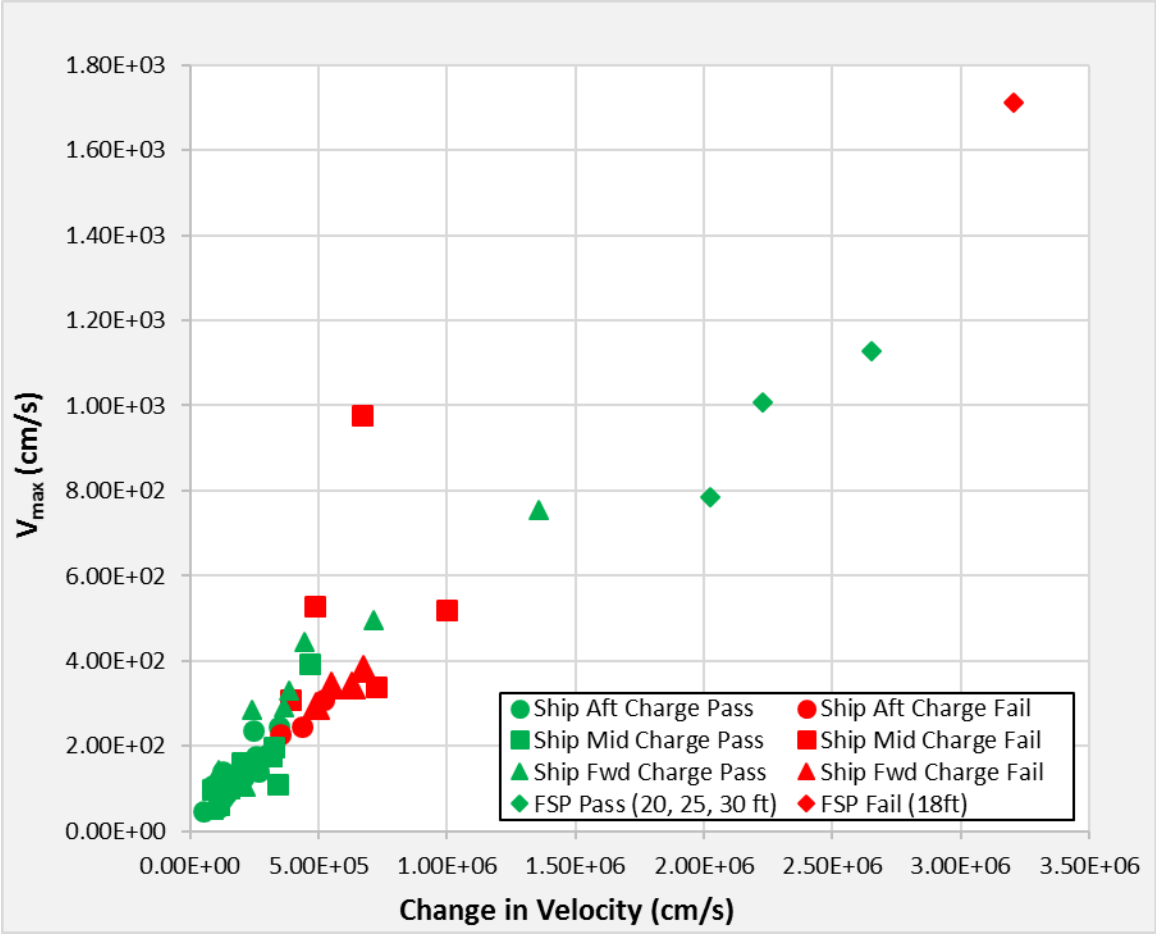

Figure 103. Maximum Velocity vs. Change in Velocity

Continuing to work with different combinations of response motion, the pair, maximum acceleration and change in velocity was plotted, as shown in Figure 104. In this plot, there is data that indicates that failure was achieved at relatively low accelerations, whereas other locations experienced no failure at much greater accelerations. Here too, there is no clear delineation of the cut off change in velocity that would indicate the onset of failure. The plot indicates that several equipment locations tolerated accelerations of greater than 1.0e5 cm/s^2 and change in velocity of 4.0e5 cm/s and higher, while others failed at less than 1.0e4 cm/s^2 with nearly the same 4.0e5 cm/s change in velocity.

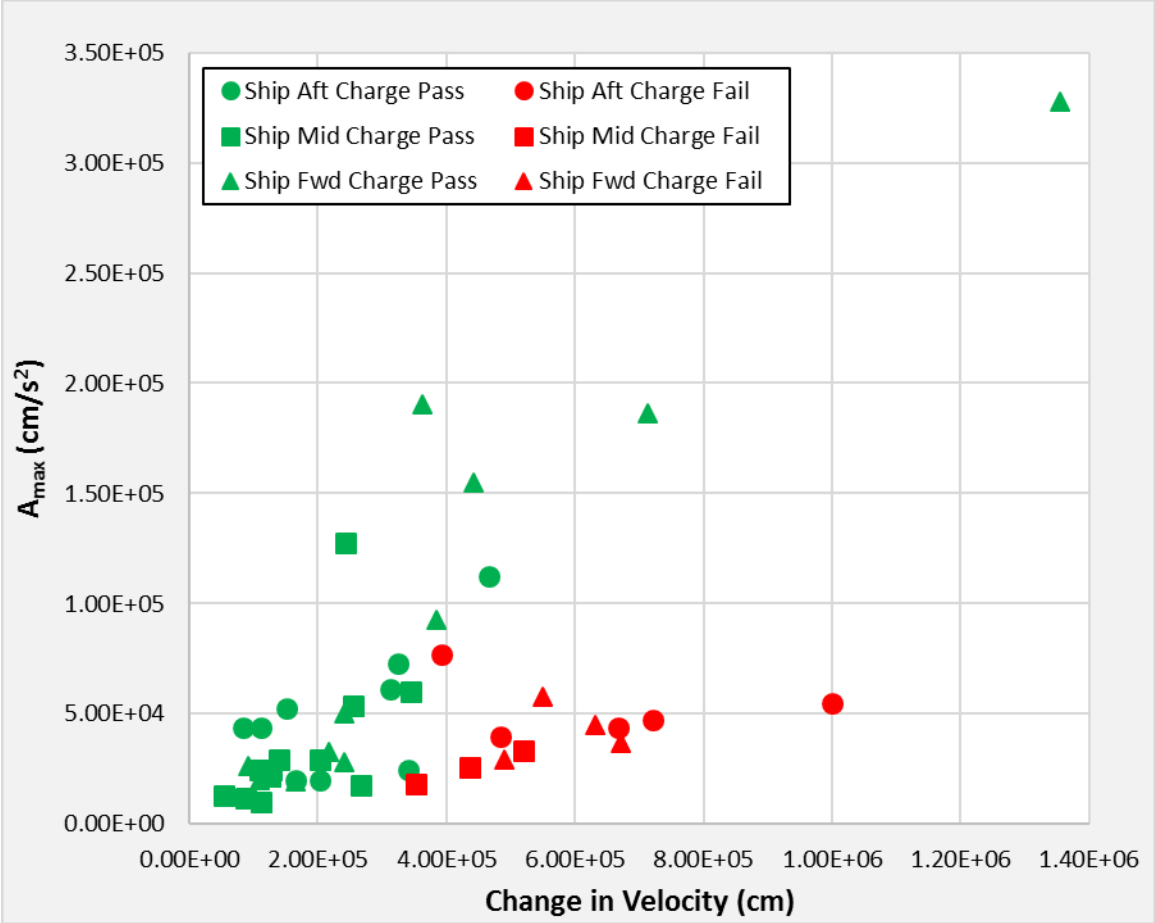

Figure 104. Maximum Acceleration vs. Change in Velocity–Ship Data

Maximum acceleration and change in displacement were investigated as well. Figure 105 provides the results of the data analysis. This attempt was inconclusive, as there is much comingling of data at lower accelerations across the board. However, an interesting occurrence was noted in that there was a threshold for failure that could be assigned as a result of the change in displacement. The value of approximately 3500 cm serves as a lower limit to all failed equipment locations in the full ship simulation.

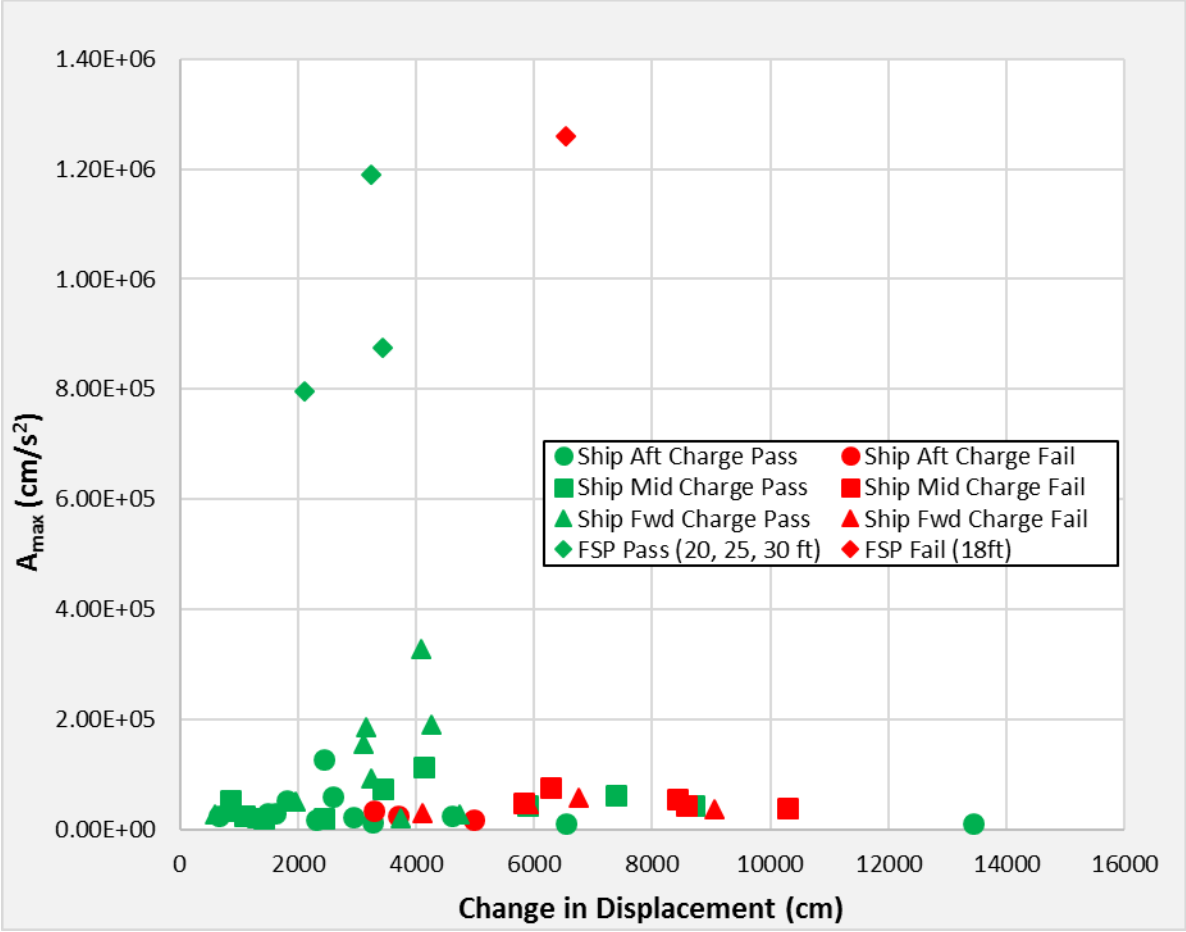

Figure 105. Maximum Acceleration vs. Change in Displacement

Again, using the damage boundary method as a guide, the data from the study was again plotted, this time with the maximum velocity and the change in displacement. The result of the midships shot, which was most severe and caused the greatest number of functional failures appears in Figure 106. The red square markers indicate failure, while the green markers represent the equipment models that "survived" the simulated UNDEX loading. The boxed area indicates a clear region of failure when examining both the maximum velocity of the response at failure and the maximum change in displacement. Values of between 200–300 cm/s maximum velocity and 4000–5000 cm in change of displacement were determined to serve as boundaries of the failure zone.

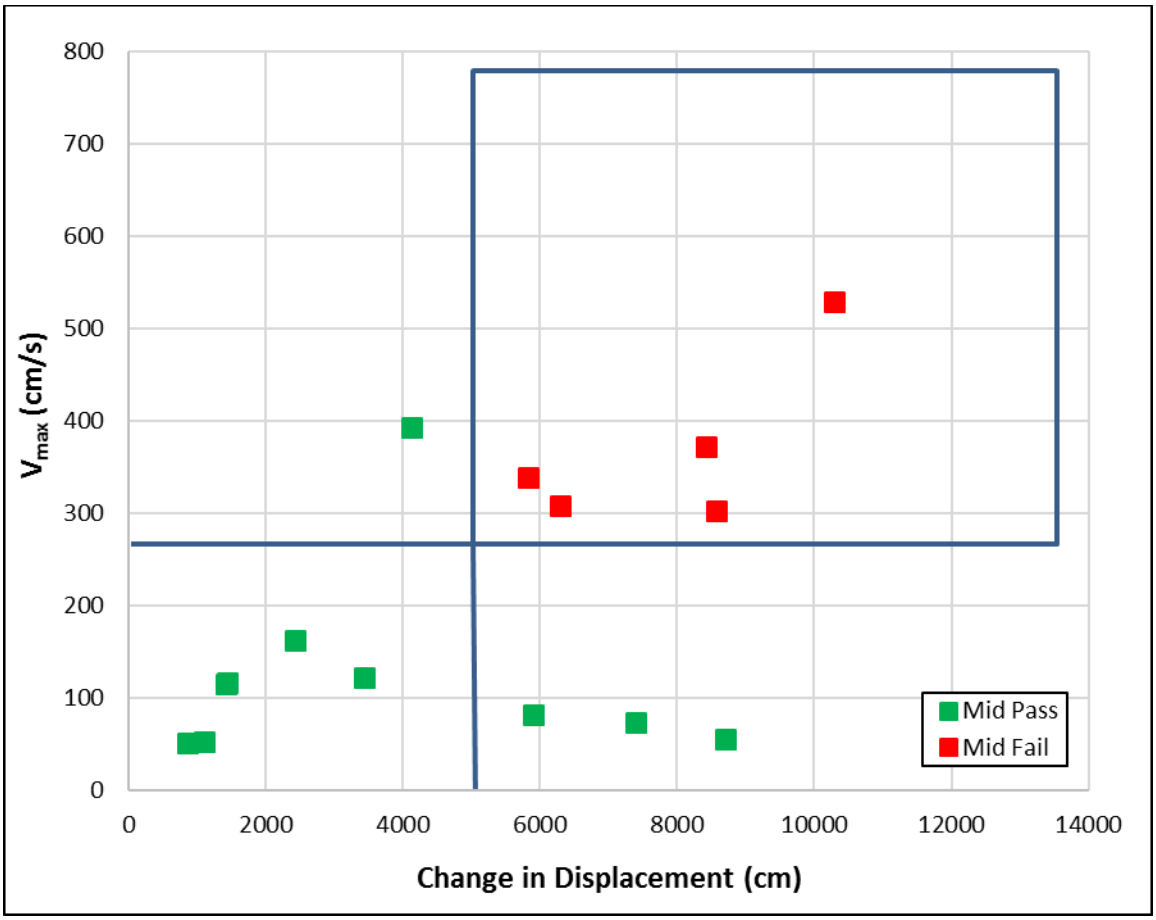

Figure 106. Maximum Velocity vs. Change in Displacement–Ship Study

This trend was then confirmed when looking at just the FSP shot data where the charge was incrementally brought in from a 15.24 m (50 ft) standoff to 5.49 m (18 ft), which exceeds the requirement of the standard shock qualification heavyweight test. When the maximum velocity and the maximum change in displacement (area) were plotted against one another, the same result appeared. All simulations exhibiting functional failure of their representative model were contained up and to the right of a lower boundary for velocity and a minimum value for the change in displacement. This is indicated by the lines in Figure 107 extending away from the lower boundaries of the enclosed failure region. The values of maximum velocity and change in displacement, approximately 300 cm/s and 5000 cm, respectively, are consistent with those found in the shipboard simulations.

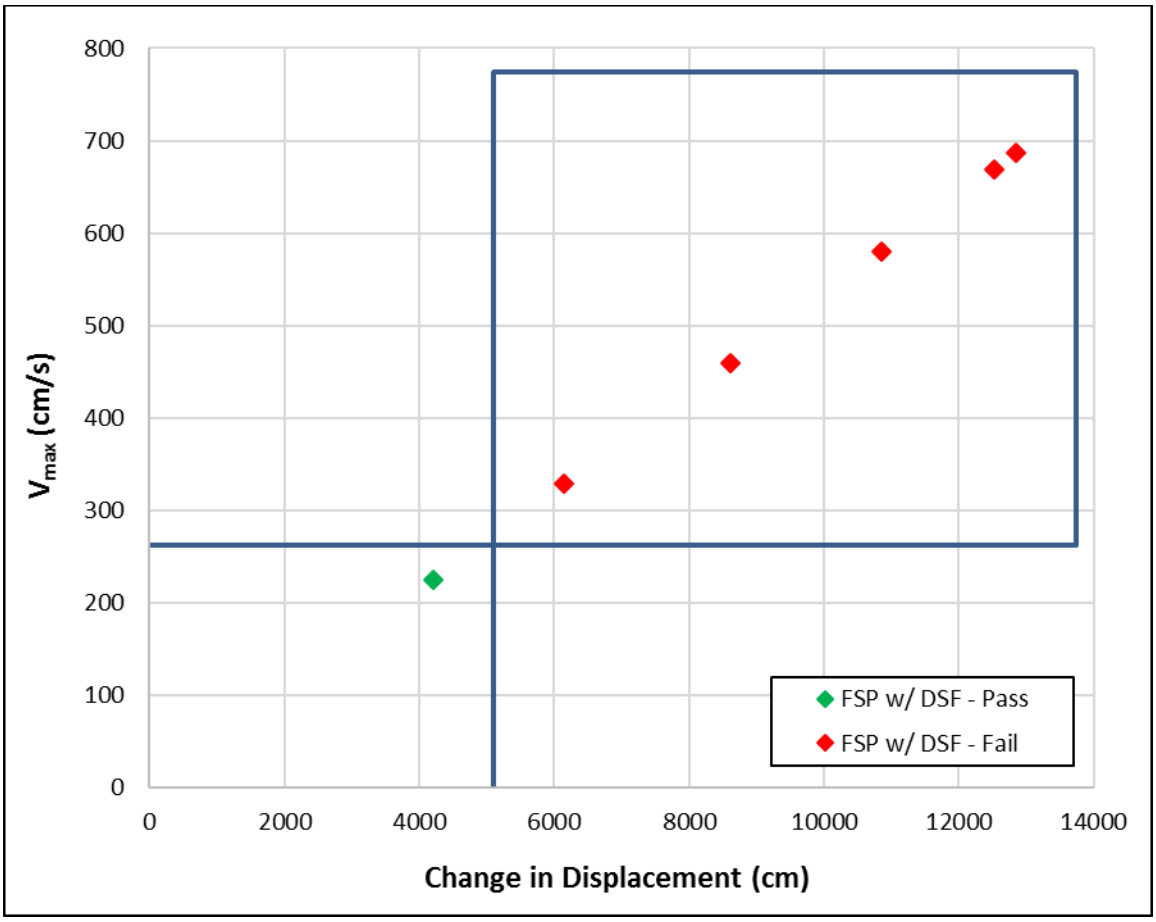

Figure 107. Maximum Velocity vs. Change in Displacement–FSP Study

D. SUPPLEMENTAL NUMERICAL EXPERIMENTATION

The following items were given a cursory review during the study but are mainly included as prospective future research areas to improve understanding and strengthen the correlations made through this current effort.

1. Improved Understanding of Equipment Response

Many factors affect the observed response of the equipment. Refinement of equipment models, improvement of measurement accuracy and enforcement of environmental controls during testing may only account for some reduction in the uncertainty of the recorded response. Knowing which factors influence the result and to what degree is required.

a. What Affects Response

Transmissibility, Q, is the ratio of the maximum output force to the maximum input force as given here.

$$Q = \frac{F_{out}}{F_{in}} \tag{5.5}$$

Investigation of transmissibility within the ship shock environment as it pertains to the ship hull, the deck and those other surrounding structures and major equipment can be performed to better understand how sensitive the equipment response is to the actual transmitted loading. This difference between the source yield and equipment loading is potentially affected by hull shape, displacement and other platform specific characteristics. The size and proximity of the other equipment, structure and attributes on the ship are also studied to determine if their response is linked to functional failure thresholds. One might ask how large and close do objects near the item of interest need to be to influence shock failure? Figure 108 is a generic depiction of what this may look like.

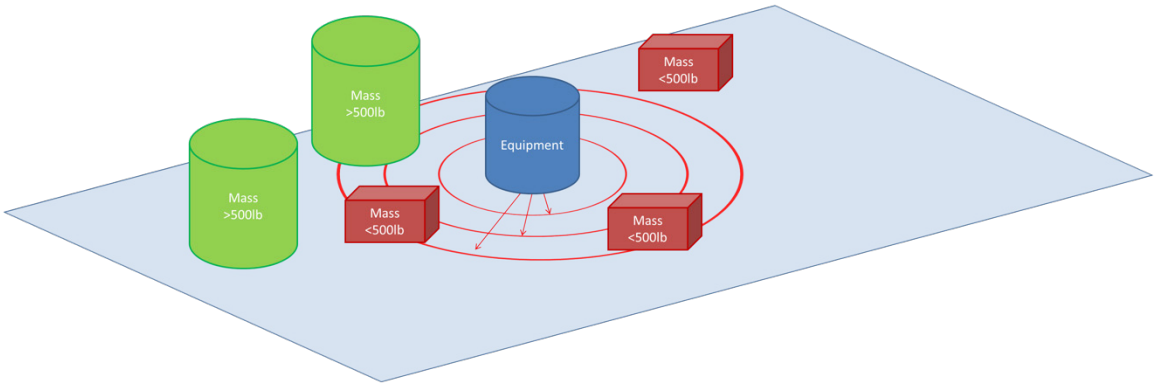

Figure 108. Influence of Equipment Location to Functional Failure

b. Mitigation of Variations

Additionally, there is the issue of variation about the ship. Specifically, the question arises as how to resolve issues of equipment location placement and mounting. One method is to incorporate the use of reduced order models to test within VV&A full ship shock

model based on appropriate functional failure mode and the desired installation location of the equipment. More is yet to be learned concerning this aspect of the M&S approach.

2. Influence of Shock Test Machine

The M&S of the FSP, LWSM and full ship model produced results that confirmed what was reported in [135], that is, the type of test machine or platform does influence the result. A DDAM comparison was also made for the generic shell box model of the equipment cabinet that was used in the study. Previous dynamic transient modeling was performed by NPS on a similar model. Figure 109 shows the dynamic transient modeling of the equipment case on the LWSM.

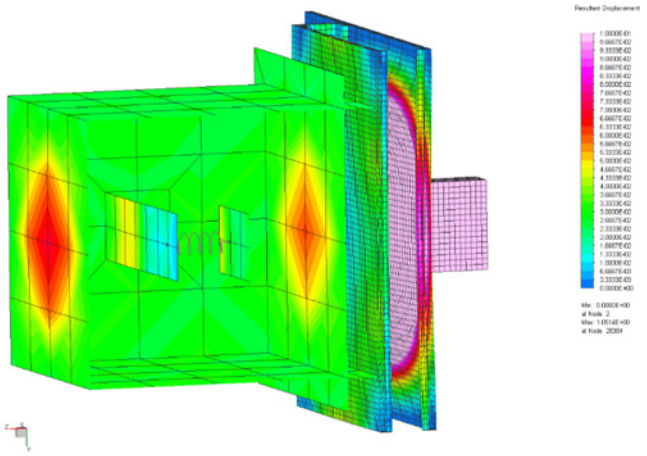

Figure 109. Dynamic Transient Modeling of System with LWSM

Because the peaks of displacement occur at different times in the dynamic transient modeling, only the maximum displacement of the equipment case is shown in Figure 109. Both displacements of the cantilever beams and case in the dynamic transient modeling were approximately 0.05 cm. While the displacement of the DDAM modeling matches the cantilever beam displacement, the casing displacement in the DDAM model results is 0.66 cm, or 10 times greater than the dynamic transient representation of the LWSM.

Another dynamic transient modeling was performed using the FSP shock input, as shown in Figure 110.

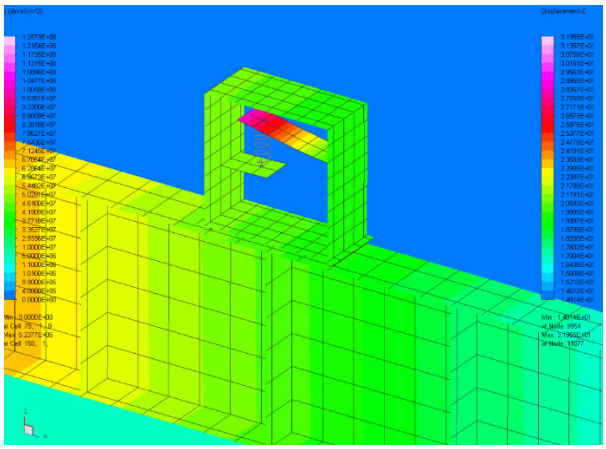

Figure 110. Dynamic Transient Modeling of System with FSP

The maximum displacement observed in the dynamic transient modeling with the FSP was approximately 15.24 cm (6 in), far greater than either the dynamic transient modeling of the LWSM or the DDAM analysis of the system. In this case the standard FSP model was used. Further work is ongoing with the tuned deck FSP model to explore the differences in the dynamic response.

THIS PAGE INTENTIONALLY LEFT BLANK

VI. RESULTS AND DISCUSSION

Considerable efforts have been made in the investigation of shipboard equipment shock qualification failure analysis using numerical experimentation of standard shock test machines, the FSP and full ship models as described in the previous chapters of this work. This chapter summarizes the finding from the failure assessment and analyses of numerical experimentation test cases and documents the development of the failure criterion. Additionally, the proposed implementation of the failure criteria is discussed as an improvement over existing practices in the qualification of shipboard equipment for shock hardness.

A. PROPOSED APPROACH TO EQUIPMENT SHOCK QUALIFICATION

In order to more definitively state that the equipment, systems and components subjected to shock qualification testing and analysis are in fact ready to go into a combat environment, an updated approach is proposed. Based on the numerical experimentation and other investigations conducted herein, an approach utilizing a multifactor failure criterion is presented. The main objective of the updated approach is to reduce the uncertainty in qualification testing by using defined thresholds for maximum velocity and change in displacement. Functional failure assessment is based on a verified shock geometry and base input time histories.

1. Development of Approach

The Pressure Impulse (P-I) diagram shown in Figure 111 is a convenient way to represent blast loading. Several common damage and failure methods use this type of chart to designate failure thresholds and damage areas [136].

Newton's Damage Boundary [63] method employs a variation of this diagram to plot peak acceleration against change in velocity. However, unlike the smooth curve that the P-I diagram produces, with an associated formula, as given in Equation 6.1 [137],

$$\left(P_o - P_{cr}\right)\left(I - I_{cr}\right) = C \tag{6.1}$$

where the change in initial and critical pressure and impulse are related by a constant value *C*, the failure criteria here, determined via the analysis of the functional failure model, result in and provide linear thresholds to separate the failure and non-failure (normal operations) regions based on the data points alone.

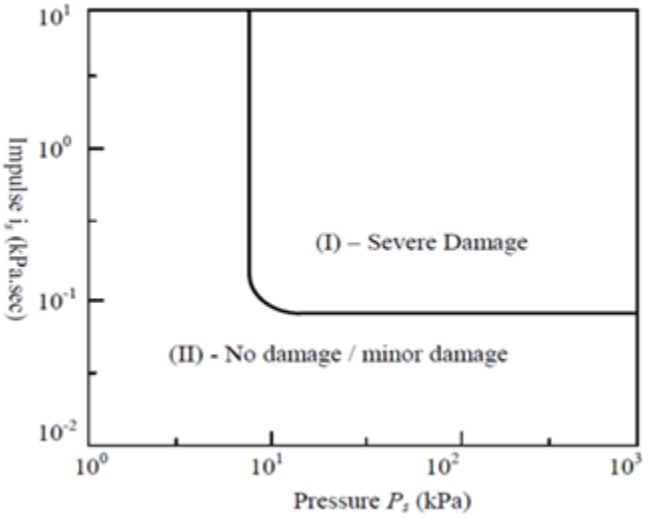

Figure 111. Typical Pressure-Impulse (P-I) diagram. Source: Adapted from [138].

2. Determination of Criteria

Maximum velocity and change in displacement were selected as the two response parameters associated with the use of functional failure as an indicator of unacceptable equipment status in the post shock event period. Detailed explanation of how these values are determined based on numerical experimentation follows.

a. Maximum Velocity

The maximum velocity, V_{max}, is taken as the absolute maximum velocity response experienced by the equipment following the application of the shock loading via base acceleration input such as through the deck, foundation, shock isolator (spring) or other attachment points. All velocities up until the time of functional failure of the representative

model are considered, with the greatest of these being selected. In Figure 112, the velocity time history is taken at the center point of the upper equipment case shell; indicated by the yellow dot in the inset pictorial. The peak amplitude is denotated as V_1, a value that is larger than V_2, which corresponds to next largest amplitude. It is noted that time at which the maximum velocity is realized may exist at any time between the time of impact t_o, and t_f, the time of functional failure, which can be thought of as the start and finish times of the velocity curve bound by the horizontal axis, which represents the equilibrium position.

Here, an important assumption must be made. The equipment structure, which is modeled as fully elastic does not succumb to some sort of material failure prior to the onset of functional failure, which again was described as the contact of two vertically offset cantilevered beams within the equipment model.

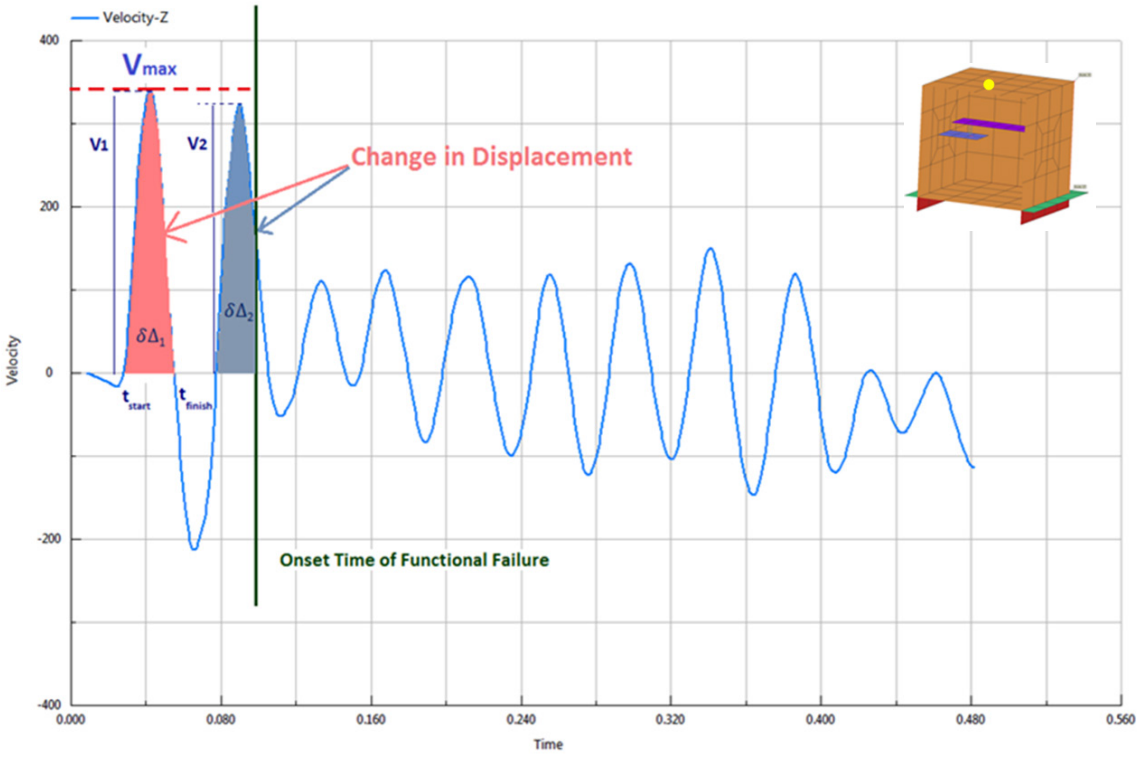

Figure 112. Sample Failure Criteria Value Determination from Velocity Time History

b. Change in Displacement

The use of change in displacement is analogous to that of change in velocity in Newton's Damage Boundary method, however is calculated from the area under the velocity curve vice the acceleration curve. A review of the basic derivation using simple harmonic motion (SHM) in place of the recorded time history is provided here.

The complex velocity curve containing all the represented frequencies of the actual response signal is represented here by simple harmonic motion function, as illustrated in Figure 113. The amplitude of the curve, A, is the local maximum displacement from the reference location, which typically represents the equilibrium (rest) position. The elapsed time, t, increases along the horizontal axis from the $t = 0$ at the start of the curve, where $y(t)$ represents the ordinate of the response in time. The hatched area under the curve is the area equal to the change in displacement.

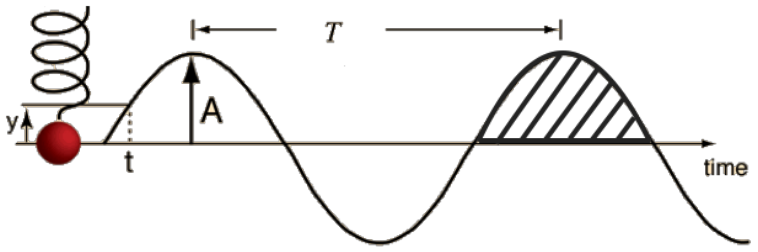

Figure 113. Simple Harmonic Motion Oscillator. Source: Adapted from [139].

If instead of looking at the detailed equipment case as our model, we use a simple spring-mass system with base acceleration (see Figure 114). The relation for motion can be expressed as

$$y = A \sin 2\pi \frac{t}{T} \tag{6.2}$$

Since the period, T, is established as

$$T = \frac{1}{f} \tag{6.3}$$

and represents the time between successive crests of the wave, we then find the relation for frequency, *f*, to be the reciprocal.

$$f = \frac{1}{T} \tag{6.4}$$

As the angular frequency, ω, and *f* are related by Equation 6.5,

$$\omega = 2\pi f \tag{6.5}$$

we can then which is measured in cycles per second (Hz).

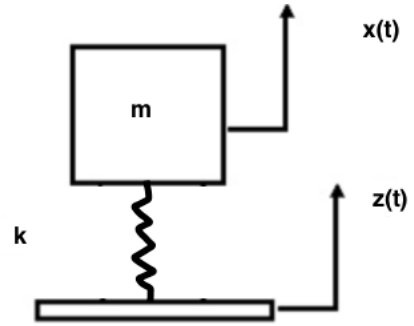

Figure 114. SDOF Spring Mass System

With the response wave fully described, the displacement, velocity, and acceleration responses in the vertical direction are then defined as,

$$y(t) = A\sin(\omega t + \phi) \tag{6.6}$$

$$v(t) = A\omega\cos(\omega t + \phi) \tag{6.7}$$

$$a(t) = -A\omega^2\sin(\omega t + \phi) \tag{6.8}$$

Of particular interest is the equation for velocity. In general, when examining the instantaneous velocity equation

$$V = \frac{dx}{dt} \tag{6.9}$$

we find that it can be rearranged into

$$dx = Vdt \tag{6.10}$$

where x represents a distance and dt the change in time.

Taking the definite integral of both sides of Equation 6.10 with respect to time, the following results

$$\int_{x_i}^{x_f} dx = \int_{t_i}^{t_f} Vdt \tag{6.11}$$

performing the integration of both sides finds that the left-hand side of the equation reduces to

$$x\Big|_{x_i}^{x_f} = x_f - x_i \tag{6.12}$$

and ultimately results in the following solution

$$\Delta = \int_{t_i}^{t_f} Vdt \tag{6.13}$$

which is then the change in displacement. The integral of the velocity with respect to time as shown in Equation 6.13 then provides the area under the velocity curve, as illustrated by the shaded section in Figure 115.

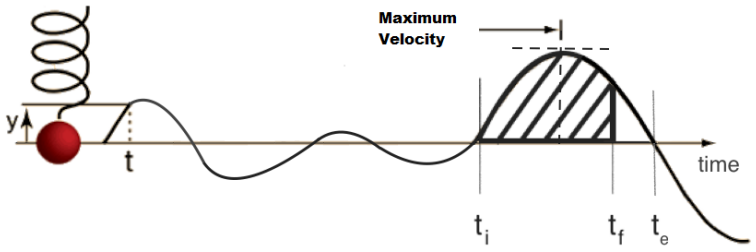

Figure 115. Change in Displacement–Area Under the Velocity Curve.
Source: Adapted from [139].

Since these equations were developed from the basic kinematic equations for the SHM, they must be expanded into a more general form based on Equation. 6.13.

The criteria are based on both the maximum velocity response, V_{max}, and the maximum change in displacement, $\delta\Delta$, as follows:

- V_{max} is taken as overall maximum velocity prior to time of failure.
- Change in Displacement is calculated from integration of velocity during incremental time periods prior to time of failure.

$$\delta\Delta_i = \frac{2}{\pi}\left(t_{finish} - t_{start}\right)_i V_i \tag{6.14}$$

$$\left.\begin{array}{c} \delta\Delta_{\max} = \max(\delta\Delta_i), where \left|\delta\Delta_1\right| > \left|\delta\Delta_2\right| \\ and \\ V_{\max} = \max(V_i) \end{array}\right\} for\ t \le t_{fail} \tag{6.15}$$

Derived from analysis of functional failure of critical component within the equipment model, the largest overall change in displacement is selected from all values prior to the point of functional failure as illustrated in Figure 112.

Figure 116 illustrates the combined results for functional failure plotted for the standard FSP, tuned deck FSP and full ship models. Additional complimentary investigations were conducted using the LWSM and DDAM, however these results are not explicitly included in this summary. The red shaded results indicate that the device failed, (i.e., contact was made between the two cantilevered beams housed within the equipment case). The green shaded markers indicate a pass was achieved and there was no contact between the same beams. The triangle shapes denote the ship case while the diamond shapes, that of the FSP. In the case of the ship, the identical charge weights were used at the three longitudinal positions and there were 15 locations throughout the ship for the equipment model. In the case of the FSP, there was only one equipment case, however the series of simulations were conducted such that the charge was moved laterally away from

the side hull starting at a minimum of 5.49 m (18ft) horizontal standoff distance to a maximum of 15.24 m (50 ft).

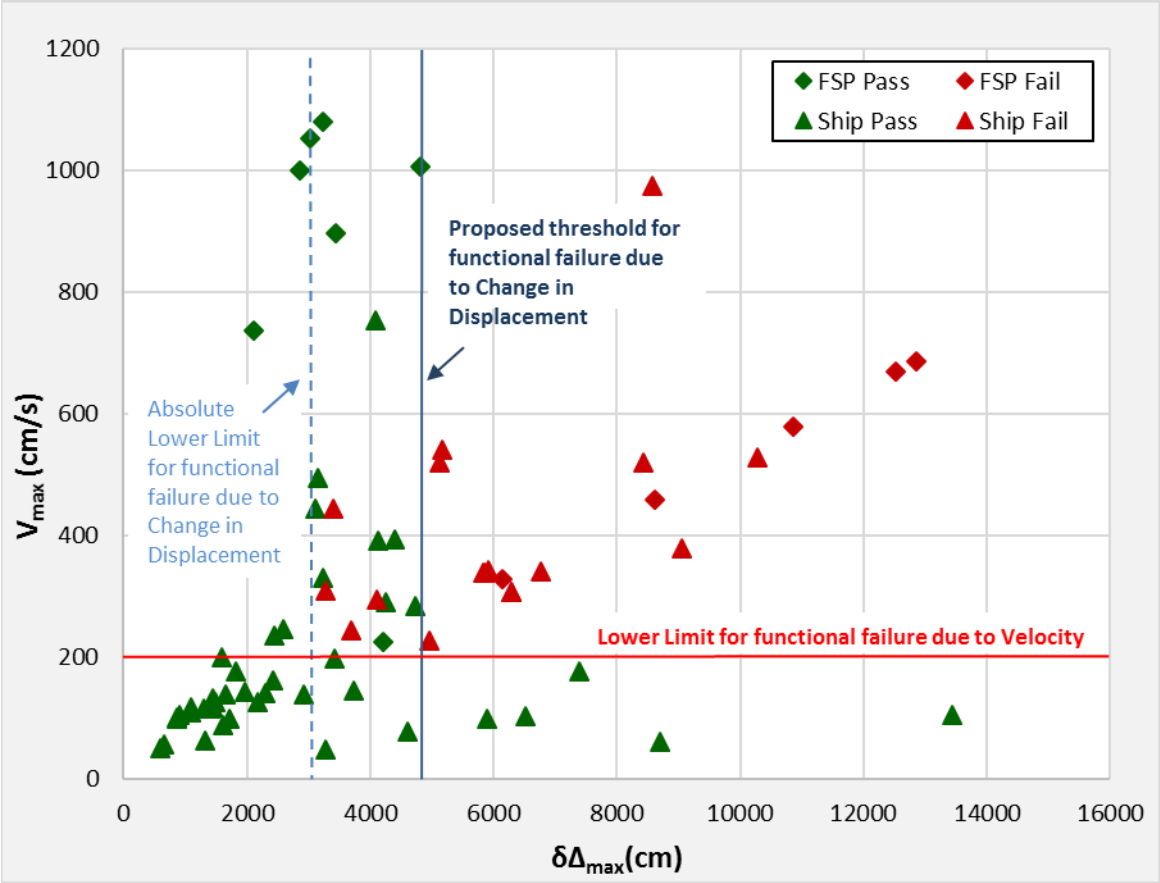

Figure 116. Combined Results of Functional Failure Analyses.

Apart from a small number of outliers, the predominance of the data indicates failure fell at a maximum velocity response of above 200 cm/s and a change in displacement of over 4800 cm. A few of the full ship and standard FSP data points with higher peak velocities, above 500 cm/s and in the range of 3200 cm change of displacement and greater, could be categorized as nearly having failed. In these cases, the cantilevered beams relative positions were plotted and found to be within 1 cm of another as illustrated in Figure 117. This example is taken from the ship simulations, equipment case No. 9, from Table 12, with the charge located aft. This is compared to the same equipment case with a

charge location at amidships, in Figure 118, and is highlighted by a green circle, showing the time of contact (failure) between the upper and lower beams of the functional failure model.

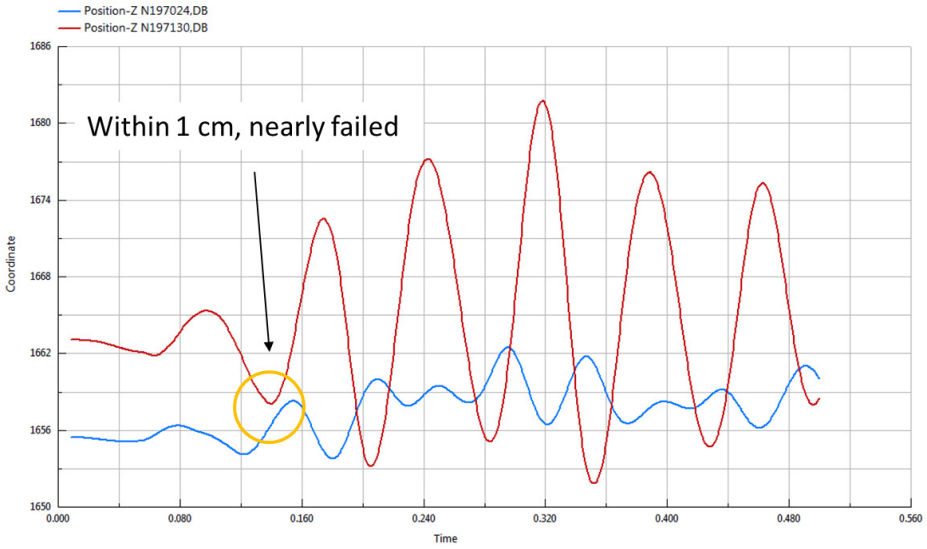

Figure 117. Relative Position of Beams–Nearly Failed

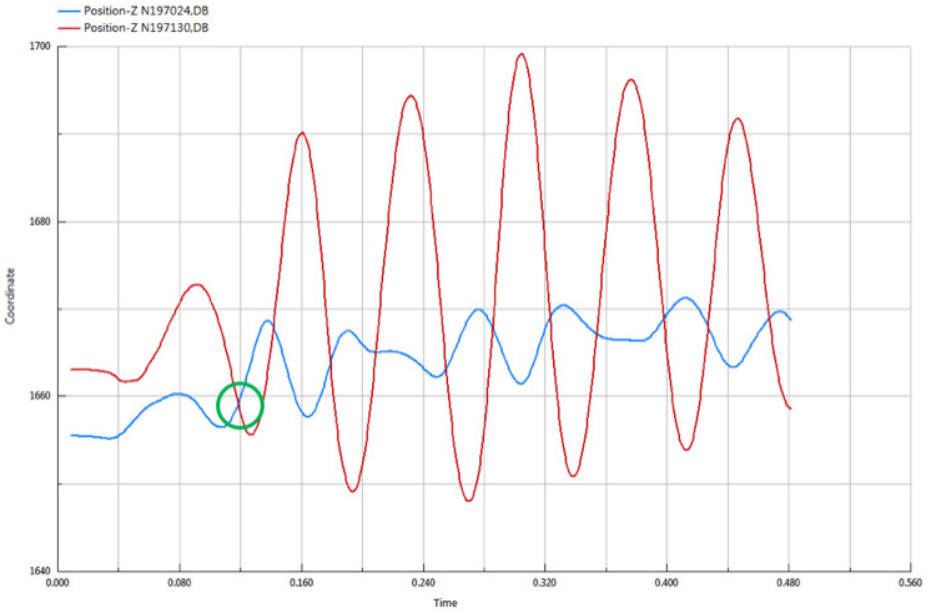

Figure 118. Relative Position of Beams–Failed

Based upon the investigations for this equipment cabinet, our surrogate shipboard equipment test article, the following functional failure diagram is provided in Figure 119.

The absolute lower limit for functional failure is consistent at a maximum vertical velocity response of approximately 200 cm/s (solid horizontal line) and the corresponding threshold for change in displacement is approximately 4800 cm (dashed vertical line). An absolute lower limit for functional failure is found for a change in displacement of 3200 cm (square dot vertical line).

It must be stressed that the multifactor criteria that was developed for this functional failure model and shipboard equipment model is not universal, rather the values are specific to this case. What transcends the particulars of the equipment model and the shock loading is the requirement for both the determined maximum velocity and the maximum change in displacement to be met in order to achieve failure within the model.

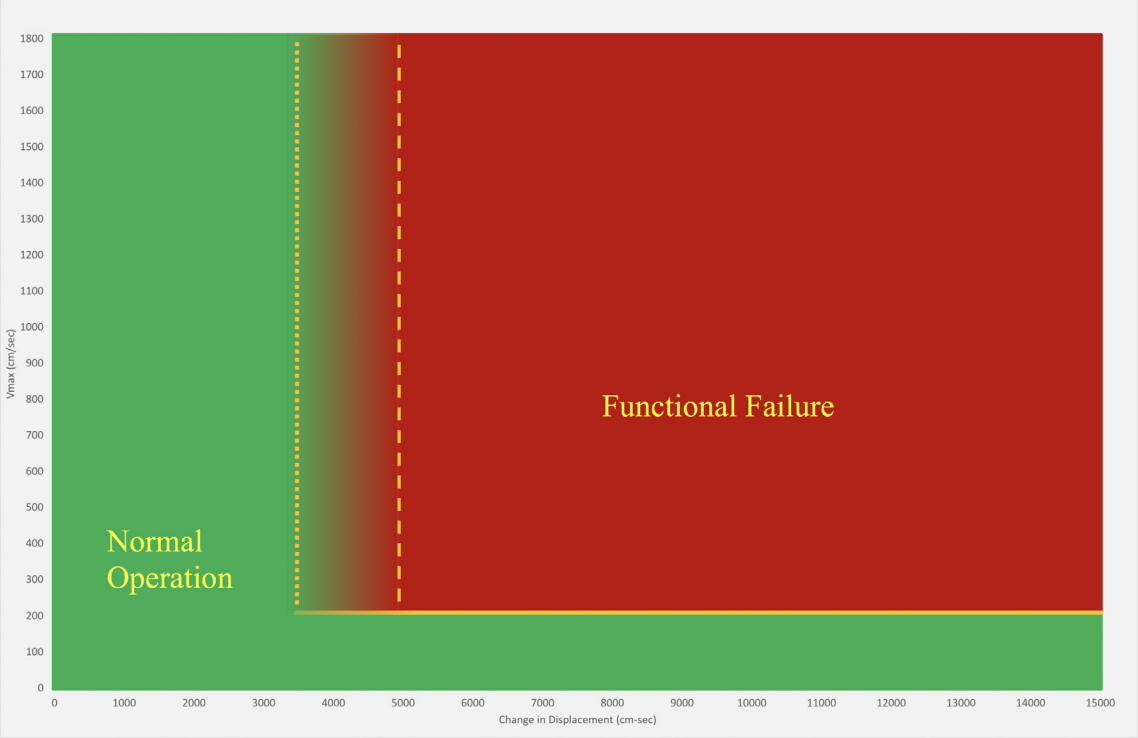

Figure 119. Functional Failure Region Mapping

Keeping in mind that this diagram was generated from various test cases, that included diverse shock factor loading conditions, different ship types, equipment locations and orientations, what this plot illustrates is the fact that there are definitive peak velocities and changes in displacement that bound a functional failure region. By using the multifactor criteria of maximum transmitted vertical velocity response and corresponding change in displacement, regardless of the excitation source, transmission path, or equipment mounting, the qualification status can be determined, as a *pass* or *fail*. However, this is contingent on the condition of satisfactory assessment of the functional failure of the critical component, in its most probable failure mode. This is in addition to the prerequisite requirements consistent with the existing shock qualification standards that no visible or detectable material failure is present in the test article, or no other contributory failure exists which renders the test failed.

Details regarding each numerical test case and the shipboard equipment location are provided in the supplemental data analyses.

B. GUIDELINES FOR USE OF UPDATED ASSESSMENT APPROACH

In the quest to determine a satisfactory failure criterion for the shock qualification of equipment, numerical experimentation was used to complete the following: 1) Develop a representative functional failure model, 2) Improve the accuracy of ship shock structural models, 3) Determine the appropriate failure criteria for assessment of equipment critical components, and 4) Assess shock hardness of the shipboard equipment via reduced order numerical models for realistic shock cases.

Based on the results of these studies, the general procedures for implementation of the proposed approach as an update to the existing shock qualification standard found in [42] are presented here.

1. Method of Application

In the case that a piece of equipment is to be shock qualified for shipboard installation and use, the following method is followed.

1. Prepare equipment in accordance with MIL-DTL 901-E procedures for shock validation of shipboard equipment based on Grade, Class, weight, form factor, etc.

2. Apply accelerometers to test article, velocity meter if practical, to record base input motion to equipment scheduled for test.

3. Measure physical response (acceleration, velocity, strain) away from base.

4. If equipment passes current test requirements, proceed with the following. (If it does not, modify, redesign and retest the equipment.)

5. Create a reduced-order MDOF equipment model via modal analysis (system identification procedure) using existing FEM model, if available.

6. Evaluate MDOF model in fully coupled ship shock FEM simulation using recorded 901-E data (installed accelerometer, velocity meters strain gauges) as input, or desired shock scenarios, if unavailable.

7. Place equipment at planned installation locations within the ship model, as known.

8. Extract acceleration, velocity and displacement response values from M&S.

9. Validate equipment against both the known failure limit (physical result from current 901-E test, ensuring visual pass) and the determined failure criteria based on V_{max} and Change in Displacement.

The author's vision of an overall updated shock assessment procedure for shipboard equipment is presented in Figure 120, while the more detailed process for evaluation of the shipboard equipment against the newly proposed failure criteria is presented in Figure 121.

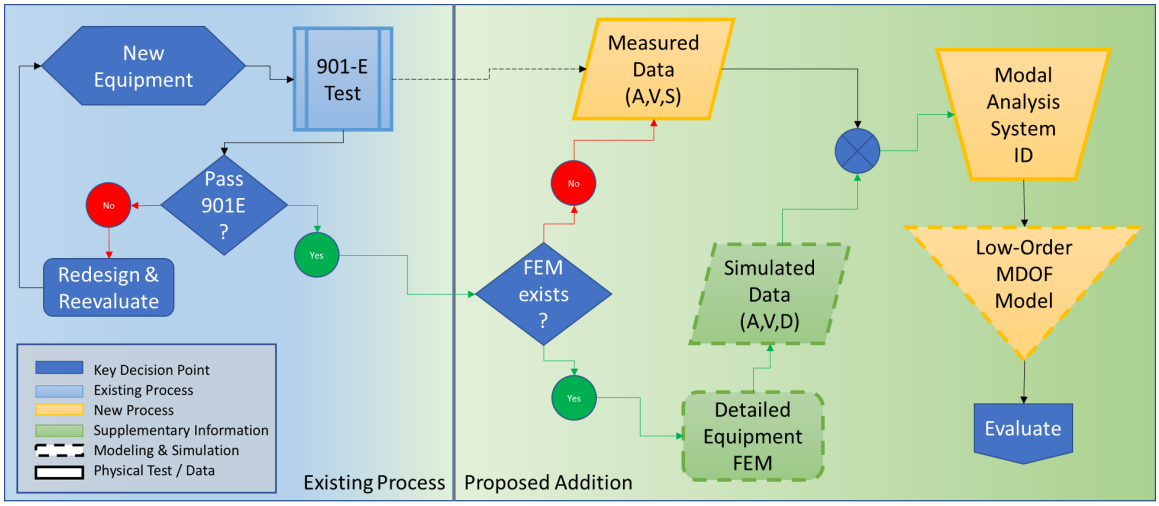

Figure 120. Updated Shock Assessment Procedure for Shipboard Equipment

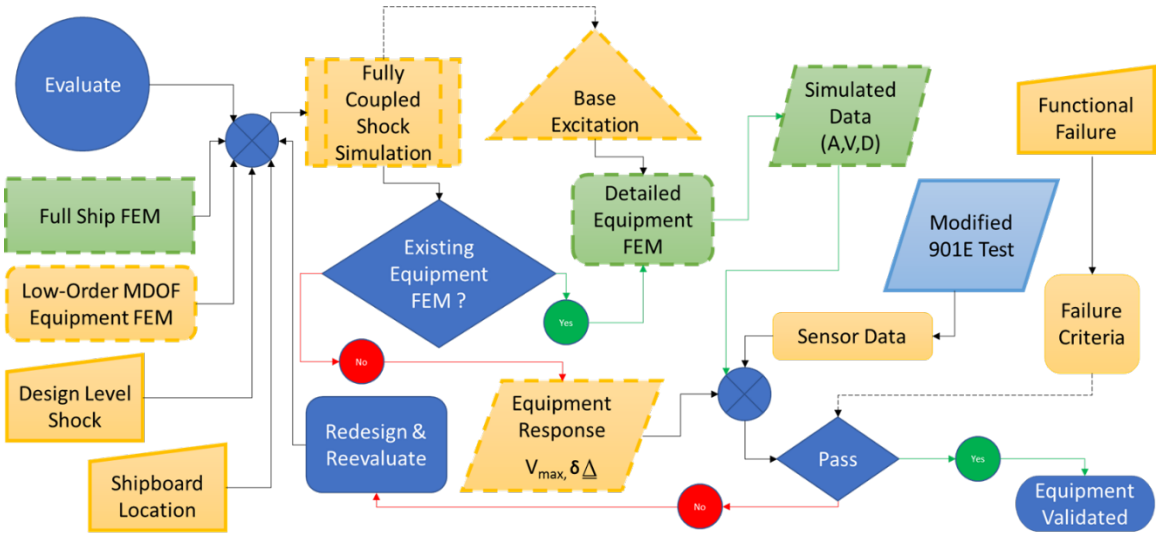

Figure 121. Proposed Shipboard Equipment Failure Assessment Process

2. Implementation of Criterion

As is evident by the preceding flowcharts, there are many inputs to be considered when evaluating the equipment with regard to shock qualification. In an ideal world, a ship shock model derived from a detailed full ship FEM model, ship construction drawings or other would be readily available. With interdisciplinary programs such as CREATE Ships [140] this prospect becomes more practical. Naval architecture, materials engineering, systems integration, electrical network and power distribution grid information are among some of the parameters that are incorporated through this system's modules of Rapid Ship Design Environment (RSDE) [141], Navy Enhanced Sierra Mechanics (NESM) [142], NavyFOAM [143], the Integrated Hydrodynamics Design Environment (IHDE) [144], and other software modules. As such, there is great potential in pushing the state of the art forward and reducing the modeling time through the continued integration of these and other modeling and simulation tools and accessibility of test data available to the engineer.

C. BENEFITS OF UPDATED APPROACH

There are several benefits that result from the updated shock assessment process for shipboard equipment as presented herein.

1. Base Motion Record

First, the inclusion of a requirement that specifies the measurement and cataloging of base acceleration input data for the component being tested is prudent. Having archived accelerometer data available for analysis regarding functional failure using the FEM model is useful in the approach described here, but also as a means of failure investigation throughout the life cycle of the equipment.

As a design tool, this can be used when both modifying the equipment, but also in investigating modifications of the ship surrounding structure, equipment relocation or future placement and perhaps orientation. The archived record facilitates the investigation of the shock response for future applications, but also enables comparison for items that may have failed later in a shock event, whether by test or attack.

2. Reduced Order Model

Use of reduced order models is highly desirable in evaluating new equipment placed in various locations throughout the ship, as was completed in these studies. It is yet to be determined how influential the global hull structure and local scantling may be in determining the functional failure, as was done here, however a reduced order model enables the simulation to focus on a particular aspect of the failure vice overall material performance. This too facilitates the inclusion of many more equipment models integrated throughout the detailed full ship model, without negative impact on the computational timestep and runtime of the simulation. It is envisioned that multiple reduced order models, representing unique functional failures can be exercised at similar locations within the full ship model to aid in the zonal mapping of equipment response. Ultimately having this quantifiable data tied to the investigation of functional failure as a criteria aids in the decision-making process regarding the acceptance and use of shipboard equipment.

a. Extends Use of M&S Tools

In general, the reduced order model approach can specifically enhance M&S by:

- Incorporating functional failure modes as well as structural failure.
- Simulating proposed equipment response via numerical analysis.
- Expanding the range of loading cases to actual threat levels.
- Investigating limitless shipboard locations (planned, desired, required).

b. Impact on Ship Design Process

As alluded to in the opening and background sections, the primary goal of shock qualification of shipboard equipment is to ensure that ship system mission capability does not deteriorate in an unacceptable manner following an UNDEX event. In the 2007 JASON report [43] it is suggested that,

> A component shock-qualification procedure which ensures the survivability of 99% of the critical components still is not good enough to ensure a ship's continued operational capability in the aftermath of a nearby underwater explosion.

Traditionally, early in the ship design process, the hull shape, stability, structure, power and propulsion all take precedence over the arrangement of compartments, placement of subsystems and performance of equipment. The latter are outfitted to the ship and adapted to meet the expected response loading transmitted from the ship which in essence acts as a giant filter of frequency and amplitude.

So instead of being used solely to help check the design performance and optimum location of equipment for installation, the reduced order models could be used early in the design to impact choices in the actual principal characteristics of the ship itself. Use of fully vetted ship shock models similar to the one used in these studies also promotes further comparison of existing ships with regard to modernization and informs new platform design.

3. Appropriate Test Selection

A longstanding question relates to what test or which procedure should be used to shock qualify a component or equipment. As was discussed, there is a bias for use of physical shock test machines in qualification testing. Associated costs of testing expensed by the vendor drive towards preferential selection of the LWSM whenever possible as it is the test series that can be performed with the least amount of preparatory work and at the lowest cost. However, this simple test, though a predominant means of shock qualification within the community, is perhaps not best suited in all cases.

Use of the functional failure criteria approach may help better inform physical test selection. By evaluating the equipment fragility and expected failure mode, and failure mechanism, the "best" test, which is the most informative based on shock loading and response may be conducted by appropriate test selection and proper gauge placement.

4. Comparison of Threat Level

Clearly one of the other benefits that this approach brings, over physical testing alone, is the ability to assess component performance beyond the known "safe" zone. Numerically exceeding the design level via increase of the shock factor provides for better

understanding of performance over the conventional extension of acceptable test levels. Additionally, it allows for different types of excitation to be applied and evaluated.

5. Potential Shortcomings of Updated Approach

As with most processes that delve further into the science of improvement, there are, as expected some potential impediments in employing the proposed updated approach to shipboard equipment shock qualification. Additionally, effort and resources, namely the time and associated costs to perform the analyses top this list. Yet other suggested items such as the mandated installation of a small quantity of gauges and recording of base input and overall equipment response of the critical component being tested may or may not be cost prohibitive. The collection of this data provides a future means of incorporating greater sample size, diversity of equipment and testing for refinement of failure criterion and further verification of numerical analysis against physical test data.

THIS PAGE INTENTIONALLY LEFT BLANK

VII. CONCLUSIONS

The topic of shipboard equipment shock qualification in the non-contact UNDEX environment was studied. Specifically, functional failure tracking through the modeling and simulation of a surrogate model was accomplished in order to enable prediction of critical component failure within representative shipboard equipment. Proposed failure criteria for realistic shock loading cases are identified based on these results.

Developed via numerical experimentation and subsequent analyses of functional failure in simplified (spring-mass) equipment models, multifactor failure criteria based on maximum velocity and maximum change in displacement of the equipment are prescribed in terms of threshold values for the same in order to inform shock qualification assessment.

Additionally, in an attempt to further increase knowledge and reduce unexpected failures in surface ship shock hardening, an improved structural modeling regimen and revised testing approach is recommended in order to reduce uncertainty in the current shock qualification processes for shipboard equipment.

A. SUMMARY

Failure is conceived in this instance as the lack of residual capacity to absorb the dominate failure mechanism in a particular failure mode as a result of shock loading applied to the system.

From basic FMEA previously performed in terms of design, function and process, it is known that failure of shipboard equipment occurs due to material dysfunction such as deformation of structure, which through elongation eventually leads to fracture. This is one of the most commonly thought of failure types, and perhaps most easily understood, yet the system or equipment considered to be failed can and does often exist absent of obvious material failure in a state where it is unable to complete its intended mission or task. Analysis of functional failure is beneficial in better understanding the limitations of current testing approaches and how they are used to qualify shipboard equipment for use in shock environments. However, unlike design (material) failure analysis, the detection of the failure mechanism can be much more elusive.

First, an improved two-stage structural damping model was presented as a means to reduce modeling inconsistencies. This proportional (Rayleigh) damping scheme not only utilized proportional constants extracted from the time history analyses of simplified representative systems of the structural model but furthermore, employed a transition time selected as a function of natural frequency and decay constant for optimal application of these constants. Implemented in the full ship finite element models, these three parameters together serve to address both mass and stiffness driven damping influences in both the early and late time, and within the low and high frequency regimes, respectively.

Next, a basic equipment cabinet finite element model constructed of fully elastic shell elements served to model the material performance. A pair of vertically offset cantilevered beams connected to one another by a soft spring at the tip and fixed at the side frame of the equipment cabinet represented the functional failure model. Contact of the beam tips indicated failure, which could be thought of simply as a critical component making undesired physical contact within the equipment case.

Numerical experimentation with the representative equipment model positioned on the LWSM model, FSP and full ship models, was conducted across various shock loading scenarios. The effects of shock severity, equipment mounting configuration, test platform location and charge source position were included in the amassed data set. As a result of this approach not all the data was available for direct comparison, yet the aggregate provided both depth and breadth in evaluation of the function failure affects within the equipment response due to the variety of cases studied.

This research demonstrated that functional failure of the critical component in this case, occurred, when both a lower boundary at a maximum velocity of 200 cm/s and a corresponding change in displacement of 4800 cm, was observed. In some cases, a small number of outliers were found to exist that potentially lower the change in displacement threshold value to approximately 3200 cm as an absolute lower limit. And while these values are not universal, as it is recognized that they are not necessarily appropriate for other equipment models, they can be applied across any non-contact UNDEX for this representative case. The ability to use this multi-factor failure criteria-based approach from the calculated response values of change in displacement and maximum velocity of the

equipment model subjected to various shock geometries provides improved ability to predict equipment shock hardness performance over physical testing alone.

B. RECOMMENDATIONS

An updated approach, as proposed here, implementing functional failure criteria, will reduce uncertainty in the shock qualification of shipboard equipment and enhance shock hardening performance of naval combatants in an UNDEX environment. These are some but not all the recommendations based on the work presented.

1. Use of Failure Criterion

The proposed failure criterion can be implemented with minimal change or cost to the current shock qualification procedure. More detailed study of actual equipment via scaled laboratory experimentation and traditional shock qualification testing (LWSM, MWSM, and FSP) should be conducted to provide further understanding of the applicability of the proposed criterion.

2. Shock Loading and Response Record

Though there is currently not a requirement to instrument equipment undergoing shock qualification testing, it is recommended that a base input and equipment response record be requested and kept for future data analysis. Building a library of typical equipment shock loading and system response time histories for each equipment tested, would provide valuable data in analyzing potential changes to equipment shock failure response determination during major ship alterations, equipment installation location changes, or in extension of qualifications to new ship classes or equipment model updates.

3. Future Work

Rather than a refined solution, the approach presented herein is a first step in advancing shipboard equipment shock qualification. Further sensitivity studies are necessary in order to expand the data set used in the numerical experimentation. Exercising additional existing full ship shock models is a logical extension of this work. The effects of shock severity caused by variance in loading cases (shock factor) resulting from changes

in charge weight, type and geometry are of particular interest. Determining the significance of other possible influencing factors such as proximity of closely spaced major equipment, consequence of ship hull forms, variations in primary ship structure and deck scantlings, the installation, mounting and placement of equipment components and the overall dependence on transmission path is also suggested.

Additionally, other types of function failure mechanisms are to be studied commensurate with the specific shipboard equipment being evaluated for shock qualification. Inevitably other representations of functional failure specific to different classes of shipboard equipment exist and should to be incorporated into the modeling and simulation of shipboard equipment shock qualification via this general approach.

Finally, construction and subsequent testing of a physical functional failure model similar to the one studied here must be completed in order to further correlate numerical experimentation results with laboratory test data to verify robustness of this method.

Related follow-on topics of study include the influence of strain rate, combinations of shock failure mechanisms, incorporation of latent component errors in the equipment and failure probability.

APPENDIX A. FLUID MODELS

The fluid domain is set up such that the explosive charge is placed in a two-dimensional (2D), XZ grid, and subsequently propagated to a preset trap condition. At this point the simulation is halted. The XZ grid pressure profile is loaded into the full 3D grid using the previous axisymmetric result. Then the body (structural model) is coupled to the fluid and the simulation is executed as a fully coupled run. This fully coupled approach allows for comprehensive fluid structure interaction through a coupler interface. The details of this process are examined in this appendix using the FSP model as the structural model coupled with the fluid.

A. 2D FLUID

The 2D fluid is used to achieve a very accurate initial shock pressure wave propagation during the initial prescribed burn phase of the explosion simulation where solid high explosive material is changed from an unburned to burned state for ideal explosive products of materials [145] following the Jones-Wilkins-Lee (JWL) [146] equations of state.

1. Grid

The DYSMAS program uses a rectangular fluid mesh generator titled GemGrid. The grid generator enables the user to select from spherical, cylindrical or rectangular coordinates. A uniform or expanding cell grid may be used in preparing the fluid domain. Figure 122 presents a combination scheme wherein the center section of the fluid domain is uniform in both the horizontal and vertical directions, while the upper and lower regions expand with a fixed ratio away from the center section. The insert of Figure 122 highlights this fanning effect which is used to reduce the overall number of cells required for the calculation while preserving the sharpness of the shock front in the immediate area of the detonation.

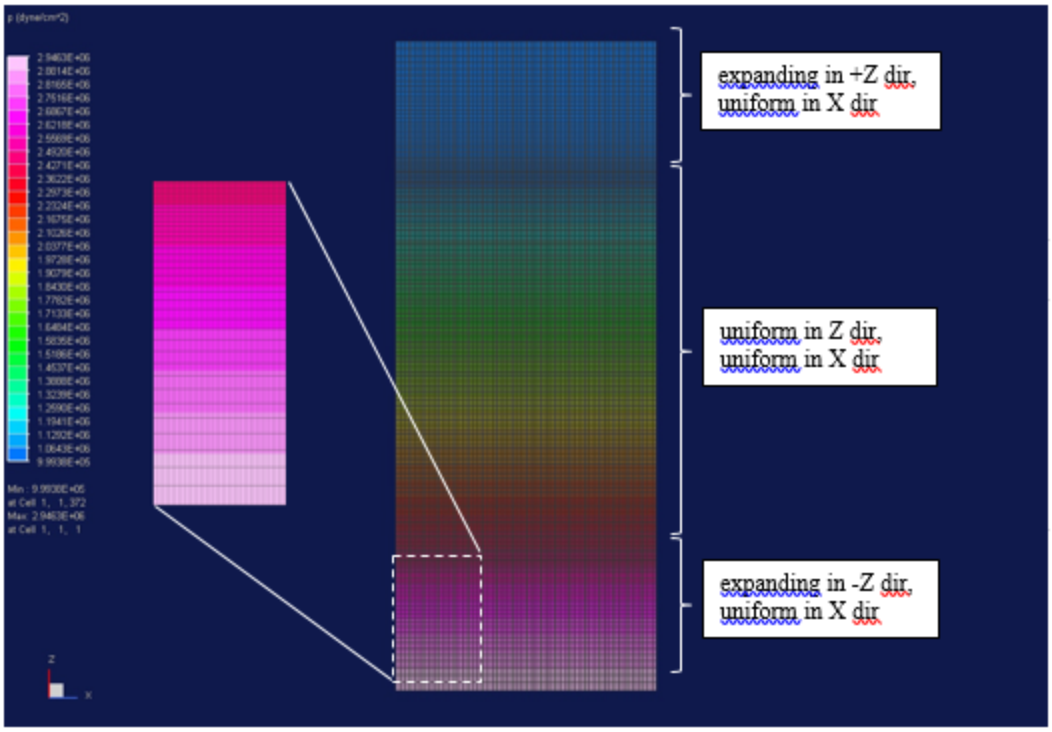

Figure 122. Grid in 2D Pregemini with Inset of Grid Expansion in Z-dir

2. Pregemini

In the Pregemini subroutine, the problem space is defined. Hydrostatic properties, explosive materials and boundary treatment such as the ocean bottom and air-water interface, are set, in a 2D space.

3. Gemini

The Gemini hydrocode was set to run out to a termination time that corresponded to the trap condition. The trap condition is set by designation a fluid cell location and specifying a fluid characteristic to be tracked as used as the trigger. In this case a change in pressure value was selected. The location of the fluid cell was chosen to be just outside of the location that the structural body, the FSP, would sit within the 3D fluid mesh once body and fluid were coupled together. The crosshair in Figure 123 indicates the location of the trap condition used in this example.

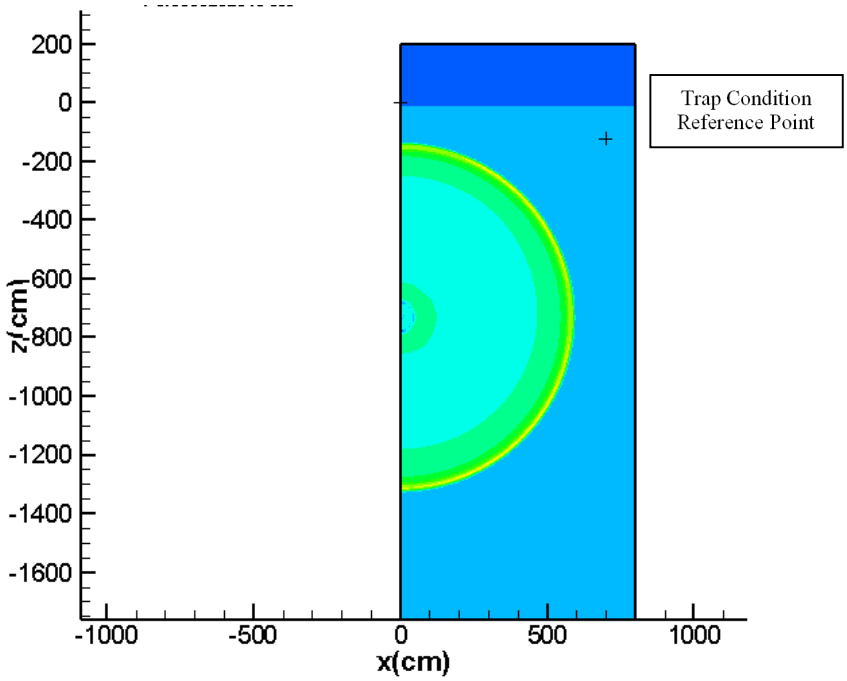

Figure 123. Fluid Mesh Geometry with Trap Location

i. Trap Condition

Trap condition is set at a predetermined distance of 0.1524 m (½ ft) from the outer edge of the FSP on its beam. This is completed in order to allow for high fidelity mesh calculation in the 2D environment, stopping the shock front just prior to the commencement of fluid structure interaction with the FSP. A cell in the fluid is selected and an extremely small pressure set so as to halt the simulation when the trap condition is met. This allows the simulation to go from 2D cylindrical to 3D Cartesian mesh. Figure 124 illustrates the propagation of the shock front toward the trap condition while Figure 125 gives a refined view of the cell grid and test cell at the achievement of the trap condition.

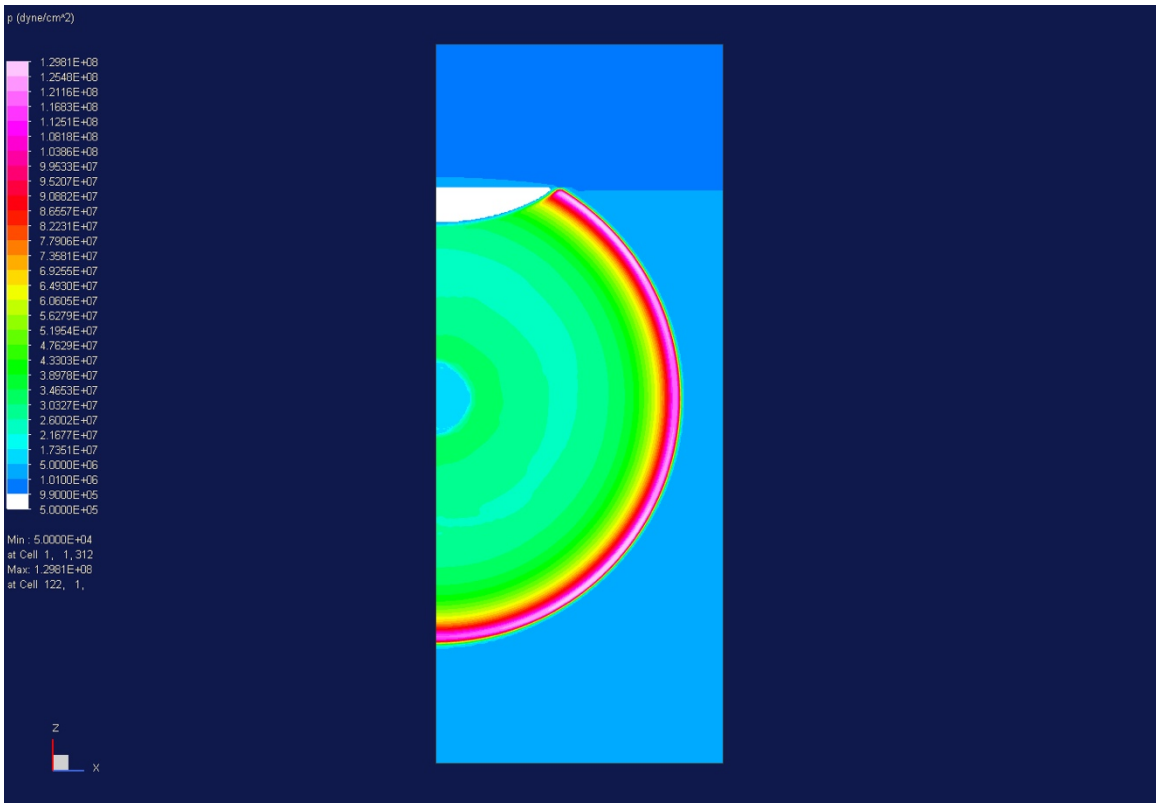

Figure 124. 2D Fluid Propagation at Trap Condition

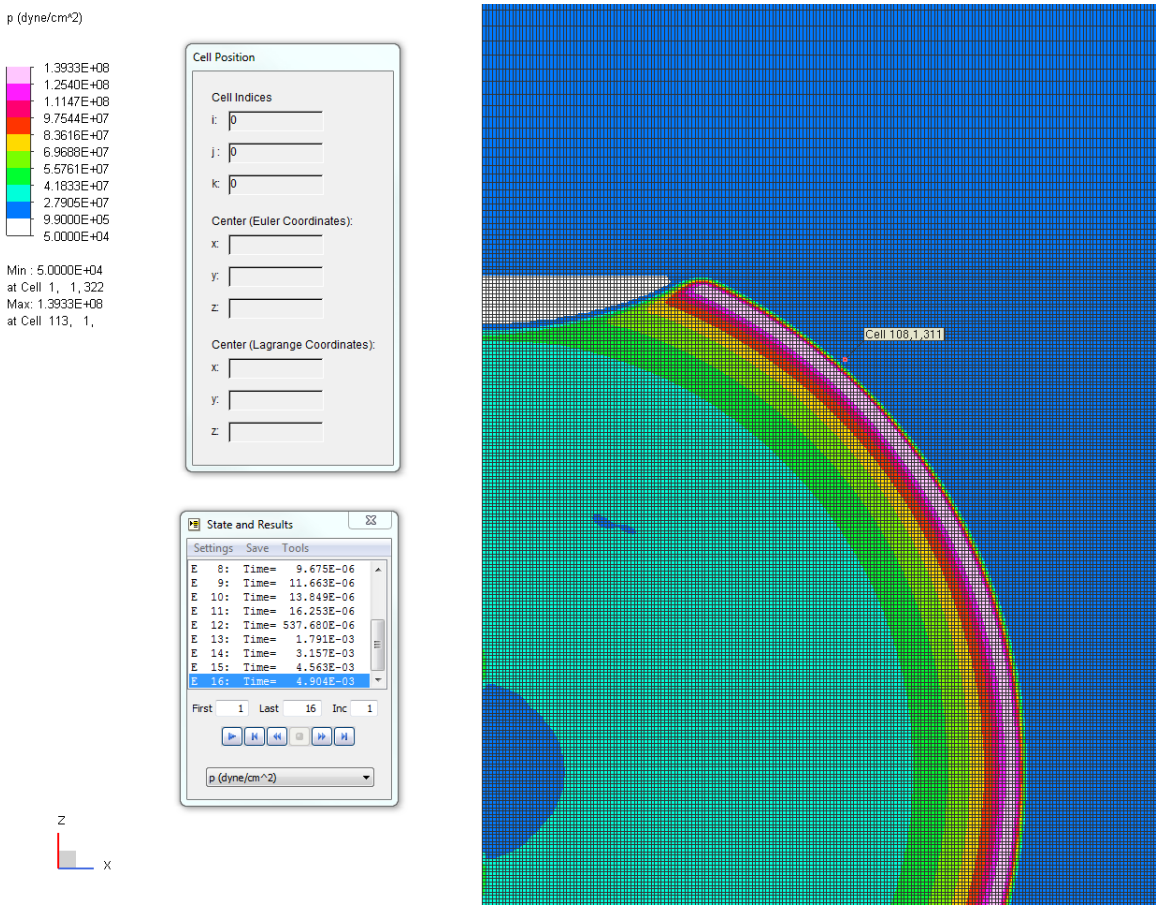

Figure 125. Euler Cell Pressure Showing Refined Mesh at Achievement of Trap Condition

The following fringe plot, Figure 126, compares the charge source detonation point at initiation (left) with the resulting propagation of the pressure front at the end of the 2D Gemini simulation (right). The initial charge location shown to the far left is marked by an arrow for clarity. Figure 127 provides verification of loading pressure to be cast into the 3D fully coupled simulation involving the FSP structure. Of note is the steep rise of the shock front, and subsequent pressure train.

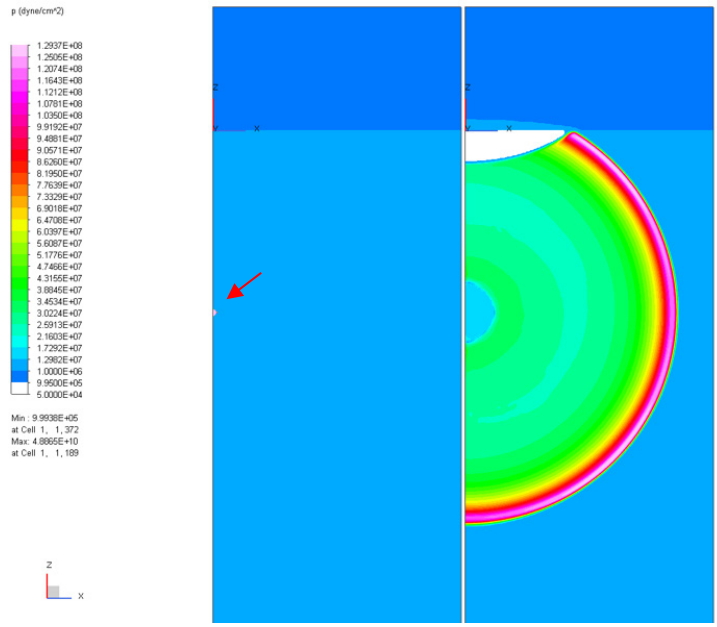

a) Charge at problem start, b) Shock front propagation at trap condition.

Figure 126. Charge Centroid Compared to Gas Globe

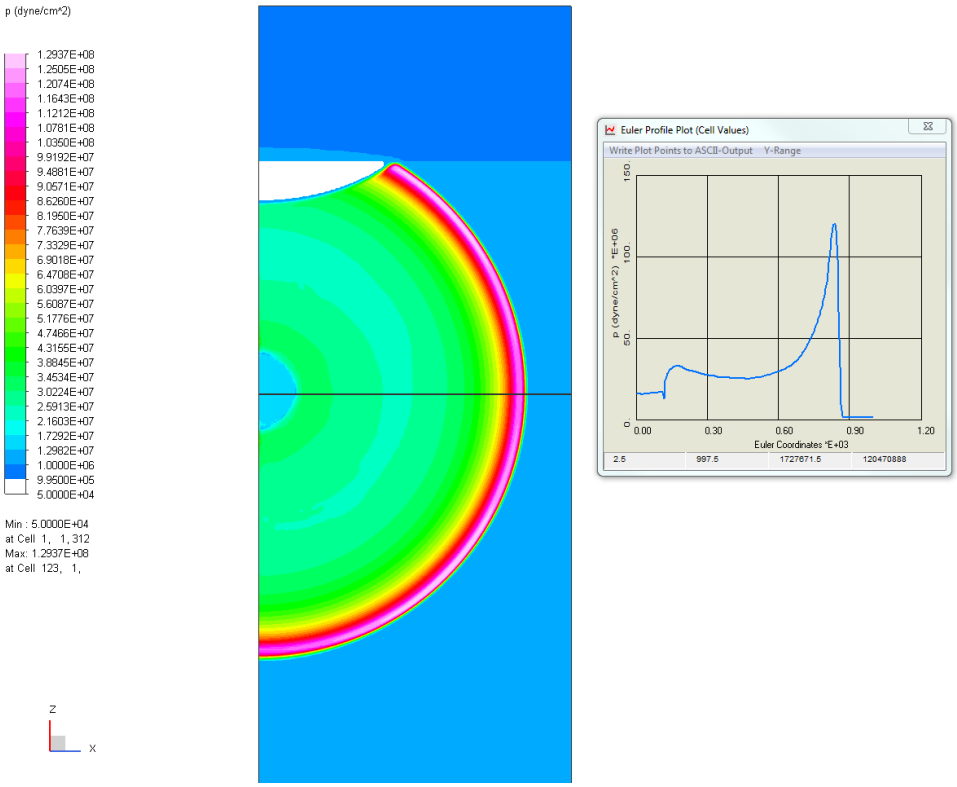

Figure 127. Propagation of Shock Front with Pressure Profile

B. 3D FLUID

1. Grid

Whereas a uniform grid is typically used in the 2D domain, a variable size fluid cell grid is employed in the 3D domain. Figure 128 illustrates sample inputs.

```
                              DIRECTION X
Reference Grid Line =     1
Reference Location =   -1800.0000000

 block    num          a1           a2          ratio          width          Xinit
                                                                        -1800.0000000
    1     45    102.0464710    10.0000000     0.9485774   1800.0000000
                                                                            0.0000000
    2    140     10.0000000    10.0000000     1.0000000   1400.0000000
                                                                         1400.0000000
    3     56     10.0000000   141.0841348     1.0492998   2800.0000000
                                                                         4200.0000000
-------------------------------------------------------------------------------------
 TOTAL   241                                              6000.0000000   4200.0000000



                              DIRECTION Y
Reference Grid Line =     1
Reference Location =   -1000.0000000

 block    num          a1           a2          ratio          width          Xinit
                                                                        -1000.0000000
    1     25     34.8227920    10.0000000     0.9493412    500.0000000
                                                                         -500.0000000
    2     50     10.0000000    10.0000000     1.0000000    500.0000000
                                                                            0.0000000
    3     50     10.0000000    10.0000000     1.0000000    500.0000000
                                                                          500.0000000
    4     26     10.0000000    32.6537670     1.0484732    500.0000000
                                                                         1000.0000000
-------------------------------------------------------------------------------------
 TOTAL   151                                              2000.0000000   1000.0000000



                              DIRECTION Z
Reference Grid Line =     1
Reference Location =   -3500.0000000

 block    num          a1           a2          ratio          width          Xinit
                                                                        -3500.0000000
    1     31     94.8151792    20.0000000     0.9494492   1500.0000000
                                                                        -2000.0000000
    2     69     20.0000000    10.0902775     0.9899893   1000.0000000
                                                                        -1000.0000000
    3    100     10.0000000    10.0000000     1.0000000   1000.0000000
                                                                            0.0000000
    4     37     10.0000000    56.4876276     1.0492708   1000.0000000
                                                                         1000.0000000
-------------------------------------------------------------------------------------
 TOTAL   237                                              4500.0000000   1000.0000000

Total Number of Cells =  8624667 (  8.625M)
```

Figure 128. Sample Gemgrid Summary Output File

2. Pregemini

Here the 2D slice from the XZ plane has been placed within the 3D domain. The symmetry axis at X=0 in 2D allows the user to "spin" the cylindrical coordinates slice through a full 360-degree revolution in 3D. Note only the XZ plane is presented in Figure 129.

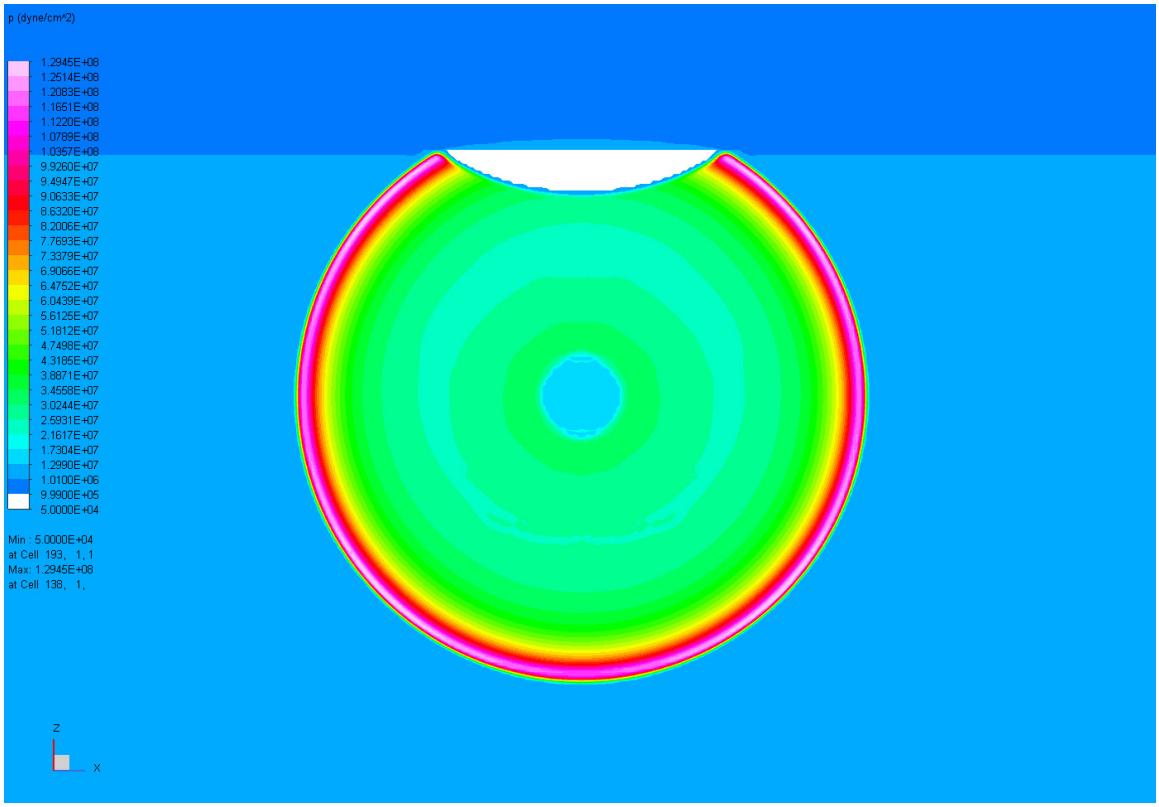

Figure 129. 3D Slice of Propagated Charge Pressure Corresponding to Trap Condition

3. Gemini

The final step in the preprocessing of the fully coupled fluid-structure model is to insert the structural body within the 3D fluid domain which has been preloaded with the previously propagated shock front.

C. FULLY COUPLED MODEL

The structural body is placed in the 3D model at the appropriate location by using the body origin location within the fluid mesh and grid datum. The fluid-structure coupling interface was selected within the DYSMAS/P pre-processor based on the structural model and written out as part of the Paradyn inputs. Appropriate fluid field plot files and structural time history response data are then collected from the fully coupled 3D simulation and post-processed using software packages such as DYSMAS/P, Tecplot and UERDtools.

As a final note, the power of high-performance computing (HPC) systems is utilized by dividing the fluid and structural models into subgrids for multiprocessor computation during the simulation. An example of the non-uniform fluid partition is shown in Figure 130. Computational processors are assigned a balanced load via the internal partitioning scheme or may be manually assigned.

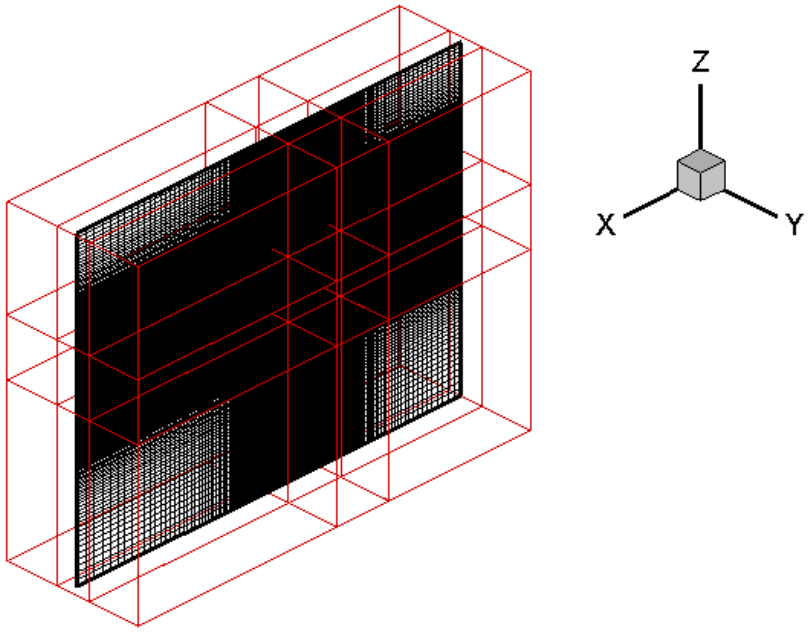

Figure 130. X-Z Plane Showing Fluid Cell Concentration

THIS PAGE INTENTIONALLY LEFT BLANK

APPENDIX B. EQUIPMENT MODEL

This appendix provides more detailed information concerning the various equipment models that were used in the research of this topic.

A. DETAILED EQUIPMENT CABINET WITH FOUNDATION MODEL

The figure shown here of the detailed shell element model represents the main equipment model used in the analysis of the functional failure and shock response. Figure 131 is a cutaway view of the model showing the vertically offset cantilevered beams attached at the ends with a soft spring joining them nearer the free end.

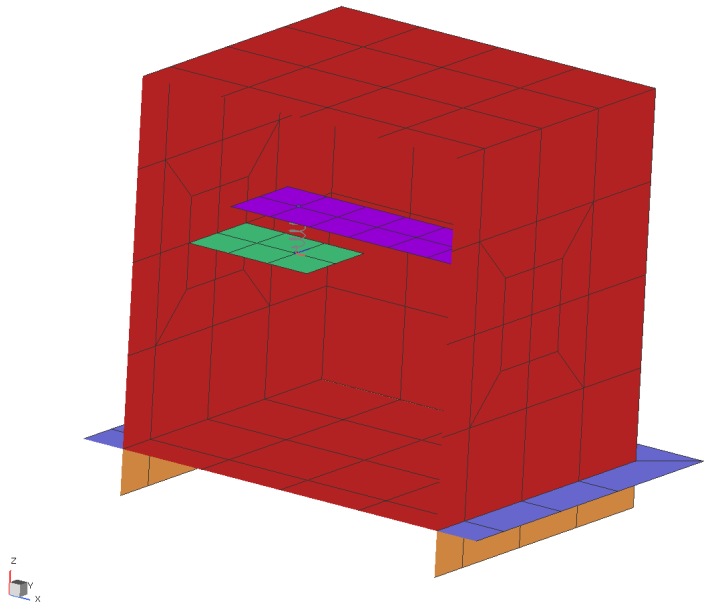

Figure 131. Detailed Shell Model of Equipment Cabinet with Foundation

The material characteristics, mass and centroid information is provided in Table 13 and Table 14.

Table 13. Material Properties of Equipment Shell Model

Edit Material Parameters (Internal Group Number and Element Type can not be changed !)

Int. No.	Ext. No.	Ele Type	Ele Form...	Ref. S...	Mat ...	Density	Youngs M...	Poisso...	Title of Element Group
1	9	QUAD4	Belytschko	0	1	7.8600E+00	2.1000E+12	0.3300	5/64 inch foundation lip
2	10	QUAD4	Belytschko	0	1	7.8600E+00	2.1000E+12	0.3300	5/64 in foundation base
3	7	QUAD4	Belytschko	0	1	7.8600E+00	2.1000E+12	0.3000	4.5 mm Flap Lower
4	8	QUAD4	Belytschko	0	1	7.8600E+00	2.1000E+12	0.3000	Equipment Case
5	11	QUAD4	Belytschko	0	1	7.8600E+00	2.1000E+12	0.3000	4.5 mm Flap Uppper

Table 14. Center of Gravity and Mass values for Equipment Shell Model

Mass/Center of Gravity/Inertia Tensor of active Set

Mass and Coordinates of Center of Gravity (C.G.) of active set

Part	Mass	C.G. Pos-X	C.G. Pos-Y	C.G. Pos-Z
Structural	1.3387E+05	-4.9094E+03	-9.9997E-02	3.7524E+03
Additional	0.0000E+00	0.0000E+00	0.0000E+00	0.0000E+00
Total	1.3387E+05	-4.9094E+03	-9.9997E-02	3.7524E+03

Inertia Tensor referred to Center of Gravity of total mass of active set

Tij	x	y	z
x	1.5093E+08	2.8537E+02	-2.9953E+04
y	2.8537E+02	1.5233E+08	3.3651E+02
z	-2.9953E+04	3.3651E+02	1.4887E+08

B. DETAILED EQUIPMENT CABINET WITHOUT FOUNDATION MODEL

A version of the detailed shell element model, this time without a foundation is represented in Figure 132. This model retained the same material properties as the previous model which included the explicitly modeled deck foundation. The mass is approximately the same while the overall center of gravity is slightly higher in the latter model, nearly centered on the vertical dimension of the cubic equipment cabinet case.

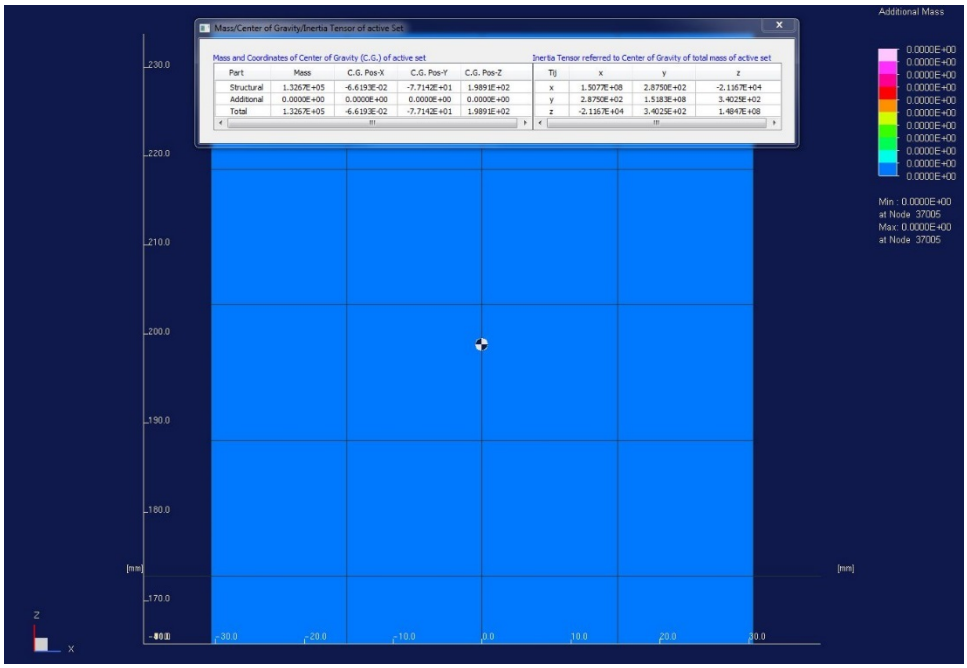

Figure 132. Equipment Shell Model without Foundation

THIS PAGE INTENTIONALLY LEFT BLANK

APPENDIX C. FEM MODELS

An investigation was conducted with the tuned deck FSP. There was a total of six cases investigated. The FSP remained the same in each case while the representation of the equipment, its attachment and foundation was altered in each case to provide a broad range of modeling options. The dynamic shock response of each is compared to the other cases as well as with previously given results from the simple FSP, full ship model and other FSP modeling efforts.

A. EQUIPMENT MODELS

1. Case 1

The first case model consisted of the equipment case and critical component representation, the cantilevered beams used for the failure model. The shell element box was attached to the FSP deck via a simple foundation consisting of shell elements. The equipment system mass was approximately 1.34e5 g (295 lb). A structural foundation was included as part of this model.

2. Case 2

In the second case, the model consisted of the equipment case without the foundation placed at the equivalent center of gravity and connected to the deck, at the same corner points of the foundation footprint as in Case 1, using 4 linear SDOF springs. The mass of the model is 1.14e5 g (250 lb) and the spring stiffness was set to 6.417e10 per isolator.

3. Case 3

In the third case, the model consisted of a single added mass of 1.34e5 (295 lb) placed at the equivalent center of gravity and connected to the deck, at the same concern points of the foundation footprint as in Case 1, using 4 linear SDOF springs. The spring stiffness was 1.06e11.

4. Case 4

This case is similar to Case 2, as there are four springs supporting a single mass, yet the mass here is only 1.14e5 g (250 lb) which accounts for only the equipment case and critical component (failure model) and not the deck foundation. The stiffness of the springs and the center of gravity have been adjusted appropriately based on modal analysis and

5. Case 5

For the model in this case, a simple rigid body structure was affixed atop four springs, at the deck mount corner points, as was done previously. The total mass of the equipment system is 1.14e5 g (250 lb) with a total stiffness split between the four springs.

6. Case 6

In the final case, a two-part tied rigid body mass supported by four simple springs was investigated. The rigid body representation of the equipment box and foundation were tied while the springs provided the equivalent elasticity to the equipment system. The center of gravity and mass were maintained with prior cases.

B. EQUIPMENT MODEL FREQUENCY

A study was conducted using ABAQUS 6.13 in order to determine the natural frequency of the equipment cabinet model. The Lanczos extraction method was used within Abaqus/Standard to analyze several variations of the same basic model as described before. The automatic multi-level substructuring (AMS) scheme was also utilized and yielded similar results to the Lanczos approach.

Figures 133–136 show the first mode plots while Table 15–17 provides the corresponding Eigenvalue data.

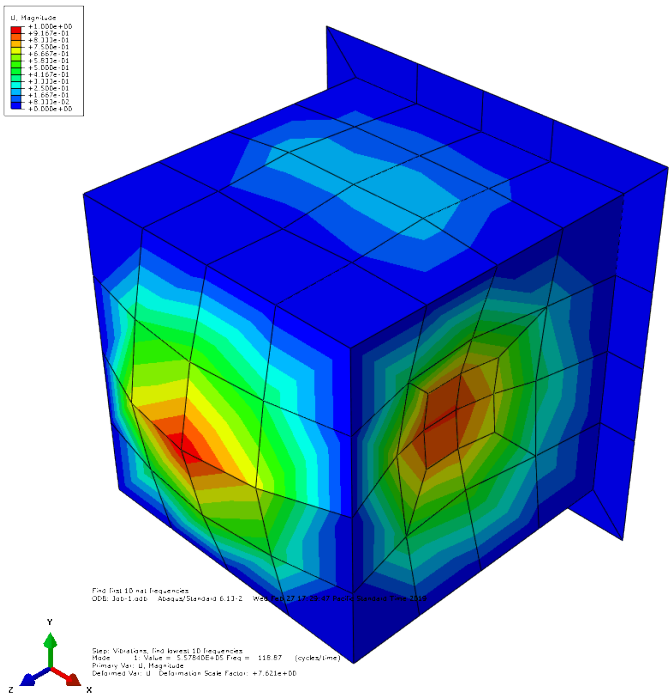

Figure 133. First Mode of Box without Flaps, Foundation Included

Table 15. Eigenvalue Output for Box Model without Flaps.

E I G E N V A L U E O U T P U T

MODE NO	EIGENVALUE	FREQUENCY (RAD/TIME)	FREQUENCY (CYCLES/TIME)	GENERALIZED MASS	COMPOSITE MODAL DAMPING
1	5.57840E+05	746.89	118.87	9556.0	0.0000
2	6.00433E+05	774.88	123.33	7760.5	0.0000
3	6.27678E+05	792.26	126.09	6709.2	0.0000
4	7.38016E+05	859.08	136.73	6066.4	0.0000
5	1.13005E+06	1063.0	169.19	9179.6	0.0000
6	1.21609E+06	1102.8	175.51	2121.4	0.0000
7	2.93980E+06	1714.6	272.88	8499.8	0.0000
8	3.68458E+06	1919.5	305.50	5309.0	0.0000
9	4.00727E+06	2001.8	318.60	5088.3	0.0000
10	4.49779E+06	2120.8	337.54	7635.1	0.0000

P A R T I C I P A T I O N F A C T O R S

MODE NO	X-COMPONENT	Y-COMPONENT	Z-COMPONENT	X-ROTATION	Y-ROTATION	Z-ROTATION
1	-2.98201E-06	-1.51776E-07	0.64451	5.31931E-04	-1.09548E-04	5.08478E-07
2	9.12379E-06	8.03590E-07	0.77872	5.93271E-04	3.95538E-04	-5.11025E-07
3	1.8339	-2.31896E-09	-2.23360E-06	2.51392E-06	75.250	-1.48771E-03
4	-6.86730E-08	1.9825	-5.96192E-08	-82.193	-1.07083E-05	-5.65833E-05
5	3.77192E-06	2.02055E-07	-0.64851	-5.38739E-04	1.33652E-04	-3.48367E-07
6	8.04956E-07	-7.32624E-08	2.0763	1.69977E-03	9.10214E-05	8.60093E-07
7	4.11468E-07	-5.35737E-06	-2.88254E-07	2.49974E-04	1.25257E-05	-36.009
8	7.96721E-02	-1.66381E-07	5.11143E-06	3.18559E-05	-37.186	-6.63794E-05

9	-2.62918E-07	4.21416E-02	-3.86294E-07	35.072	-2.35190E-05	7.16616E-05
10	-3.74570E-07	0.33430	-1.38586E-06	1.1494	-7.49053E-05	-1.69060E-05

E F F E C T I V E M A S S

MODE NO	X-COMPONENT	Y-COMPONENT	Z-COMPONENT	X-ROTATION	Y-ROTATION	Z-ROTATION
1	8.49757E-08	2.20132E-10	3969.5	2.70389E-03	1.14680E-04	2.47072E-09
2	6.46009E-07	5.01138E-09	4705.9	2.73146E-03	1.21413E-03	2.02662E-09
3	22565.	3.60793E-14	3.34721E-08	4.24008E-08	3.79917E+07	1.48494E-02
4	2.86093E-11	23843.	2.15628E-11	4.09834E+07	6.95621E-07	1.94228E-05
5	1.30602E-07	3.74768E-10	3860.6	2.66429E-03	1.63974E-04	1.11403E-09
6	1.37455E-09	1.13862E-11	9145.4	6.12906E-03	1.75753E-05	1.56930E-09
7	1.43907E-09	2.43958E-07	7.06257E-10	5.31132E-04	1.33357E-06	1.10213E+07
8	33.699	1.46965E-10	1.38706E-07	5.38753E-06	7.34116E+06	2.33925E-05
9	3.51733E-10	9.0364	7.59290E-10	6.25875E+06	2.81455E-06	2.61303E-05
10	1.07122E-09	853.24	1.46641E-08	10086.	4.28389E-05	2.18220E-06
TOTAL	22598.	24705.	21681.	4.72522E+07	4.53329E+07	1.10213E+07

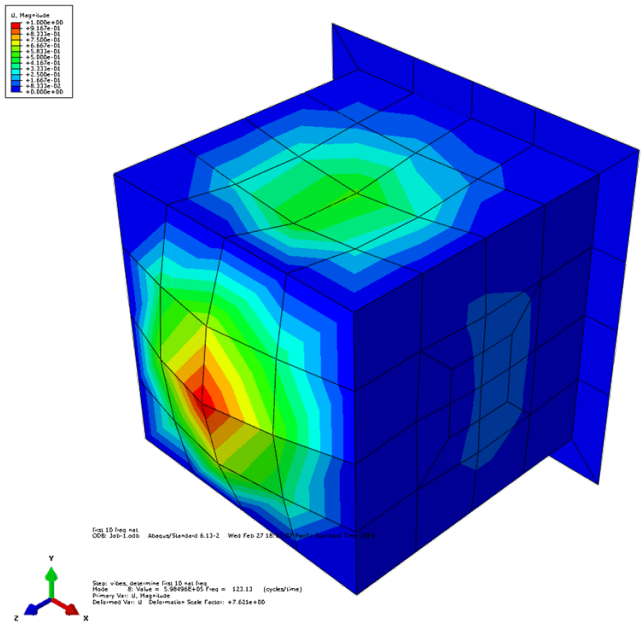

Figure 134. First Mode for Box with Flaps and Foundation Included

Table 16. Eigenvalue Output for Box Model with Flaps and Foundation

E I G E N V A L U E O U T P U T

MODE NO	EIGENVALUE	FREQUENCY (RAD/TIME)	FREQUENCY (CYCLES/TIME)	GENERALIZED MASS	COMPOSITE MODAL DAMPING
1	6915.1	83.157	13.235	721.83	0.0000
2	1.93122E+05	439.46	69.942	313.01	0.0000

3	2.42896E+05	492.84	78.439	1013.6	0.0000
4	2.88135E+05	536.78	85.432	720.20	0.0000
5	3.52391E+05	593.63	94.478	441.13	0.0000
6	3.79948E+05	616.40	98.103	6790.6	0.0000
7	4.77681E+05	691.14	110.00	4908.5	0.0000
8	5.98496E+05	773.63	123.13	5002.4	0.0000
9	7.56385E+05	869.70	138.42	6166.1	0.0000
10	1.04808E+06	1023.8	162.94	7923.4	0.0000

P A R T I C I P A T I O N F A C T O R S

MODE NO	X-COMPONENT	Y-COMPONENT	Z-COMPONENT	X-ROTATION	Y-ROTATION	Z-ROTATION
1	-3.33519E-02	-1.78406E-08	1.5642	1.25193E-03	11.629	2.68622E-05
2	-0.15785	3.81434E-08	1.4443	1.15282E-03	11.937	1.25925E-04
3	3.41795E-06	0.85255	-1.17547E-06	-42.315	1.51085E-04	-19.724
4	0.86054	-3.09164E-07	-0.83561	-6.51615E-04	51.518	-6.78598E-04
5	2.32904E-07	1.77398E-02	-1.21830E-07	9.1013	1.02330E-05	-0.26117
6	1.2116	1.78574E-07	-0.22030	-1.85852E-04	51.575	-9.69622E-04
7	1.7225	-3.07190E-07	0.25930	2.27037E-04	70.107	-1.39000E-03
8	0.10110	6.67650E-07	1.2284	9.63393E-04	4.3443	-8.48626E-05
9	-4.67430E-07	1.9627	1.62423E-08	-81.952	-2.78820E-05	-2.8573
10	6.57622E-02	6.42193E-08	-0.68283	-5.62468E-04	1.2500	-5.76552E-05

E F F E C T I V E M A S S

MODE NO	X-COMPONENT	Y-COMPONENT	Z-COMPONENT	X-ROTATION	Y-ROTATION	Z-ROTATION
1	0.80292	2.29747E-13	1766.2	1.13134E-03	97610.	5.20853E-07
2	7.7991	4.55401E-13	652.95	4.15983E-04	44598.	4.96336E-06
3	1.18411E-08	736.72	1.40052E-09	1.81487E+06	2.31368E-05	3.94309E+05
4	533.33	6.88383E-11	502.88	3.05798E-04	1.91146E+06	3.31649E-04
5	2.39286E-11	0.13882	6.54743E-12	36541.	4.61921E-08	30.089
6	9968.4	2.16543E-10	329.55	2.34555E-04	1.80631E+07	6.38432E-03
7	14564.	4.63195E-10	330.03	2.53014E-04	2.41255E+07	9.48372E-03
8	51.128	2.22988E-09	7548.1	4.64290E-03	94413.	3.60259E-05
9	1.34724E-09	23752.	1.62668E-12	4.14119E+07	4.79357E-06	50341.
10	34.266	3.26772E-11	3694.4	2.50674E-03	12381.	2.63384E-05
TOTAL	25160.	24489.	14824.	4.32633E+07	4.43491E+07	4.44680E+05

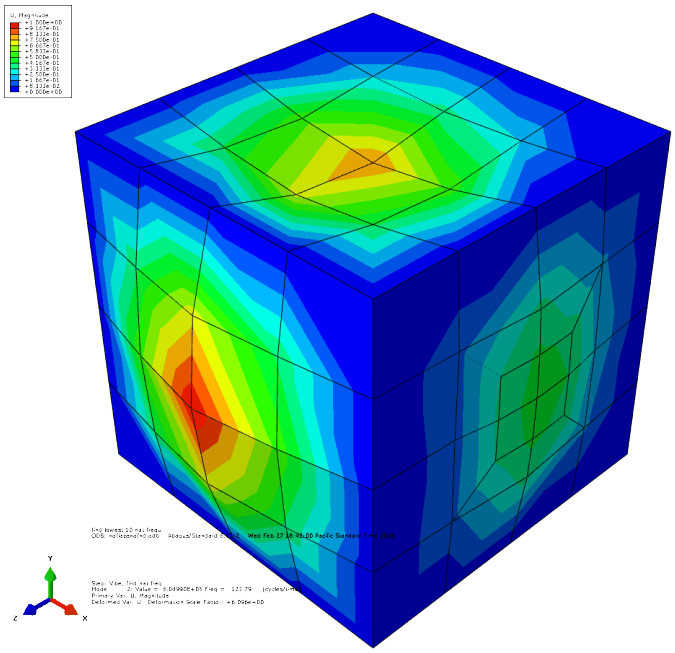

Figure 135. First Mode for Box without Flaps or Foundation

Table 17. Eigenvalue Output for Box Model without Flaps or Foundation

E I G E N V A L U E O U T P U T

MODE NO	EIGENVALUE	FREQUENCY (RAD/TIME)	FREQUENCY (CYCLES/TIME)	GENERALIZED MASS	COMPOSITE MODAL DAMPING
1	5.61175E+05	749.12	119.23	8083.7	0.0000
2	6.04990E+05	777.81	123.79	9057.6	0.0000
3	6.38420E+05	799.01	127.17	6652.8	0.0000
4	7.52458E+05	867.44	138.06	6012.6	0.0000
5	1.13654E+06	1066.1	169.67	8959.8	0.0000
6	1.23697E+06	1112.2	177.01	2065.3	0.0000
7	2.95810E+06	1719.9	273.73	8419.0	0.0000
8	3.74415E+06	1935.0	307.96	5096.6	0.0000
9	4.05432E+06	2013.5	320.46	5293.0	0.0000
10	4.52785E+06	2127.9	338.66	8122.9	0.0000

P A R T I C I P A T I O N F A C T O R S

MODE NO	X-COMPONENT	Y-COMPONENT	Z-COMPONENT	X-ROTATION	Y-ROTATION	Z-ROTATION
1	-2.66134E-06	-8.50603E-08	0.76338	6.21661E-04	-9.38843E-05	2.70794E-07
2	7.69404E-06	7.85356E-08	0.66624	5.36141E-04	3.35817E-04	-1.26184E-07
3	1.7934	-4.21178E-08	-1.76024E-06	2.13302E-06	74.186	-1.45019E-03
4	3.54601E-08	1.9323	4.91031E-08	-80.866	1.93041E-06	-5.47281E-05
5	3.75603E-06	1.65443E-07	-0.52899	-4.34509E-04	1.37251E-04	1.17972E-08
6	-9.31445E-11	-2.27774E-12	2.2478	1.81929E-03	6.03309E-05	9.37636E-14
7	1.13066E-07	-5.12296E-06	4.97978E-09	2.49223E-04	5.95484E-06	-34.857
8	2.44372E-02	-6.79778E-08	4.69859E-06	1.09893E-05	-38.112	-2.04544E-05
9	-1.95614E-08	-1.64969E-02	1.23771E-07	33.557	1.23703E-05	7.30978E-05
10	-5.29929E-08	0.26937	1.90098E-08	4.0819	-6.38246E-06	-8.29604E-06

E F F E C T I V E M A S S

MODE NO	X-COMPONENT	Y-COMPONENT	Z-COMPONENT	X-ROTATION	Y-ROTATION	Z-ROTATION
1	5.72547E-08	5.84876E-11	4710.7	3.12404E-03	7.12518E-05	5.92773E-10
2	5.36195E-07	5.58659E-11	4020.4	2.60358E-03	1.02145E-03	1.44219E-10
3	21398.	1.18014E-11	2.06133E-08	3.02686E-08	3.66143E+07	1.39911E-02
4	7.56031E-12	22449.	1.44969E-11	3.93182E+07	2.24056E-08	1.80086E-05
5	1.26403E-07	2.45242E-10	2507.2	1.69160E-03	1.68785E-04	1.24698E-12
6	1.79179E-17	1.07147E-20	10435.	6.83563E-03	7.51714E-06	1.81569E-23
7	1.07627E-10	2.20954E-07	2.08775E-13	5.22918E-04	2.98537E-07	1.02294E+07
8	3.0436	2.35512E-11	1.12516E-07	6.15486E-07	7.40291E+06	2.13230E-06
9	2.02535E-12	1.4405	8.10847E-11	5.96032E+06	8.09960E-07	2.82820E-05
10	2.28111E-11	589.42	2.93538E-12	1.35341E+05	3.30893E-07	5.59053E-07
TOTAL	21401.	23040.	21674.	4.54138E+07	4.40172E+07	1.02294E+07

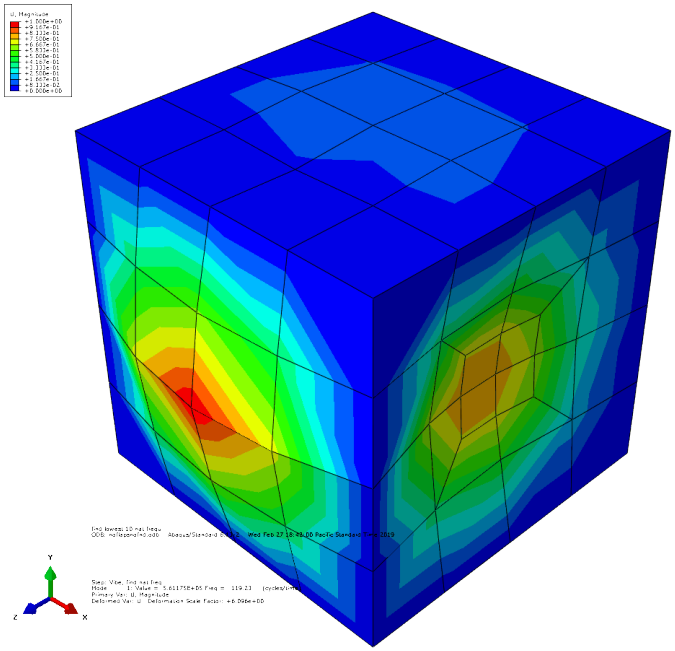

Figure 136. Higher Mode for Box with Flaps and Foundation Included

The FFT evaluation of the series of masses gave 27 Hz as the dominant lowest frequency and 133 Hz for the equipment shell model equivalent weight of 1.14e5 g (250 lb) when using a lumped mass system. The results are listed in Table 18. These investigations were performed using a spring mass atop of the backing plate LWSM model. The corresponding FFT is shown in Figure 137.

Table 18. Summary of Frequencies for Various Mass Weights Representing the Equipment Model

Case	Mass Total	Equip Mass	Peak 1 Base		Peak 2 Base		Peak 1 Top		Peak 2 Top	
1000msec	g	g	Freq (Hz)	Amp	Freq (Hz)	Amp	Freq (Hz)	Amp	Freq (Hz)	Amp
1 lb	4.06E+05	4.536000E+02	110	7.66E+03	222	1.53E+04	110	7.94E+03	222	1.78E+04
64 lb	4.34E+05	2.902000E+04	51	6.04E+03	139	3.13E+03	51	1.15E+04	139	1.25E+03
75 lb	4.39E+05	3.401943E+04	47	5.99E+03	142	3.47E+03	47	1.13E+04	142	1.04E+03
125 lb	4.63E+05	5.669905E+04	37	3.76E+03	136	2.68E+03	37	7.27E+03	136	4.78E+02
250 lb	5.19E+05	1.133981E+05	27	1.40E+03	133	2.97E+03	27	2.96E+03	133	2.59E+02

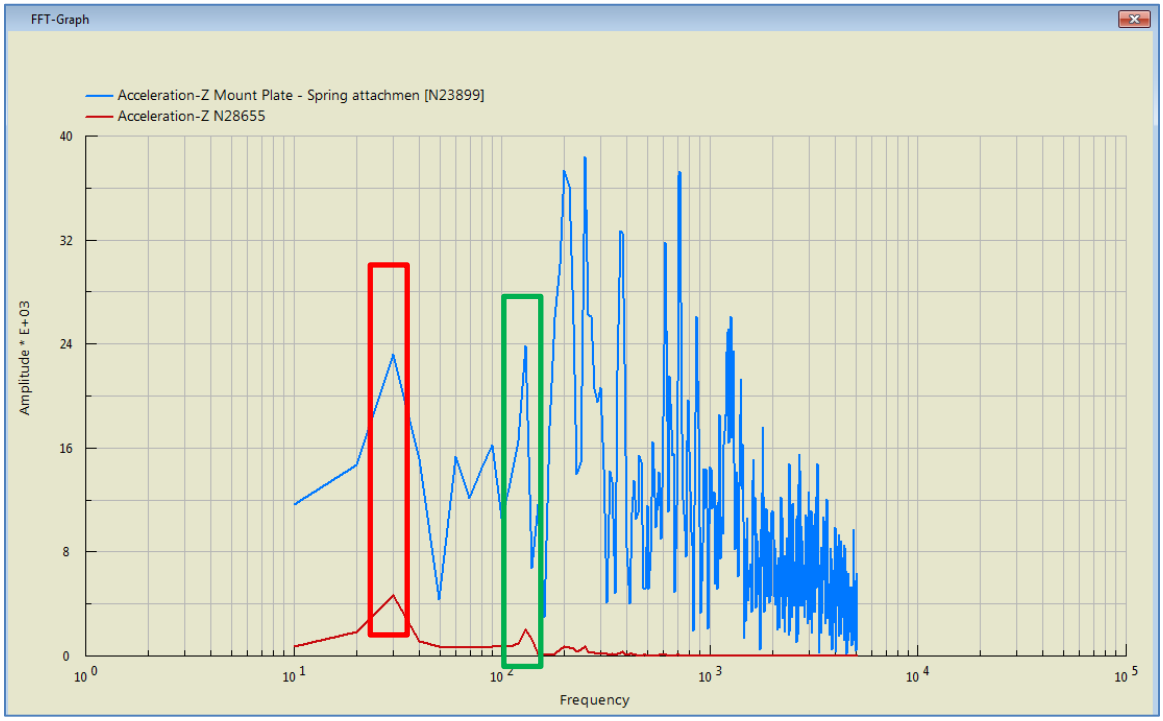

Figure 137. FFT of Acceleration Response from Spring Mass System on LWSM

This was repeated with a refined 7.62 cm (3 in) nominal, instead of 15.24 cm (6 in) nominal mesh spacing for equipment case in order to see the effects on the lowest frequency for the 1.11e5 g (245 lb) system model. Various details of this model are presented in Figure 138.

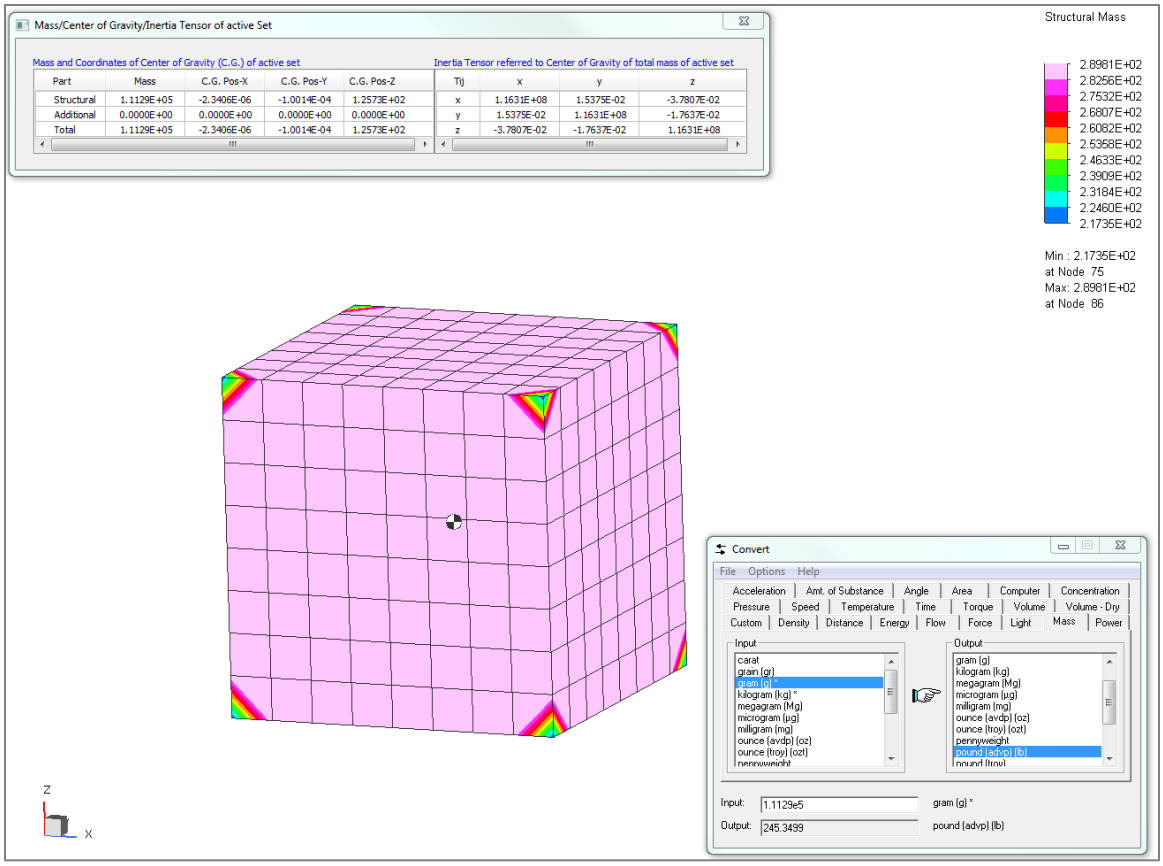

Figure 138. The 245 lb System Model

Some additional details on the model include a 0.635 cm (¼ inch) shell thickness, a density of 7.86 g/cm^3 and dimensions of 60.96 x 60.96 x 60.96 cm (2 ft) cube box with uniform mesh spacing.

The dominant frequency is clearly at 113.31 Hz with a close frequency of 116 Hz that can be considered spurious with almost no mass participation. Here we find that Mode 7 is rotational about z axis at 239 Hz while at 285 Hz there is a Y translation mode. See Figure 139 and Table 19.

There are also several higher repeated modes with mirrored x, y component direction modes with values of 127 Hz, 158 Hz, and 255 Hz. The assumption here is that this is due to the perfect symmetry of the box.

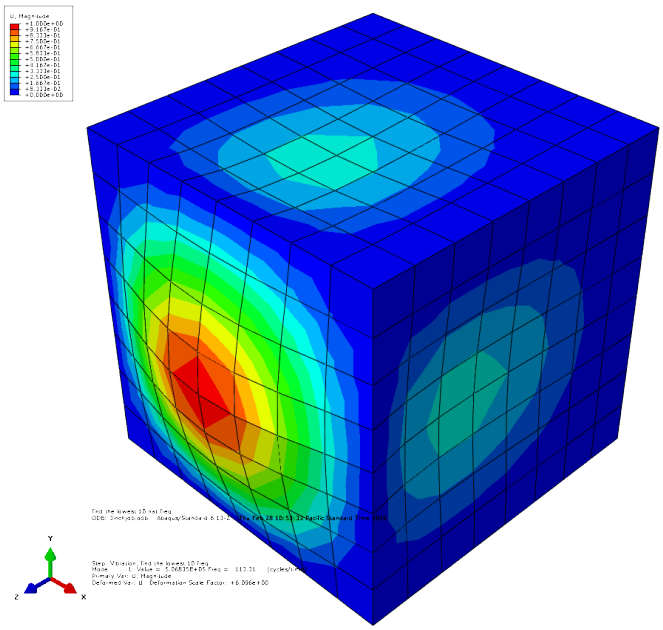

Figure 139. First Mode for Box with Flaps and Foundation Included

Table 19. Eigenvalue Output for Box Model without Flaps or Foundation.

E I G E N V A L U E O U T P U T

MODE NO	EIGENVALUE	FREQUENCY (RAD/TIME)	FREQUENCY (CYCLES/TIME)	GENERALIZED MASS	COMPOSITE MODAL DAMPING
1	5.06835E+05	711.92	113.31	4848.6	0.0000
2	5.37659E+05	733.25	116.70	14972.	0.0000
3	6.42381E+05	801.49	127.56	7320.9	0.0000
4	6.42381E+05	801.49	127.56	7320.9	0.0000
5	9.85579E+05	992.76	158.00	14016.	0.0000
6	9.86614E+05	993.28	158.09	2801.7	0.0000
7	2.25746E+06	1502.5	239.13	14148.	0.0000
8	2.56789E+06	1602.5	255.04	6170.9	0.0000
9	2.56789E+06	1602.5	255.04	6170.9	0.0000
10	3.22763E+06	1796.6	285.93	8124.2	0.0000

P A R T I C I P A T I O N F A C T O R S

MODE NO	X-COMPONENT	Y-COMPONENT	Z-COMPONENT	X-ROTATION	Y-ROTATION	Z-ROTATION
1	-6.28551E-12	-1.81021E-10	1.3526	-1.35371E-04	-5.61841E-09	1.93171E-13
2	3.23676E-10	2.52749E-10	-3.28803E-07	-3.19040E-08	4.31204E-08	-6.06042E-13
3	1.7079	6.24965E-07	7.44695E-11	-8.09637E-05	221.25	1.70951E-04
4	-6.24965E-07	1.7079	6.31637E-11	-221.25	-8.09637E-05	-8.86665E-10
5	-2.40234E-11	2.41972E-10	0.36769	-3.68341E-05	-5.47418E-09	-9.15662E-13
6	1.61019E-15	-1.90698E-15	1.8292	-1.83092E-04	-1.28025E-08	1.29610E-14
7	3.32392E-10	-4.67360E-10	8.94092E-15	3.32682E-08	4.84258E-08	28.135
8	2.38856E-08	6.14553E-02	-3.14901E-10	25.122	-9.76396E-06	5.36780E-08
9	-6.14553E-02	2.38856E-08	7.83369E-10	9.76396E-06	25.122	-6.16385E-06
10	4.14265E-10	0.12914	-6.64588E-11	-7.9439	2.54863E-08	-9.70257E-09

E F F E C T I V E M A S S

MODE NO	X-COMPONENT	Y-COMPONENT	Z-COMPONENT	X-ROTATION	Y-ROTATION	Z-ROTATION
1	1.91555E-19	1.58881E-16	8871.2	8.88514E-05	1.53053E-13	1.80924E-22
2	1.56854E-15	9.56433E-16	1.61863E-09	1.52394E-11	2.78382E-11	5.49897E-21
3	21354.	2.85940E-09	4.05994E-17	4.79892E-05	3.58382E+08	2.13946E-04
4	2.85940E-09	21354.	2.92077E-17	3.58382E+08	4.79892E-05	5.75549E-15
5	8.08883E-18	8.20632E-16	1894.8	1.90159E-05	4.20007E-13	1.17514E-20
6	7.26399E-27	1.01886E-26	9374.3	9.39200E-05	4.59208E-13	4.70652E-25
7	1.56308E-15	3.09017E-15	1.13095E-24	1.56581E-11	3.31767E-11	1.11990E+07
8	3.52064E-12	23.306	6.11928E-16	3.89450E+06	5.88306E-07	1.77805E-11
9	23.306	3.52064E-12	3.78690E-15	5.88305E-07	3.89450E+06	2.34452E-07
10	1.39423E-15	135.49	3.58826E-17	5.12678E+05	5.27707E-12	7.64806E-13
TOTAL	21377.	21513.	20140.	3.62790E+08	3.62277E+08	1.11990E+07

From the ABAQUS solver, the lowest dominant frequency is determined to be approximately 120 Hz for the shell equipment case (box). Based on the FSP simulation a mode at approximately 120 Hz is also found. A summary of cases is provided in Table 20.

Table 20. Summary of Lowest Dominant Frequencies per Model Variation

Model	Mode	Lowest Dominant Freq (Hz)	Particiaption Factor	Participation Direction	Effective Mass	Effective Mass Direction
Box w/ fnd w/ flaps	7	110.00	70.11	Y-rotational	2.41E+07	Y-rotational
Box w/ fnd w/o flaps	1	118.87	0.64	Z-translational	3969.5	Z-translational
Box w/o fnd w/o flaps (6 in)	1	119.23	0.76	Z-translational	4710.7	Z-translational
Box w/o fnd w/o flaps (3 in)	1	113.31	1.35	Z-translational	8871.2	Z-translational

From the analysis of the acceleration response it was found that the simulation produced a base (deck) frequency of 27 Hz, and higher natural frequency of 133 Hz for the 1.14e5 g (250 lb) standard shell equipment model when impacted on the LWSM model. Figure 140 illustrates the FFT response data. Figure 141 gives a sample of the very normal oscillation early time acceleration response, while Figure 142 illustrates FFT content and Figure 143 a simulation fringe plot of the vertical acceleration.

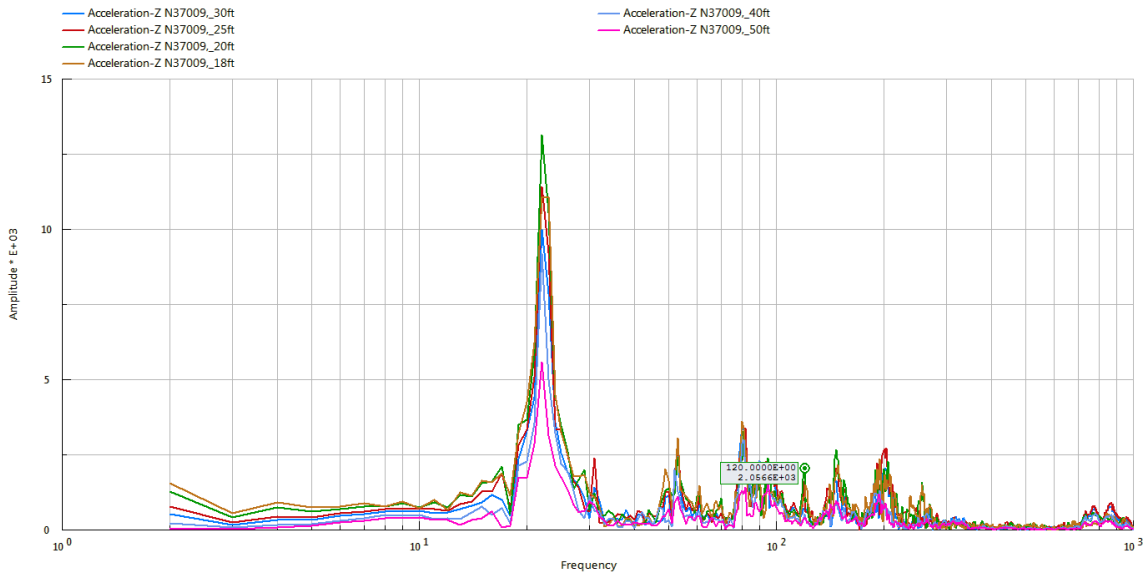

Figure 140. Frequency Content of Shell Model Simulation on LWSM

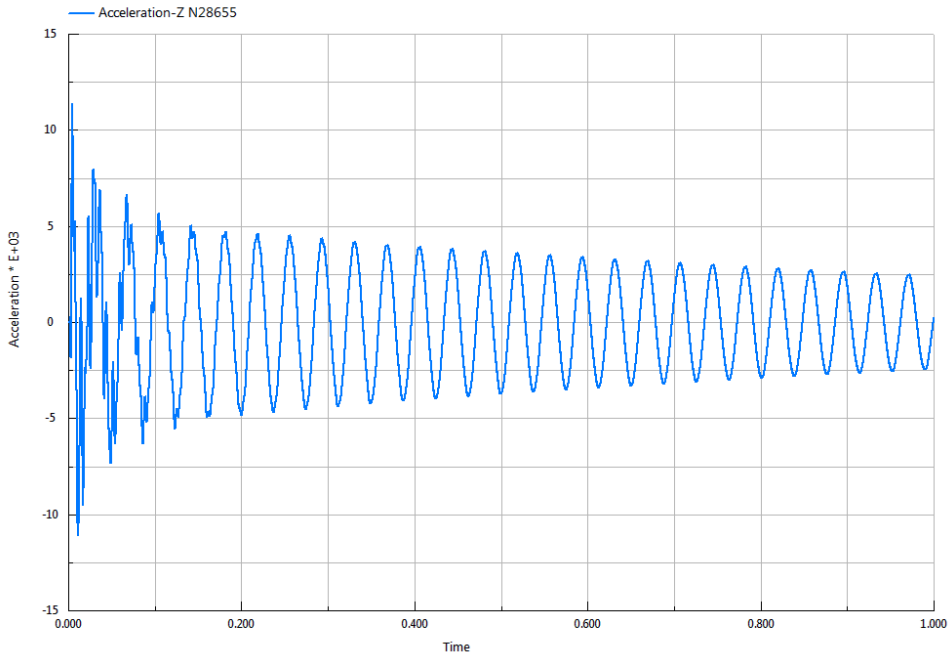

Figure 141. Early Time Acceleration Response of Mass atop Spring on LWSM

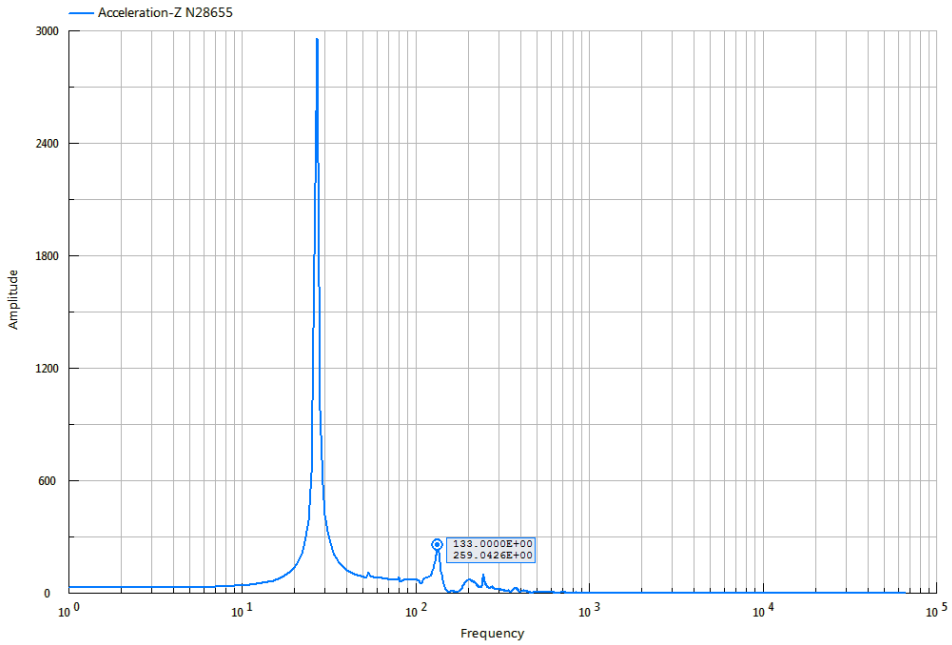

Figure 142. Dominant Response Frequency Based on FFT of Acceleration

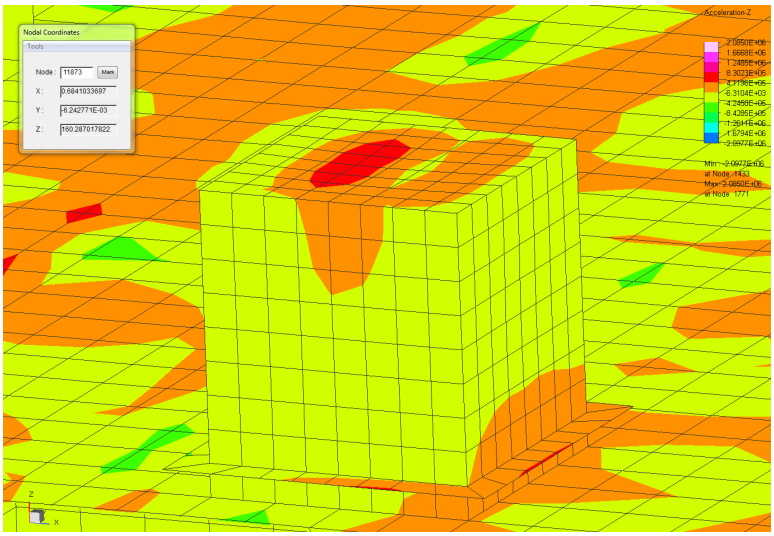

Figure 143. Example of FSP and Equipment Model Response

THIS PAGE INTENTIONALLY LEFT BLANK

SUPPLEMENTAL 1. DATA ANALYSES FOR IMPROVED SHIP DAMPING MODEL

In addition to the FSP, a full ship shock model is used to examine the proposed proportional damping model. The ship model contains the necessary complexity and diversity in structure in order to be able to discern the damping affects.

A brief description of the ship model is given, along with details regarding the shock geometry set up used in the M&S effort. Additionally, data results are summarized, and analyses documented for the ship proportional damping study.

For those interested in obtaining the supplemental document for review, please contact the NPS Dudley Knox Library.

THIS PAGE INTENTIONALLY LEFT BLANK

SUPPLEMENTAL 2. DATA ANALYSES OF FULL SHIP SHOCK FAILURE MODEL

In addition to the FSP, a full ship shock model is used to examine the functional failure model. The ship model contains the necessary complexity and diversity in structure in order to compare the same equipment cabinet model in various installations throughout the ship. The ship model itself is an excellent FEM model used in many previous studies.

A description of the ship model is given, along with details regarding the shock geometry set up used in the M&S effort. Additionally, data results are summarized, and analyses documented for the ship equipment study.

For those interested in obtaining the supplemental document for review, please contact the NPS Dudley Knox Library.

THIS PAGE INTENTIONALLY LEFT BLANK

LIST OF REFERENCES

[1] D. Inman, *Engineering Vibration,* 2nd ed. Upper Saddle River, NJ: Prentice Hall, 2001.

[2] R.G. Weingardt, "Engineering legends–Stephen P. Timoshenko, ASCE Leadership and Management in Engineering, vol. 8, issue 4. Oct 2008, doi: 10.1061/(ASCE)1532-6748(2008)8:4(309).

[3] S.P. Timoshenko. *As I Remember; the autobiography of Stephen P. Timoshenko.* Princeton, NJ: D. Van Nostrand Company, 1968.

[4] I. Korsak, *Harrow in a Strange Field (Борозна у чужому полі)*. Kiev, Ukraine: Yaroslaviv Val (in Ukrainian), 2014.

[5] R. Soderberg, *Stephen P. Timoshenko–A Biographical Memoir*, Washington, D.C., National Academy of Sciences, 1982.

[6] S. Timoshenko, *Vibration Problem in Engineering*, 2nd ed. New York, NY: D. Van Nostrand Company, 1928.

[7] G.I. Taylor, "The Pressure and Impulse of Submarine Explosion Waves on Plates," in Underwater Explosion Research, vol. I, Office of Naval Research, 1950, 1155–1173.

[8] H.G. Snay and E.A. Christian, "The Response of Air-Backed Plates to High-Amplitude Underwater Shockwaves," NAVORD Report 2462, 1952.

[9] W.P. Welch, "Mechanical Shock on Naval Vessels as Related to Equipment Design," Journal of American Society of Naval Engineers, 1946. [Online]. Available: https://onlinelibrary.wiley.com/doi/abs/10.1111/j.1559-3584.1946.tb02715.x

[10] R.H. Cole, *Underwater Explosions*, Princeton University Press; 1948.

[11] C.M. Harris and C.E. Crede, *Shock and Vibration Handbook*, 2nd ed. Kingsport, TN: Kingsport Press, 1976.

[12] G.J. O'Hara, "Background for Mechanical Shock Design of Ships Systems," NRL Report 6267, Washington, DC, 1965

[13] H.C. Pusey, "Two Generations of Shock and Vibration Technology–Progress Over Sixty Symposia," *Proceedings of Shock and Vibration Symposium* No. 60, November 1989.

[14] H.U. Mair, Preliminary Compilation of Underwater Explosion Benchmarks, *Proceedings of the 67th Shock and Vibration Symposium*, Volume I (1996), SAVIAC, 361–379.

[15] R.P. Carlisle, *Where the Fleet Begins: A History of David Taylor Research Center, 1898–1998*, Naval Historical Center, Dept. of the Navy, Washington, D.C., 1998.

[16] H.C. Pusey, "Progress in Shock and Vibration Technology Over 80 Symposia," in *Rotating Machinery, Structural Health Monitoring, Shock and Vibration*, Volume 5, Springer New York, 2011.

[17] Rogers Corporation, "Shock Control Design Guide," Accessed: Aug 22, 2019. [Online]. Available: http://www.rogerscorp.com/documents/992/hpf /poron/industrial/Shock-Control-Design-Guide.aspx

[18] RAND Corporation, Sustaining U.S. Nuclear Submarine Design Capabilities, Appendix D, pp. 179–190 "U.S. Navy's Technical Warrant Holders," 2007 Accessed: Aug 22, 2019. [Online]. Available: https://www.jstor.org/stable/10.7249/mg608navy.21

[19] R.N. Bonny, "The effect of non-contact explosions on warship machinery design," *Naval Engineers Journal*, vol. 60, no.3 pp. 365–388, Aug. 1948.

[20] War Damage Report No.47, U.S.S. Chincoteague (AVP24) Bomb Damage, NAVSHIP 47(424), Bureau of Ships, 1944, Accessed: Aug 22, 2019. [Online]. Available: https://www.history.navy.mil/research/library/online-reading-room/title-list-alphabetically/w/war-damage-reports/uss-chincoteague-avp24-war-damage-report-no-47.html

[21] IHS Jane's Fighting Ships [series].

[22] M.R. Doyle, D.J. Samuel, T. Conway, and R.R. Klimowski, "Electromagnetic Aircraft Launch System–EMALS," Naval Air Warfare Center, Aircraft Division, Lakehurst, NJ, IEEE Transactions on Magnetics, vol. 31, no. 1., January1995 accessed: Aug 22, 2019. [Online]. Available: https://ieeexplore.ieee.org/iel1/20/8355/00364638.pdf

[23] OPNAV Instruction 9072.2A, "Shock Hardening of Surface Ships," 19 February 2013.

[24] NAVSEA 0908-LP-000-3010A, Shock Design Criteria for Surface Ships, October 1994.

[25] NAVSEA, *Shock Design Criteria for Surface Ships*, T9070-AJ-DPC-120/3010, Washington, D.C., 2017.

[26] Investigation into the attack on the U.S.S. Cole, Report of the House Armed Services Committee Staff, May 2001.

[27] USS Cole Bombing. [Online]. Available: https://www.hsdl.org/c/resources/uploads/2017/12/USS-Cole.jpg

[28] J.M. Gilmore, "Director, Operational Test and Evaluation FY 2016 Annual Report," DOT&E, Washington, D.C., Dec. 2016.

[29] U.S. Navy photo by Mass Communication Specialist 2nd Class Michael Bevan.

[30] F.A. Costanzo, "Underwater Explosion Phenomena and Shock Physics," Proceedings of the IMAC-XXVIII, February 1–4, 2010, Jacksonville, Florida.

[31] Major Systems and Munitions Programs: Survivability Testing and Lethality Testing required before Full-Scale Production, U.S.C. Title 10 Part IV Chapter 139 section 2366. 2017. [Online]. Available: https://www.gpo.gov/fdsys/pkg/

[32] H.M. Schauer, "Shock Resistance Testing of U.S. Naval Vessels," presented at the Spring Meeting of The Society of Naval Architects and Marine Engineers, Hampton Roads, Virginia, April 1962.

[33] W.J. Sette and K.W. Goben, "Shock in ships," Naval Engineers Journal, vol. 75, no. 3 pp. 525–534, 1963.

[34] A.H. Keil, "The Response of ships to underwater explosions," David Taylor Model Basin, Bethesda, MD, Technical Report 1576, Nov. 1961.

[35] W.A. Fensterer, "Design level ship shock simulation of Winston Churchill (DDG-81)," M.S. thesis, Dept. of Mech. and Aerosp. Eng., NPS, Monterey, CA, USA, 2004.

[36] E.W. Clements, "Shock performance of a shipboard electrical switchgear," NRL Memorandum Report 4003, NRL, Washington, D.C.,1979.

[37] I. Vigness, "Navy High-Impact Shock Machines for Lightweight and Mediumweight Equipment," NRL Report 5618, NRL, Washington, D.C., 1961.

[38] A Guide for Design of Shock Resistant Naval Equipment, NAVSHIPS 25 0–660-30, 1949.

[39] Military Specification, MIL-S-90lB (NAVY), 9 April l954.

[40] T.L. Bradey, Jr. T.M. Daves, S.L. McCampbell, J.I. Ykema, "Comparison of shock test methods of MIL-S-901 derived from tests on a circuit breaker & Switchboard," *Naval Engineers Journal*, Vol 104, No. 3, May 1992.

[41] Military Specification, MIL-S-901D, Shock Tests, High Impact Shipboard Machinery, Equipment and Systems, Requirements for, March 1989.

[42] Shock Test, H.I. (High-Impact) Shipboard Machinery, Equipment, and Systems, Requirements for, MIL-DTL-901E, 2017.

[43] M. Brener et al., Navy Ship Underwater Shock Prediction and Testing Capability Study, Technical Report, MITRE Corporation, JSR-07-200, McLean, Virginia, Oct. 2007.

[44] J.M. Fowler, "Recent Trends in Ship Shock," ASE, 24th Annual Technical Symposium, Washington, D.C., 1987.

[45] E.T. Moyer, J.C. Stergiou, G.M. Reese, and N.N. Aboud, "Navy Enhanced Sierra Mechanics (NESM): Toolbox for predicting navy shock and damage," Computing in Science & Engineering, Vol. 18, No. 6, 2016.

[46] H.U. Mair, R.M. Reese, and K. Hartsough, "Simulated Ship Shock Tests/Trials?," [Online]. Available: https://www.researchgate.net/publication /2825129_Simulated_Ship_Shock_TestsTrials

[47] Y.S. Shin, and S.Y. Park, "Ship Shock Trial Simulation of USS John Paul Jones (DDG 53) Using LS-DYNA/USA: Three Dimensional Analysis," *70th Shock and Vibration Symposium Proceedings*, Vol. I, November 1999.

[48] J.M. Didoszak, Y.S. Shin, and D.H. Lewis, "Shock Trial Simulation for Naval Ships," Proceeding ASNE DAY 2004 Conference, Crystal City, VA, June 2004.

[49] Naval Sea Systems Command Evaluation of Alternative to Meet Surface Ship and Submarine Live Fire Test and Evaluation Requirements, NAVSEA, Ser 05p-153/195, May 2013.

[50] G.L. Chahine, K.M. Kalumuck, M. Tanguay, J. Galambos, M. Rayleigh, R.D. Miller, and C. Mairs, "Development of a Non-Explosive Ship Shock Testing System SBIR Phase I Final Report," DYNAFLOW Report 2M3030-1-DTRC, 2004.

[51] G.L. Chahine, C.T. Hsiao, and J.K. Choi, "Development of a Non-Explosive Ship Shock Test System: SBIR Phase II Final Report," DYNAFLOW, INC. Report 2M5011-2-NSWCCD, December 2007.

[52] A. Corbishdale, B. Lang, B. Klenow, R. Javier, S. Yamada, S. Drake, and S. Mixer, "Test Plan: Floating Shock Platform Airgun and Underwater Explosion Test Series for the Full Ship Shock Trial Alternative Program," Technical Report. NSWCCD-66-TR–2012/06, May 2012.

[53] J. Venne, J. and F.A. Costanzo, "Non-Explosive Testing Working Group FY11/12 Progress for the Full Ship Shock Trial Alternative Program," Technical Report NSWCCD-66-TR-2013/40, Nov 2013.

[54] A.W. Hapij, and C.G. Van Valkenburgh, "Modeling and Simulation for a Full Ship Shock Trial Alternative: FY11/12 Progress," Naval Surface Warfare Center Carderock Division, Technical Report, NSWCCD-66-TR–2013/006, Jan. 2013.

[55] S. Rutgerson, R. Javier, and F.A. Costanzo, "A Review of Recent Full Ship Shock Trial (FSST) Costs and Potential Cost Avoidance Measures," NSWCCD, Technical Report, NSWCCD-66-TR–2011/00, Jan. 2011, unpublished.

[56] B. Lang et al., "Test Report: Floating Shock Platform Airgun and Underwater Explosion Test Series for the Full Ship Shock Trial Alternative Program," Naval Surface Warfare Center Carderock Division, Technical Report, NSWCCD-66-TR-2013/18, May 2013.

[57] B. Lang, D.C. Merrill, and D. Manko, "Equipment Operability Working Group FY11/12 Progress for the Full Ship Shock Trial Alternative Program," Naval Surface Warfare Center Carderock Division, NSWCCD-66-TR-2013/29, October 2013.

[58] Y.W. Kwon, J.M. Didoszak and D.A. Nussbaum, "Assessment of Ship Shock Hardening Validation Options," NPS, Monterey, CA, Technical Report NPS-MAE-17-002R, June 2017.

[59] Y.W. Kwon, and J.M. Didoszak, "Development of Shipboard Equipment Shock Survivability Assessment Technique," Naval Postgraduate School, Monterey, CA, Interim report, October 2018.

[60] C. Lalanne, *Mechanical Vibration and Shock Analysis–Mechanical Shock*, 2nd ed. Vol 2, John Wiley & Sons, Inc., New Jersey, 2014.

[61] D.S. Steinberg, *Vibration Analysis for Electronic Equipment*, 3rd ed. John Wiley & Sons, Inc., New York, 2000.

[62] G.J. O'Hara, *Background for Mechanical Shock Design of Ships Systems*, Naval Research Laboratory; 1965

[63] R.E. Newton, "Fragility Assessment Theory and Test Procedure," Monterey Research Laboratory, Inc., Monterey, California, 1968.

[64] G.J. O'Hara, and R.O. Belsheim, *Interim design values for shock design of shipboard equipment*, National Technical Information Service, 1963.

[65] ANSI Equipment Ruggedness Specification, ANSI/ASA S2.62-2009: Shock Test Requirements for Equipment in a Rugged Shock Environment.

[66] R.E. Newton, "Damage Boundary Theory Revisited," American Society of Mechanical Engineers paper, 89-WA/EEP-24, ASME, New York, NY, 1989.

[67] H.H. Schueneman,"Vibration Testing of Products and Package Systems," Westpak, Inc., San Jose, CA, 1995.

[68] H.H. Schueneman "Package Engineering, Design and Testing," Westpak, Inc., San Jose, CA, 1996.

[69] D. Root, "6-Step Product/Package Development Method," Lansmont Corporation, Monterey, CA, 1992. [Online]. Available: http://www.lansmont.com/resources/six-step-method/

[70] Military Specification, MIL-STD-810G, 31 October 2008.

[71] M.M. Swisdak, Jr., Explosion effects and properties: Part II–Explosion effects in water, Naval Surface Weapons Center, White Oak Lab, Silver Spring MD. NSWC/WOL TR 76–1, February 1978.

[72] E. Lee, M. Finger, W. Collins, JWL Equation of State Coefficients for High Explosives, Lawrence Livermore National Laboratory. Report UCID-16189, January 1973.

[73] R.J. Scavuzzo, and H.C. Pusey, *Naval Shock Analysis and Design*. 2000: Shock and Vibration Information Analysis Center, Booz-Allen and Hamilton, Incorporated.

[74] A.B. Arons, et. al., "Long Range Shock Propagation in Underwater Explosion Phenomena II," *Underwater Explosion Compendium*, Vol. I, Oct. 10, 1943.

[75] F.A. Costanzo, J.D. Gordon, "An Analysis of Bulk Cavitation in Deep Water," Underwater Explosion Research Field Unit Report 511, May 1980.

[76] A.P. Walters, J.M. Didoszak and Y.W. Kwon, "Explicit Modeling of Solid Ocean Floor in Shallow Underwater Explosions," *Journal of Shock and Vibrations*, Vol. 20, Number 1/2013. doi:10.3233/SAV-2012-0737.

[77] H. Lamb, *Hydrodynamics*, 6th Edition, Cambridge Press, 1932 and by Dover Press, 1945.

[78] A.P. Walters, "Investigation of an explicitly modeled solid ocean floor on a shallow water UNDEX event," M.S. thesis, Dept. of Mech. and Aerosp. Eng., NPS, Monterey, CA, USA, 2012.

[79] H.G. Snay, "Hydrodynamics of underwater explosions," Naval Hydrodynamics Publication 515, National Academy of Sciences – National Research Council, 1957.

[80] R. Ilamni, "Analyses of the Baltic Sea test site UNDEX shock environment," Naval Surface Warfare Center Indian Head, Indian Head, Report IHTR 2785, 2006.

[81] United States Department of Defense (24 November 1980). MIL-STD-1629A– Procedures for performing a failure mode effect and criticality analysis. Department of Defense (USA).

[82] MIL-DTL-1629, "Procedures for Performing a Failure Mode, Effects and Critically Analysis," August 1998.

[83] SAE (2008). Potential Failure Mode and Effects Analysis in Design (Design FMEA) and Potential Failure Mode and Effects Analysis in Manufacturing and Assembly Processes (Process FMEA) and Effects Analysis for Machinery (Machinery FMEA). SAE International.

[84] K. M. Adams, *Non-functional Requirements in Systems Analysis and Design, Topics in Safety, Risk, Reliability and Quality*, Springer, DOI 10.1007/978-3-319-18344-2.

[85] J.E. Shigley and C.R. Mischke, *Mechanical Engineering Design,* 5th Edition, McGraw-Hill, 2002.

[86] Ship Structure Committee, "Ship Design Vibration Guide," SSC-350, 1990. [Online]. Available: http://www.shipstructure.org/pdf/350.pdf

[87] D.S. Steinberg, *Preventing Thermal Cycling and Vibration Failures in Electronic Equipment*, 1st ed. John Wiley & Sons, Inc., New York, 2001.

[88] H.A. Gaberson, and R.H. Chalmers, "Modal Velocity as a Criterion of Shock Severity," *Shock and Vibration Bulletin* 40, Part 2, Dec 1969, pp. 31–49.

[89] Craig, B.D. J Fail. Anal. and Preven Material failure modes, part I: A brief tutorial on fracture, ductile failure, elastic deformation, creep, and fatigue. (2005) 5: 13. https://doi.org/10.1361/154770205X70732. *Journal of Failure Analysis and Prevention*, October 2005, Volume 5, Issue 5, pp. 13–14.

[90] Craig, B.D. J Fail. Anal. and Preven. (2005) 5: 7 https://doi.org/10.1361/154770205X762407Material failure modes, part II: A brief tutorial on impact, spalling, wear, brinelling, thermal shock, and radiation damage. *Journal of Failure Analysis and Prevention*, December 2005, Volume 5, Issue 6, pp. 7–12.

[91] Craig, B.D. J Fail. Anal. and Preven. (2006) 6: 12. https://doi.org/10.1361/154770206X99262. Material failure modes, part III: A brief tutorial on corrosion-related material failure modes Journal of Failure Analysis and Prevention April 2006, Volume 6, Issue 2, pp. 12–19.

[92] International Electrotechnical Commission (IEC). Internet: http://www.iec.ch

[93] IEC-60068-2-27:2008, Environmental testing–Part 2-27: Tests –Test Ea and guidance: Shock, Edition 4.0 date 2008–02.

[94] IEC 60068-2-6:2007, Environmental testing–Part 2–6: Tests–Test Fc: Vibration (sinusoidal), Edition 7.0 date: 2007–12.

[95] ETSI EN 300 019–2-4, Environmental conditions and environmental tests for telecommunications equipment, Part 2-4: Specification of environmental tests; Stationary use at non-weatherprotected locations, Edition 2.5.1 date 2018–07.

[96] IEC 60068-2-57:2013, Environmental testing–Part 2-57: Tests Ff: Vibration – Time-history and sine-beat method.

[97] R.H. Anderson and R.O. Hundley, "The Implications of COTS Vulnerabilities for the DOD and Critical U.S. Infrastructures: What Can/Should the DOD Do?" RAND Corporation, Santa Monica, CA, P-8031, 1998.

[98] B.W. Lang, "A New American National Standard for Shock Testing Equipment," pp. 13–14, Sound and Vibration, April 2010.

[99] "Standard Test Methods for Mechanical-Shock Fragility of Products, Using Shock Machines," American Society of Testing and Materials (ASTM) Standard D3332-99, January 2010.

[100] Shock Hardening of Surface Ship, NAVSEA Tech Pub T9072-AF-PRO-010, January 2017.

[101] NRL report 7396, "Shipboard Shock and Navy Devices for its Simulation," by Clements, E.W., dated July 14, 1972.

[102] NRL report 8631, " "Procedures for Conducting Shock Tests on Navy Class HI (High Impact) Shock Machines for Lightweight and Mediumweight Equipment," by Clements, E. W., dated 30 September 1982.

[103] Lightweight Shock Machine. [Online]. Available: http://www.e-labsinc.com/dynamics-hammer-shock-testing.shtml.

[104] V. Bateman, "Mechanical Shock Test Techniques and Data Analysis." Slides, SAVIAC, Arvonia, VA, USA, 2009.

[105] Floating Shock Platform. [Online]. Available: http://hitestlabs.com

[106] FSP Deck Simulating Fixture. [Online]. Available: https://www.nts.com/content/uploads/2014/08/901-figure1.jpg

[107] Deck Shock Simulator Module. [Online]. https://www.nts.com/ntsblog/nts-deck-simulator-901d/

[108] Qualification Testing. May 1970. National Aeronautics and Space Administration https://ntrs.nasa.gov/search.jsp?R=19710019569

[109] Heavyweight High Impact (H.I.) Shock Test Report for Argon Ship Exploration Equipment Increment E (SSEE-E) System, Dynamic Testing Corp. July 2003.

[110] Medium Weight Shock and Vibration Test Report on 3 x 1.5 x 8 Pump with 30 HP Motor, Sims Pump Valve Company, Inc. April 2006.

[111] D.V. Caletka, R N. Caldwell and J.T. Vogelmann, "Damage Boundary Curves: A Computational (FEM) Approach, " ASME Journal of Electronic Packaging, Vol. 102, September 1990.

[112] R.L. Iman and J.C. Helton, "Computer simulations are used to study engineering uncertainty," *An Investigation of Uncertainty and Sensitivity Analysis Techniques for Computer Models*, Risk Analysis, Volume 8, Issue 1, pages 71–90, March 1988, DOI: 10.1111/j.1539-6924.1988.tb01155.x] [Online]. Available: https://en.wikipedia.org/wiki/Uncertainty_quantification#/media/File:Bias_Correction.png

[113] G. Harris, J.A. Luton, T. McGrath, R.M. McKeown, J. St. Clair, W. Babcock, and A.B. Wardlaw, Jr., "Overview of the Dynamic System Mechanics Advanced Simulation Code (DYSMAS)," NSWC Indian Head EOD Technology Division, IHSP 14-04, Oct. 11, 2014.

[114] A.B. Wardlaw, Jr., J.A. Luton, J.R. Renzi, K.C. Kiddy, and R.M. McKeown, "The Gemini Euler Solver for the Coupled Simulation of Underwater Explosions," NSWC-IHD Technical Report IHTR 2500, Nov. 30, 2003.

[115] J.I. Lin, *DYNA3D: A Nonlinear, Explicit, Three-Dimensional Finite Element Code for Solid and Structural Mechanics*, User Manual. Lawrence Livermore National Laboratory. Report UCRL-MA-107254, June 2005.

[116] C.G. Hoover, A.J. De Groot, and R.J. Sherwood. *ParaDyn User Manual, ParaDyn: A Parallel Nonlinear Explicit, Three-Dimensional Finite-Element Code for Solid and Structural Mechanics*. Lawrence Livermore National Laboratory. Report UCRL-MA-140943-revised, January 2004.

[117] J.M. Didoszak and Y.S. Shin, "Modeling & Simulation of Ship Shock Trials: Comparison of DYSMAS, LS-DYNA/USA and Beam Code Simulations with Live Fire Test Results," NPS Technical report, Monterey, CA, NPS-MAE-07-001, January 2007.

[118] J.M. Didoszak, L.H. Bollock, J.J. Lepe and Y.S. Shin, "LPD-17 Class Pretrial Ship Shock Response Predictions: Coupled Ship-Fluid Model Generation," in *Proceedings 76th Shock and Vibration Symposium*, Destin, FL, 2005.

[119] D.T. Hart, "Ship Shock Trial Simulation of USS Winston S. Churchill (DDG-81): Surrounding Fluid Effect," M.S. thesis, Dept. of Mech. and Aerosp. Eng., NPS, Monterey, CA, USA, 2003.

[120] S.H. Ahn, "Investigation of Shallow UNDEX in Littoral Ocean Domain," M.S. thesis, Dept. of Mech. and Aerosp. Eng., NPS, Monterey, CA, USA, 2014.

[121] R. Ilamni, personal communication, May 2010.

[122] Y.S. Shin and I.B. Ham, "Damping Modeling Strategy for Naval Ship System," NPS Technical report, NPS-ME-03-003, Monterey, CA, September 2003.

[123] J. H. Gordis and J.M. Didoszak, "Analysis of the Complex Exponential Method for Modal Parameter Estimation from FSST Data," unpublished.

[124] R. Bishop, "A note on structural damping of ship hulls," *Journal of Sound And Vibration*, 1978, Vol.56(4). DOI: 10.1016/0022-460X(78)90291-2.

[125] Y.W. Kwon and J.M. Didoszak, "Improved Structural Damping Models in UNDEX Modeling and Simulation," NPS Technical report, Monterey, CA, July 2016.

[126] S. Rutgerson, "Damping Summary," unpublished.

[127] W.T. Thomson, *Theory of Vibration with Applications*, 3rd ed., Prentice Hal, Englewood Cliffs, New Jersey, 1988.

[128] C.T. Sun and Y.P. Lu, *Vibration Damping of Structural Elements*, Prentice Hall PTR, Englewood Cliffs, New Jersey, 1995.

[129] A.M. Iglesias, "Investigating Various Modal Analysis Extraction Techniques to Estimate Damping Ratio," M.S. Thesis, VPI&SU, June 2000.

[130] K. Harris, T. Wailiko, T. Brodrick and E.T. Moyer, Validation Testing of UNDEX Induced Injuries: Test Report, NSWCCD-66-TR–2012/29 December 2012.

[131] ABAQUS (2018), "ABAQUS Documentation," Dassault Systèmes, Providence, RI, USA.

[132] Damaged PCB components. [Online]. Available: http://i.imgur.com/P7vkbUE.jpg

[133] H. Gaberson, "Shock Severity Estimation," *Sound & Vibration*, January 2012.

[134] H.A. Gaberson, and R.A. Eubanks, "Simplified Shock Design for Equipment Installation," NCEL Technical Note, N-1622, March 1982.

[135] H.A. Gaberson, "Pseudo Velocity Shock Spectrum Rules for Analysis of Mechanical Shock"; IMAC XXV, Orlando, FL; Society of Experimental Mechanics; Bethel, CT, http://www.sem.org, Feb 2007, p 367.

[136] L. Chernin, M. Vilnay, I.Shufrin, and D.Cotsovos, "Pressure-Impulse Diagram Method–A Fundamental Review," *Journal of Engineering and Computational Mechanics*, March 2019, DOI: 10.1680/jencm.17.00017

[137] J. Sperrazza, "Modelling of Air Blast," In Use of models and scaling in shock and vibration. Philadelphia, Pennsylvania. Winter annual meeting of the ASME, 1963.

[138] T. Ngo, P. Medis, A. Gupta and J. Ramsay, "Blast loading and blast effects on structures–An overview," *Electronic Journal of Structural Engineering*, vol. 7, 76–91, January 2007.

[139] Simple harmonic motion oscillator. [Online].
Available: http://hyperphysics.phy-astr.gsu.edu/hbase/shm.html

[140] D.E. Post, C.A. Atwood, K.P. Newmeyer, R.L. Meakin, M.M. Hurwitz, S. Dey, J.N. D'Angelo, R.L. Vogelsong, N. Hariharan, S. Morton, R. Strawn, J. Livingston, A. Mackenna, J.Gorski, E. Moyer, R.P. Kendall, L.G. Votta, P.A. Gibson, D. Borovitcky, L.K. Miller, O.A. Goldfarb and S.B. Allwerdt, "The CREATE Program–A Suite of Physics-based High Performance Computing Software Applications for the Design and Analysis of Air Vehicles, Naval Vessels, Radio Frequency Antennas, and Ground Vehicles," IEEE Computing in Science and Engineering, Nov/Dec 2015.

[141] A. Mackenna, "Rapid design and integration," presented at the Physics-based Modeling in Design & Development for U.S. Defense Conference, Denver, CO, Nov. 14–17, 2011.

[142] C. Van Valkenburgh and E.T. Moyer, "Validation Study of Navy Enhanced Sierra Mechanics Using the Floating Shock Platform Model," NSWC Carderock Division, NSWCCD-66-TR- 2013/025, April 2013.

[143] H. Shan et al., "Guide to NavyFOAM V1.0, NSWCCD, Technical Report, NSWCCD-50-TR–2011/025, April 2011.

[144] W. Wilson, T. Quezon, V. Trinh, C. Saries, J. Li and J. Gorski, "HPCMP CREATE-SH Integrated Hydrodynamic Design Environment," *Computing in Science & Engineering*, 18(6): 47-56, November 2016. doi:10.1109/MCSE.2016.109.

[145] B. M. Dobratz and P. C. Crawford, *LLNL Explosive Handbook: Properties of Chemical Explosives and Explosive Simulants*, Livermore: Lawrence Livermore National Laboratory, 1985.

[146] Lee, E., Finger, M., and Collins, W. *JWL equation of state coefficients for high explosives*. United States: N.p., 1973. Web. doi:10.2172/4479737.

INITIAL DISTRIBUTION LIST

1. Defense Technical Information Center
   Ft. Belvoir, Virginia

2. Dudley Knox Library
   Naval Postgraduate School
   Monterey, California